Roles of a major *O*-acetylserine (thiol) lyase (OASTL) in cysteine biosynthesis, innate immunity and disease resistance in *Arabidopsis*

A thesis presented in partial fulfilment of the requirements for the degree of

Doctor of Philosophy

in

Plant Biology

at Massey University, Palmerston North,

New Zealand

Jibran Tahir

2012

Blank Page

Blank Page

Blank Page

Abstract

O-Acetylserine (thiol) lyases (OASTLs) are evolutionary conserved proteins among many prokaryotes and eukaryotes that carry out sulphur acquisition and synthesis of cysteine. OASTL catalyses cysteine biosynthesis using O-acetylserine (OAS) and sulfide as substrates. OASTL also interact with another enzyme Serine acetyltransferase (SERAT) to facilitate the production of OAS. Cysteine-derived thiols and metabolites play an important function in regulating cellular redox conditions and modulate abiotic and biotic stress responses. The *Arabidopsis thaliana* genome encodes multiple OASTL isoforms that are targeted to different sub-cellular compartments. The cytosolic OASTL-A1 or known as **O**NSET OF **L**EAF **D**EATH3 (OLD3) is the major OASTL isoform due to its high OASTL activity. The *old3-1* mutation causes a dysfunctional oastl-a1/old3-1 protein *in vitro* and was previously shown to cause autonecrosis in specific *Arabidopsis* accessions. To investigate why a mutation in a major OASTL isoform causes cell death and necrosis in some but not other accessions different mutations in OASTL-A1 were characterised in *Arabidopsis* accessions. Here it is shown that the *old3-1* mutation causes an autoimmune syndrome and metabolic disorder, in the L*er*-0 accession (parent) genetic background, but not in the reference accession Col-0. This is not the result of lack of functional OASTL-A1 or impaired cysteine biosynthesis. A *Recognition of Peronospora Parasitica 1* (*RPP1*)-like disease resistance *R* gene, from an evolutionary divergent *R* gene cluster in L*er*-0, shows a negative epistatic interaction to old3-1 and activates autonecrosis. The severity of autonecrosis was found to be dependent upon variations in temperature and day length. Next, the role of OASTL-A1 was also identified in resistance against infection with virulent and non-virulent *Pseudomonas syringae* pv. *tomato DC3000* strains. Since OASTL also interacts with SERAT, old3-1 was found to negatively affect the interaction with SERAT *in vivo*, highlighting that the release of R-mediated immunity is associated with the loss of key functions associated with OASTL. Finally various mutations were generated in OASTL-A1 isoforms to identify the relevance between the loss of OASTL functions and R-mediated immunity. These results indicated that motifs in close proximity of *old3-1* mutation play an important role in cysteine biosynthesis and therefore likely an important interface to affect R-mediated immunity. The study indicates a novel cross-talk between cysteine procuring a major OASTL isoform and components of plant immunity and further support emerging evidence that cysteine-derived metabolites function in immune signalling across kingdoms.

Blank Page

Acknowledgements

I am thankful to my supervisor Paul Dijkwel and co-supervisor Donald Hunter who have put immense effort in guiding and helping me out through all times of my PhD. Here I would especially like to thank Paul for his help in the process of thinking, performing and analysis of my experiments and preparation of my manuscript and thesis. I am also very grateful on Paul's help for obtaining funding from HEC and IMBS during the thesis writing and paper submissions. Special thanks to Don for the moral and intellectual support during solving some hard problems of PhD. I am also grateful for his help in providing access to tools such as "RNAi" that led my experiments successful. Thanks to Michael McManus for his support and putting massive pressure of lab meeting that shaped our scholarly attitudes to some extent.

I am thankful to Mutsumi Watanabe, from Max Plank Institute of Germany who helped me by performing metabolic profiling and analysis of enzymatic activities. I am also thankful to Rainer Hoefgen, Alisdair Fernie and Yariv Brotman from Max Plank Institute of Germany, on their guidance in experimental work and helping in disease resistance experiments. For criticism and ideas related to my work, thanks to many anonymous reviewers who have critically reviewed our work during submissions in peer-reviewed journals. I am highly thankful to my friend Jay Jarayaman for insightful discussions and ideas. Special thanks to Dr. Xiao Song in our lab and Marion Verdanaud from INRA for help in yeast hybrid experiments and accessing bioinformatics tools. I am thankful to my colleagues (Muhammad, Alvina, Mathew, Susana, Afsana, Srishti, Jun, Trish, Diantha, Phong, Aluh, Sam, Ihsan, and Daniel) for their support and help and good times in New Zealand. Rubina, who has always stood by my side in life as well as in academics deserves more than acknowledging. Special thanks to my two loving daughters who have given me the endless happiness of life and peace to work on my thesis. Deeply, I acknowledge my parents who have passed tough times during my PhD studies but provided me with the moral and financial support in hard times. Thanks to HEC for being a financial supporter of my PhD and IMBS-Massey and Plant and Food Research for providing a scientific enclave to thrive. Thanks God & may God bless the role of academia in the friendship of Pakistan and New Zealand.

Blank Page

Table of Contents

Abbreviations

ABA	Abscisic Acid
ACD6	Accelerated Cell Death 6
AOX	Alternative Oxidase
APK	APS Kinase
APS	Adenosine 5′-PhosphoSulfate
APR	Adenosine 5′-Phosphosulfate Reductase
ATPS	ATP Sulfurylase
Avr	Avirulence
BSAS	β-Substituting Alanine Synthase
Cys	Cysteine
Col-0	Columbia-0
COX	Cytochrome Oxidase
CAS	β-Cyanoalanine Synthase
CLT	Chloroquine-resistance Transporter
cad-2	cadmium sensitive -2
CgS	Cystathionine γ-Synthase
CFU	Colony Forming Units
CamV	Cauliflower Mosaic Virus
CAPS	Cleaved Amplified Polymorphic Sequences
DES	DESulfhydrase
DM	Dobzhansky and Muller
DAB	Di-amino benzidine
EF-Tu	Elongation Factor-Tu
EMS	Ethylmethane sulphonate
EDS1	Enhanced Disease Susceptibility 1
ETI	Effector-Triggered Immunity
ETS	Effector-Triggered Susceptibility
γ-EC	Gamma-glutamylcysteine.
GC-MS	Gas Chromatography- Mass spectrometery
GSH	Glutathione
γ-ECS	γ-glutamyl-cysteine ligase
GSH2	Glutathione Synthetase

GR	Glutathione Reductase
GSNO	S-Nitrosoglutathione
GMO	Genetically Modified Organisms
GSBs	Genetic Sequence Blocks
GABA	γ-AminoButyric Acid
HCA	Hierarchical Clustering Analysis
HPLC	High-Performance Liquid Chromatography
HEPES	4-2-Hydroxyethyl-1-piperazineethane sulfonic acid
Hom	Homozygous
Het	Heterozygous
HR	Hypersensitive response
hrpA-	hypersensitive reaction and pathogenicity A gene
IDT	Integrated DNA Technologies
ICSI	Isochorismate synthase 1
I3M	Indole-3-yl-methyl glucosinolate
JA	Jasmonic Acid
LC-MS	Liquid Chromatography- Mass Spectrometery
L.D.	Long Days
L*er*-0	Landsberg *erecta*-0
LRR	Leucine-Rich Repeat
mETC	mitochondrial Electron Transport Chain
MAMPs	Microbe-Associated Molecular Patterns
MHC	Major Histocompatibility Locus
4MI3M	4-Methoxy-Indol-3-ylMethyl-glucosinolate
PTI /MTI	PAMPS / MAMPs-Triggered Immunity
NADP	Nicotinamide Adenine Dinucleotide Phosphate
NIL	Near-Isogenic Line
NBS	Nucleotide Binding Site
NPR1	Non-expresser of Pathogenesis Related 1
PPi	inorganic Pyrophosphate
PAD4	Phytoalexin deficient 4
PR-1	Pathogenesis Related-1
3PGA	Glyceraldehyde 3-Phosphate
PEP	Phosphoenoylpyruvate

OAS	O-acetylserine
ORF	Open Reading Frame
Os	*Oryza sativa*/ Rice
OPT	Oligopeptide Transporters
OASTL	O-acetylserine (thiol) lyase
OLD3/old3	Onset of Leaf Death3
PRR	Pattern Recognition Receptors
PCD	Programmed Cell Death
PAPS	3′-phosphoadenosine ate 5′-phosphosulfate
PLP	Pyridoxal-Phosphate
PPDB	Plant Proteome Database
CS26	S-sulfocysteine synthase 26
Pst	Pseudomonas syringe
PCRs	Polymerase Chain Reactions
qRT-PCR	Quantitative real-time PCR
QTL3	Quantitative Trait Locus 3
R	Resistance
RCR3	Required for full *Cladosporium. fulvum r*esistance3
Cf-R	*Cladosporium. fulvum* Resistance
R.H	Relative Humidity
RD-19	RESPONSIVE TO DEHYDRATION19
RPM1	RESISTANCE TO *PSEUDOMONAS SYRINGAE* 1
RNS	Reactive Nitrogen Species
ROS	Reactive Oxygen Species
RPP1	RESISTANCE TO *PERENOSPORA PARASITICA* 1
riml 1	*root meristemmless* 1
RNAi	RNA interference
SULTRs	Sulfate Transporters
SLIM1	Sulfur LIMitation1
SiR	Sulphite Reductase
SA	Salicylic Acid
SERAT	Serine acetyltransferase
STAS	Sulfate Transporters and AntiSigma-factor Antagonists
SAR	Systemic Acquired Resistance

S.D.	Short Days
SAM	S-adenosylmethionine
SLIM	Site-Directed Ligase Independent mutagenesis
SSLP	Simple Sequence Length Polymorphism
SID2	Salicylic acid (SA) induction–deficient mutant
TIR	Toll-Interleukin-1-Resistance
TAIR	The Arabidopsis Information Research
TTSS	Type-III Secretion System
TCA	Tricarboxylic acid
UTRs	Un-Translated Regions
WRKY	WRKYGQK (amino acid sequence in the transcription factors)
WT	Wild-type
Ws	Wassilewskija
ZM	*Zea Mays* /Maize

List of Figures

List of Tables

Blank Page

Blank Page

Chapter 1

General Introduction

For millions of years plants have co-existed with many organisms that gained the ability to infect and access the energy and nutrient resources generated in plant cells. Pathogens such as biotrophs have adapted to "slowly steal" plant-synthesized nutrients without rapid host killing whereas necrotrophs are relatively "notorious" as they force brutal host-cellular damage and cause nutrient loss. Unlike immune systems in mammals, plants do not have specialized cells to detect foreign molecules. Plants are also of sessile nature and so cannot avoid pathogenic environments. Even under such natural limitations, plants are evolved with an effective immune system to resist pathogen attacks. Various forms of defence in plants can be seen in the form of cell walls, thorny leaves and waxy cuticles over leaf surface that can withstand many foreign invasions. However a number of pathogenic organisms such as fungi and bacteria are able to deploy cell wall degrading enzymes and intrude through leaf stomatal openings to cause infection. To counter such an invasion, plants are equipped with an inducible immune system that is based on detection of foreign molecules by specific receptor proteins which then activate innate immune responses. Interestingly, the functional domains of the plant immune receptors display striking similarities to those of the mammalian immune receptors suggesting a remarkable conservation of an ancestral immune system (Ausubel, 2005; Dardick and Ronald, 2006).

Various receptor proteins have been identified in plants, which develops a layer of immune system, as they detect divergent activities of pathogenic/foreign molecular patterns (Dangl and Jones, 2001; McDowell and Woffenden, 2003; Jones and Dangl, 2006; Takken et al., 2006; Dodds and Rathjen, 2010; Glowacki et al., 2011; Heidrich et al., 2011; Schulze-Lefert and

Panstruga, 2011; Takken and Goverse, 2012). Some of the receptor proteins are conserved among many plant species, which act as the main components of the basal immune system. These proteins are extracellular and termed as Pattern Recognition Receptors (PRRs) which can detect conserved microbe associated molecular patterns (MAMPS). The resistance employed by PRRs, however, can be challenged when certain pathogens specific virulence molecules are released inside plant cells which suppress the basal defence. Such an intrusion is dealt with by plant Resistance (R) proteins that are usually intracellular or localised at the plasma membrane. R proteins activate cell death upon sensing signatures that are typical of virulence activity. This mode of immunity is termed as specific/monogenic immunity and provides strong resistance against specific pathogen pressures in respective habitats. Regardless of these two layers of immune system, a common stream of metabolic and biochemical reactions are being employed during pathogen resistance. As our knowledge of the mechanisms of the plant immune system has widened, it is further intriguing to understand how systems of plant growth and development are connected with the functioning of innate immune system, as they do in mammals (Becker et al., 2010). Furthermore, the role of R-mediated "autoimmunity" has raised new questions about the evolution and mechanisms of detection of self and non-self (modified-self) in plants (Kruger et al., 2002; Yang and Hua, 2004; Bomblies et al., 2007).

In this study, an enzyme *O*-acetyl serine (thiol) lyase (OASTL-A1), which is involved in cysteine biosynthesis and sulfur assimilation, was identified to have a novel role in basal defence and disease resistance. Cysteine biosynthesis and sulfur assimilation is already implicated in abiotic stress tolerance. As cysteine and its derived metabolites are also required in the synthesis of immune-associated metabolites, role of the OASTL-A1 enzyme seems to be universal in biotic as well as abiotic stress. This study has also identified a novel genetic interaction between R protein encoding gene(s) and a mutation in the *OASTL-A1* gene. The nature of the genetic interaction is such that dysfunctional oastl-a1 protein triggers R-mediated autoimmunity indicating reception of modified-self by the R-protein(s). These findings provide evidence for genetic cross-talks between components of cysteine biosynthesis and innate immunity in plants. Finally this study shed new light on the metabolic basis of autoimmunity in plants, a view previously unknown. In conclusion, the work present novel and new insights into the roles of an OASTL isoform in cysteine metabolism, biotic stress and R-mediated innate immunity.

Blank Page

Blank Page

Chapter 2

Role of *Arabidopsis β*-Substituting Alanine Synthase (*BSAS*) gene family in cysteine metabolism and stress defence- A Literature review

Cysteine (Cys) is a sulfur-containing amino acid which functions as the major sulfur-carrier in the cellular system. Cysteine is required for synthesis of proteins and metabolites and is therefore indispensable for growth and development in cells of both prokaryotic and eukaryotic origin. In plants the β-Substituting Alanine Synthase (BSAS) gene family encodes enzymes which are involved in cysteine biosynthesis and homeostasis. The functions of the BSAS isoforms have been reported to be crucial in sulfur assimilation as well as in the mechanism of tolerance under a variety of stress responses. Furthermore recent studies link cysteine-thiol metabolism to plant immunity (Spoel and Loake, 2011). However a comprehensive and global overview on the role of BSAS isoforms in sulfur and cysteine metabolism and plant stress defence is lacking. This review therefore aims to cover the established facts and emerging concepts about sulfur reduction and assimilation and the functions of BSAS isoforms in cysteine metabolism and mechanisms of stress-defence in plants.

2.1 Sulfur acquisition, transport and enzymatic reduction in plants

(i) Sulfate transporters/SULTRs

Plants take up sulfur from the soil in form of the sulfate anion. This is achieved by plasma-membrane localised **SUL**fate **TR**ansporter proteins (**SULTRs)**, which symport SO_4^{-2} and H^+ ions at a ratio of 1:3, against the proton gradient (Leustek and Saito, 1999; Saito, 2000). Detailed insights into SULTRs have been obtained from studies in *Saccharomyces cerevisiae* and various plant species including the model plant *Arabidopsis thaliana*. Fourteen putative *SULTR* genes have been identified in both *Arabidopsis* and rice genomes (Kaul et al., 2000; Takahashi, 2010; Takahashi et al., 2011a). Most of the *SULTRs* encode proteins with 12 membrane spanning domains and a C-terminal domain which is exposed into the cytosol (Aravind and Koonin, 2000). The C-terminal domain is evolutionary conserved (among **S**ulfate **T**ransporters and **A**nti**S**igma-factor antagonists) and named as **STAS** (Aravind and Koonin, 2000). Mutations in the STAS domain has been shown to affect sulfate uptake by interfering with the correct localization of the SULTRs (Shibagaki and Grossman, 2004; Rouached et al., 2005). Furthermore the STAS domain is involved in SULTR homodimerization, which may be important for sulfate transporter activity (Rouached et al., 2005).

SULTRs are spatially expressed in root hairs, root tips, epidermal and cortical root cells, in xylem and phloem cells of shoot, seeds, leaves and nodules (Figure 2.1) (Smith et al., 1995; Smith et al., 1997b; Takahashi et al., 2000; Vidmar et al., 2000; Shibagaki et al., 2002; Yoshimoto et al., 2002; Howarth et al., 2003; Maruyama-Nakashita et al., 2003; Yoshimoto et al., 2003; Buchner et al., 2004; Krusell et al., 2005; Zuber et al., 2010). Based on their affinity for sulfate transport, SULTRs are divided into five different groups, *SULTR1-SULTR5* (Hawkesford, 2003). High affinity SULTR isoforms belong to the *SULTR1* group and are typically expressed in roots tissues. Lower affinity SULTR isoforms belonging to groups *SULTR2-4* are differentially expressed in roots, phloem and xylem and seed tissues (Figure 2.1) (Takahashi et al., 1997; Takahashi et al., 2000; Yoshimoto et al., 2003; Zuber et al., 2010). Group 5 contains a SULTR isoform that lacks a STAS domain (Buchner et al., 2004).

(ii) Transcriptional regulation of *SULTRs*

Promoter *cis*-elements have been identified that drive sulfur-related expression of *SULTR* genes (Maruyama-Nakashita et al., 2005; Maruyama-Nakashita et al., 2006). The Sulfur-Responsive Element (SURE) of the *SULTR1;1* promoter drives transcription of the *Arabidopsis SULTR1;1* and other genes involved in sulfur reduction and/or assimilation (Maruyama-Nakashita et al., 2005). However the identity of the transcription factor(s) which target the SURE elements in the promoter of *SULTR* genes has remained elusive. Sulfur LIMitation1 (SLIM1) is a transcriptional regulator of *SULTRs* and modulates sulfate transport and assimilation (Figure 2.1) (Maruyama-Nakashita et al., 2006). However, SLIM1 does not target the SURE *cis*-elements (Maruyama-Nakashita et al., 2006; Kawashima et al., 2011). More recently, a microRNA395-encoding gene was found to regulate sulfate transport by degrading *SULTR2;1* transcripts (Figure 2.1) (Liang et al., 2010). Interestingly, a transcription factor PHR1, which is involved in phosphate homeostasis has been also shown to regulate transport of sulfate in plant shoots (Rouached et al., 2011). Identifying other transcription factors that targets SURE and modulates the expression of *SULTRs* therefore seems the next step in understanding the regulation of sulfate transport in plants.

(iii) Signals activating SULTRs and sulfate uptake

SULTR transcription is regulated by the concentration of sulfate available in plants and in the rhizosphere. When sulfate availability declines in the soil, mRNA and protein abundance of SULTRs increases, which in turn affects sulfate uptake and total sulfate levels in plants (Takahashi et al., 1997; Lappartient et al., 1999; Shibagaki et al., 2002; Maruyama-Nakashita et al., 2006; El Kassis et al., 2007; Rouached et al., 2008). For example, in *Arabidopsis*, the mRNA abundance of a high affinity sulfate transporter *SULTR1;2* increases rapidly in root tissues under conditions when sulfur is limited, which suggests SULTR1;2 functions to efficiently scavenge the scarce amounts of available sulfur (Shibagaki et al., 2002; El Kassis et al., 2007). The role of SULTR1;2 as a major sulfate transporter is further highlighted by the reduced capacity of the *sultr1;2* mutant roots to uptake sulfate (Shibagaki et al., 2002; Yoshimoto et al., 2002; El Kassis et al., 2007).

Metabolites in the sulfur assimilation pathway also affect *SULTR* gene expression. Accumulation of O-acetylserine (OAS), a substrate required in reductive assimilation of sulfate into cysteine, triggers *SULTRs* gene expression (Smith et al., 1997a), suggesting a positive feedback effect of OAS on sulfate uptake. By contrast, higher concentrations of the end-products in sulfate assimilation pathway, including cysteine and glutathione, are shown to exert negative feedback effect on the expression of *SULTR* genes and consequently result in reduced sulfate uptake (Figure 2.1) (Lappartient and Touraine, 1996; Vauclare et al., 2002). How OAS and cysteine-thiols signal the transcriptional activation or suppression of *SULTR* genes in the nucleus, is however less explored. It is possible that OAS and thiols influence activity of transcription factors that regulate expression of the *SULTRs*. This is consistent with the GSH being targeted to the nucleus and modulating signalling and redox changes which affects the expression of various genes (Pellny et al., 2009; Vivancos et al., 2010). Regardless, the response of *SULTRs* and acquisition of sulfate under sulfur-limiting or demanding conditions confirm that uptake of sulfate in plants is a demand-driven mechanism (Lappartient and Touraine, 1996).

SULTRs gene expression and consequently sulfate uptake is affected by nitrogen availability, heavy metals and plant hormones. The expression of *SULTRs* is suppressed in soils that are low in nitrogen leading to reduced sulfate uptake (Clarkson et al., 1989; Maruyama-Nakashita et al., 2004a). Toxic metals, including selenate and cadmium also trigger up-regulation of *SULTR* gene expression in plants presumably because sulfur is required for tolerance to heavy metal stress (Shibagaki et al., 2002; Nocito et al., 2006). Of particular note is that some *SULTRs* specifically from group *SULTR1* and *5* have been associated with transport of metals including molybdate and selenate (Shibagaki et al., 2002; Tomatsu et al., 2007; Fitzpatrick et al., 2008) suggesting specialised functions of some *SULTR* isoforms.

Plant hormones associated with growth and development such as auxin and cytokinin also affect expression of *SULTR*s and sulfate uptake (Grossman and Takahashi, 2001; Maruyama-Nakashita et al., 2004b; Sakakibara, 2006; Dan et al., 2007). On the other hand, plant defence hormones such as salicylic acid (SA) and jasmonic acid (JA) were shown to affect the expression of genes in the sulfur assimilation pathway (Xiang and Oliver, 1998; Harada et al., 2000; Freeman et al., 2004; Freeman et al., 2005; Jost et al., 2005). However, it needs to be further explored how these

defence hormones regulate *SULTRs* gene expression as well as sulfate uptake. Recently abiotic and biotic stresses were found to modulate expression of various *SULTR* genes (Barberon et al., 2008; Rouached et al., 2009). Considering the mounting evidence that sulfur is a component of a broad range of defence compounds (Rausch and Wachter, 2005; Mugford et al., 2009), *SULTRs* may have an important role in providing sulfur for strengthening plant immune responses.

(iv) Sulfate flux between sub-cellular compartments

Transport of sulfate between various sub-cellular compartments of plant cells decides the fate of the sulfur taken up by the plants (Figure 2.1). Sulfate is present in the cytosol but is largely stored in the vacuole which appears to serve as an internal nutritional reservoir of sulfur (Buchner et al., 2004). The flux of sulfate between sub-cellular compartments was initially suggested to be passive, i.e., depend on a concentration-gradient (Buchner et al., 2004). However, the identification of a tonoplast membrane-localised group of SULTRs suggests that at least a few SULTRs are involved in symport of sulfate from vacuole to cytosol (Kataoka et al., 2004; Parmar et al., 2007). By contrast, no SULTR isoforms have been shown to transport sulfate among other sub-cellular compartments. Reductive assimilation of sulfate into sulphide takes place in the plastids (Figure 2.1). For long, the channel for sulfate import into plastids has remained unclear. Similarly the efflux of sulfate from plastids is also not well defined and needs further elucidation. An ABC bacterial type transporter has been found in green-algae to transport sulfate into chloroplasts, but surprisingly it has no close homologues in plants (Chen et al., 2003). Very recently, SULTR;3-1 has been identified to be a chloroplast-specific transporter suggesting symport as one of the mechanism involved in sulfate transport into chloroplast (Cao et al., 2012).

(v) Reduction of sulfate; a multi- enzymatic process towards assimilation

a. ATP Sulfurylase/ATPS: Sulfate to APS

ATP sulfurylase (ATPS) catalyses the assimilation of sulfur by coupling inorganic phosphate, from ATP, with sulfate to generate phosphate-sulfate anhydride also known as adenosine 5′-phosphosulfate (APS) (Figure 2.1). Since biosynthesis of APS is the starting point of sulfate assimilation, lack of functional ATPS results in enhanced levels of sulfate in plants (Liang et al., 2010). Two ATPS isoforms have been identified in some plants; one is located in the plastid whereas the other is targeted to the cytosol (Kopriva et al., 2009). The plastidic isoform contributes most to the total ATPS activity (Lunn et al., 1990; Renosto et al., 1993; Klonus et al., 1994; Rotte and Leustek, 2000). In the model plant species including *Arabidopsis*, rice, and *Populus trichocarpa*, four isoforms of ATPS have been identified, all of which contain localisation signals for plastids (Leustek et al., 1994; Murillo and Leustek, 1995; Hatzfeld et al., 2000a; Kopriva et al., 2009).

b. APS Kinase/APK: APS to PAPS

In plants, APS has two fates; either to undergo reductive assimilation towards sulphite or to be metabolised into 3′-phosphate adenosine 5′-phospho-sulfate (PAPS) by an enzyme APS kinase (APK) (Figure 2.1). APK synthesizes PAPS by phosphorylating APS in an ATP dependent manner. Multiple isoforms of APK exist in different plant species and are localised to both plastids and cytosol (Leustek et al., 2000; Rotte and Leustek, 2000; Koprivova et al., 2001; Koprivova and Kopriva, 2008; Mugford et al., 2009). In bacteria, fungi and lower plants, conversion of APS to PAPS is part of the reductive assimilation of sulfate as these organisms encode a PAPS reductase enzyme (Kredich, 1971; Koprivova et al., 2002). By contrast, higher plants lack PAPS reductase and therefore PAPS cannot be further utilised into reductive assimilation of sulfate in plants (Kopriva, 2006). PAPS synthesis in plant sulfate metabolism is related to its utilization in sulfation reactions, performed by sulfotransferases (Klein and Papenbrock, 2004; Komori et al., 2009). Sulfotransferases utilize PAPS for incorporation of

sulfate directly into the synthesis of other secondary metabolites such as flavonoids, phenolic acids, steroids, coumarins, sulfate esters, gibberellic acids, hydroxy- jasmonates and glucosinolates (Hernàndez-Sebastiá et al., 2008). Therefore the APK-dependent PAPS production pathway in plants contributes to sulfated secondary compounds, proteins and peptides mostly involved in plant growth and defence (Halkier and Gershenzon, 2006; Bednarek et al., 2009; Komori et al., 2009).

Arabidopsis and other *Brassicaceae* family members produce higher amounts of sulfated compounds i.e., glucosinolates which are involved in plant defence against various pathogens (Mugford et al., 2009). Analysis of the APK isoforms in *Arabidopsis* show that there is functional redundancy between APK isoforms, but that APK activity is essential for plant viability (Mugford et al., 2009). Moreover PAPS are suggested to be diffusible between plastids and cytosol (Klein and Papenbrock, 2004; Kopriva et al., 2009). As both ATPS and APK are localised to cytosol and plastids in various plant species (Koprivova and Kopriva, 2008; Kopriva et al., 2009), it seems that the synthesis of PAPS is facilitated in major compartments for sulfation, before APS is irreversibly converted into sulphite.

c. APS reductase/APR: APS to Sulphite

The second to last step in the reductive assimilation of sulfur is the reduction of APS to sulphite, which occurs in plastids only and is catalysed by APS reductase (APR) (Figure 2.1). It is thought that APR uses glutathione, a tri-peptide thiol, as a source of electrons for the reduction of APS (Leustek and Saito, 1999) . Three isoforms for APR are encoded in the *Arabidopsis* genome all of which are targeted to chloroplasts (Kopriva et al., 2001). APR is considered the major enzyme of sulfate assimilation among *Arabidopsis* population (Vauclare et al., 2002; Loudet et al., 2007). Lack of either of the APR isoforms, individually, however does not affect the plant growth but results in the accumulation of sulfate in plants (Loudet et al., 2007). On the other hand over-expression of APR was shown to result in the accumulation of sulphite and thiosulfate which caused toxicity and adverse effects on the plant phenotype (Martin et al., 2005). The transcriptional regulation and enzymatic activity of APR is affected by various environmental signals including sulfate limitation, heavy metal toxicity and other stresses. Existence of multiple

APR isoforms in plastids has been further implied in additional but novel functions considering their differential tissue-specific mRNA expression profiles (Kopriva et al., 2009).

d. Sulphite reductase/SiR: Sulphite to Sulphide

In the final step of sulfate reduction, sulfite is reduced to sulphide via sulphite reductase (SiR), which is exclusively targeted to plastids (Figure 2.1). SiR is encoded by only a single gene copy in *Arabidopsis* and is a key enzyme in sulfur assimilation (Khan et al., 2010). SiR performs the reduction of sulphite into sulphide using siroheme and FeS centers as prosthetic group/cofactors and ferredoxin as an electron donor. Sulphide is directly used in the synthesis of cysteine. As cysteine biosynthesis takes place in various sub-cellular compartments, diffusion of sulphide from plastids into other sub-cellular sites appears to facilitate cellular cysteine biosynthesis.

Figure 2.1. Sulfate transport systems, cellular compartmentation of sulfur metabolism and signals and components regulating SULTR gene expression and sulfate transport in *Arabidopsis*.

A. Sulfate is absorbed from roots via red circled sulfate transporters (*SULTRs*) and is transported from root tissues into xylem. Sulfate can also be stored inside the vacuoles of root tissues. Sulfate is transported in xylem to the shoot and mesophyll cells of leaf tissues as well as to seed tissues. Within the cell, sulfate is transported into plastids, for its reductive assimilation into sulphide and then its assimilation into cysteine via multi-enzymatic reactions. Enzymes involved in reduction of sulfate are indicated in **bold** *italics*. Dashed lines indicate putative channelling for transport of sulfate or other metabolites. In parallel to its reductive assimilation, sulfate is also converted to PAPS to fuel the synthesis of sulfated compounds including glucosinolates. Arrows in red represent pathways for sulfate transport, reduction and assimilation. Arrows in black represent pathways further downstream including those involved in cysteine (Cys), methionine (Met) and glutathione (GSH) biosynthesis. Cys, Met and GSH interact with glucosinolate metabolism and Met is also in involved in the synthesis of ethylene via the Yang cycle. The theme of the figure is adapted from (Takahashi et al., 2011b).

B. Different signals are reported to affect the expression of SULTRs and consequently sulfate uptake. An arrow indicates induction and a T refers to suppression of the targeted factors including SULTRs and sulfate uptake. The role of auxin modulating SULTRs and sulfate uptake is not completely understood and is therefore indicated by a dashed line. The role of ethylene (ET), brassinosteroids (BR) and defence hormones including salicylic acid (SA) and jasmonic acid (JA), and methionine, glucosinolates and sulfation metabolism in modulating SULTRs expression is not well explored and is therefore represented by an arrow with an asterisk head.

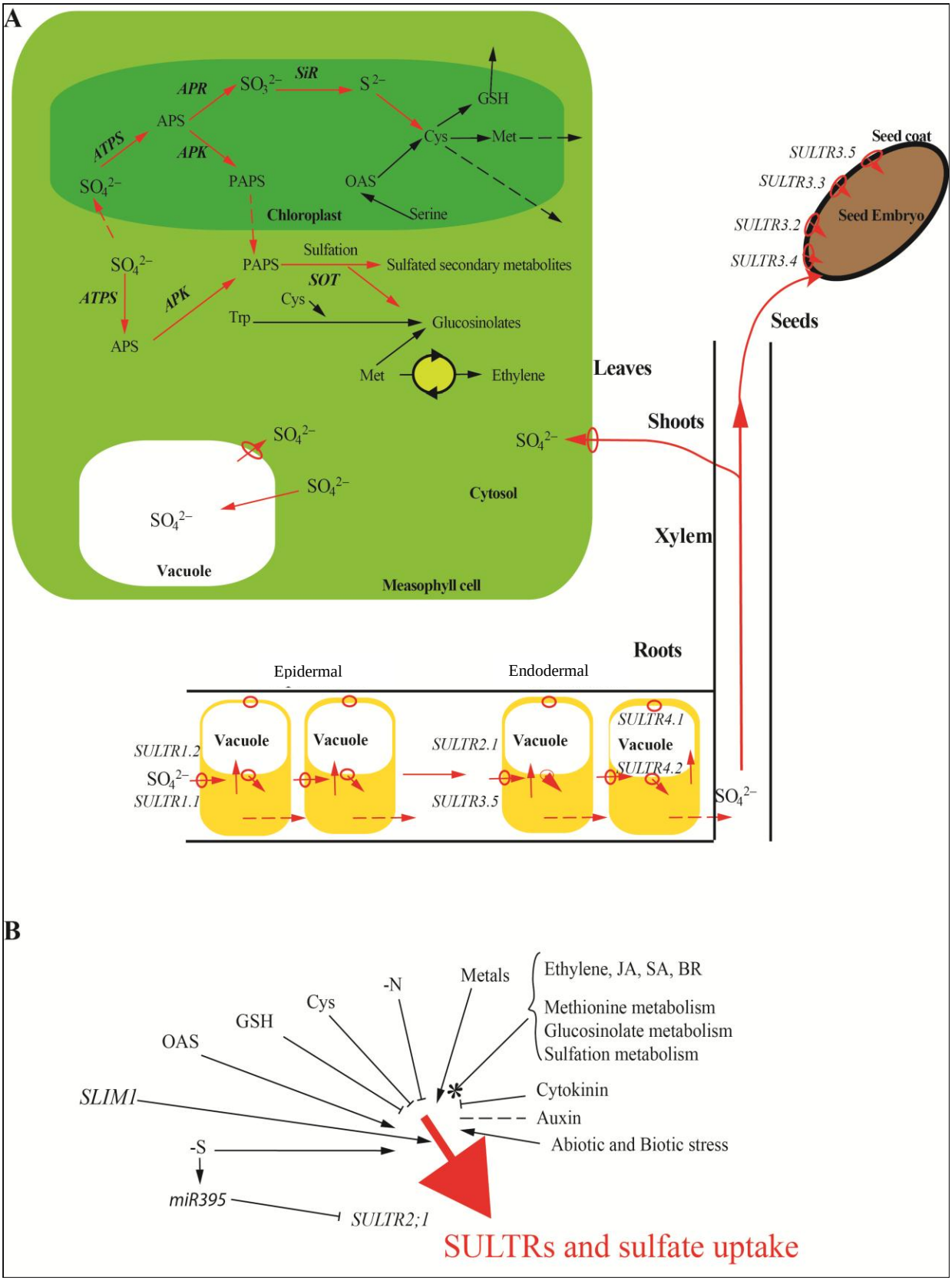
A
APR
SiR
ATPS
APK
APS
PAPS
Chloroplast
GSH
Cys
Met
OAS
Serine
Sulfation
SOT
Sulfated secondary metabolites
Trp
Glucosinolates
Ethylene
Cytosol
Vacuole
Measophyll cell
Leaves
Shoots
Xylem
Roots
Seeds
Seed coat
Seed Embryo
SULTR3.5
SULTR3.3
SULTR3.2
SULTR3.4
Epidermal
Endodermal
SULTR1.2
SULTR1.1
SULTR2.1
SULTR3.5
SULTR4.1
SULTR4.2
B
Metals
-N
Cys
GSH
OAS
SLIM1
-S
miR395
SULTR2;1
Ethylene, JA, SA, BR
Methionine metabolism
Glucosinolate metabolism
Sulfation metabolism
Cytokinin
Auxin
Abiotic and Biotic stress
SULTRs and sulfate uptake

2.2 Cysteine biosynthesis in *Arabidopsis*

(i) Serine acetyltransferase (SERAT) and *O*-acetylserine (thiol) lyase (OASTL) complex: Serine to OAS

Biosynthesis of cysteine is a convergent point in the assimilation of two macronutrients; nitrogen and sulfur, as the serine amino acid is metabolised to acquire sulphide, which yields cysteine (Figure 2.2). In plants, cysteine biosynthesis is known to take place in three sub-cellular compartments, plastids, cytosol and mitochondria. Serine acetyltransferase (SERAT or SAT; EC 2.3.1.30) interacts with *O*-acetylserine (thiol) lyase (OASTL) to make a hetero-oligomeric complex (Figure. 2.2). SERAT complex catalyses the acetylation of the hydroxyl group in serine using acetyl-CoA to produce O-acetylserine (OAS). Free OASTL dimers then catalyses the addition of sulphide to OAS to yield cysteine. This two-step OASTL-SERAT catalytic process is evolutionary conserved among bacteria and plants (Hell and Wirtz, 2008).

At the cellular level, SERAT is much less abundant than OASTL (1:60) and catalyses the rate limiting step in cysteine biosynthesis (Droux et al., 1998; Heeg et al., 2008). Plant SERAT is also able to perform a catalytically functional interaction with the bacterial OASTL/CysK of *E. coli*. (Droux et al., 1998), suggesting a remarkable conservation of the molecular interaction between these two proteins from different species. In *Arabidopsis* five nuclear *SERAT* genes have been identified (Kawashima et al., 2005; Watanabe et al., 2008b). These have been divided into three groups (*SERAT1-3*), which contain localisation signals to various sub-cellular compartments. The SERAT1;1 (encodes an isoform targeted to cytosol), *SERAT2;1* (encodes an isoform targeted to plastid) and *SERAT2;2* (encodes an isoform targeted to mitochondrial) are highly expressed genes in various tissues of plants compared with the group 3 genes *SERAT3;1* and *SERAT3;2*, which encode cytosolic-targeted isoforms and are relatively lowly expressed (Kawashima et al., 2005; Watanabe et al., 2008b). The substrate affinities of the isoforms of Group 3 are also low compared with the isoforms of the other two groups (Kawashima et al., 2005). Thus SERAT1;1, SERAT2;1 and SERAT2;2 appear to be the major isoforms regulating OAS production in *Arabidopsis*.

Two homodimers of OASTL enzymes bind to a dimer of homotrimers of SERAT enzymes in the OASTL-SERAT complex. The OASTL-SERAT interaction in the complex formation affects the kinetic properties of SERAT resulting in positive co-operativity of SERAT to its substrates, Ser and acetyl-CoA (Droux et al., 1998). Thus OASTL acts as an important subunit of SERAT for the production of OAS (Leustek and Saito, 1999). Formation of the complex enables SERAT to produce OAS but also inactivates the OASTL enzyme (Saito et al., 1995; Bogdanova and Hell, 1997; Droux et al., 1998; Wirtz et al., 2001; Wirtz and Hell, 2006). This is because the C-terminal residues of the SERAT competes with the OAS for the α-carboxyl region, which is the active site of the OASTL (Campanini et al., 2005; Francois et al., 2006; Kumaran and Jez, 2007; Feldman-Salit et al., 2009; Kumaran et al., 2009). This inhibits the catalytic activity of the OASTL towards cysteine biosynthesis.

The precursors of cysteine also regulate the formation of OASTL-SERAT complex (Droux et al., 1998; Berkowitz et al., 2002; Wirtz and Hell, 2006). Under conditions when sulfur is limited, OAS levels can increase in the plant cell because limited sulphide reduces OAS consumption in cysteine biosynthesis (Figure 2.2). In this case, OAS has been shown to affect the stability of the OASTL-SERAT interaction in the complex. Higher OAS concentration has been shown to negatively affect the binding of the C-terminal domain of SERAT with the active site of OASTL and results in disassociation of the two enzymes (Figure 2.2). On the other hand higher concentration of OAS has been already known to stimulate the expression of sulfate transporter genes which consequently leads to sulfate uptake and availability of sulphide in cells. This can re-activate OAS sequestration into cysteine biosynthesis (Figure 2.2) (Hell and Wirtz, 2011). Conversely, sulfide is reported to exert a positive feedback effect on the stabilization of the OASTL-SERAT complex, which drives the OAS production (Figure 2.2). In conclusion, both OAS and sulfide antagonistically affect the OASTL-SERAT complex formation which is a key regulatory step in cysteine biosynthesis (Droux et al., 1998; Berkowitz et al., 2002; Wirtz and Hell, 2006).

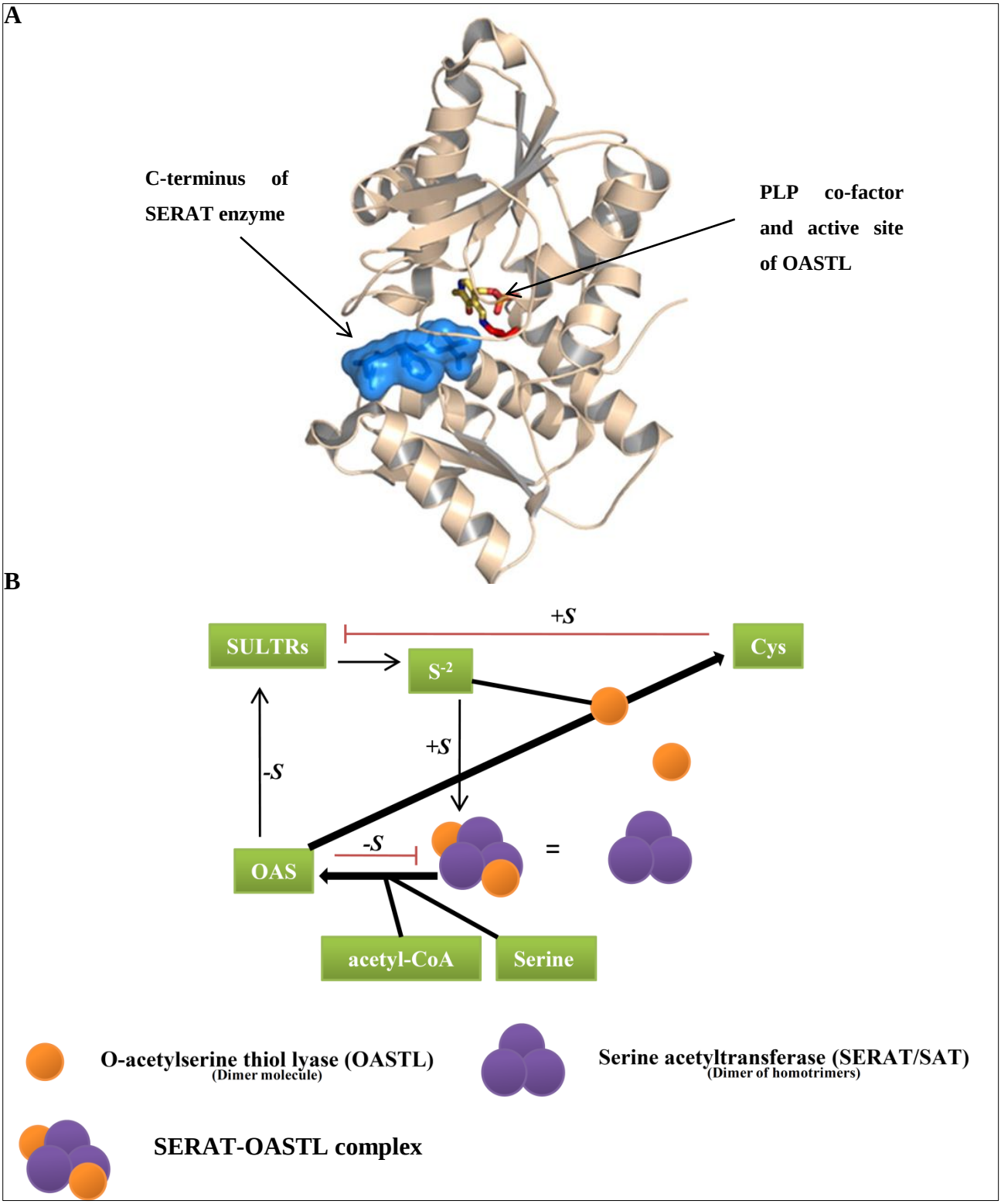
A
C-terminus of SERAT enzyme
PLP co-factor and active site of OASTL
B
SULTRs
+S
Cys
S-2
+S
-S
-S
OAS
=
acetyl-CoA
Serine
O-acetylserine thiol lyase (OASTL)
(Dimer molecule)
Serine acetyltransferase (SERAT/SAT)
(Dimer of homotrimers)
SERAT-OASTL complex

Figure 2.2. Sulfur assimilation and cysteine biosynthesis in a two-step enzymatic process.

A. The figure is adapted from (Francois et al., 2006) and shows the binding of the C-terminal peptide of SERAT to OASTL. C-terminal peptide of SERAT is shown in blue. PLP is indicated by rainbow coloured stick and the 3-D OASTL structure is indicated.

B. SERAT produces *O*-acetyl serine (OAS) from serine and acetyl-CoA in OASTL-SERAT complex. Free active OASTL catalyses the substitution of the acetyl group in OAS with sulphide to form cysteine. Under conditions when sulfur is limited (as indicated -S), higher concentrations of OAS disassociate the OASTL-SERAT complex (as indicated by red suppressing arrown) as well as trigger the expression of SULTRs (as indicated by black arrow) and consequently sulfate uptake. This then increases the availability of sulphide for cysteine biosynthesis. Acquisition and reduction of sulfate (as indicated by +S) will feed the cysteine biosynthesis as well as stabilizes the OASTL-SERAT complex for OAS production. Cysteine can have a repressing effect on *SULTR* gene expression under these conditions. The lines in red show a repressing effect whereas lines in black show a positive effect on the activity of the components.

(ii) OASTL: OAS + sulphide to cysteine

In plant cells, OASTL proteins can make a stable homodimer which catalyses the synthesis of cysteine by substituting the acetyl group of OAS with sulphide (Saito, 2000; Hell et al., 2002). OASTLs are encoded by members of the *BSAS* gene family in *Arabidopsis.* OASTLs contain a pyridoxal-phosphate (PLP) binding site in which the acetyl moiety of OAS is substituted for the sulphide group. OASTL-like proteins are conserved among many prokaryotes and eukaryotes. In plants OASTLs are evolutionary related from cyanobacteria (Kopriva et al., 2009). In *E. coli* bacteria, two thiolase genes, *CysK* and *CysM* have been found (Kredich et al., 1969; Zhao et al., 2006). In plants, the number of *OASTL*-like or *BSAS* genes varies (Kopriva et al., 2007). A total nine *BSAS* genes have been identified in *Arabidopsis* from which only eight have been shown to encode functional isoforms (Table 2.1;) (Watanabe et al., 2008a).

Transcript abundance of the *BSAS*/*OASTL* genes in *Arabidopsis* is tissue dependent. Transcript accumulation of the cytosolic *BSAS1;1* is high in roots and shoots, the plastidic *BSAS2;1* and mitochondrial *BSAS3;1* are higher in leaves than in roots, and the transcript abundance of the other mitochondrial *BSAS2;2* is relatively high in roots, compared to the leaves (Watanabe et al., 2008a). Other *BSAS/OASTL* genes are relatively lowly expressed suggesting a lesser role for their encoded isoforms in cysteine biosynthesis.

OASTL isoforms are targeted to different sub-cellular compartments in plant cells including the cytosol, mitochondria and plastids. A detailed genetic, biochemical and molecular characterisation report on BSAS/OASTLs in *Arabidopsis* is presented in Table 2.1. The OASTL enzymes that carry out cysteine synthesis are only considered authentic or true if they also interact with SERAT (Droux et al., 1998; Wirtz and Hell, 2006). Only five of the eight *BSAS*-encoded OASTLs in *Arabidopsis* have been shown to interact with SERAT and therefore are true OASTLs. Of these, only three make a significant contribution to the total OASTL activity in plants (Table 2.1) (Wirtz et al., 2004; Heeg et al., 2008; Watanabe et al., 2008a). These are the cytosolic BSAS1;1 (OASTL-A1), plastidic BSAS2;1 (OASTL-B) and mitochondrial BSAS2;2 (OASTL-C) (Table 1.1). OASTL-A1 contributes ~50% of the total leaf cellular OASTL activity; OASTL-B up to 25-40% of the leaf cellular OASTL activity and OASTL-C contributes up to 5%

and 18% of the total OASTL activity in leaves and roots, respectively (Table 2.1). The other two true OASTLs are cytosolic CysD1 and CysD2 isoforms and contribute very little to total OASTL activity. Among the true OASTLs, OASTL-A1 and OASTLB contribute most to the total OASTL protein pool (23-65%) of the cell compared with OASTL-C (11%) and the two other cytosolic CysD1 and CysD2 isoforms (1-0.25) (Heeg et al., 2008). However, of all five isoforms, OASTL-A1 is the dominating protein (Wirtz et al., 2010).

(iii) Protein structure of OASTL

Protein sequence analysis of the major OASTL isoforms indicates that many residues are conserved between OASTL-A1 and the two other major plastidic (OASTL-B) and mitochondrial (OASTL-C) isoforms (Bonner et al., 2005; Heeg et al., 2008; Watanabe et al., 2008a). Most of these residues are also conserved between the OASTL-like CysK from *Salmonella typhimurium* and *E. coli* (Bonner et al., 2005; Heeg et al., 2008). OASTL proteins make homodimers of 68-75 kD, with 303-315 amino acid residues per monomer. The 2.2 Å resolution crystal structure of the OASTL-A1 protein revealed a symmetric homodimer, which resembles the Cys thiolase structure of *Salmonella typhimurium* (Bonner et al., 2005). In each OASTL monomer, the N-terminal region consists of six β-sheets (β1A, β2A, β3B-β6B) and four α-helices (α1- α4), comprising from 1-150 residues (Figure 2.3). While the C-terminal region of the monomer consist of 151-303 amino acid residues containing four β-sheets (β7A-β10A) and four α-helices (α5- α9) (Figure 2.3). The active PLP site of the OASTL enzyme is buried in a cleft formed between the folding of the N and C terminal regions of the protein (Figure 2.3) (Bonner et al., 2005). The α9-helix from the C-terminal domain makes part of the dimer interface between the two monomers. The dimer interface accounts for approximately 19% of the accessible surface area of each monomer (Bonner et al., 2005). The active site of each of the monomer faces the same side and the monomers are oriented in an anti-parallel manner (Bonner et al., 2005).

(iv) Active sites of OASTL involved in enzymatic activity and protein-protein interactions

PLP acts as a cofactor in various enzymatic reactions mediated by aminotransferases and transaminases. In a shallow cleft between the N and C terminal domain of OASTL, PLP is linked

to Lys^{41} by a covalent bond forming the Schiff base between the alpha-amino group of the Lys^{41} and the pyridine ring of the PLP (Figure 2.3). It is important to note that the PLP interacting residue Lys^{41} is conserved between all the BSAS encoding isoforms in *Arabidopsis* (a detailed protein alignment of all eight functional BSAS is provided in Appendix 1) The synthesis of cysteine from OAS and sulphide involves two steps. In the first step, OAS displaces the interaction between Lys^{41} and PLP by its alpha-amino group resulting in quinonoid α-aminoacrylate, as an intermediate linked to PLP. This results in the release of the acetyl moiety from OAS, which then diffuses away from the active site enabling sulfide to interact with the Cβ of α-aminoacrylate to produce cysteine (Rabeh and Cook, 2004; Bonner et al., 2005; Chattopadhyay et al., 2007).

OASTL activity is abolished when Lys^{41} is mutated to Arg^{41} (K46A) demonstrating the importance of Lys in PLP function (Bonner et al., 2005). Further hydrogen bonds between the oxygen and the nitrogen of the pyridine ring with the Asn^{77} and Ser^{269} residues of OASTL stabilize the PLP cofactor (Figure 2.3). The phosphate group of PLP makes hydrogen bonds with the Gly^{181}, Thr^{182}, Gly^{183}, Thr^{185} and His^{157} residues. Amino acid substitution in these residues has been also shown to affect OASTL enzymatic activity. For example mutations in α5 helix, at residues H157Q and H157N, resulted in an ~2 fold reduction in the catalytic activity of OASTL as compared to wild-type. However mutations of residues, between β7A sheet and α6 helix at Thr^{182} and in α6 helix at Thr^{185} resulted in 50 and 400–1600-fold decrease in the OASTL activity suggesting that these residues are crucial in PLP stabilization.

Mutations in different sites, including Thr^{74}, Ser^{75}, and the Gln^{147}, affected the catalytic activity of the OASTL indicating that these residues are involved in positive cooperativity of the enzyme towards its substrates, OAS and sulphide (Bonner et al., 2005). Mutation in these residues also affected the interaction with the SERAT enzyme. This indicated that these residues are selected for both the functions associated with OASTL (Figure 2.3). During OASTL-SERAT complex formation the C-terminal peptide of the SERAT interacts with these residues reducing the ability of PLP to interact with its substrate OAS and hence OASTL becomes inactive in the OASTL-SERAT complex (Francois et al., 2006). In this scenario, the active site of only one of the OASTL subunits is occupied by the C terminus of SERAT. This allosterically affects the active

site of the other un-occupied subunit in the dimer, rendering the bounded OASTL dimer completely inactive for cysteine biosynthesis (Feldman-Salit et al., 2012).

The residues between β8A and β9A sheets (217-223) in OASTL, which are on the lower side in the entrance of the active site cleft, are also conserved among bacterial and some plant OASTL isoforms (Figure 2.3) (Bonner et al., 2005). Mutation in residues between β8A to β9A sheets (K217A, H221A, and K222A) have been shown to negatively affect the interaction of OASTL with SERAT showing that these residues are involved in SERAT interaction. However, these mutations did not affect the catalytic activity of the mutant oastl-a1 protein (Bonner et al., 2005).

OASTL also interacts with proteins other than SERAT. For example, OASTL interacts with ATPS in *E. coli* and the plant OASTL-A1 has recently been shown to interact with the STAS domain of the SULTR protein (Wei et al., 2002; Shibagaki and Grossman, 2010). These findings are consistent with the suggestion that OASTLs are involved in sulfate homeostasis in addition to their primary role in cysteine biosynthesis. Moreover recently, OASTL-A1 was found to interact with the phosphoserine binding 14-3-3 proteins and this interaction is shown to exert a positive effect on the OASTL activity of the protein (Shin et al., 2011). Thus it is possible that OASTLs may participate in other more diverse protein-protein interactions required for tis functions but the subtlety in which this occurs *in planta* will likely require more sophisticated methods for verification.

(v) Post-translational modification of OASTLs

Post-translational modification of proteins is an important regulatory step that has evolved in nature to enable diversification of protein function and control protein abundance and activity. Proteomic profiling of purified true OASTL proteins in *Arabidopsis* show that OASTL-A1, B and C proteins exhibit modifications. Various sub-species of the proteins encoded from the individual OASTL genes were detected on 2-D gels showing variation in total molecular weight and overall charge of the protein species (Table 2.1) (Heeg et al., 2008; Wirtz et al., 2010). OASTL-A1 and OASTL-C showed four and three different sub-species, respectively, while seven sub-species were identified for the OASTL-B and only one protein spot was observed for

CysD1 and CysD2 isoforms (Heeg et al., 2008; Wirtz et al., 2010). Different protein spots for each OASTL protein suggest post-translational modifications.

In contrast, alternative splicing and consequently variation in protein models can also contribute to variation in the total size and thus variation in total charge of the protein (Wirtz et al., 2010). Analysis of the protein-coding gene models suggests that although OASTL-A1 and OASTL-B encode alternative 5′ and 3′ splice variants, all contribute to one protein sequence and hence a standard molecular weight (Appendix 2). In contrast, OASTL-C shows alternative splice variants in its Open Reading Frame (ORF), which encode for three different protein models (Appendix 2). Thus in the case of OASTL-C, alternative splicing was suggested to be responsible for the different protein species. On the other hand, OASTL-A1 and OASTL-B protein sub-species are likely the result of post-translational modification as they encode a standard molecular weight of protein (Wirtz et al., 2010).

Analysis of the OASTL-A1 protein sub-species (A1-A4) suggested that the dominant sub-species of the OASTL-A1, the A2, experiences N-terminal acetylation. This was suggested on the basis of ~ 42 Da of difference in the molecular weight which corresponds to N-terminal acetylation modification (Wirtz et al., 2010). Other species also showed differences in their molecular weight ranging from 42-179 Da, suggesting further modification in the protein other than N-terminal acetylation. Similarly, the OASTL-B species showed significant variation in their molecular weights and seven sub-species were identified, some of which were suggested to undergo N-terminal acetylation modification. This is consistent with results from a chloroplast proteomic study which revealed the presence of acetylated sub-species of OASTL-B (Zybailov et al., 2008). N-terminal acetylation of the nuclear-encoded chloroplast proteins in cytosol is required for proper chloroplast functioning (Pesaresi et al., 2003). As N-terminal acetylation is mainly involved in the degradation and the over-all turn-over of the proteins (Hwang et al., 2010), it seems that acetylation is also required for the homeostasis of abundant OASTL proteins in different sub-cellular compartment of plant cell.

Table 2.1. Genetic, biochemical and molecular characterisation of *BSAS*/*OASTL* gene family in *Arabidopsis*.

Name	Gene/ AGI No.	Evolutionary relationship[c]	Subcellular Localization	Protein coding gene models	Enzymatic Reaction	Interaction with SERAT	Contribution in total cellular activities (Shoot/Root) *in planta*				Post-translational modifications	
							OASTL	CAS	DES	SCS	Sub-species	Nature of modification
OAS-TL A1	Bsas1;1 AT4G14880	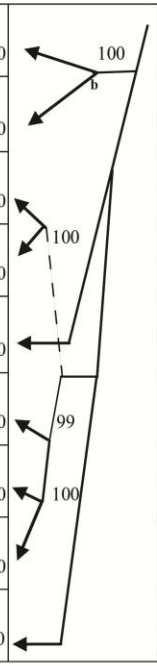	Cytosol	1	O-acetylserine (thiol) lyase ($OAS + S^{-2} = Cys + acetyl$)	Yes	~50-60% ~75%	~20% ~35%	N.D. N.D.	N.D. N.D.	4	Nitration N-terminal Acetyl.
OAS-TL A2[a]	Bsas1;2 AT3G22460		Cytosol	1	N.D.	N.D.	N.D.	N.D.	N.D.	N.D.	N.D.	N.D.
OAS-TL B	Bsas2;1 AT2G43750		Plastids	1	O-acetylserine (thiol) lyase ($OAS + S^{-2} = Cys + acetyl$)	Yes	~25-40% ~20%	*U.D.* *U.D.*	N.D. N.D.	N.D. N.D.	7	N-terminal Acetyl.
OAS-TL C	Bsas2;2 AT3G59760		Mitochondria	3	O-acetylserine (thiol) lyase ($OAS + S^{-2} = Cys + acetyl$)	Yes	~ 5% ~20%	*U.D.* *U.D.*	N.D. N.D.	N.D. N.D.	3	N-terminal Acetyl.
CysC1	Bsas3;1 AT3G61440		Mitochondria Cytosol[c]	3	β-cyanoalanine synthase (CAS) ($Cys + CN = CA + S^{-2}$)	No	*N.S.* *U.D.*	~65% ~55%	*U.D.* N.D..	N.D. N.D.	N.D.	N.D.
CysD1	Bsas4;2 AT3G04940		Cytosol	1	O-acetylserine (thiol) lyase ($OAS + S^{-2} = Cys + acetyl$)	Yes	<1% *U.D.*	*U.D.* *U.D.*	*U.D.* N.D.	N.D. N.D.	1	*U.D.*
CysD2	Bsas4;1 AT5G28020		Cytosol	2	O-acetylserine (thiol) lyase ($OAS + S^{-2} = Cys + acetyl$)	Yes	<1% *U.D.*	*U.D.* *U.D.*	*U.D.* N.D.	N.D. N.D.	1	*U.D.*
DES1	Bsas4;3 AT5G28030		Cytosol	1	Cysteine desulfhydrase (DES) ($Cys = S^{-2} + Pyruvate + NH_3$)	No	*U.D.* *U.D.*	*U.D.* *U.D.*	~20-25% N.D.	N.D. N.D.	N.D.	N.D.
CS26	Bsas5;1 AT3G03630		Plastids	1	S-sulfocysteine synthase (SCS) ($OAS + S_2O_3^{2} = S\text{-}Cys$)	No	*N.S.* *U.D.*	*U.D.* *U.D.*	*U.D.* N.D.	100% N.D.	N.D.	N.D.

The information is obtained from various reports (Jost et al., 2000; Hell et al., 2002; Heeg et al., 2008; Watanabe et al., 2008a; Alvarez et al., 2010; Bermúdez et al., 2010b; Wirtz et al., 2010; Alvarez et al., 2011); **a** *BSAS1;2* encodes a truncated or non functional protein; **b** BSAS1;2 protein is a hypothetical model, derived from the available protein sequence in TAIR, as the mutation in mRNA cause a truncated protein; **c** *BSAS3;1* is an alternatively spliced protein-coding gene model as available from TAIR and suggest that the encoded protein version may not contain the mitochondrial target peptide signal and therefore probably resides in the cytosol; **d** The nature of modification is identified and predicted in the reports. **e** Neighbouring joining tree based on alignments of conserved sequences. The values represents consensus support% based on 10,000 bootstrap values. *N.D.* is not determined; *U.D.* is un-detectable in the analysis performed; *N.S.* is non-significant for the value obtained. OAS is *O*-acetyl serine; Cys is Cysteine, CN is cyanide; CA is β-Cyanoalanine; S-Cys is Sulfo-cysteine.

Post-translational modifications affecting OASTL function has been shown for OASTL-A1 only, which involves nitration of the protein (Alvarez et al., 2011). Nitric oxide mediates nitration of Cys and Tyr residues of the OASTL-A1 protein. Further the OASTL-A1 was shown to be catalytically inactivated by nitration with peroxynitrite, which targets the Tyr residue for nitration. Nitrated OASTL-A1 is incapable of binding to its substrate OAS and has impaired OASTL activity. As nitric oxide production is associated with stress, OASTL-A1 activity therefore can be inhibited in response to activated reactive nitrogen species (RNS) in plant cell. This may have implications in RNS induced stress signalling (Alvarez et al., 2011). Other OASTLs were also found to be affected by nitration, but to a relatively less extent than OASTL-A1(Alvarez et al., 2011).

In conclusion, these studies indicate the extent of post-translational modifications among OASTL isoforms. It further raises questions about the nature and requirement of these post-translational modifications for function of the OASTLs. Furthermore, although phosphorylation of OASTLs has not been shown yet, putative sites for phosphorylation have been suggested in OASTL-A1(Alvarez et al., 2011). Therefore, future investigation on the nature of various novel modifications of OASTLs and their impact on cysteine biosynthesis and homeostasis are areas of research that would greatly extend our knowledge on OASTL function.

Figure 2.3. Structure of the OASTL-A1 protein of *Arabidopsis thaliana*.

Ribbon diagram of the 3D crystal structure of OASTL-A1. Coloured regions indicate the interaction of SERAT with OASTL. The PLP co-factor buried in the cleft between the N and C terminal domains is indicated by the rainbow coloured stick structure in the middle of the protein. The function of the residues indicated in colour is highlighted in the sequence annotation. The OASTL-A1 amino acid sequence is presented below the figure. Various annotations are indicated in the sequence. Grey cylinders represent α-helices whereas grey arrows are β-sheets. The regions coloured in the crystal structure are highlighted in the same colour in the sequence. A small surface diagram of the OASTL protein is also presented to the left of the ribbon diagram. The residues involved in interaction (as shown by colour) and PLP stick in the cleft highlights the topology of the active protein interaction sites of OASTL-A1. Information regarding the function of residues and the structure and natural variation (provided in Appendix 3) in Arabidopsis OASTL-A1 is obtained from (Bonner et al., 2005; Francois et al., 2006; Weigel and Mott, 2009). The 3-D crystal structure was made using Pymol Software using the crystal structure file of OASTL-A1 obtained from the Plant Databank (http://www.rcsb.org/pdb/home/home.do).

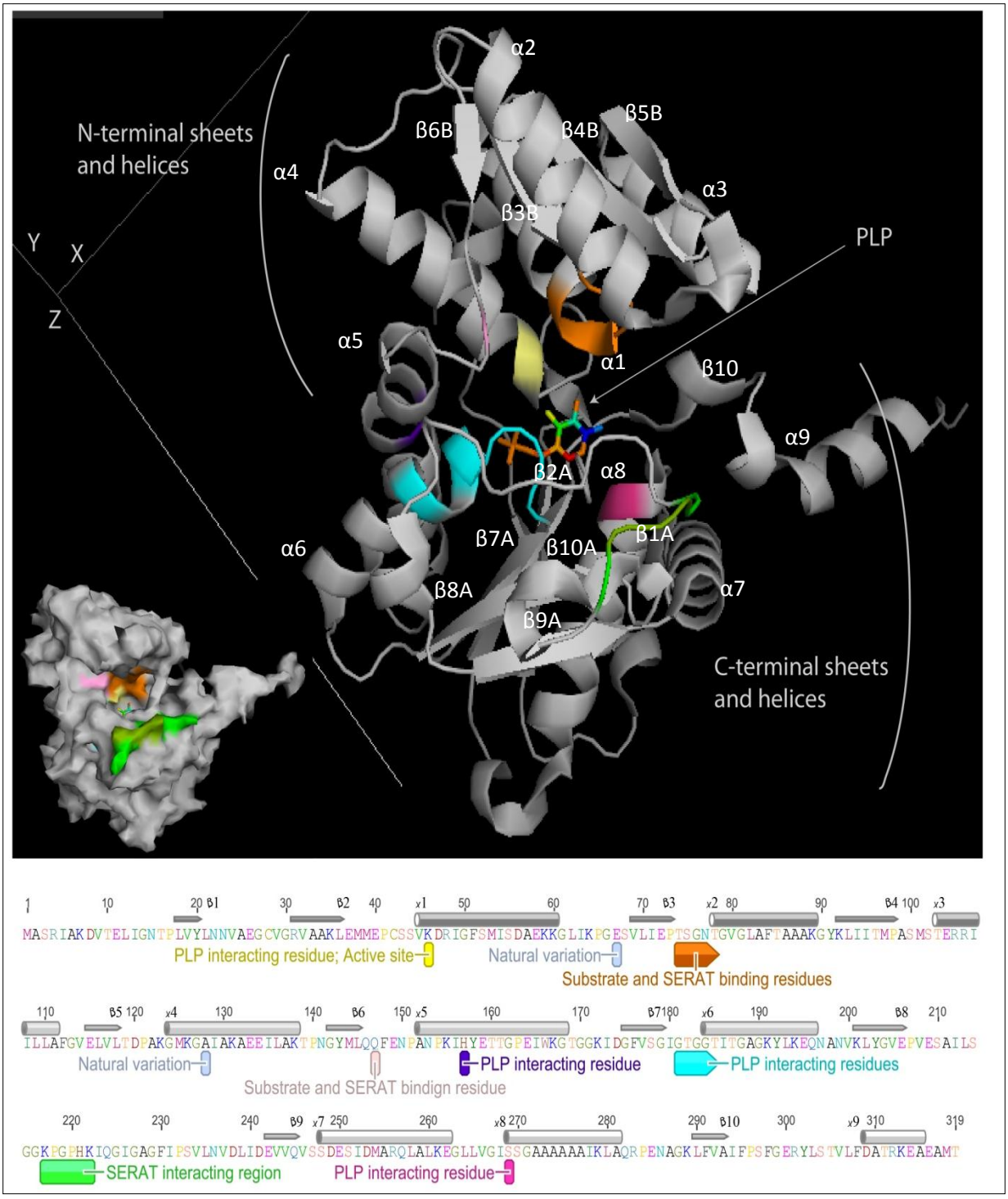
α2
β6B
β4B
β5B
N-terminal sheets
and helices
α4
α3
β3B
Y
X
Z
PLP
α5
α1
β10
α9
β2A
α8
β7A
β10A
β1A
α6
β8A
α7
β9A
C-terminal sheets
and helices
MASRIAKDVTELIGNTPLVYLNNVAEGCVGRVAAKLEMMEPCSSVKDRIGFSMISDAEKKGLIKPGESVLIEPTSGNTGVGLAFTAAAKGYKLIITMPASMSTERRI
PLP interacting residue; Active site
Natural variation
Substrate and SERAT binding residues
ILLAFGVELVLTDPAKGMKGAIAKAEEILAKTPNGYMLQQFENPANPKIHYETTGPEIWKGTGGKIDGFVSGIGTGGTITGAGKYLKEQNANVKLYGVEPVESAILS
Natural variation
Substrate and SERAT bindign residue
PLP interacting residue
PLP interacting residues
GGKPGPHKIQGIGAGFIPSVLNVDLIDEVVQVSSDESIDMARQLALKEGLLVGISSGAAAAAAIKLAQRPENAGKLFVAIFPSFGERYLSTVLFDATRKEAEAMT
SERAT interacting region
PLP interacting residue

2.3 Coordination between sub-cellular compartments involved in OAS and cysteine biosynthesis

In *Arabidopsis*, five isoforms of both SERAT and OASTL enzymes are potentially involved in OAS and cysteine biosynthesis. Three isoforms of SERATs (SERAT1;1, 3;1, and 3;2) and OASTLs (OASTL-A1, CysD1 and CysD2) are localised to the cytosol and a single isoform of each is targeted to the plastids (SERAT2;1, OASTL-B) and mitochondria (SERAT2;2, OASTL-C). How these sub-cellular compartments coordinate during OAS and cysteine biosynthesis at specific sub-cellular site is well-understood recently.

(i) SERATs

SERAT carries out OAS biosynthesis using serine and acetyl-CoA as substrates. A detailed genetic dissection for SERATs in *Arabidopsis*, shows that lack of each isoform in individually knock-out *serat* mutants, does not significantly affect the total SERAT activity in leaves, except in mitochondrial *serat2;2* mutant, under non-stressed growth conditions (Watanabe et al., 2008b). This showed functional redundancy between all SERAT isoforms, except for mitochondrial SERAT2;2. However the study also showed that lack of individual mitochondrial SERAT does not impact the total OAS, cysteine and thiol levels, in leaf, root, stem and silliques, under non-stressed growth conditions (Watanabe et al., 2008b). This indicates efficient transport of OAS across compartments which can contribute to cysteine and thiol biosynthesis at the cellular level. Nevertheless, the role of mitochondrial SERAT2:2 in OAS and also cysteine production is further highlighted in another study in which the *serat2;2* mutant, showed reduced accumulation of radioactively labelled cysteine and GSH levels in the mutant as compared to wild-type, when supplemented with the radiolabelled Ser (Haas et al., 2008). Thus SERAT2;2 mediated OAS production plays an important role in cysteine production as well (Haas et al., 2008).

The role of each SERAT isoform is further illuminated by analysis of the quardruple mutants, in which except one of the isoform, other *SERAT* isoforms were knocked-out (Watanabe et al., 2008b). These mutants also confirmed that mitochondrial *SERAT2;2* predominantly contributes

to the total cellular SERAT activity. Analysis of *serat* quardruple mutants also showed that the enzymatic activity of each SERAT isoform and total OAS production was found to be differentially regulated in different tissue, suggesting that each isoform may contribute to OAS production in a tissue-dependent manner in plants. On the other hand, mitochondrion is indicated to be the major site for the production of serine (Voll et al., 2006), which acts as the precursor of OAS. This further adds significance to mitochondrial-specific OAS production and mitochondria were suggested to be relatively major organelles contributing to total cellular OAS production (Haas et al., 2008; Watanabe et al., 2008b).

The cytosolic SERAT1;1 was identified as another important isoform in contributing cellular OAS biosynthesis, more so than the plastidic and two other cytosolic SERAT isoforms (SERAT3;1 and SERAT3;2) (Watanabe et al., 2008b). The cytosolic SERAT1;1 activity is inhibited by cysteine (Noji et al., 1998; Saito, 2000), which suggests that cytosolic SERAT1;1 may be important for OAS production under conditions when sulfur is limited and cytosolic cysteine levels are reduced. This is consistent with the suggestion that the cytosol is the secondary major site for OAS production after mitochondria (Watanabe et al., 2008b). A quintuple mutant, in which all five *SERAT* isoforms were knocked-out showed embryo lethality suggesting that no other pathway exists for OAS production and that these five isoforms are the only functional SERATs (Watanabe et al., 2008b).

(ii) OASTLs

Three independent studies have shown that loss of cytosolic OASTL-A1, which contributes ~50% of the total OASTL activity, does not substantially reduce the total cysteine and GSH levels in the cell although a slight and significant reduction, of 15 to 28% in total cysteine concentration was observed in various studies (Heeg et al., 2008; Watanabe et al., 2008a; Shirzadian-Khorramabad et al., 2010). Lack of plastidic OASTL-B however did not affect total cysteine and GSH levels. These changes coincided with the absence of a noticeable phenotype. in, both *oastl-a1* and *oastl-b* mutants (Heeg et al., 2008; Watanabe et al., 2008a; Shirzadian-Khorramabad et al., 2010). In contrast, a strong decrease of ~34% in total cysteine levels coupled with development of an oxidative burst and cell death in *oastl-a1* mutants was reported (Lopez-

Martin et al., 2008), a phenotype not noticed in earlier studies. The question remains why independent groups found different results? It is possible that discrepancies in the observations are linked with the particular growth conditions used for the experiment, perhaps in combination with plant age. This would be consistent with a role of OASTL in stress.

Simultaneous lack of both OASTLs (A and B) in the *oastl-ab* mutant affected plant growth under non-stressed growth conditions indicating that under these conditions both isoforms are important for cysteine biosynthesis and are functionally redundant (Heeg et al., 2008). Studies using radioactively labelled sulfate media supplementation have further indicated that cytosolic OASTL-A1 is the major enzyme driving *de novo* cysteine biosynthesis because significantly lower amount of radioactively labelled sulfate was incorporated into cysteine in the *oastl-a1* mutant only compared with the *oastl-b* and *oastl-c* mutants (Heeg et al., 2008). By contrast, GSH biosynthesis appears equally dependent on OASTL-A1 and OASTL-B, but not OASTL-C activity (Heeg et al., 2008).

Interestingly, Heeg et al (2008) also found that loss of OASTL-C severely affected plant growth despite it not being a major contributor to total OASTL activity. However, this OASTL-C loss of function phenotype was not observed by others (Watanabe et al., 2008a). Nevertheless, results from previous studies (Haas et al., 2008; Heeg et al., 2008) indicated that SERAT2;2 and OASTL-C mediated mitochondrial OAS and cysteine biosynthesis, respectively, is equally crucial for plant growth as well. Although the SERAT and OASTL proteins are present in all sub-cellular compartments, the studies suggested that relative to other compartments cytosol is preferred as a major site for cysteine biosynthesis while plastids as major suppliers of reduced sulphide. In contrast, OAS production seems to be favoured in mitochondrion. Based on these findings a model was proposed which predicts facilitated diffusion of sulphide, OAS and cysteine among sub-cellular compartments that regulates cysteine biosynthesis at the cellular level (Figure 2.4) (Haas et al., 2008; Heeg et al., 2008; Watanabe et al., 2008a; Watanabe et al., 2008b).

2.4 Role of true OASTLs and functionally divergent *BSAS* isoforms in cysteine biosynthesis and homeostasis and stress responses

(i) Cytosolic cysteine biosynthesis and the role of a major BSAS1;1/OASTL-A1 isoform in stress response

The cytosol, as mentioned above, is the major site for cysteine biosynthesis in *Arabidopsis*. Five genes are predicted to encode cytosolic-specific *BSAS* isoforms. Two of these, the *BSAS1;1/OASTL-A1* and *BSAS1;2/OASTL-A2*, are closely related at the coding level suggesting an early duplication event in the ancestral cytosolic OASTL-A isoform in plants (Table 2.1) (Watanabe et al., 2008a). However *BSAS1;2/OASTL-A2* mRNA contains a stop codon within the ORF causing a truncated protein; thus *BSAS1:2/OASTL-A2* is considered a pseudogene (Jost et al., 2000). Other cytosolic targeted BSAS isoforms includes BSAS4;3/DES, which is involved in the degradation of cysteine (Alvarez et al., 2010), and two other isoforms BSAS4;1/ CysD1 and BSAS4;2/ CysD2 (Hatzfeld et al., 2000b; Yamaguchi et al., 2000; Heeg et al., 2008; Watanabe et al., 2008a). Based on its contribution to total OASTL activity, BSAS1;1/OASTL-A1 is considered the major OASTL isoform in the cell (Heeg et al., 2008; Lopez-Martin et al., 2008; Watanabe et al., 2008a). It is also the most abundant OASTL isoform in *Arabidopsis* (Heeg et al., 2008; Wirtz et al., 2010). It is still unclear however, what genetic and molecular factors contribute to the high activity of OASTL-A1. Similarly, the evolutionary significance of high OASTL-A1 expression in *Arabidopsis* plant remains an open question.

Making use of the *Arabidopsis* accessions genome sequences database (Weigel and Mott, 2009) (1001genomes.org/datacenter/), it was found that among widely dispersed natural populations, cytosolic *OASTL-A1 /AT4G14880* is highly conserved at the coding level (Appendix 3). Orthologs of OASTL-A1 in rice and maize can also be found in the Plant Proteome Database (PPDB) (Figure 2.5). Although the cellular function of the evolutionary conserved OASTL-A1 in *Arabidopsis* is not fully understood, its role in resistance to abiotic stresses has been suggested over a decade ago. Exposure of the *Arabidopsis* and other plant species to high salt concentration increased OASTL activity and levels of cysteine-thiols in plants (Barroso et al., 1999; Fediuc et al., 2005). Similarly when plants were exposed to heavy metal and other toxic factors, a rapid

increase in transcript abundance of OASTL-A1 along with the accumulation of cysteine and GSH was detected in plants (Noji et al., 1998; Domínguez-Solís et al., 2001; Fediuc et al., 2005). These studies suggested that rapid induction of cysteine/thiols biosynthesis is associated with adaptation to a variety of adverse conditions, presumably because cysteine is incorporated into GSH and other sulfur-containing metabolites involved in resistance to abiotic stress.

The direct role of OASTL-A1 in stress defence was demonstrated by finding that yeast cells, *Arabidopsis* and tobacco plants over-expressing *OASTL* were better able to tolerate oxidative stress and higher concentrations of salt and cadmium (Noji et al., 2001; Youssefian et al., 2001; Dominguez-Solis et al., 2004; Lopez-Martin et al., 2008; Shirzadian-Khorramabad et al., 2010). By contrast, the susceptibility of the *Arabidopsis oasa1.1* mutant (knock-out of OASTL-A1) to cadmium toxicity was found to be correlated with lower cysteine and reduced thiols levels which likely compromised the antioxidant response and phyto-chelation capacity for heavy metals (Lopez-Martin et al., 2008). Since an increased flux of cysteine in thiols and other metabolites could be required in various mechanisms of protection, the role of the OASTL-A1 isoform in the cytosol seems to be tightly linked with adaptation to adverse environments.

(ii) Role of Mitochondrial specific BSAS3;1/ Cys-C1/ *β*-cyanoalanine synthase in cyanide detoxification

The BSAS gene family in *Arabidopsis* is functionally diverged and a few of the OASTLs do not interact with SERAT or show negative cooperativity towards sulphide for cysteine biosynthesis. One of these divergent OASTLs is BSAS3;1/CYS-C1 which encodes *β*-cyanoalanine synthase (CAS). BSAS3;1/CYS-C1/*β*-CAS does not interact with SERAT and shows poor OASTL activity (Hatzfeld et al., 2000b; Warrilow and Hawkesford, 2000; Yamaguchi et al., 2000). Instead *β*-CAS is involved in detoxification of endogenous cyanide which is produced as a by-product during biosynthesis of the stress hormone ethylene and the defence compound camalexin (Peiser et al., 1984; Bottcher et al., 2009). Cyanide is toxic as it inhibits the activity of various enzymes including catalase, nitrate and nitrite reductase, nitrogenase, peroxidase, and cytochrome c oxidase which is part of the mitochondrial respiratory chain (Siegień and Bogatek, 2006; Cooper and Brown, 2008). Detoxification of cyanide is hence required in mitochondria

and other sub-cellular compartments for normal plant growth and development. Moreover the detoxification of cyanide can be a major requirement particularly under abiotic/biotics stress conditions which induce higher amounts of ethylene and camalexin in plants and consequently increase cyanide release in the cellular system. *β*-CAS sequesters cysteine for the conversion of cyanide into *β*-cyanoalanine and this reaction generates hydrogen sulphide as a by-product. *β*-cyanoalanine is then funnelled downstream into nitrogen metabolism and incorporated into Asn or Asp by nitrilase, which releases ammonia as a by-product (Piotrowski, 2008). The sulphide meanwhile gets incorporated back into cysteine. Therefore *β*-CAS regulates cysteine homeostasis and biosynthesis by sequestering cysteine and providing its precursor sulphide (Figure 2.4).

β-CAS is the most abundant CAS enzyme in *Arabidopsis* and significantly contributes to total CAS activity in *Arabidopsis* root and leaf tissues (Hatzfeld et al., 2000b; Yamaguchi et al., 2000; Watanabe et al., 2008a). Two other cytosolic BSAS isoforms, Cys-D1 and Cys-D2 were also suggested to be member of *β*-cyanoalanine synthase family. However, they do not possess CAS activity and contribute a minor fraction of the total OASTL activity in the cell (Table 2.1) (Hatzfeld et al., 2000b; Yamaguchi et al., 2000; Jost et al., 2005; Watanabe et al., 2008a). Even though *β*-CAS significantly contributes to cyanide detoxification, plant lacking functional *β*-CAS i.e., *bsas3;1*, have been previously shown to exhibit leaf and shoot development, comparable to wild-type plants (Watanabe et al., 2008b). Interestingly, lack of *β*-CAS in *Arabidopsis* was shown to impair the growth and development of root structures which correlates with the accumulation of cyanide in roots only but not in the shoots (García et al., 2010). Lack of functional *β*-CAS was shown to cause reduced total CAS activity and high respiration rates in the roots along with transcriptional suppression of genes involved in root development and ethylene signalling (García et al., 2010). Therefore the activity of *β*-CAS interacts directly and indirectly with 1) cyanide detoxification, 2) root hair growth and development 3) ethylene signalling and 4) cysteine homeostasis and biosynthesis.

Protein sequence comparison of the *Arabidopsis β-CAS* with rice and maize suggests that these species have orthologs of *β-CAS* (Figure 2.5). However, *β*-CAS appears to be the only mitochondrial OASTL isoform in species such as potato and spinach in contrast to the presence

of a pair of BSAS isoforms (i.e., OASTL-C along with β-CAS) in *Arabidopsis* mitochondria (Hatzfeld et al., 2000b; Warrilow and Hawkesford, 2000). Thus requirement of cysteine in cyanide detoxification in these species may be compensated by facilitated diffusion of cysteine from the cytosol into the mitochondria. Nevertheless, the authentic OASTLs still share high similarity in the protein structure with *β*-CAS. It was also proposed that the true OASTLs may perform, to some extent, both the cysteine and *β*-cyanoalanine synthesis *in vivo* (Hell and Wirtz, 2008). Evidence for such an argument also comes from the observation that, the total CAS activity was reduced in the mutant lacking the cytosolic OASTL-A1 (Watanabe et al., 2008a).

In *Arabidopsis*, the *β*-CAS activity is predominantly localised in mitochondria. However *β-CAS* gene shows three different protein-coding gene models that arise from alternative splicing (Appendix 2). Analysis of the N-terminal region of these gene models suggests that in contrast to gene model 1, model 2 and 3 do not contain mitochondrial localization signals and indicate that these isoforms may localise to cytosol and peroxisomes (Appendix 2). This raises the possibility that *β*-CAS may also function to detoxify cyanide in the cytosol and peroxisomes as well as mitochondria (Figure 2.4), however this needs further investigation.

(iii) Requirement of OASTL-C and OASTL B in detoxification of sulphide

Mitochondrial OASTL-C may have an important role in providing cysteine for cyanide detoxification and for quenching build-up of toxic sulphide levels in the mitochondria (Figure 1.4). Alvarez and co-workers (2012a) have shown that the *oastl-c* mutant is impaired in overall root growth and root hair development. The *oastl-c* mutant also accumulates a substantial amount of cyanide and sulphide. Elevated amounts of these compounds seem to inhibit root and shoot development, cause higher respiration rates, oxidative burst, cell death, and activate Alternative Oxidase (AOX) expression (Alvarez et al., 2012a). AOX is part of the mitochondrial electron transport chain (mETC), which is activated to alleviate the stress caused by ROS production (Maxwell et al., 1999). This is because AOX allows passage of electrons for the reduction of ROS, as an alternative pathway to the primary cytochrome oxidase (COX) mediated electron flux in the mETC. The need of OASTL-C to rectify the growth defects of *oastl-c* mutant suggest its function in sequestrating toxic sulphide levels in mitochondria via cysteine

biosynthesis which can further aid in detoxification of cyanide. Interestingly impaired root hair development in *oastl-c* mutant mimics the root phenotype of mutant plants lacking *β*-CAS, which is directly involved in cyanide detoxification (García et al., 2010). In another study, Birke and co-workers (2012) have shown the lethal effects of elevated levels of sulphide and cyanide on mitochondrial COX activity. The lower COX activity in the *oastl-c* mutant further suggested that sulphide and cyanide toxicity impairs the function of the mETC in the *oastl-c* mutant (Birke et al., 2012). Since the work of Birke et al. (2012) suggests that the *oastl-c* mutant does not contain significantly higher amounts of cyanide, it seems that sulphide toxicity can be a major factor causing impaired mETC function and repressed growth in the *oastl-c* mutant.

Furthermore, Birke and co-workers (2012) also suggested the presence of a novel cyanide detoxification mechanism in the mitochondrion of the *oastl-c* mutant without the localised cysteine production. These findings were consistent with their observation that the enzymatic activity of Fe-S cluster proteins were comparable between the *oastl-c* mutant and wild-type indicating the cysteine concentration in the *oastl-c* mitochondria was not limiting. These result impress on the notion that OASTL-C-mediated cysteine biosynthesis in mitochondria is a necessity in the process of sequestration of toxic sulphide levels.

Sulfide toxicity in the mitochondrion suggests that sulphide diffusion out of the mitochondrial membrane into the cytosol is not efficient. Sulphide is shown to diffuse through the lipid bilayer membrane easily in form of hydrogen sulphide gas suggesting no requirement of facilitator channelling via transporter proteins in bacteria (Mathai et al., 2009). In mitochondrion, however, proton pumping from the inner mitochondrial matrix via mETC is suggestive of an increase in the pH of the mitochondrial matrix as compared to cytosol which may not facilitate H_2S production and therefore results in poor diffusion of sulphide from mitochondria into the cytosol (Lowicka and Beltowski, 2007; Alvarez et al., 2012a).

Surprisingly, inclusion of sucrose in the plant growth medium was shown to rescue the growth defects in both shoots and roots in the *oastl-c* mutant (Alvarez et al., 2012a). Moreover a defective growth of the *oastl-c* mutant was observed in short-days (Heeg et al., 2008) in

comparison to long-days (Watanabe et al., 2008a). These results points to potential connections between photosynthesis, sucrose catabolism and resistance to sulphide toxicity.

In contrast to mitochondria, plastids contain higher concentrations of sulphide, in part due to them having sulphite reductase, which carries out the reduction of sulphite into sulphide. Despite the plastids hosting sulfate reduction, lack of the plastidic OASTL-B has no demonstrated effect on the plant phenotype suggesting efficient sulphide transport across plastidic membrane into the cytosol (Heeg et al., 2008; Watanabe et al., 2008a). Release of hydrogen ions from the inner thylakoid into the chloroplast stroma can allow excess sulfide to escape as H_2S (Mathai et al., 2009; Birke et al., 2012) which may protect the plastids from sulfide toxicity (Figure 1.4). Regardless, a recent finding suggests positive feedback effects of sulphide on plant photosynthesis (Chen et al., 2011) supporting the co-evolution of the sulfate reduction and carbon fixation during the evolution of photosynthetic organisms.

Phylogenetic analysis suggests that the plastidic OASTL-B and mitochondrial OASTL-C have originated from an early duplication event in *Brassicaceae* instead of being transferred from an early endosymbiotic event or later during the evolution of higher land plants (Table 2.1; Figure 2.5) (Watanabe et al., 2008b). However the OASTL activity of the OASTL-B isoform is relatively very high as compared to OASTL-C. Recently, cysteine was shown to cause inhibitory effects on the mitochondrial SERAT enzyme activity and OAS production i.e., independent of OASTL-C (Wirtz et al., 2012). In this regard, it may be of evolutionary significance to maintain lower OASTL activity and consequently reduced cysteine production in mitochondria.

(iv) Cytosolic specific *BSAS4;3/* L-Cys Desulfhydrase (DES) is involved in cysteine degradation

Cytosolic Bsas4:3 or known as DES1 of *Arabidopsis* encodes L-Cys Desulfhydrase (DES) activity which results in in the degradation of Cys into sulphide, pyruvate and ammonium (Alvarez et al., 2010). DES does not interact with SERAT and is therefore not a true OASTL (Heeg et al., 2008; Alvarez et al., 2010; Wirtz et al., 2010). This is consistent with the difference in the amino acid sequence, between DES and a true OASTL, in the residues between β8A and

β9A sheets, which is the acknowledged site for interaction with SERAT (Bonner et al., 2005; Alvarez et al., 2010). Furthermore, there is a Gly to Ser substitution at residue 75 in DES, which is part of a highly conserved motif involved in interaction with the OASTL substrates as well SERAT enzyme.

DES contribute up to 20-25% of the total DES activity in *Arabidopsis* (Table 2.1; Figure 2.4) (Alvarez et al., 2010). This is because DES is not the only enzyme involved in the degradation of cysteine as cysteine lyases have been identified in *Arabidopsis* that may contribute to cysteine degradation as they do in mammals (Cooper, 1983; Jones et al., 2003). The *des1* null mutant shows premature senescence and constitutive activation of systemic acquired resistance (SAR), a disease resistance response under non-stressed/pathogenic conditions (Alvarez et al., 2010; Alvarez et al., 2012b). This is associated with the accumulation of Cys in plants. DES is therefore proposed to function in Cys homeostasis at the cytosolic and probably at the cellular level during plant development. However, why the *des1* mutant shows constitutive biotic stress response has remained unclear although higher amounts of Cys in the mutant is suggested to be toxic in plants (Park and Imlay, 2003). Interestingly no BSAS isoform closely related to DES was identified in rice or maize (Figure 2.4).

(v) Plastidic BSAS5;1 /S-sulfocysteine synthase /CS26 plays an important role in chloroplastic functions

The plastidic BSAS5;1 or known as CS26 lacks the loop of residues in between β8A and β9A sheets that is required for interaction with SERAT and therefore is not an authentic OASTL (Figure 2.4) (Bermúdez et al., 2010b). CS26 synthesizes sulfocysteine (S-Cys) using thiosulfate and OAS in chloroplasts and is the only enzyme that contributes to SSCS activity in *Arabidopsis* (Bermúdez et al., 2010b). A CS26-like BSAS isoform was also identified in both rice and maize (Figure 2.5). Lack of CS26 results in higher glutathione levels in plants without significant variation in total cysteine levels and these changes are associated with oxidative burst and premature leaf senescence in the *cs26* null mutant.

Interestingly, the *cs26* null mutant phenotype is dependent on day length. Transcriptional analysis of *cs26* null lines showed that the mutants express activation of abiotic and biotic stress responses under long days (L.D.) which is consistent with the development of the growth defects in plants (Bermúdez et al., 2010b). In contrast, this spectrum of transcriptional responses was found to be suppressed in a short-days (S.D.) condition which rescues the mutant phenotype. However the basis of the major flux in plant transcriptome towards a stress response in the *cs26* null mutants remains unknown. Nevertheless, the results suggest that CS26 contributes towards SSCS activity in plastids and mutation in CS26 have pleiotropic effects on various metabolic and stress responses (Bermúdez et al., 2010b).

(vi) Function of CysD1 and CysD2; relatively low abundance and poor OASTL activity of these isoforms questions their evolutionary significance

CysD1 and CysD2 contribute ~1 and 0.5% of the total OASTL activity and abundance of the OASTL proteins, respectively (Heeg et al., 2008; Watanabe et al., 2008a). Lack of these isoforms individually does not affect the abundance of other OASTLs. A relatively low expression of CysD1 and CysD2 as compared to other true OASTLs in wild-type or other *oastl* mutants concomitant with relatively low OASTL activity and abundance of these isoforms suggest that these isoforms may not play an active role in cysteine biosynthesis in plants (Heeg et al., 2008; Watanabe et al., 2008a).

The protein accumulation patterns of these isoforms across plant organs, obtained from the AT proteome TAIR7, suggests that CysD2 is relatively more abundant in flower buds and open flowers compared with CysD1, which generally showed very low abundance. Phylogenetic analysis of all the *BSAS*-encoded isoforms revealed that both cytosolic CysD1 and CysD2 are closely related to cytosolic DES (Table 2.1). This is in contrast to the previous suggestion that CysD1 and CysD2 are closely related to *β*-CAS in the BSAS gene family (Hatzfeld et al., 2000b; Yamaguchi et al., 2000). Regardless, previous studies indicate that CysD1 and CysD2 do not show β-CAS (Watanabe et al., 2008a) or significant DES activity (Alvarez et al., 2010). It is possible that CysD1 is functionally redundant to CysD2 and therefore lack of both isoforms is required to reveal their function. In comparison to CysD1, CysD2 exhibits multiple splicing patterns in the protein coding gene models and may contribute different sizes of proteins possibly

for altered functions (Appendix 2). Enzymatic analysis of these isoforms for other substrates and the role of these isoforms, possibly under different environmental conditions, may reveal their function in plant metabolism.

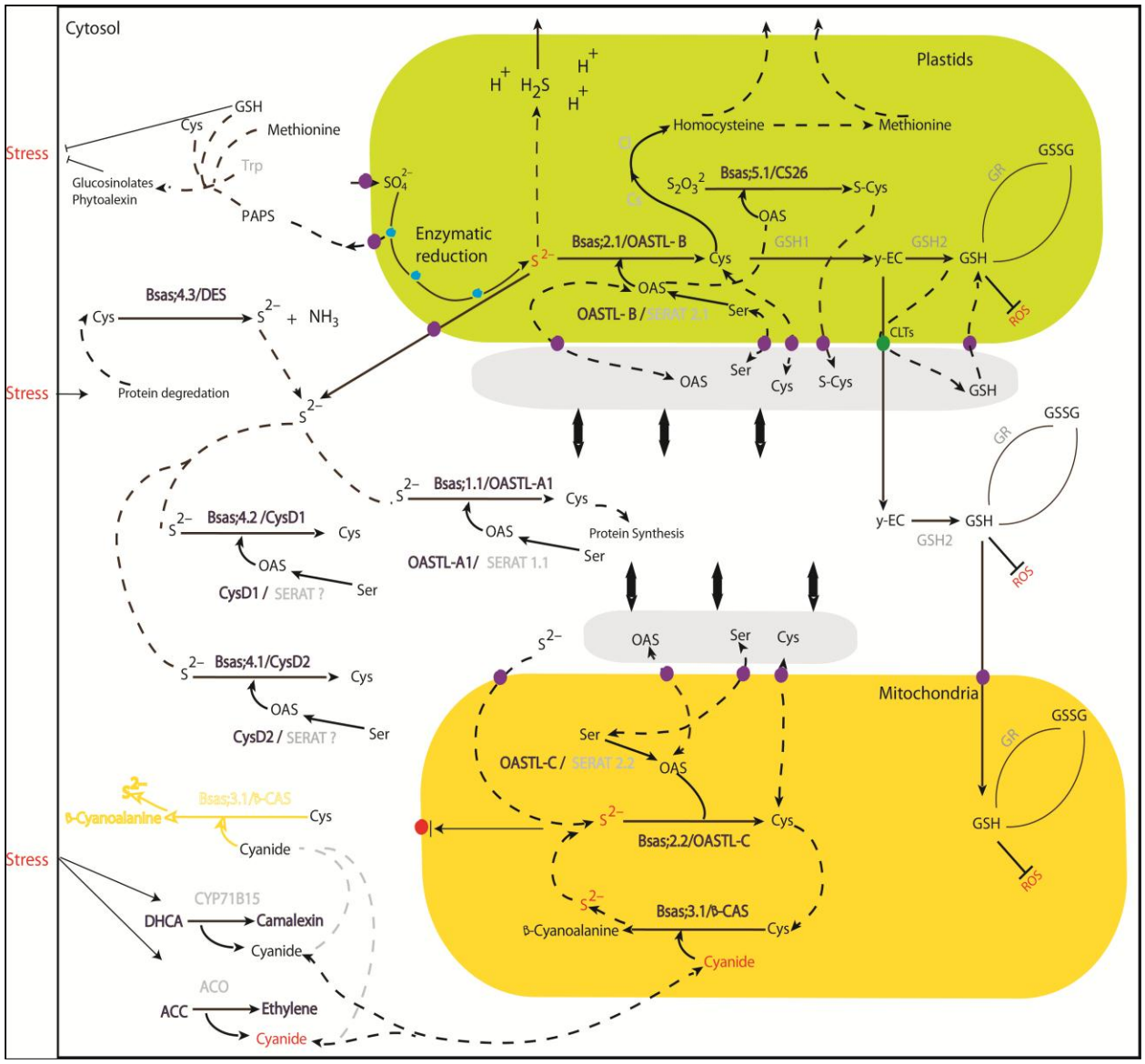

Figure 2.4. Biochemical routes and biological routers (enzymes and proteins) involved in cysteine metabolism and homeostasis in plant cell. The figure shows the pathways and enzymes in sulfur assimilation, cysteine biosynthesis and homeostasis and metabolism of thiol biosynthesis and homeostasis. The solid arrows indicate reactions and paths of metabolites passages identified previously. The shaded arrows indicate putative pathways and reactions suggested in various studies. The purple spots at membrane of the organelles suggest putative transporters of the metabolites of sulfur reduction, assimilation and thiol pathways. The green spot is the identified true transporter of the metabolite. The red spot suggest absence of a transporter for a specific metabolite. The reaction in yellow is suggested to be a putative phenomenon based on the findings in this review. The grey shaded area is a hypothetical metabolite pool sharing the transport of the metabolites and ions. Abbreviations; Glutathione (GSH), Cysteine (Cys), 3′-phosphate adenosine 5′-phospho-sulfate (PAPS), S-sulfocysteine (S-cys), Serine (Ser), γ-glutamylcysteine (y-EC), chloroquine-resistance transporter (CLTs), oligopeptide transporters (OLTs), Di-hydro camalexic acid (DHCA), 1-aminocyclopropane-1-carboxylic acid (ACC). The information is compiled from; (Peiser et al., 1984; Bleecker and Kende, 2000; Hatzfeld et al., 2000b; Yamaguchi et al., 2000; Koprivova et al., 2002; Heeg et al., 2008; Watanabe et al., 2008a; Watanabe et al., 2008b; Bottcher et al., 2009; Krueger et al., 2009; Mugford et al., 2009; Alvarez et al., 2010; Bermúdez et al., 2010b; García et al., 2010; Maughan et al., 2010; Wirtz et al., 2010; Hell and Wirtz, 2011; Takahashi et al., 2011b; Alvarez et al., 2012a; Birke et al., 2012; Noctor et al., 2012).

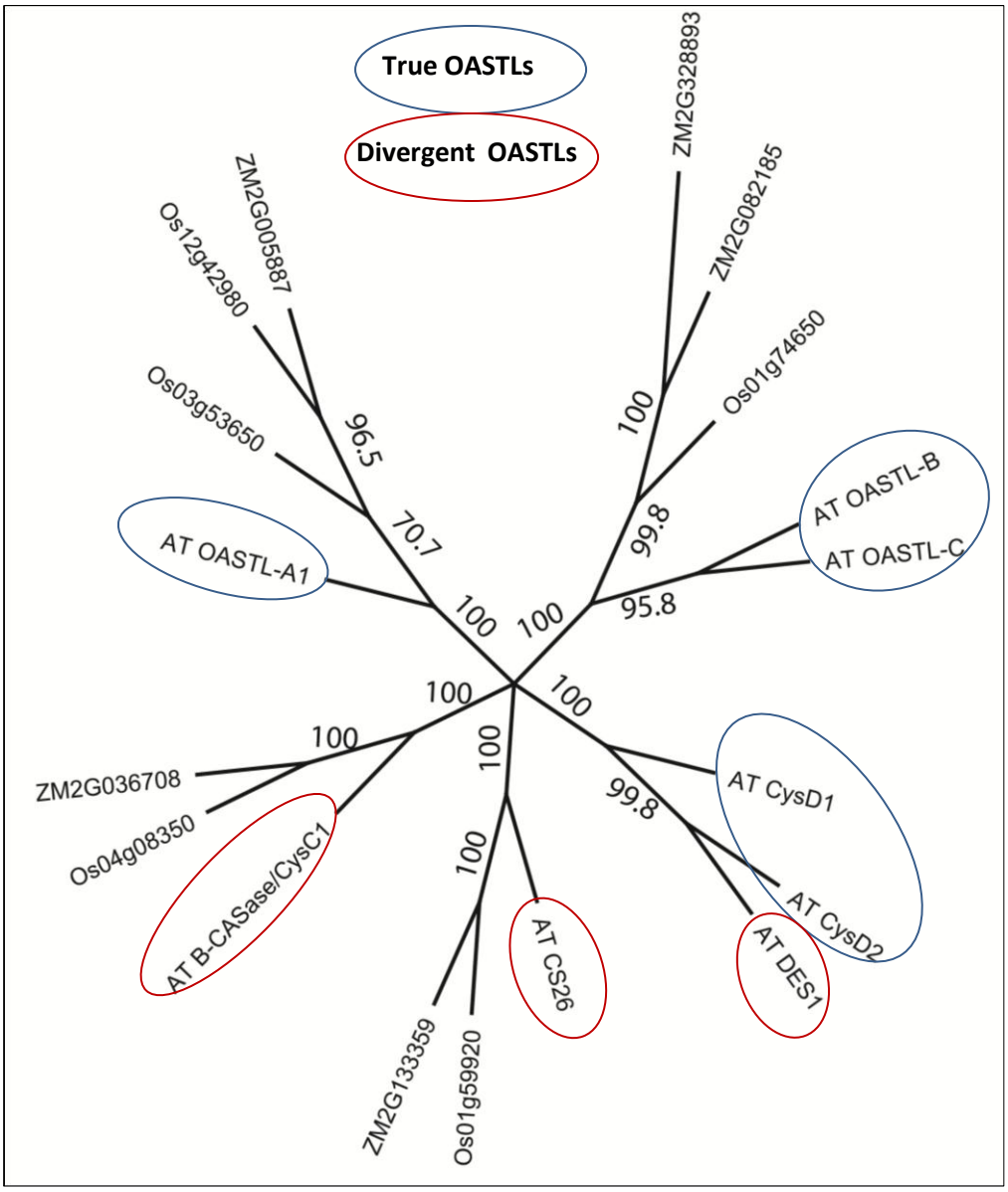

Figure 2.5. Phylogenetic analysis of BSAS/OASTL isoforms in Maize, Rice and *Arabidopsis*. Figure shows neighbouring-joining tree of the alignment of the conserved protein sequences of BSAS isoforms in three plant species. Sequence obtained from TAIR and Plant Protein Database. AT is *Arabidopsis thaliana*; Os is *Oryza sativa* /Rice and ZM is *Zea Mays* /Maize. Values represent consensus support (%) between lineages based on 10,000 bootstrap values.

2.5 Requirement of cysteine in glutathione biosynthesis and other metabolites involved in growth and defence metabolism

Cysteine is an indispensable molecule in the synthesis of various proteins. Biosynthesis of cysteine in the major sub-cellular compartments ensures sufficient availability of cysteine to fuel various functions of the cellular machinery. The reduced form of sulfur in cysteine, known as the thiol group (Cys-SH) is an important mediator of redox reaction. This is because sulfur is highly nucleophilic and an efficient donor of free electrons. The thiol group also enables di-sulphide bridge formation between Cys residues which aids in modification of the protein structure as well as protein-protein interactions. Further cysteine is also required in the synthesis of metabolites essential for plant growth as well as stress defence. For example, the thiol group of the Cys provides the reducing power of glutathione (GSH) which mitigates oxidative stress and metal toxicity in the cells.

(i) Glutathione

The tripeptide glutathione or GSH (L-γ-glutamyl-L-cysteinylglycine) is the most abundant sulfur-containing peptide in plants. GSH is involved in various stress migitation reactions in plants such as detoxification of ROS, reactive nitrogen species (RNS), xenobiotics and heavy metals.

The first step in GSH synthesis is carried out by the enzyme γ-glutamyl-cysteine ligase (GSH1 or γ-ECS). GSH1 is encoded by a single copy gene and catalyses the rate-limiting step in GSH biosynthesis. GSH1 is localised to plastids in many plants (Richman and Meister, 1975; May and Leaver, 1994) but in some species including pea and spinach, is present in both cytosol and plastids (Hell and Bergmann, 1990). GSH1 catalyses the synthesis of γ-glutamylcysteine (γ-EC) from two substrates, L-glutamate and L-cysteine. GSH1 acts as a monomeric protein and has not been found to interact with any other enzyme.

The final step in GSH biosynthesis involves the addition of glycine to γ-EC. This is catalysed by glutathione synthetase (GSH2 or GSH-S) (Rawlins et al., 1995). GSH2 is localised to both

cytosol and plastids in *Arabidopsis*. It is encoded by a single copy gene, which shows multiple transcriptional splicing patterns (Wachter et al., 2005). In absence of GSH2 localisation to plastids, the cytosolic GSH2 is sufficient for GSH biosynthesis in plants (Pasternak et al., 2007). This is because the precursor of GSH, γ-EC, can diffuse from plastids into the cytosol via a specific transporter and contribute to GSH biosynthesis. γ-EC transporters are localised to the plastidic membrane and are orthologs of the *Plasmodium falciparum* chloroquine-resistance transporter (CLT) (Maughan et al., 2010). Further the study also suggests that GSH can also be transported from plastids into cytosol via these transporters. GSH biosynthesis does not take place in mitochondria and depends upon import of GSH from the cytosol. Although plasma and plastidic membrane-specific transporters of GSH are suggested to be oligopeptide transporters (OPT) and CLTs in plants, respectively, mitochondrial specific transporters of GSH are yet to be revealed. The null *GSH1* mutant lines show an embryo-lethal phenotype whereas *GSH2* null lines are seedling lethal. These findings assert that γ-EC and GSH are required in plant development and viability (Vernoux et al., 2000; Cairns et al., 2006; Pasternak et al., 2008).

(ii) GSH functions in redox balance and resistance against ROS and RNS

The cysteine of GSH molecule provides the antioxidant capacity of GSH against ROS. ROS include various species such as superoxide and the hydroxyl radical. Excess concentration of ROS can damage the cellular system by oxidising proteins and enzymes as well as altering redox-sensitive reactions (Van Breusegem and Dat, 2006). ROS oxidise GSH and therefore GSH acts as a scavenger for these species to prevent them from oxidising important proteins and enzyme.

The oxidation of the thiol group in GSH results in the formation of a disulphide bridge between the two oxidised GS^- anions which yields a stable molecule, GSSG (Foyer and Noctor, 2003; Noctor et al., 2012). GSSG is reduced back into GSH by Glutathione reductase (GR) which uses reducing equivalents from NADPH. The redox status in the cells is often measured by the ratio of GSH to GSSG, which is greater than 0.9 under non-stressed conditions. GR is localised to plastids, cytosol and mitochondria to ensure the reduction of GSSG. This maintains the

antioxidant capacity of plant cells and is therefore a crucial point in redox balance. Reduced biosynthesis of cysteine due to lack of OASTL-A1 has been shown to affect the cytosolic redox status and result in lower GSH:GSSG ratio which suggests that cytosolic cysteine production is an important player in modulating oxidative stress conditions (Lopez-Martin et al., 2008).

GSH also reacts with nitric oxide which results in the formation of S-nitrosoglutathione (GSNO). GSNO was unravelled to be a key player in signalling as it performs nitrosylation of cysteine residues which results in post-translational modification of the proteins (Lindermayr et al., 2005; Romero-Puertas et al., 2008; Lindermayr and Durner, 2009). Recently GSNO mediated post-translation modification was found to be a key step in ethylene biosynthesis (Lindermayr et al., 2006) and activation of defence signalling during disease resistance (Tada et al., 2008).

(iii) Role of GSH in immunity and disease resistance

Reduced GSH biosynthesis can lead to oxidised cytosolic environment which can negatively affect the metabolic processes. The role of GSH in plant immunity has been highlighted by the reduced resistance of *pad2* and *cad2* mutants against the avirulent pathogen strain of *Pseudomonas syringae* (Ball et al., 2004; Parisy et al., 2007). Moreover mutants lacking cytosolic GSH biosynthesis, either due to impaired γ-EC transport into the cytosol or lacking GS enzymes showed reduced expression of *PATHOGENESIS RELATED-1* defence genes and enhanced disease susceptibility in *Arabidopsis* plants (Maughan et al., 2010). Similarly plants lacking cytosolic GR, which is involved in reducing GSSG to GSH, also showed reduced *PR-1* transcript abundance and SA accumulation (Mhamdi et al., 2010). Redox changes in the cytosolic environment are shown to be involved in defence signalling in response to the disease resistance hormone salicylic acid (Tada et al., 2008). Therefore the cytosolic redox status is a key factor in defence signalling pressing the importance of cytosolic cysteine and thiol production in plant immunity (Foyer and Noctor, 2005). Moreover cysteine and GSH are also required in synthesis of plant defence compounds including indol-glucosinolates and camalexin which are actively involved in resistance against disease caused by bacterial and fungal pathogens as well as herbivory (Schlaeppi et al., 2008; Bednarek et al., 2009; Bottcher et al., 2009; Clay et al.,

2009; Su et al., 2011). Therefore the availability of cysteine and GSH seems a crucial factor in modifying plant-pathogen interactions (Rausch and Wachter, 2005).

(iv) Role of cysteine derived metabolites in resistance to metal toxicity

The role of cysteine and its derived metabolites γ-EC and GSH is already highlighted in protection against metal toxicity (Zhu et al., 1999a; Zhu et al., 1999b; Gullner et al., 2001; Dominguez-Solis et al., 2004; Lopez-Martin et al., 2008; Shirzadian-Khorramabad et al., 2010). Mutations in GSH1 (*root meristemless 1/ rml 1 and cadmium sensitive -2/ cad-2*) which causes reduced GSH levels lead to impaired root meristem development and shoot growth and enhanced susceptibility to cadmium toxicity (Cobbett et al., 1998; Vernoux et al., 2000). The GSH-mediated-antioxidant shield further prevents the damage in the cellular system caused by heavy-metal-induced ROS accumulation. GSH also acts as a scavenging molecule of heavy metals in form of phytochelatins. Phytochelatins are oligomers of GSH and synthesized by the cytosolic phytochelatins synthases (PCS) enzymes in *Arabidopsis* (Ha et al., 1999; Cazale and Clemens, 2001). Phytochelatins complex heavy metals which are transported to vacuoles for degradation (Cobbett and Goldsbrough, 2002).

(v) Cystathionine, Methionine and Fe-S cluster

Cysteine is converted in plastids into cystathionine by cystathionine γ-synthase (CgS) enzyme, which catalyses the substitution of the phosphate group of O-phospho-homoserine by the sulfhydryl group of cysteine (Ravanel et al., 1998). The synthesis of cystathionine from cysteine and O-phospho-homoserine is the starting point for the biosynthesis of the other sulfur containing amino acid, methionine. Cystathionine is converted into homocysteine by another enzyme Cystathionine β-lyase. Homocysteine is then methylated to form methionine. The three enzymatic reactions converting cysteine to methionine takes place in plastids (Ravanel et al., 2004). Methionine is transported from plastids into cytosol; however homocysteine can be converted into methionine in the cytosol as well. Methionine is further converted into S-adenosylmethionine (SAM) which is fed into the Yang-cycle that regulates ethylene

biosynthesis. Availability of reduced sulfur in the form of cysteine therefore plays a major role in methionine, SAM and ethylene biosynthesis. Cysteine is also required in the synthesis of Fe-S cluster which makes an important component of electron transport chain of chloroplast and mitochondria (Balk and Pilon, 2011).

2.6 Conclusions and outlook

Cysteine is an important component of proteins and metabolites which control plant growth and stress responses. Consistent with this the function of BSAS enzymes involved in cysteine biosynthesis and homeostasis seems to strongly integrate with plant stress-defence. These observations suggest a network of BSAS proteins in plant cells acting as biological routers (active proteins) that modulate stress responses in varying capacities and mechanisms, distinct environments and specific sub-cellular locations. This review also highlights an important role of various external signals in the transcriptional activity of *BSAS* genes. Considering the mounting evidence about the indirect role of BSAS in plant defence it seems plausible to argue that during the expansion of *BSAS* gene family in plants, recruitment of enzymatic functions of various BSAS must be tightly connected to acclimation in hostile habitats, including drought and saline lands as well as exploitation of niches with pathogen pressures. It is furthermore interesting to pinpoint the key genetic changes and predict evolutionary mechanism that today set the basis of divergence in the functionality of various BSAS isoforms.

2.7 Aims of the research

Roles of the major OASTL isoforms in sulfur assimilation and cysteine biosynthesis have been widely accepted and clearly demonstrated in recent studies (Haas et al., 2008; Heeg et al., 2008; Watanabe et al., 2008a; Krueger et al., 2009). Previously, an ethylmethane sulphonate (EMS) induced single nucleotide substitution was identified in the *OASTL-A1* gene in the L*er*-0 accession of *Arabidopsis*, which was found to cause an early leaf death phenotype/autonecrosis under non-stressed growth conditions, was referred to as *onset of leaf death3(old3-1)* (Shirzadian-Khorramabad et al., 2010). OASTL-A1 encodes high OASTL activity and provides resistance to cadmium toxicity. The old3-1 mutation caused a dysfunctional enzyme and this was

consistent with the development of intolerance to cadmium toxicity in the *old3-1* mutants. Interestingly mutation in another BSAS isoform encoding *DES* has been also shown to cause early senescence and premature leaf yellowing (Alvarez et al., 2010). However the mechanistic basis of premature leaf senescence and cell death in *bass* mutant remained obscured in the previous and recent studies (Jing et al., 2002; Alvarez et al., 2010; Shirzadian-Khorramabad et al., 2010; Alvarez et al., 2012b). The aim of this study was to characterise the basis of the mechanism of activation of cell death associated with a dysfunctional OASTL-A1 under non-stressed growth conditions. The study mainly comprised of different genetic, biochemical and metabolic approaches to identify the link between cysteine metabolism, an OASTL isoform and pathways of cell death which could help in understanding the molecular basis of the phenomenon in the *bsas* mutants.

Blank Page

Chapter 3

Materials and Methods

3.1 Plant Lines

Wild-type *Arabidopsis* accessions used in the study are Col-0 and L*er*-0. Col-0 is the reference accession in *Arabidopsis* whose whole genome sequence is well–drafted and annotated (www.arabidopsis.org/ TAIR). Col-0's origin is from Colombia, North America. L*er*-0 is one of the widely studied *Arabidopsis* accession after Col-0, whose origin is from Landsberg, Germany, Europe. L*er*-0 is the abbreviation of Landsberg *erecta*, where errecta is the EMS induced mutation in the *ERRECTA* gene of the Landsberg accession. Thus L*er*-0 itself is not a wild-type accession and is derived after mutation of the La-1 or Landsberg accession.

Mutant lines used in this study are, 1) *old3-1*, 2) *old3-2*, 3) *old3-1*^{rec}, 4) *old3-2 odd-ler.* 1) The *old3-1* mutant, also known as the *old3-1 odd-ler*, is an EMS mutant in the L*er*-0 genetic background and is described in detail in Chapter 4. The *old3-1* mutant is homozygous for the *old3-1* and *odd-ler* region. The *old3-1* mutant has a dysfunctional oastl-a1 /old3-1 protein (Jing et al., 2002; Shirzadian-Khorramabad et al., 2010). 2) The *old3-2* or *oas.a1.1* mutant line is a T-DNA knock-out of *OASTL-A1/At4g14880/OLD3* gene in Col-0 genetic background and has been previously characterised in various studies (Lopez-Martin et al., 2008; Watanabe et al., 2008a; Shirzadian-Khorramabad et al., 2010). 3) The *old3-1*^{rec} mutant line has a mixed Col-0 /L*er*-0 genetic background and is homozygous for the *old3-1* and *odd-col* region/locus. This line was prepared in another study and previously referred to as *old3-1 odd-col* (Shirzadian-Khorramabad et al., 2010). 4) The *old3-2 odd-ler* line is homozygous for the *old3-2* and *odd-ler* region/locus

and contains a mixed Col-0 / L*er*-0 genetic background. The *old3-2 odd-ler* line was prepared in this study. This was achieved by crossing L*er*-0 with the *old3-2* mutant (Lopez-Martin et al., 2008; Watanabe et al., 2008a). The F1 progeny samples were genotyped for the *old3-2* and *odd-ler* region/locus and plants were selected. Primers used for genotyping are listed in Appendix 4.6. (sub-section-Genotyping). From the F2 population of the cross, more than four different seedlings were identified which were homozygous for both the *old3-2* and *odd-ler* alleles. These lines are referred here as the *old3-2 odd-ler* lines.

3.2 General plant growth conditions

Seeds were sterilized according to methods described (Weigel and Glazebrook, 2002) and vernalized at 4 °C in dark for 3-4 days. Mutant and wild-type seedlings were grown, in wet Seed Raising Mix® from Orderings (autoclaved and dried prior to use), at 28 °C or 21 °C (as indicated) in 60% Relative Humidity (R.H) in Long Days (L.D.) conditions (16hrs Day light of 280µE and 8hr dark). For short days (S.D.) plants were grown at 21 °C (8 hr day light of 280µE and 16 hr dark) in 60% Relative Humidity.

3.3 Metabolic profiling and enzymatic activities

The plants lines, Col-0, *old3-2*, the *old3-1* mutant, L*er*-0 and *old3-1*^{rec} were prepared and sent to the Max Plank Institute of Germany for the experiment of metabolic profiling and analysis of enzymatic activities. The growth experiment, metabolic profiling and enzymatic activities were performed and analysed by Mutsumi Watanabe in Germany. Plants were cultured on soil (type 'GS-90 Einheitserde', Gebrüder Patzer, Germany) in a L.D. growth chamber (16 h day, 140-160 mmol m^{-2} s^{-1}, 28°C; 8 h night, 28°C) for 16 days and transferred to either 20°C or kept at 28°C and grown for an additional 2-5 days. The plants were harvested, immediately frozen in liquid nitrogen, and stored at -80°C until use. Three biological replicates were harvested for each genotype at each time point. The data obtained from metabolic profiling was analysed at Massey using various software. For the hierarchal cluster analysis, the data was analysed using MeV software (www.tm4.org/mev/). Statistical analysis on the data was performed using Student's-*t* test, two-tailed type-2 error.

i) OASTL and SERAT enzymatic activity assay

Plant materials were homogenized in 5-10 volumes (fresh weight basis) of extraction buffer containing 250 mM potassium phosphate, pH 8.0, 0.5 mM ethylenediaminetetraacetic acid and 10 mM 2-mercaptoethanol. The enzymatic activity of OASTL was determined in the reaction mixture (50 µL) containing 50 mM potassium phosphate (pH 8.0), 5 mM Na_2S and 12.5 mM OAS. The reaction was performed at 30 °C for 10 min and terminated by the addition of 10 µL of 7.5% (w/v) TCA. The Cys produced was quantified by spectrophotometry using the acid-ninhydrin method at 560 nm (Gaitonde, 1967).

The enzymatic activity of SERAT was determined in reaction mixtures (100 µL) containing 50 mM Tris-HCl, pH 8.0, 1 mM acetyl-CoA, and 10 mM Ser. The reaction was performed at 30 °C for 10 min and terminated by the addition of 10 µL of 7.5% (w/v) trichloroacetic acid. SERAT activity was determined for the production of OAS, which was derivatized with *O*-phthalaldehyde using HPLC (Lindroth and Mopper, 1979; Kim et al., 1997).

ii) Protocol for measuring ion concentration

Plant materials were homogenized in 10 volumes (fresh weight basis) of 0.1 mM HCl. Samples were centrifuged for 5 min at 14,000 *g* and 4 °C. The supernatant was transferred to Ultrafree MC 5000 MC NMWL Filter Unit (Millipore, Schwalbach, Germany) and was centrifuged for 90 min at 5,000 *g* and 4 °C. After filtration, samples were diluted 10 times with de-ionized water and analyzed by HPLC with conductivity detection facilitating a Dionex ICS-2000 system (Dionex, Idstein, Germany). Ions were eluted using a KOH gradient.

iii) Protocol for measuring Cys and GSH levels

Quantitative analyses of reduced forms of Cys and GSH were performed by a combination of monobromobimane fluorescent labeling and HPLC (Anderson, 1985; Fahey and Newton, 1987). Plant materials were homogenized in 3 volumes of 0.1 M HCl (fresh weight basis) with mixer

mill. A mixture of 20 µL of extract and 40 µL of 25 mM *N*-acetyl-Cys as the internal standard was reacted with 5 µL of 30 mM monobromobimane in acetonitrile and 10 µL of 8.5 mM *N*-ethylmorpholine for 20 min at 37 °C in the dark. The labeling reaction was terminated by the addition of 10 µL of acetic acid and the resulting solution was then subjected to HPLC analysis. HPLC was carried out as described previously (Saito et al., 1994).

iv) Protocol for measuring OAS and amino acid concentrations

OAS and amino acids were extracted following a modified protocol from (Kim et al., 1997). 20-30 mg of freshly ground frozen plant tissue was extracted with 200 µL 80% (v/v), 200 µL 50% (v/v) aqueous ethanol (buffered with 2.5 mM HEPES/KOH, pH 6.2) and 100 µL 80% (v/v) aqueous ethanol. Ethanol/water extracts were subjected to HPLC analysis using a Hyperclone C_{18} base-deactivated silica (BDS) column (Phenomenex, Aschaffenburg, Germany) connected to an HPLC system (Dionex). OAS and amino acids were measured by pre-column online derivatization with *O*-phtalaldehyde in combination with fluorescence detection (Lindroth and Mopper, 1979; Kim et al., 1997).

v) Protocol for measuring secondary metabolites by GC-TOF-MS

Metabolites were extracted from aliquots of 50 mg tissue fresh weight in 2 ml Eppendorf tubes as described by (Lisec et al., 2006): by thoroughly shaking for 15 min at 70 °C in a mixture of 1400 µL methanol supplemented with 60 µL 1.3 µM ribitol in water. The supernatant was transferred to glass vial with 60 µL 1.3 µM ribitol in water. Water-soluble metabolites were separated by adding 750 µL chloroform and 400 µL water to the extract. Subsequently, the aqueous phase was transferred into to clean Eppendorf tubes. Samples were dried at room temperature by vacuum centrifugation for 3 hours. Derivatisation of the metabolites was performed by a methoxyamination reaction prior to GC-TOF-MS analysis. After baseline correction (ChromaTOF software version 1.00, Pegasus driver 1.61, LECO, St Joseph, MI, USA), peak heights of the mass (m/z) fragments were normalized to the internal standard (ribitol) and fresh weight of the samples. Annotation of the mass fragments was manually

supervised using TagFinder (Luedemann et al., 2008). These experiments were compliant with the recommendations given for metabolomics in (Fernie et al., 2011).

vi) Protocol for measuring secondary metabolites by LC–ESI–MS

Secondary metabolite analysis by LC-MS was performed as described previously (Tohge and Fernie, 2010). All data were processed using Xcalibur 2.1 software (Thermo Fisher Scientific, Waltham, USA). The obtained data matrix was normalized using the internal standard (isovitexin, CAS: 29702-25-8). Metabolite identification and annotation were performed using comparison with the previous publications, metabolite databases, and standard compounds. These experiments were compliant with the recommendations given for metabolomics in (Fernie et al., 2011).

vii) Protocol for measuring sugar concentrations

Plant materials (20-30 mg) were extracted in 1 mL of 80% (v/v) ethanol at 80 °C for 1 hour, and centrifuged at 20,000 g for 15 min. Sugars were detected as described by (Stitt et al., 1989) with volumes adapted to a microplate format. 50 µL of extract was incubated with 150 µL of reaction mixture (15.5 µL buffer containing 80 mM HEPES, pH 7.0, 3 mM magnesium chloride, 480 µL of 45 mM NADP, 480 µL of 100 mM ATP and 60 units Glc6P dehydrogenase grade II). Hexokinase (0.9 units), phosphoglucose isomerase (0.2 units), and invertase (1 µL of the enzyme powder re-dissolved to saturation) were successively added. Sugar levels were quantified by spectrophotometric measurement at 340 nm.

viii) Protocol for measuring starch levels

Starch levels were measured as described previously (Hendriks et al., 2003). Plant materials (20-30 mg) were homogenized twice in 1 mL of 80% (v/v) ethanol at 80 °C for 1 hour. For starch determination, the pellets of the ethanol extraction were solubilized by heating them to 95 °C in 0.2 M NaOH for 30 min. After acidification to pH 4.9 with an HCl/sodium-acetate, pH 4.9, part of the suspension was digested overnight with amyloglucosidase and alpha-amylase. The glucose

concentration of the supernatant was then used to assess the starch concentration of the sample (see Determination of sugar concentration).

ix) Determination of chlorophyll contents

Plant materials were homogenized in 100 volumes (fresh weight basis) of absolute ethanol. After centrifugation at 2500 g for 5 min, the chlorophyll in the supernatant was quantified by spectrophotometric measurement at 652 nm (Bruinsma, 1961). For determination of chlorophyll a and chlorophyll b contents, plant materials were homogenized in 100 volumes (fresh weight basis) of 80% (v/v) ethanol. After centrifugation at 2500 g for 5 min, the chlorophyll in the supernatant was quantified by spectrophotometric measurement at 645/655 nm.

x) Protocol for measuring for measuring soluble protein levels

Plant materials were homogenized in 10 volumes (fresh weight basis) of extraction buffer containing 250 mM potassium phosphate, pH 8.0, 0.5 mM ethylenediaminetetraacetic acid, and 10 mM 2-mercaptoethanol. Soluble protein amounts were measured with the Bio-Rad Bradford reagent (Bio-Rad Laboratories) according to the manufacturer's instructions.

3.4 Histochemical staining

Trypan blue and DAB staining for cell death and reactive oxygen species, respectively, were performed as described previously (Parker et al., 1993; Thordal-Christensen et al., 1997).

3.5 DNA and RNA extractions

The DNA extraction was performed on frozen leaf tissues using method from (Dellaporta et al., 1983). Quantitative and qualitative analysis of genomic DNA was preformed using NanoDrop ND-1000 Spectrophotometer and by running at 1-2% TAE Agarose Gel at 100-110 V for 60-80 mins.

Total RNA was isolated from frozen powdered leaf tissue using the Trizol Reagent (Life Technologies-Invitrogen) according to the manufacturer's instructions. Total RNA was also isolated using Zymo RNA extraction kit and used for real-time transcriptional analysis. Quantitative and qualitative analysis of RNA was preformed using NanoDrop ND-1000 Spectrophotometer (at 260/280 and a 260/230 nm ratio) and by running at RNA TAE Agarose Gel at 80 V for 40 mins. RNA gels were prepared in RNAse free apparatus.

3.6 Polymerase Chain Reactions (PCRs)- Genomic, Real-time and Site-directed mutagenesis

Polymerase Chain Reactions (PCRs) were carried out using high fidelity Taq polymerases (ExTaq and LaTaq enzymes) provided from TaKaRa Bio Inc., Taq Polymerase-PCR Master Mix (Promega Co.), KAPA Hi-Fi polymerase (Kapa Biosystems), Expand Reverse Transcriptase and Expand High Fidelity (Roche Applied Sciences). Primers were ordered from Invitrogen and Integrated DNA Technologies (IDT) and 10µM primer concentration was used as working solution. PCR reaction cycles were carried out at variable annealing temperature for the primers listed in Appendix 4.6. Reactions with various enzymes systems were performed according to the protocols provided by the companies. Amplified DNA fragments were scored by running at 0.8-1% agarose gel along with 1 kb Hyperladder and viewed under BIORAD UV Gel-Doc. PCR product cleaning was carried out using SureClean Plus Kit from BIOLINE and ExoSAP-IT PCR clean-up kit from GE Healthcare.

Typical PCR reactions were set as; 95 °C/ 3 min: 30cycles (98 °C/ 10 secs ; 50-58 °C/30 sec; 68-72 °C/ 1 min/kb): 68-72 °C/5-10 mins: 4-10 °C forever. For genetic fragments <2kb following reaction was employed; Promega MM = 12.5 µL + Primer Sens and Anti-sense = 2 µL + DNA (~150-300 ng was 10X diluted) = 1 µL + Doubled Distilled H_2O = 9.5 µL. For genetic fragments >3kb up to 5 Kb following reaction was employed; Takara ExTaq buffer = 2.5 µL + dNTP = 2.0 µL + Primer pair Sense and Anti-sense = 2 µL + DNA (~150-300 ng was 10X diluted) = 0.5 µL + Doubled Distilled H_2O = 17.5 µL + ExTaq enzyme 0.125 µL. For Hot-start PCR, reactions were placed at higher temperatures i.e., 98 °C from ice. For genetic fragments

>6Kb following reaction was employed; Takara LaTaq buffer = 2.5 µL + dNTP = 2.0 µL + Primer pair Sense and Anti-sense = 2 µL + DNA (~150-300 ng was 10X diluted) = 0.5 µL + Doubled Distilled H_2O = 17.5 µL + LaTaq enzyme 0.25 µL. For Hot-start PCR, reactions were placed at higher temperatures i.e., 98 °C from ice.

Generally, cDNA synthesis was performed using Expand Reverse Transcriptase (from Roche Applied Sciences) according to the protocol. A ~ 1000-2000 ng of good quality RNA was used for the cDNA synthesis.

Colony PCR was performed with gene-specific primers or in combinations with vector primers using Promega MM Taq polymerase. The colony was pierced by a sterile tooth pick or yellow tip and mixed in the already prepared PCR reaction, lacking any genomic DNA. Soon afterwards the tubes were placed in the machine under hot-lid.

For Site-Directed Mutagenesis, the OASTL-A1 cDNA including 5 and 3′ UTR regions was amplified from L*er*-0 cDNA using proof-read enzyme Expand Long Reverse Transcriptase (Roche Applied Sciences) and cloned into pGEMT easy vector (Promega Co.) and was subsequently sequenced. The primers used are listed in Appendix 4.6. (sub-section-Over-expression of OASTL-A1 in plants) For site-directed mutagenesis, Site-Directed Ligase Independent (SLIM) protocol was used (Chiu et al., 2004) and modified accordingly (Hay et al., 2010). The primers used to carry out SLIM are listed in Appendix 4.6. (sub-section-Site-directed mutagenesis of OASTL-A1) and were used to induce single or two mutations, as required to obtain targeted mutagenesis.

For quantitiative real-time PCR, RNA (1.5 µg), isolated from the tissues, was treated with DNAse I (Roche Applied Sciences) and used as a template for cDNA synthesis. cDNA synthesis was performed using Superscript III Reverse transcriptase (Life Technologies-Invitrogen). The cDNA was diluted 20-fold and used as a template for quantitative Reverse Transcriptase PCR (qRT-PCR) employing a LightCycler® 480 SYBR Green 1 Master PCR labelling kit (Roche Applied Sciences) and RotorGene 3000 Real time PCR machine (Corbett Research, Sydney,

Australia). qRT-PCR was performed as described (Hunter et al., 2011). The qRT-PCR data was analysed using the standard comparative quantification equation as described (Pfaffl, 2001).

Auto-sequencing PCR was performed using BigDye™ Terminator Version 3.1 as described online at AWC website (http://awcmee.massey.ac.nz/Data/BDTv3.1_Protocol_04337035.pdf).

3.7 Vectors and Cloning

The pGEM-T Easy Vector System (Promega Co.) and pBlue-script were used as shuttle vectors for the cloning of PCR fragments. The pGreen 0229 and pGreen 0029 plasmids are binary vectors and were used for transformation into plants (Hellens et al., 2000). Maps of these vectors are provided in Appendices 4.1 and 4.2. For the over-expression of the ORF, cDNA figments were cloned into the pART7 vector (map is provided in Appendix 4.3) containing the CaMV 35S promoter cassette (Gleave, 1992). The pDAH2 vector was used for the RNA interference (RNAi) and was provided by Dr Donald Hunter, NZ Institute for Plant & Food Research, Palmerston North, NZ (map is provided in Appendix 4.4). The hair-pin construct is driven by the CaMV 35S promoter in the pDAH2 vector. The pSoup vector was also used to aid the replication of the binary vectors in the *Agrobacterium* strain. The over-expression constructs in the bacterial system were prepared in the pET32 vector (map is provided in Appendix 4.5).

PCR fragments, amplified using Taq polymerase were used for the TA cloning into the pGEM-T Easy Vector System (Promega Co.). For direct cloning into the binary vectors or RNAi vector, specific restriction sites were added in 5′ of the Sense and Anti-sense primers. PCR products obtained were gel-purified and directly subjected to enzyme restriction digestions for directional cloning in destination vectors. Restriction digestions were performed using enzymes and standard protocol from New England Biolabs, Roche Applied Sciences and Fermentas. Ligations of the PCR fragments and the open vector were performed using T4 DNA ligase according to the protocol (Roche Applied Systems).

3.8 Preparation of competent *Escherichia coli* (*E. coli)* and *Agrobacterium* cells for transformations

Ultra-Chemical competent *E. coli* (DH5*α* strian) cells were prepared using the method as described by Inoue et al. (1990). Transformations of the ligations in the Ultra-Chemical competent *E. coli* (DH5*α* strian) cells were performed using a Heat-shock method according to Inoue et al. (1990). Electrocompetent *E. coli* (DH5*α* strian) cells preparation and transformations were carried out as described in (BIO-RAD Electroporation Mannual. Electrocompetent *Agrobacterium* (*GV3101*) cells preparation and transformation was carried out by standard methods as described in BIORAD Manual and others (Weigel and Glazebrook, 2006). Chemical competent *E. coli* (NK3 strain) cells were prepared using the method as described (Inoue et al., 1990).

Transformation reactions were generally plated at LB medium plates (10g peptone+5g yeast Extract+10g Nacl + 18g Bacto-Agar/ 1000 ml water at pH 7.5: autoclaved) supplemented with appropriate selection antibiotics required for specific vectors. For blue-white screening of the colonies, which identifies positive for the insertion in the cloning site/ *Lac Z* gene of the vector, ligation reaction were plated over LB plates containing IPTG/X-Gal concentrations as described in the pGEM-T Easy Vector System I Manual (Promega Co.). Plates were incubated at 37°C overnight and positive colonies were selected using overnight blue and white screening at 4 °C. Colonies were further cultured for plasmid DNA isolation using mini/maxi prep.

3.9 Plasmid preparations

Plasmid DNA isolations were performed from *E. coli* strain culture using MINIPREP and MAXIPREP alkaline-lysis method as described (Sambrook, 2001). For transformation of the plasmids into the *Agrobacterium* or yeast strains, plasmid DNA isolations from the *E. coli* were performed with the Plasmid DNA isolation kit (Roche Applied Systems). Plasmid DNA isolation from *Agrobacterium* strain was performed as described (Wise et al., 2006). Cleaning of the

Plasmid DNA product from *E. coli* was occasionally carried out using SureClean Plus Kit from BIOLINE. Quantitative and qualitative analysis (at 260/280 and a 260/230 nm ratio) of plasmid DNA was preformed using NanoDrop ND-1000 Spectrophotometer. Restriction enzyme digestions were performed using enzymes and standard protocol from New England Biolabs, Roche and Fermentas.

For Site-directed mutagenesis, positive clones i.e., mutants were initially detected by sequencing plasmid preps from randomly selected colonies. To detect positive clones, restriction digestion was also performed on plasmid preps from various colonies. For this purpose, enzymatic sites were identified arising due to the mutations induced in the OASTL-A1 sequence. For mutations, which generated or abolished the restriction site, associated enzymes were used to cut the clones and changes in the restriction pattern were observed at 2% TAE Agarose gel to identify the positive clones.

3.10 Synthesis of constructs for RNAi, over-expression and complementation experiments

Initially, development of the RNAi and over-expression constructs was performed *in silico* cloning using the SeqBuilder Software at Plant and Food Research and Geneious software at Massey University.

The RNAi constructs were designed by amplifying 150-300 bp fragments from the genomic DNA and were subsequently cloned in a hair-pin orientation in the RNAi-vector pDAH2. RNAi cassettes were subsequently cloned into the binary pGreen 0229 (Hellens et al., 2000) Primers, used to amplify two different *RPP1*-specific sequences (A and B) and At3g44620 and At3g44610 sequences, are listed in Appendix 4.6 (sub-section-RNAi of candidate genes). Multiple *old3-1* +RNAi-*RPP1* transgenic lines were identified that rescued the necrosis phenotype using the two different *RPP1*-specific sequences. *B40-12 and B41-13* are the T3 lines and suggested to be homozygous for a single cassette insertion. This is based on the segregation ratio 3(resistant):1(susceptible) against BASTA selection in the T1 and T2 progenies. Lines from the T3 progenies which then segregated as 1(resistant):0(susceptible) against BASTA selection were

suggested to be homozygous for the T-DNA i.e., also containing the *bar* gene providing resistance against BASTA .

For the knock-down of groups of *RPP1*-like *R* genes, the putative 5 and 3' un-translated regions were identified in the *R* genes (Alcázar et al., 2009) using Augustus (http://augustus.gobics.de). These regions were aligned to identify which *R* genes show homology with each other over at least 21nt. Based on this criterion RNAi fragments were amplified that were designed to target two or more *R* genes. The RNAi constructs were transformed to the *old3-1* mutants and analysis of RNAi of one group targeting *R4*, *R7* and *R8* is shown here. Primers for specific RNAi of R genes are listed in Appendix 4.6 (sub-section-UTR specific RNAi of R genes). Multiple RNAi lines targeting the putative 3' end of *R4*, *R7* and *R8* were identified in the *old3-1* mutant that rescued the autonecrosis phenotype, while a few were found that did not completely rescue the mutant at low temperature. T1 and T0 lines were used for analysis.

For the complemetation of *R* genes in *old3-1*^{rec}, primers were designed flanking the 2kb region upstream and 0.5kb downstream of each *R* gene at the *odd-ler* region. Primers designed for each gene is listed in Appendix 4.6 (sub-section-Primers for complementation of *R* genes in *old3-1*^{rec}). Since most *R* genes ranged from 7-10 kb, including the extra region required for complementation, the *R* gene fragments were amplified using high fidelity ExTaq and LaTaq (TaKaRa Bio Inc) enzymes and were initially cloned into the pGEM-T-Easy vector. Genes were sequenced from the ends (~1kb) and were then subsequently cloned into pGreen 0229 vector.

For over-expression studies, the cDNA of OASTL-A1 and various *oastl-a1*/ *old3* mutants, generated from SLIM, were cloned into pART7 vector i.e., downstream of the CaMV 35S promoter. The 35S;cDNA;OCS-terminator cassette was then cloned into the binay pGreen 0229 vector for the T-DNA mediated transformation in plants. The constructs were transformed in the *old3-2 odd-ler* lines. For the over-expression of OASTL-A1 and oastl-al/old3 mutants in the bacterial system, the ORF from the previously cloned cDNA was amplified using proof-read Expand High Fidelity enzyme (Roche Applied Sciences) and cloned into pET32 vector for the expression in *E. coli*. The primers used for this step excludes the UTR regions (that was

previously included for the cDNA over-expression study) and are listed in Appendix 4.6. (sub-section-Over-expression of OASTL-A1 in NK3-strains).

3.11 Transformation of *Arabidopsis* plants and *E. coli*-NK3 strain

Arabidopsis were transformed with *Agrobacterium*-floral-dip method as described (Weigel and Glazebrook, 2006; Zhang et al., 2006). The *old3-1* mutant is rescued at high temperature and therefore plants were grown at high temperature for rescue in all experimental studies. However it was difficult to transform the *old3-1* mutant with the *Agrobacterium* at high temperature. This is because the bacteria damage the inflorescence at high temperature conditions. Conversely, at low temperature, the *old3-1* mutant exhibited autonecrosis and immune response which was not suitable for transformation with the *Agrobacterium*. Therefore, the *old3-1* mutants plants were first grown in high temperature as described above, until bolting and then transferred to GMO glass where plants were grown under 24 hr continuous light at 22 °C. Under these conditions, most of the time, the *old3-1* mutant grew better than growing in 21 °C (without continuous light). Nevertheless the mutant plant showed symptoms of early senescence and yellowing in leaves and therefore multiple sets of plant populations were required for successful floral-dip transformations. A high transformation efficacy was achieved through this process. Transgenic plants were selected by spraying BASTA @ 125mg/L concentration on 3-4 days old seedlings. In total 3-4 sprays were conducted to select the positive transformants. Transformants were also tested for the presence of the *bar* gene to confirm positive for the BASTA resistance. Primers for testing the presence of bar gene are listed in the Appendix 4.6. (sub-section-BASTA-resistance gene).

To test the ability of the oastl-a1 mutants to carry out cysteine biosynthesis *in vivo*, the mutants were transformed into the *E. coli*-NK3 strain, which lacks the native OASTL isoform, the CysK. OASTL-A1 and old3 mutants were cloned into the pET32 and transformed into the NK3 strains. Transformed strains were selected on the LB medium using Ampicillin as a marker for resistance provided by pET32. NK3 strains with OASTL-A1 and old3 mutants were then tested for cysteine auxotrophy by streaking on M9 minimal medium supplemented with or without cysteine. For growth analysis, plates were grown at 37 °C for 24 hr.

3.12 Genome walking for the *odd-ler* region

Sequencing of the *odd-ler* region was performed from L*er*-0 genomic DNA and previously identified L*er*-0 10G16 BAC (Paul Dijkwel's Lab, University of Groningen, Netherlands). Initial primers were designed on the basis of Col-0. Primers were designed using Primer3 (version 0.4.0; http://frodo.wi.mit.edu/) and Perl Primer software (http://perlprimer.sourceforge.net/) (Marshall, 2004) and screened for homology with Col-0 genome using FASTA tool at TAIR. Primers used for walking are listed in Appendix 4.6. (sub-section-Genome walking of *odd-ler*, BAC end-sequencing). Amplified fragments were cloned in pGEM-T Easy Vector System and 454 sequencing was performed using services from Allan Wilson Centre and Massey University. Sequence data from trace files were analyzed and aligned at SeqMan Expert Sequence Alignment software. Sequence similarity searches were performed using Clustal W (http://www.ebi.ac.uk/Tools/msa/clustalw2/) and NCBI's BlastN and Megablast Algorithms (http://blast.ncbi.nlm.nih.gov/Blast.cgi). Protein sequence analysis was performed at Predict protein Online Software (http://www.predictprotein.org/).

3.13 Analysis of the innate immune response and *R* gene expression

For temperature shift experiments plants were grown on soil (Seed Raising Mix-Oderings, NZ, autoclaved and dried prior to use) in a growth chamber under L.D. conditions (16 h day, 180µE, 8 h night) with 60% relative humidity at 28 °C for 16 days. Biological replicates were harvested at 0, 8 and 16 h after transfer to 21°C. Relative transcript abundance was determined relative to *Actin2*. Fold change values were calculated relative to 0 h. Primers used in transcriptional analysis of innate immune response-associated genes and housekeeping genes are presented in Appendix 4.6. (sub-section-Transcriptional analysis through Real-time PCR) and designed using Quant-prime (Arvidsson et al., 2008). Data are presented as the mean value with the standard deviation. Values were analysed using two-tailed type-2 error Student's-*t* test.

Primers for detection of the *R* genes were designed manually in the putative coding regions. For this purpose regions conserved in the TIR-NBS-LRR domains of the *R* genes, showing gene-specific SNPs in the amplified region were selected and the primers flanking these regions are

listed in Appendix 4.6. (sub-section-Transcriptional analysis through Real-time PCR). Primer analysis for these primers was performed in Perl-Primer (Marshall, 2004). Primer products for each of the *R* gene i.e., amplified from cDNA were sequenced to confirm the identity of the *R* genes.

3.14 *In silico RPP1* and *OASTL-A1* gene analysis

Analysis of the rearrangements of genetic sequence blocks in the *RPP1*-like *R* gene family in Col-0 (TAIR) and between *RPP1*-like *R* genes from the *odd-ler* region in L*er*-0 as described by (Alcázar et al., 2009) was done using *progressiveMAUVE* software with the auto-detect settings (Darling et al., 2010). Using low-seed weight for collinear blocks, the sensitivity of the program was increased to detect genetic rearrangements in small regions. Homologous Genetic Sequence Blocks (GSBs) are presented in similar colours. The information regarding the domains of the R proteins i.e, TIR-NBS-LRR (TNL) was obtained by alignment of the sequences with the annotated *RPP1* genes in Col-0 (TAIR) and independent protein prediction tools online. Graphics for the alignments and Mauve output files were made with Geneious software (Drummond et al., 2011).

Coding sequences for OASTL-A1/AT4G14880 in *Arabidopsis* accessions were extracted from the Arabidopsis accession data-centre of the 1001 Genomes Project (1001genomes.org/datacenter/) (Weigel and Mott, 2009) and aligned using ClustalW in Geneious.

3.15 Pathogen infections

Pathogen infections were carried out with *Pseudomonas syringae* pv. tomato *DC3000* strain as described previously (Katagiri et al., 2002). Bacteria were grown on LB plates, supplemented with rifampicin, for 24 hr at 30 °C and subsequently collected in sterile 10 mM MgCl2. The bacterial culture was adjusted to OD600 = 0.01 (5×106 bacteria ml^{-1}) for infections and sterile 10 mM $MgCl_2$ was used as the mock solution. Bacterial infection was performed via needle-less syringe in the abaxial side of the leaves of wild-type and mutant plants. Plants were grown for 4

weeks in 12 h light; 12 h dark conditions. Four-five leaves/plant and a set of 20-25 plants were infected with bacterial culture for each line. The experiment was repeated twice.

The quantification for bacterial infections was performed at 0, 2 and 4 days post-infection as described (Tornero and Dangl, 2001). Approximately 100-150 mg of tissue, pooled from each biological replicates, was crushed in 500 µl of sterile 10 mM MgCl2. A volume of 20 µl from each solution was diluted in 180 µl of sterile 10 mM MgCl2 and serial dilutions were made. This was performed for three biological replicates for each line at each time point. 3 µl from each dilution was plated on LB supplemented with rifampicin and incubated at 30 °C for 48 hrs. Bacterial counts were measured as Colony Forming Units/ CFU mg^{-1} F.W.

Pathogen infections carried out using *Pseudomonas syringae* (*Pst*) *hrpA*- strain (Roine et al., 1997; Wei et al., 2000) were performed at various concentrations as indicated and 10mM $MgCl_2$ (as mock inoculation) via syringe infiltration and spray. For this experiment, lines were sent to the Max Plank Institute of Germany, due to the unavailability of permit to modify *Pst* at Massey University facility. Yariv Brotman from Max Plank Institute, Germany helped by doing the *Pst hrpA*-experiments. Plants were grown for 6-7 weeks at short days (8 h light; 16 h dark) as indicated in the figures and the assay for disease index was performed at the 3rd day after syringae infection. Disease levels were rated from 1 (no visible symptoms) to 5 (complete water-soaking chlorosis of the infiltrated regions).

3.16 Protein-Protein interaction

The Yeast-2-hybrid system from Clontech Laboratories, Inc. was employed to test the protein-protein interaction between the old3-1 and the cytosolic SERAT1;1/SAT5 protein. cDNAs for OASTL-A1, old3-1 and SERAT1;1 were amplified from *Arabidopsis* cDNA using gene-specific primers listed in Appendix 4.6. (sub-section-Expression of plant genes in yeast). PCR products were amplified, cut with *Eco*R1 and *BamH1* and cloned into frame using the *Eco*R1 and *BamH1* sites in the appropriate bait and prey yeast-2-hybrid vectors and sequenced. The OASTL-A1 and old3-1 cDNAs were cloned into the bait vector pGBKT7 (by Dr. Xiao Song in Paul Dijkwel's lab IMBS, Massey University) and the SERAT1;1 cDNA was cloned into the prey vector

pGADT7. Expression of the OASTL-A1 and old3-1 proteins in yeast was previously confirmed by western blot analysis using the His-tag and found to be similar to wild-type (by Dr. Xiao Song in Paul Dijkwel's lab IMBS, Massey University). AH109 yeast strains carrying the OASTL-A1 or old3-1 bait plasmids were transformed with the SERAT prey plasmid. Empty prey pGADT7 was also transformed in the OASTL-A1 or old3-1 bait carrying AH109 strains and used as a control. After transformation, colonies were re-streaked on the Specific Drop-out (SD) media, -Trp –Leu, to confirm the presence of both vectors. To test the protein-protein interactions, clones were streaked on -Trp,-Leu,-His and -Leu,-Trp,X α-gal. Plates were grown for two days at 30 °C and then subsequently for 11 days at room temperature and then photographed. Yeast transformations and media preparations were performed as described in the Clontech User manual.

3.17 Microarray data analysis from the Genevestigator

The microarray data was obtained from the public database collected in the Genevestiagtor tool online (Hruz et al., 2008). Each *BSAS* gene was specifically selected for analysis of its expression under various treatments and growth conditions. The data for each gene was further filtered by manually choosing the criteria of selection. In this criterion, only those treatments were selected that resulted in $\geq$ 2-fold change in the expression of the gene. To set the statistical significance of the data, the criterion for the *P* values was set to 0.05. Results were obtained in the form of the heat map with the quantitative changes in table format. The quantitative results were then subjected to display in the graphical format.

Blank Page

Chapter 4

Genetic incompatibility involving *R*-dependent innate immune responses and a dysfunctional *O*-acetylserine (thiol) lyase (OASTL-A1)

Introduction

Cytosolic OASTL-A1 is the most abundant protein among the major OASTL isoforms in *Arabidopsis* and is highly conserved at the coding level (Wirtz et al., 2010) (Appendix 3). Furthermore it physically interacts with the sulfur-transporter protein *in vitro* and *in vivo* suggesting an intricate involvement of OASTL-A1 in affecting sulfur homeostasis in plants (Shibagaki and Grossman, 2010). These findings are consistent with the suggestion that OASTL-A1 is evolutionary selected for maintaining sulfur-homeostasis in plants. Although the cellular function of OASTL-A1 in *Arabidopsis* is not fully understood, its role in resistance to abiotic stresses has been suggested over a decade ago (Barroso et al., 1999; Domínguez-Solís et al., 2001; Noji et al., 2001; Dominguez-Solis et al., 2004; Lopez-Martin et al., 2008; Shirzadian-Khorramabad et al., 2010).

The *old3-1* mutation identified previously results in the glycine, at position 162 of OASTL-A1, to be substituted with glutamic acid which disrupted the OASTL activity of the enzyme *in vitro* (Shirzadian-Khorramabad et al., 2010) (Figure 4.1). A seedling lethal phenotype was observed in plants homozygous (Hom) for the *old3-1* mutation (*old3-1old3-1*), whereas heterozygous (Het) mutant plants (*old3-1OLD3*) produced viable seeds but showed premature leaf yellowing and senescence (Figure 4.1). The phenotype arising due to the *old3-1* mutation is however dependent

upon environment and the genotype of the plant. The *old3-1* phenotype was shown to be rescued when grown at the permissive temperature of 28 ºC but developed autonecrosis and dwarfism when grown at 21 ºC (non-permissive temperature (Shirzadian-Khorramabad et al., 2010). Similarly the *old3-1* allele was identified to cause early onset of autonecrosis in its parent accession L*er*-0 but not in the reference accession Col-0. Backcross of the Het mutant (*old3-1OLD3*) to its wild-type (Wt) L*er*-0 parent yielded a 1(Wt):1(Het) ratio in the F1 progeny while F2 progeny segregated as 1(Wt):2(Het):1(Hom) (Table 4.1). This showed that *old3-1* is a semi-dominant mutation. In contrast when the *old3-1* Het mutant was crossed to Col-0, the F1 progeny segregated as 1(Wt):0(Het), while F2 segregated as 11(Wt): 4(Het): 1(Hom) (Table 4.1). These findings suggested that the *old3-1* phenotype is affected by the genetic background, as Col-0 and L*er*-0 differed in their control of the phenotype.

Initial mapping of the *old3-1*mutation revealed that the phenotype of the mutant is linked to two markers: an SSLP marker at chromosome III and a CAPS marker at chromosome IV (Jing et al., 2002; Shirzadian-Khorramabad et al., 2010). The *old3-1* mutation was mapped to the CAPS marker at chromosome IV. Thus, in addition to *old3-1,* another natural locus in the parent background on chromosome III was identified to be required for the mutant phenotype. The natural variant allele in the *Arabidopsis* populations that was involved in autonecrosis in combination with the *old3-1* allele was designated as ***odd-ler*** (***o****l****d****3****d****eterminant* identified in parent ***ler*** /L*er*-0). Further, the results from the genetic analysis showed that the *odd-col* allele, in the Col-0 genetic background, does not result in autonecrosis when combined with the *old3-1* allele (Shirzadian-Khorramabad et al., 2010).

The *odd-ler* region was mapped using ~5,000 F2 seedlings with an autonecrosis phenotype in a cross between the *old3-1* mutant and Col-0 (Jing et al., 2002). The *odd-ler* allele was fine-mapped using SNP-based markers (Jing et al., 2002), to a ~52 kb genomic region on chromosome 3, flanking the At3g44600 and At3g44630 genes in the Col-0 genome. In Col-0, this region is referred to as *odd-col* and contains 5 annotated open reading frames (Appendix 5). The map of the region and the identity of the *odd-ler* allele however remained unknown (Shirzadian-Khorramabad et al., 2010).

The nature of genetic interaction between the *old3-1* and the *odd-ler* allele was found to be dosage dependent i.e., strictly dependent upon the number and ratio of interacting alleles and is described in Table 4.1. A lethal phenotype was observed in plants when the alleles at both loci were homozygous i.e., *old3-1old3-1* and *odd-lerodd-ler*. However, when either of the locus was heterozygous in comparison to the other locus i.e., *old3-1old3-1 odd-lerodd-col* OR *old3-1OLD3 odd-lerodd-ler*, the plants showed an intermediate phenotype i.e., they survived but showed late-onset of necrosis (Table 4.1). No obvious phenotype was observed if both loci were heterozygous i.e., *old3-1OLD3 odd-lerodd-col*. It is to be noted that the autonecrosis was linked to only two loci.

Moreover, autonecrosis was also observed among the the F1 hybrids obtained by crossing the *old3-1* mutant with other *Arabidopsis* accessions (Shirzadian-Khorramabad et al., 2010). While the *old3-1* mutation did not result in onset of autonecrosis in the genetic background of various other *Arabidopsis* accessions, a few of the tested crosses showed the mutant phenotype (Table 4.2). This implicated that a few other *Arabidopsis* accessions may also contain *odd-ler* like alleles that resulted in negative epistatic interaction with *old3-1*. This was supported by showing that *old3-1* resulted in autonecrosis in *Arabidopsis* accessions that are positive for an *odd-ler*-specific marker but not in accessions that are positive for an *odd-col*-specific marker (Table 4.2,).

Based on the quantitative nature of the *old3-1 odd-ler* genetic interaction observed for the gene-dosage effect, a two-locus model of genetic incompatibility and effect on plant growth is therefore proposed (Figure 4.2). The interaction resembles the genetic incompatibility model that proposed by Dobzhansky and Muller (DM) (Coyne and Orr, 2004). The DM model first proposed that the genetic antagonism arises due to negative epistatic interactions between at-least 2 genes, one from each of the 2 parents (Coyne and Orr, 2004). The mechanisms underlying the DM type incompatibility are diverse and links to the functions of the genes involved in this interaction. In this study, the genetic map of the *odd-ler* region was determined and the candidate *odd-ler* genes were identified and characterised. Further, the causal mechanism of autonecrosis was explored by doing transcriptional analysis of the genes associated with the function of the *odd-ler* locus which activates hypersensitive response (HR) and cell death in the *old3-1* mutants.

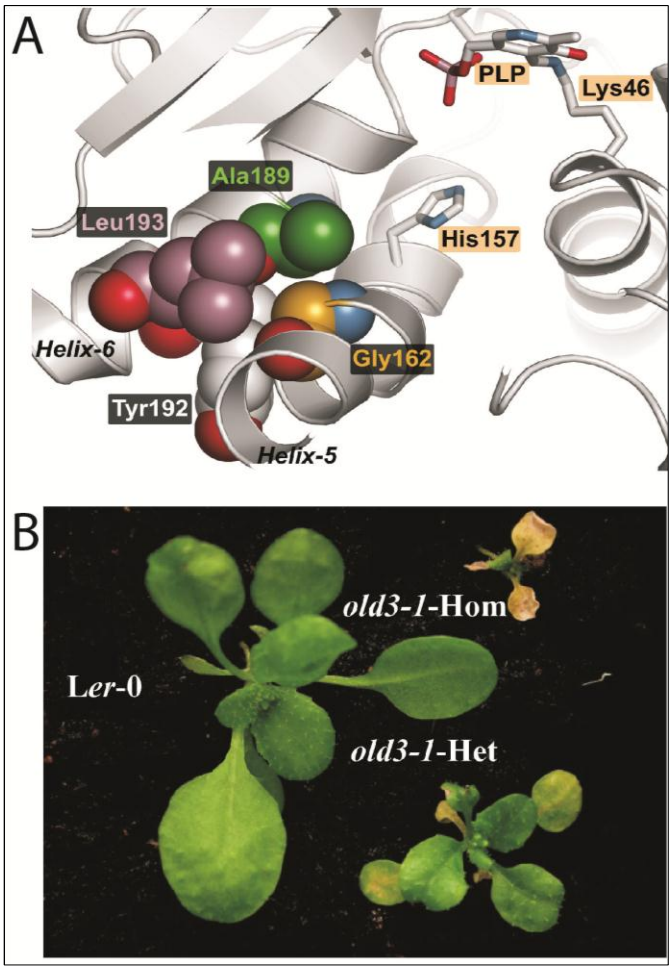

Figure 4.1. *old3-1* mutation and mutant phenotype. A. The location of Gly162 (gold) which is changed to Glu162, in α5 helix of old3-1 protein is shown. PLP is the co-factor that binds to the active catalytic site of OASTL. Lys46, the residue which forms a covalent bond (the Schiff base) with cofactor PLP and His157 which is involved in interacting with PLP are shown by stick drawings (highlighted black on orange). B. Representative wild type (L*er*-0), *old3-1* (Hom) and *old3-1* (Het) plants, grown for 21-days in standard conditions at 21 ^{o}C. Figure adapted from (Shirzadian-Khorramabad et al., 2010).

Table 4.1. Genetic and phenotypic analysis of *old3-1* mutation in different genetic backgrounds of *Arabidopsis* accessions. A. Phenotypes and segregation of F1 and F2 progeny of crosses between heterozygous *old3-1* plants and various wild-type *Arabidopsis* accessions. B. Genotypes and corresponding phenotypes of *OASTL-A1*/*OLD3* and *old3-1* in combination with different *odd* alleles. Table adapted from (Shirzadian-Khorramabad et al., 2010).

A

		F_1 phenotype		F_2 phenotype and segregation				
Male	Female	Wild type	*old3-1* Het	Wild type	*old3-1* Het	*old3-1* Hom	χ^2	Segregation
old3-1	L*er*-0	13	12	115	241	123	0.197	1:2:1
Het	Di-2	29	24	183	382	166	0.74	1:2:1
old3-1	Col-0	49	0	237	88	19	0.337	11:4:1
Het	Ws-0	53	0	341	119	32	0.18	11:4:1

B

Genotype	Phenotype
OLD3OLD3odd-colodd-col	Wild type
OLD3old3-1odd-colodd-col	Wild type
old3-1old3-1odd-colodd-col	Wild type
OLD3OLD3odd-lerodd-col	Wild type
OLD3old3-1odd-lerodd-col	Wild type
old3-1old3-1odd-lerodd-col	Het-*old3-1*
OLD3OLD3odd-lerodd-ler	Wild type
OLD3old3-1odd-lerodd-ler	Het-*old3-1*
old3-1 old3-1odd-lerodd-ler	Hom-*old3-1*

Table 4.2. Genotyping for an *odd* specific marker in *Arabidopsis* accessions. Data obtained from the thesis (Jing, 2005).

Arabidopsis accessions	Origin	F1 phenotype of cross to *old3-1* Het	Amplified fragment specific to *odd*-region (Marker flanks the region between AT3G44610 and AT3G44620)
Bu-18	Germany	*old3-1* Het	~10 kb
Di-2	France		
L*er*-0	Germany		
Wa-1	Poland		
Rsch-0	Russia		
Ak-1	Germany	Wild type	2.5 kb
Bd-0	Germany		
Bla-2	Spain		
Bs-2	Switzerland		
Col-0	USA		
Litva	Lithuania		
Mt-0	Libya		
Nok-0	Netherlands		
Rubezh	Belarus		
Tsu-1	Japan		
Wil-2	Russia		
Ws-0	Russia		

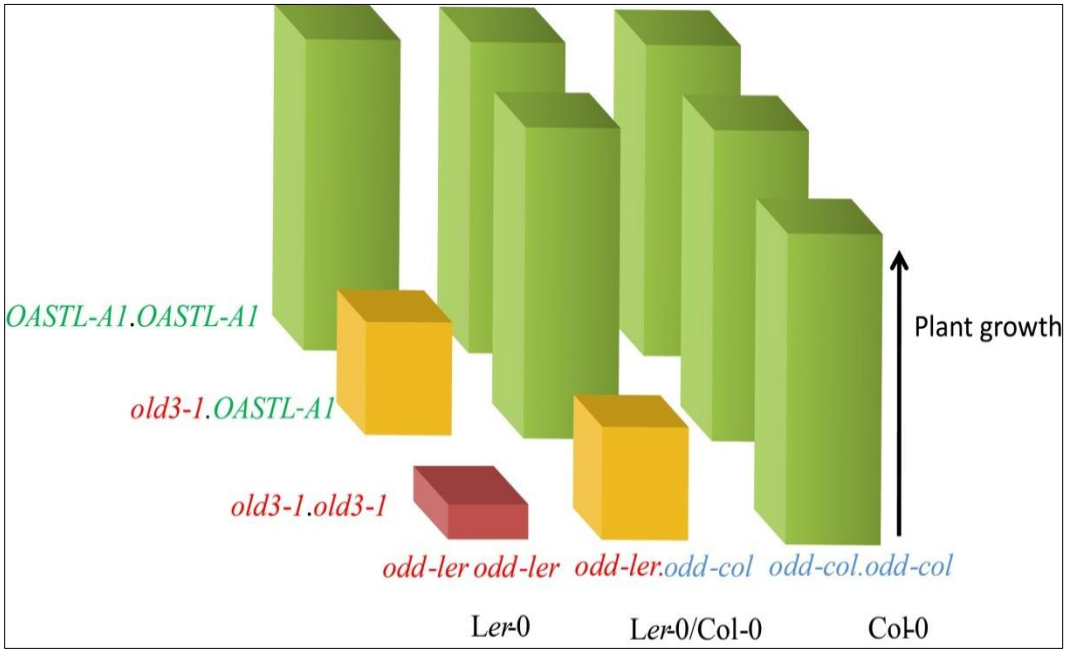

Figure 4.2. A two-locus model of negative epistasis between the *old3-1* and the *odd-ler* allele. The height of the bars represents plant growth, whereas the colour is represented as green is similar to wild-type, yellow is *old3-1* (Het) and red is *old3-1* (Hom). The OASTL-A1 alleles are on *y*-axis whereas the *odd* alleles are on *x*-axis.

Results

4.1 Autonecrosis in the *old3-1* mutant is modulated by temperature and day-length

Previously, the *old3-1* mutation was found to cause temperature-dependent autonecrosis and dwarfism. The *old3-1* autonecrosis phenotype was found to be abolished at 28 ºC as compared to 21 ºC (Shirzadian-Khorramabad et al., 2010). To identify how the variation in temperature affects the *old3-1* phenotype, the *old3-1* mutant and wild type L*er*-0 plants were first grown at 28 ºC for 16 days and was shifted to 21 ºC. Results showed that the *old3-1* mutant developed chlorosis within 4-5 days of temperature shift (Figure 4.3). These changes coincided with the reduction in further growth of the mutant (Figure 4.3).

The effect of lower temperature on the growth of the mutant was examined. When grown at 14 ºC, the *old3-1* mutant displayed a more severe phenotype, then seen at 21 °C, as the cotyledons didn't develop and the seedling turned necrotic (Figure 4.3). Thus the effect of the negative interaction between the *old3-1* and the *odd-ler* allele results in a more severe phenotype at relatively lower temperatures.

Next it was identified that autonecrosis and dwarfism was highly reduced when the *old3-1* mutant was grown at low temperature under short-day conditions (8 h light; 16 h night) (Figure 4.4). Thus day-length also modulates the onset of leaf death phenotype in the *old3-1* mutant. As both light and day-length regulated the autonecrosis, further characterisation of the mechanism associated with the autonecrosis was performed in different temperatures at long-days (16 h light; 8 h night) only.

Figure 4.3. Characterisation of the *old3-1* mutant phenotype at different temperatures. (A) shows the *old3-1* mutant and wild-type L*er*-0 plants.. Plants were grown for 16 days at 28°C and then shifted to 21°C, where further allowed to grow for 5 days to observe onset of leaf senescence. (B) shows phenotype of the *old3-1* mutant (1) as indicated by an arrow and wild type L*er*-0 (2) at 14 ºC. Bar indicates scale of 0.5 cm. The red arrow indicates the onset of reproductive phase in the *old3-1* mutant earlier than wild-types.

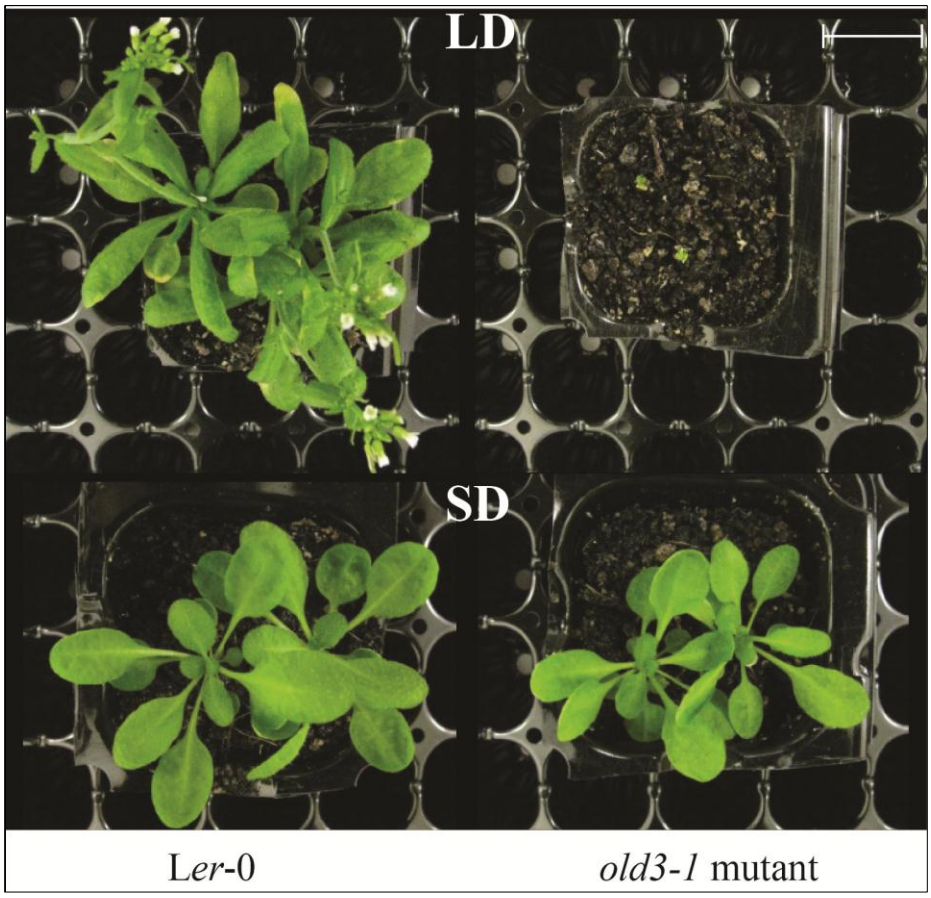

Figure 4.4. Autonecrosis in the *old3-1* mutant is modulated by day length. Phenotypes of 30 day-old L*er*-0 and the *old3-1* mutant plants grown in L.D. (16 h light/ 8 h dark) and S.D. (8 h light / 16 h dark) conditions at 21 °C. Scale bar is 2 cm.

4.2 *RPP1* gene(s) show negative epistasis to the *old3-1* mutation

The *odd-ler* genomic region required for the autonecrosis was mapped to a ~52 kb region on Chromosome 3 in the reference genome sequence of Col-0 (Shirzadian-Khorramabad et al., 2010) (Appendix 5). In Col-0, this region contains a cyclophillin protein coding gene At3g44600, a serine/threonine protein kinase coding gene AT3G44610, a protein tyrosine phosphatase coding gene-At3g44620 , 2 *RESISTANCE TO PERENOSPORA PARASITICA 1 (RPP1)* like disease resistance *R* genes-At3g44630 and At3g44670, a histone deacetylase coding gene-At3g44660 and three transposable elements (At3g44- 605, -640 and -650) (Appendix 5).

To identify potential candidates for the *odd-ler* gene, the protein coding genes in the previously mapped *odd-ler* region were sequenced. Sequencing of the At3g44610 and At3g44620 in the *odd-ler* region showed significant nucleotide variation leading towards various amino acid substitutions in the putative protein-coding gene models (Appendix 6). The primers that were designed to amplify the disease resistance *R* gene At3g44630, on the basis of genome sequence map in Col-0, did not amplify any gene fragment from L*er*-0 but were successful in amplifying the target gene from Col-0. This indicated polymorphism(s) in the L*er*-0 At3g44630 gene and therefore multiple primer sets were designed to amplify the gene in overlapping fragments. Using these primer sets, various genetic fragments were amplified. Unfortunately, these fragments showed extensive polymorphism in the *R* gene sequence and failed to overlap with each other (Appendix 6). This suggested multiple or highly diverged *RPP1*-like *R* gene(s) at the *odd-ler* region in comparison to the *odd-col* region. As *R* genes evolve rapidly in comparison to other genes (Meyers et al., 2005), the genetic variation observed in the *odd-ler* region was likely caused by the duplication, deletion or insertion of the *R* genes. Regardless, the At3G44610 (serine-threonine protein kinase), At3G44620 (encoding a protein tyrosine phosphatase) and the highly variant *RPP1*-like *R* gene(s) were identified as candidate *odd-ler* genes.

An attempt was made to silence these genes in the *old3-1* mutant using an RNAi approach. Transformation of the RNAi construct aimed for targeting the At3g44610 or At3g44620 gene in the *old3-1* mutant did not rescue the phenotype at 21 ºC (Figure 4.5). For RNAi-mediated suppression of *RPP1*-like *R* genes expression, two specific constructs were designed, named *A*

and *B*. These constructs targeted *RPP1*-specific sequences in the N and C terminal part of the *RPP1* protein-coding genes on chromosome 3 (See methods). Targeting of the *RPP1*-like *R* genes only, employing two independent constructs, rescued the lethal phenotype of the *old3-1* mutants (Figure 4.5). The rescue of the phenotype was consistent with the decrease in expression of the *RPP1*-like *R* gene(s), tested using a conserved *RPP1* specific marker (Figure 4.5).

Further the mapped *odd-ler* region was also found to overlap with Quantitative Trait Locus 3 (QTL3) which contains a cluster of 8 *RPP1*-like disease resistance (*R*) genes (Alcázar et al., 2009) in contrast to the two *R* genes present in Col-0 (Appendix 6). This confirmed the nature of *R* gene polymorphisms in the *odd-ler* region. Transcript accumulation of the *RPP1*-like *R* genes in the *odd-ler* region was therefore determined in the old3-1 mutants and rescued lines in a temperature shift experiment. Gene-specific primers were designed to the putative coding regions and tested for their ability to detect the expression of each *R* gene specifically. Measurements of the relative gene expression of *RPP1*-like *R* alleles using qRT-PCR showed that the transcript abundance of *RPP1*-like *R1*, *R2*, *R3*, *R4*, *R5*, *R7* and *R8* genes was up-regulated in the *old3-1* mutant, 24 hr post-temperature shift from 28 to 21ºC (Figure 4.6). The transcript accumulation of the truncated *R6t* allele was however not determined. In comparison, the rescued *old3-1* mutant line *B40-12* transformed with RNAi-*RPP1* construct, showed decreased transcript accumulation of all *R* genes at either growth temperature (Figure 4.6).

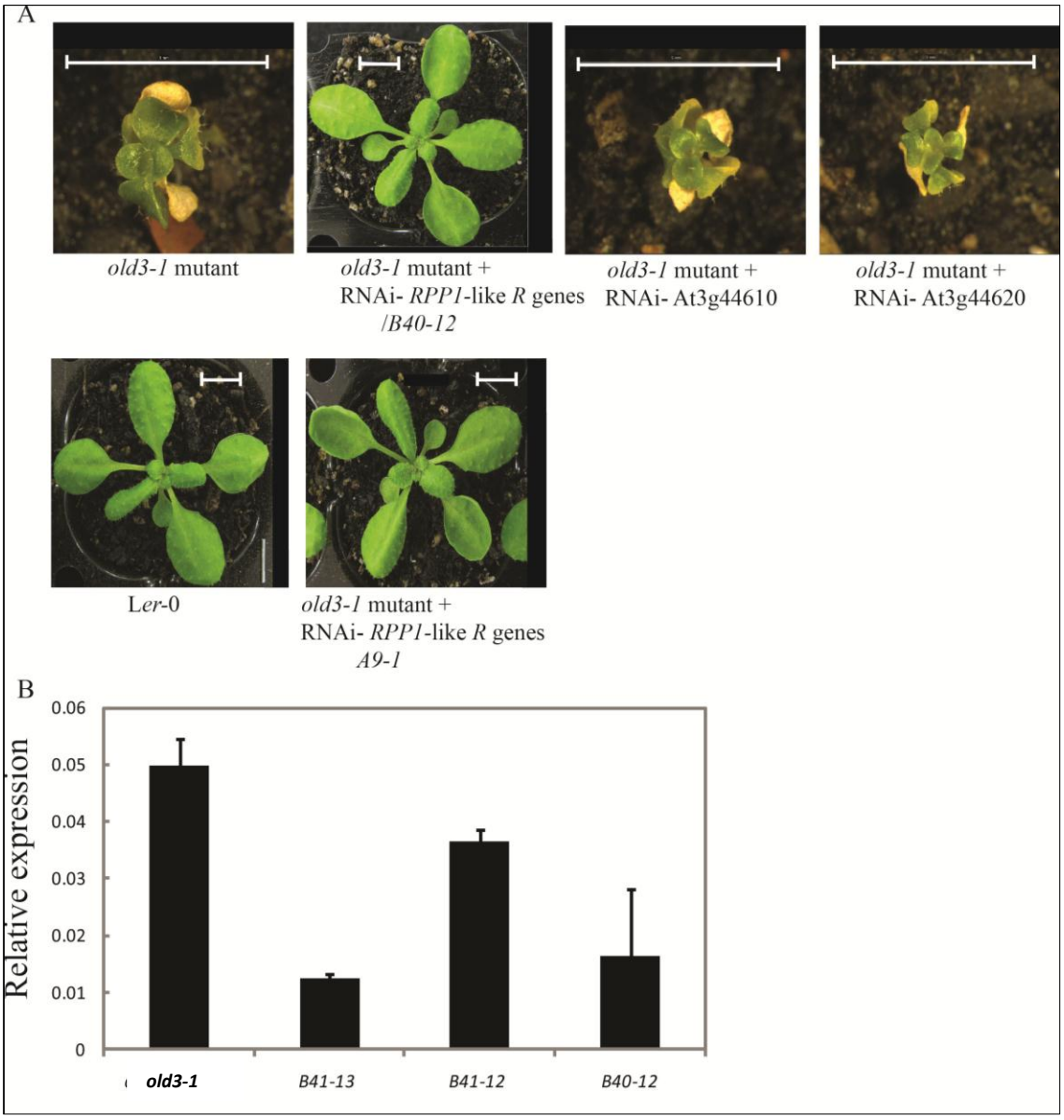

Figure 4.5. *RPP1* gene(s) show negative epistasis to the *old3-1* mutation. (A) shows phenotypes of the *old3-1* mutant, transgenic *old3-1* mutant and wild-type L*er*-0. Plants were grown for 21 days at 21 °C. Representative plants are shown. Bar indicates 5 mm. (B) shows the expression of *RPP1*-like *R* genes in the *old3-1* mutant and three T3 homozygous independent transgenic lines from construct *B*. Plants were grown for 24 days at 21 ºC and harvested for analysis. Data shows mRNA abundance of *RPP1*-like *R* genes, using an *RPP1* cDNA specific marker, relative to *Actin2*. Data are the mean of two biological replicates and each biological replicate is the mean of 3 technical replicates. Error bars represent standard deviation of the mean.

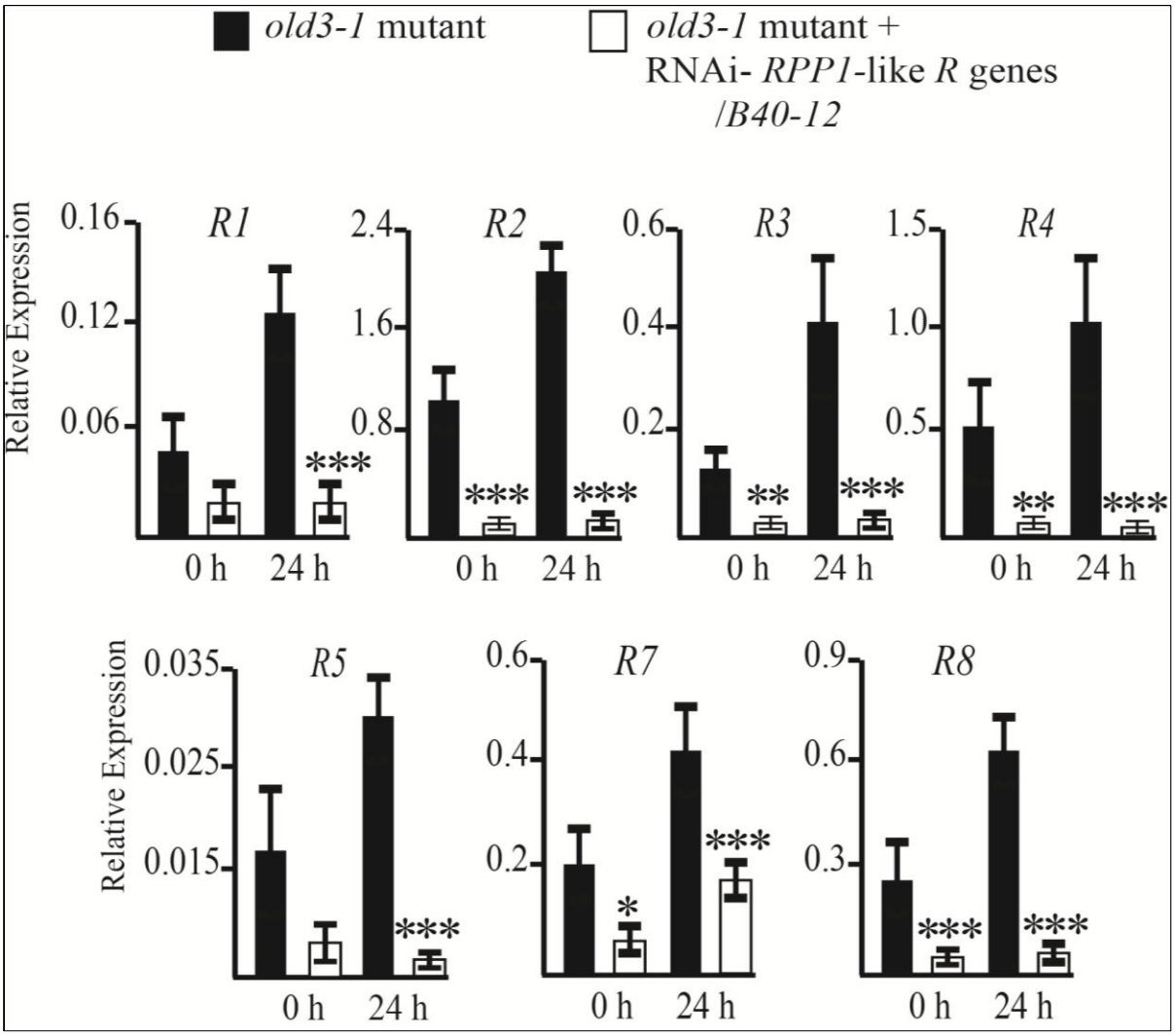

Figure 4.6. Transcript abundance of *RPP1*-like *R* genes present in the *odd-ler* region is affected upon activation of autonecrosis in the *old3-1* mutant. Figure shows the quantification of the expression of full-length *RPP1*-like *R* gene(s) in the *old3-1* mutant and the rescued line *B40-12*. Relative expression was measured by qRT-PCR using gene-specific primers at 0 and 24 hr after temperature shift from 28 to 21°C. Data represents relative expression levels of each *R* gene to the expression values of *Actin2*. The data represents mean of 3 biological replicates at each time point. Error bars represents standard deviation. Statistically significant differences in the value of the gene expression between transgenic rescued *B40-12* and the *old3-1* mutant using Student's *t* test are shown by * at $P< 0.05$, ** at $P< 0.01$ and *** at $P< 0.005$.

4.3 An innate immune response drives oxidative burst and cell death in the *old3-1* mutant but not in the *old3-1*^{rec} line

A temperature-dependent immune response was shown to be associated with the autoactivation of innate immunity (Bomblies et al., 2007). Therefore the transcript abundance of hallmarks of the R-mediated innate immune response in the *old3-1* mutants and the wild type L*er*-0 was measured during a temperature shift experiment. For this purpose the *ENHANCED DISEASE SUSCEPTIBILITY 1* (*EDS1*), *PHYTOALEXIN DEFICIENT 4* (*PAD4*) and *WRKY 18* markers were selected as they are recruited in R-mediated signalling towards the activation of immune response (Feys et al., 2001; Wiermer, 2005). In addition to these, the expression of the markers of basal disease resistance, the *ISOCHORISMATE SYNTHASE 1* (*ICS1*) /*SID2* which is involved in the production of SA and the defence related *PATHOGENESIS RELATED GENE 1*(*PR-1*), were also tested. Results showed that the transcript levels of these markers increased greatly in *old3-1* only, within 8-16 h of change in temperature (Figure 4.7; Appendix 7). These results indicated specific activation of an innate immune response signal in the *old3-1* mutant. These changes mimic an R-mediated immune response known as **E**ffector-**T**riggered **I**mmunity (**ETI**) in plant cells. R-mediated ETI can be activated upon direct or indirect recognition of pathogen effector-induced activity on various host proteins which results in host cell death at the site of infection and inhibition of pathogen growth (Dangl and Jones, 2001).

As ETI is coupled with hypersensitive response and cell death, microscopic observations of Trypan blue and Di-amino benzidine (DAB) stained leaf tissues furthermore showed oxidative burst and cell death in the *old3-1* mutants only (Figure 4.8). The results indicate that growth of the *old3-1* mutant at the non-permissive temperature leads to an innate immune response, ultimately leading to a hypersensitive response (HR)-like cell death.

To analyse the effect of the *old3-1* in the absence of the haplotype *odd-ler RPP1*-like *R* genes, *old3-1 odd-col* was examined. This line has a mixed Col-0/L*er*-0 genetic background but is homozygous for *old3-1* and *odd-col* and therefore does not show an autonecrosis phenotype (Shirzadian-Khorramabad et al., 2010). This line is referred to here as *old3-1*^{rec}. Results showed that no increase in *PR-1* expression was found in *old3-1*^{rec} tissues, even after 24 hrs of

temperature-change, consistent with no indication of cell-death or oxidative burst in this mutant line (Figure 4.9). The rescued phenotype of the transgenic *old3-1* mutant + RNAi *RPP1* also had reduced transcript abundance of defence related *PR-1* in comparison to the *old3-1* mutant consistent with reduced *R*-mediated immune response (Figure 4.9). In conclusion, the results suggest that a mutation in OASTL-A1 results in *R*-mediated innate immunity and an ETI-like response that leads to onset of leaf death.

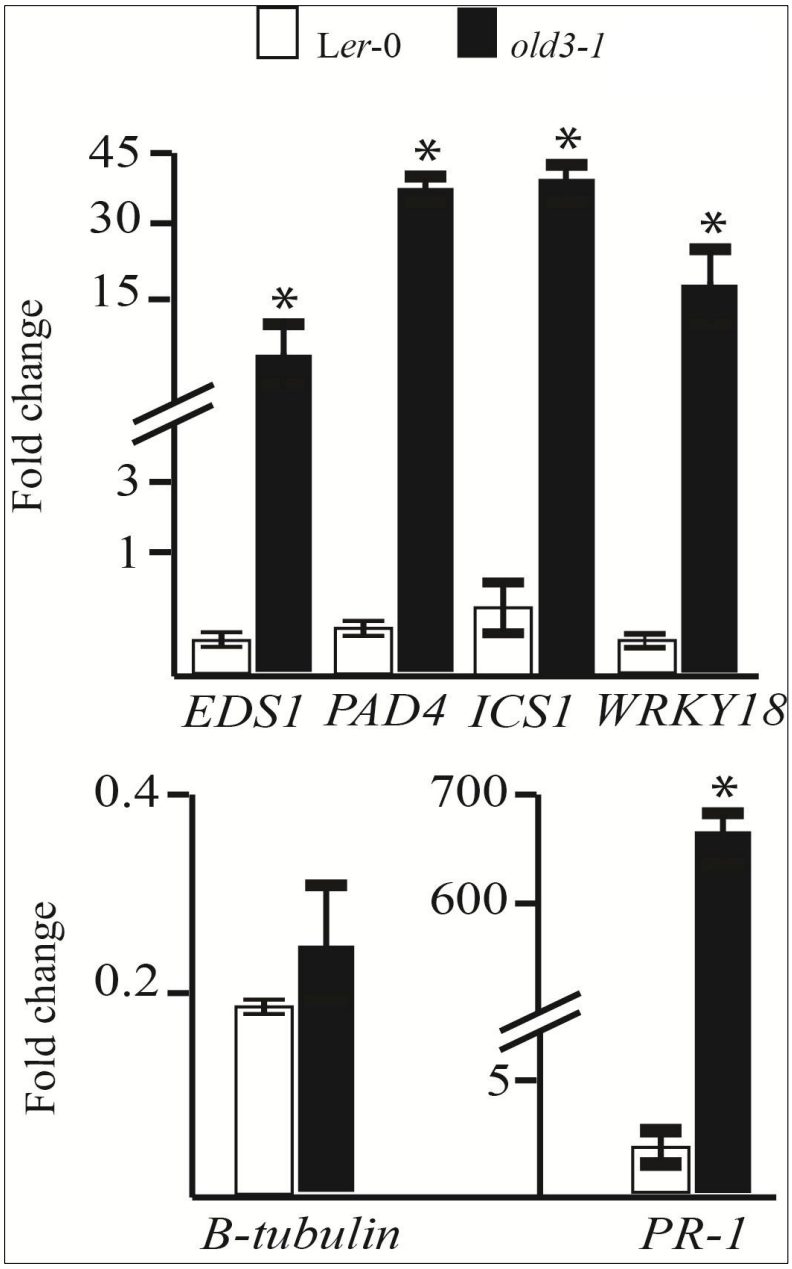

Figure 4.7. Activation of innate immune response signal in the *old3-1* mutant. Figure shows real-time quantification of the expression of markers associated with innate immune response in L*er*-0 and the *old3-1* mutant after 16 h of temperature shift from 28 to 21 °C. Expression values relative to *Actin2* were calculated and fold-change in expression values at 16 h to 0 h is presented; white and black bars represent L*er*-0 and the *old3-1* mutant, respectively. Expression of *β-tubulin* is presented as an independent control. Data represents mean of three biological replicates. Error bar represents S.D. * indicates statistically significant differences in the fold change value of the gene expression in between both genotypes using Student's *t* test ($P< 0.01$).

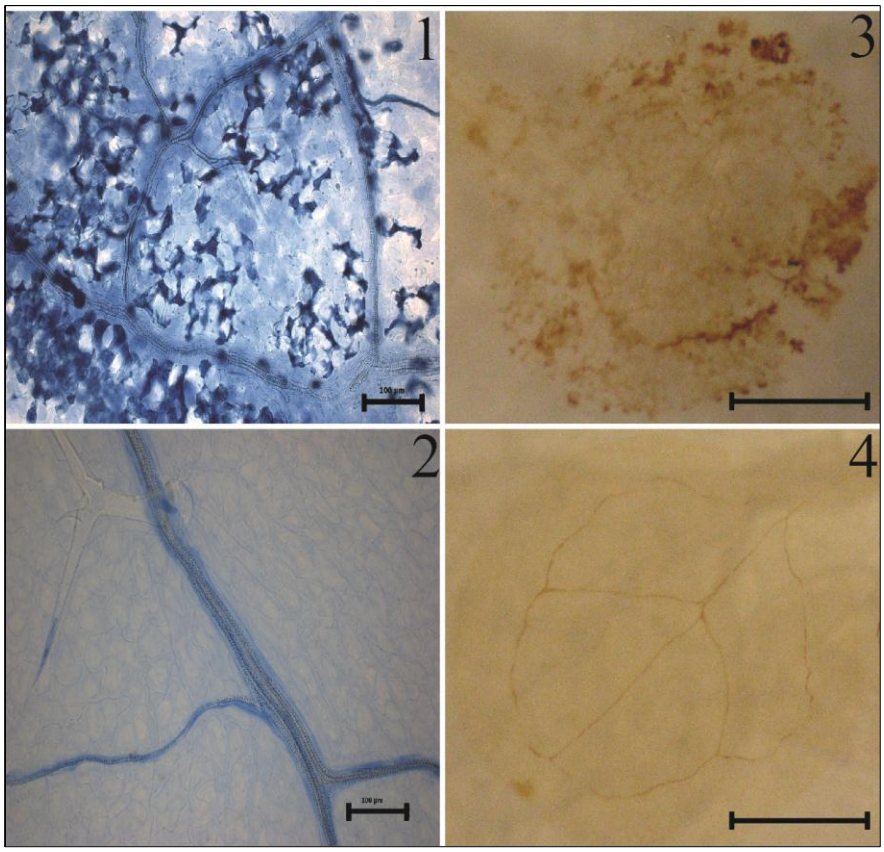

Figure 4.8. Cell death and oxidative burst in the *old3-1* mutants. Trypan blue stained leaf tissues for cell death analysis of (1) *old3-1* mutant and (2) L*er*-0 plants. Scale bar is 100 µm. DAB stained cotyledons for the detection of H_2O_2 production in tissues of (3) *old3-1* mutant and (4) L*er*-0 plants. Scale bar represents 5 mm.

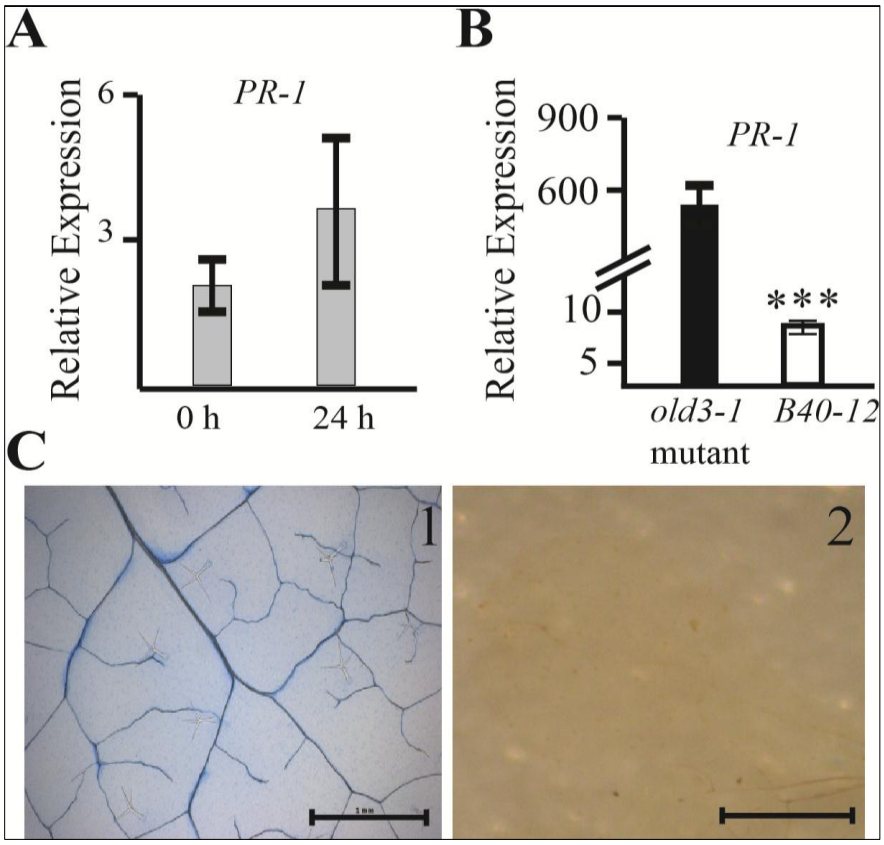

Figure 4.9. *old3-1*^{rec} does not exhibit immune response, cell death and oxidative burst. (A) shows relative expression levels of *PR-1* in *old3-1*^{rec} plants at 0 and 24 h of temperature shift. Expression values were normalised to the relative levels of *Actin2*. Expression values were tested using Student's *t* test and were insignificantly different between two time points ($P< 0.01$). (B) shows quantification of *PR-1* expression in the *old3-1* mutant and *old3-1* mutant +RNAi *RPP1*/ line *B40-12* plants 24 h post-temperature shift from 28 to 21 °C. The expression values are relative to *Actin2*. Data represent the mean value of three biological replicates. Error bars represent standard deviation. Statistically significant differences in the value of the gene expression between transgenic rescued *B40-12* and the *old3-1* mutant using Student's *t* test are shown by *** at $P< 0.005$. (C) shows (1) Trypan blue stained leaf tissues for cell death staining in *old3-1*^{rec} plants grown at 21 °C, Scale bar represent 1 mm. (2) DAB stained cotyledons for the detection of H_2O_2 production in *old3-1*^{rec} plants grown at 21 °C. Scale bar represent 5 mm.

4.4 Phylogenetic analysis of *RPP1*-like *R* genes involved in autonecrosis in the *old3-1* mutant and race-specific resistance against the downy mildew pathogen

RPP1 genes were initially found to provide ETI resistance against *Hyaloperonospora arabidopsidis*, a natural pathogen of *Arabidopsis*, which causes downy mildew disease in the plants (Botella et al., 1998). Three genetically linked *RPP1* alleles- *A*, *B* and *C* were identified in the Ws accessions of *Arabidopsis* in conferring resistance against *H.arabidopsidis*, suggesting each *R* allele is involved in recognition of a different avirulence effector (Botella et al., 1998). There are 8 *RPP1*-like *R* genes in the *odd-ler* region, however, to date, no *RPP1* alleles from L*er*-0 are characterised for resistance against *H.arabidopsidis* or autonecrosis in DM incompatibility cases. In order to understand the evolutionary relationship between the resistance conferring active *R* alleles from Ws and the clustered *RPP1* alleles at the *odd-ler* region, a phylogenetic analysis was first performed.

RPP1 phylogeny was constructed using full-length gene sequences from 2 *RPP1*-like *R* genes from the *odd-col* and *2 RPP1* genes upstream of *odd-col* on chromosome 3 in Col-0, with 8 *RPP1*-like alleles from the *odd-ler* region and three *RPP1* alleles from Ws (Figure 4.10). Results show that the *RPP1* genes from the 3 sister accessions, Col-0, L*er*-0 and Ws split into six distinct sub-clades (Figure 4.10). From the *odd-ler* region, *R8* seems to be the closest homologue of At3g44670 in *odd-col*. This is consistent with previous observations (Alcázar et al., 2009). Moreover the results also suggest that at the *odd-ler* region the *R2* and *R7* genes represent a duplication event in the ancestral gene closely related to At3g44630 in *odd-col*. None of the active resistance allele from Ws is closely related to *R2*, *R7* and At3g44630 in L*er*-0 and Col-0 respectively.

The active Ws-C *RPP1* allele is closely related to At3g44480 gene which is upstream of the *odd* region in Col-0 (Figure 4.10). The other active resistance allele Ws-*B* was found to be the closest homologue of At3g44670 and *R8* in the *odd-col* and *odd-ler* region, respectively (Figure 4.10). Finally, the *R4* in the *odd-ler* region was found to be closely related to the active Ws-*A* allele and

AT3G44400 in Col-0. These results indicated that some alleles in the *odd-ler* region are closely related to the active *R* alleles from Ws accessions as they are also present in Col-0 as well.

In contrast the L*er*-0 *R3* and *R5* appear to constitute a separate sub-clade in the *RPP1* gene family and may encode relatively new isoforms (Figure 4.10). *R6t*, however, is a truncated allele and likely a pseudo *R* gene (Alcázar et al., 2009). Only *R1* was found to be highly distinct from others, likely because of the absence of some key domains required in the function of *R* genes in its putative protein coding gene model (Figure 4.10).

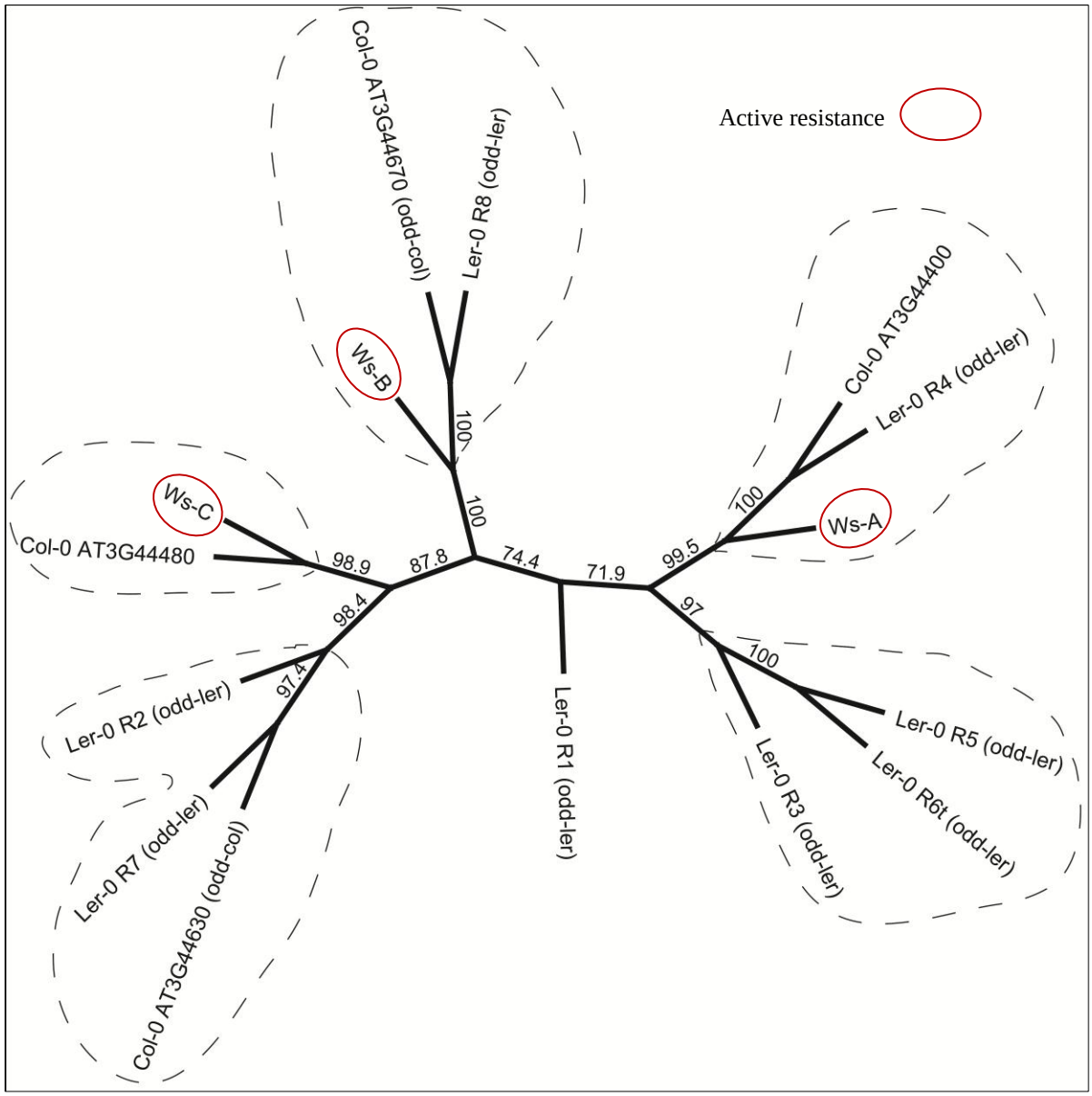

Figure 4.10. Phylogenetic analysis of the *RPP1*-like alleles in three *Arabidopsis* accessions. Figure shows a neighbouring-joining consensus tree of all *RPP1*-like alleles, from Ws, Col-0 and L*er*-0 accessions. Values at branch points show consensus support at 10,000 boot-strap values..

4.5 Genetic recombination analysis of *RPP1*-like *R* genes at the *odd* region

RPP1 genes contain Toll-interleukin-1-resistance Nucleotide Binding Site-Leucine-Rich Repeat (TIR-NBS-LRR/TNL) domains. The extent of recombination occurring within the *RPP1*-like *R*-gene family (*R1-R8*) at the *odd-ler* region and the two *RPP1*-like *R* genes present in the *odd-col* accession, At3g44630 and At3g44670, was further compared to infer recombination events within this gene family (Figure 4.11). The results are consistent with the suggestion that *RPP1*-like *R8* is the L*er*-0 homolog of *RPP1*-like disease resistance gene At3g44670 in Col-0 (Alcázar et al., 2009). However, the genetic sequences blocks (GSBs) encoding TNL domains in other *RPP1*-like *R* alleles show patterns of rearrangements with respect to two *R* genes from *odd-col* (Figure 4.11; detailed images are in Appendix 8). The GSBs for the LRR domains of the *RPP1*-like alleles at the *odd-ler* region appear to be a result of multiple recombination events, while the GSBs for the TIR domain in all *R* alleles, except *R8*, are mostly similar to that of At3g44630. The NBS domain of *R1*, *R4* and *R5*, exhibit patterns of recombination while those of *R3* and *R7* alleles and *R2* are close to that of At3g44670 and At3g44630, respectively (Figure 4.11). Thus, while extensive recombination in the LRR domains was predicted, fewer recombinations appeared to have occurred in the NBS domains, while the least recombination patterns were predicted in the TIR encoding GSBs. Therefore the evolution of new allelic variation in haplotype *R* gene clusters (Figure 4.11; detailed insights are in Appendix 8) is linked to multiple recombination and rearrangement events during evolutionary history.

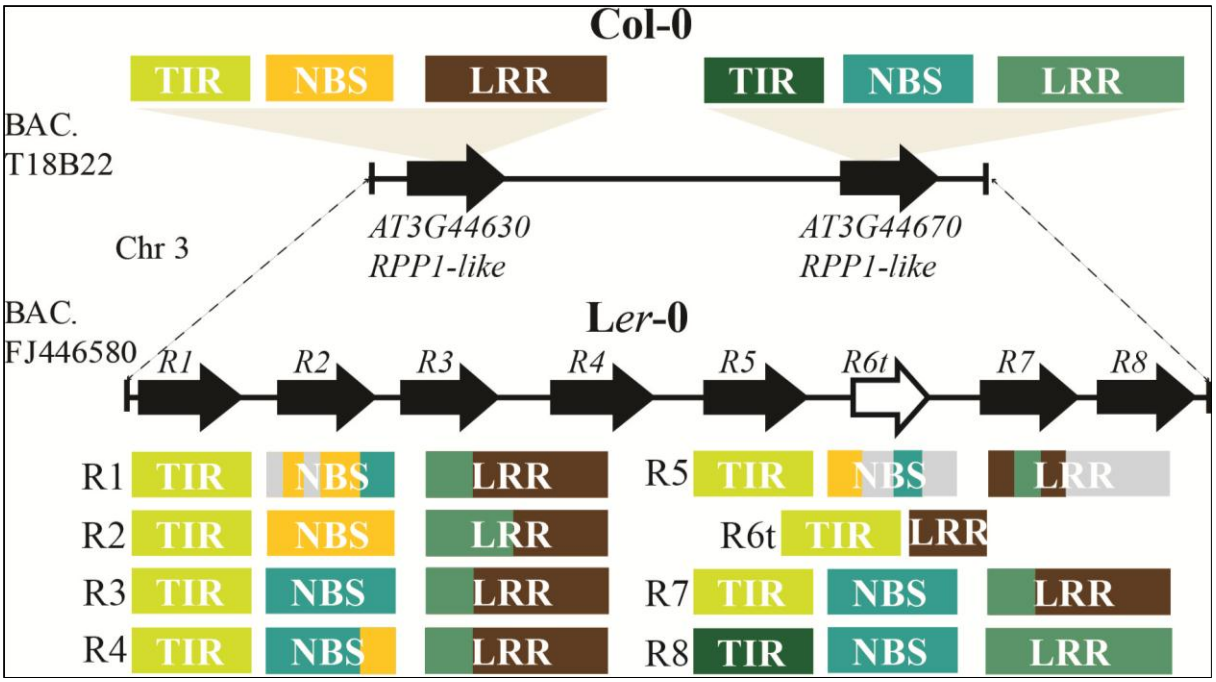

Figure 4.11. Complex evolution of TNL domains in *RPP1*-like *R* genes. Schematic representation of the 2 *RPP1*-like genes present in the *odd-col* region of Col-0 (BAC.T18B22) and 7 full-length gene models and one truncated (*R6t*-white colour) *RPP1*-like *R* genes in the *odd-ler* region (BAC.FJ446580) of L*er*-0, at chromosome 3. Lines connect markers flanking the *R* genes in the odd region. Genetic Sequence Blocks (GSBs) encoding putative TIR-NBS-LRR domains are shown. GSBs of similar colour were identified as more homologous to each other, while grey boxes represents in/dels in the alignment comparison between the 2 *R* genes at the *odd-col* region with each *R* gene from the *odd-ler* region (Detailed images of full-gene length are shown in the Appendix 8).

4.6 Identification of the potential candidate *R* gene(s) involved in autonecrosis- a complementation approach

To identify which candidate *R* gene is involved in autonecrosis, individual *R* genes from the *odd-ler* region were cloned in the *old3-1*^{rec} line. For this purpose, the 2 kb region upstream of the promoter and 500bp downstream of the stop codon of the putative *R* gene was included. *R* genes were amplified using a high-fidelity PCR TaKaRa enzyme. Only *R1*, *R2*, *R3*, *R6*, and *R8* were successfully transformed into the *old3-1*^{rec} line, individually. After transformation into *old3-1*^{rec}, multiple transgenic lines (i.e., 6-15) for each transformed gene/T-DNA construct were selected. Since expression of the candidate *R* gene from the *odd-ler* region in *old3-1*^{rec} line can activate autonecrosis phenotype, the positive transformants were screened at high temperature. Once plants were established they were exposed to low temperature and screened for the temperature-dependent autonecrosis phenotype (Figure 4.12). All the T1 plants, from each line, obtained showed phenotypes comparable to *old3-1*^{rec} i.e., without any growth defects at low temperature. Phenotypic analysis was also performed for the T2 and T3 segregating population of the transgenic lines but no plants were identified exhibiting the autonecrosis phenotype (Figure 4.12). In conclusion the results indicate that these genes, individually, may not be involved in autonecrosis in combination with the *old3-1* allele. Transformation of the *old3-1*^{rec} line with other *R* genes including *R4*, *R5* and *R7* is still awaited.

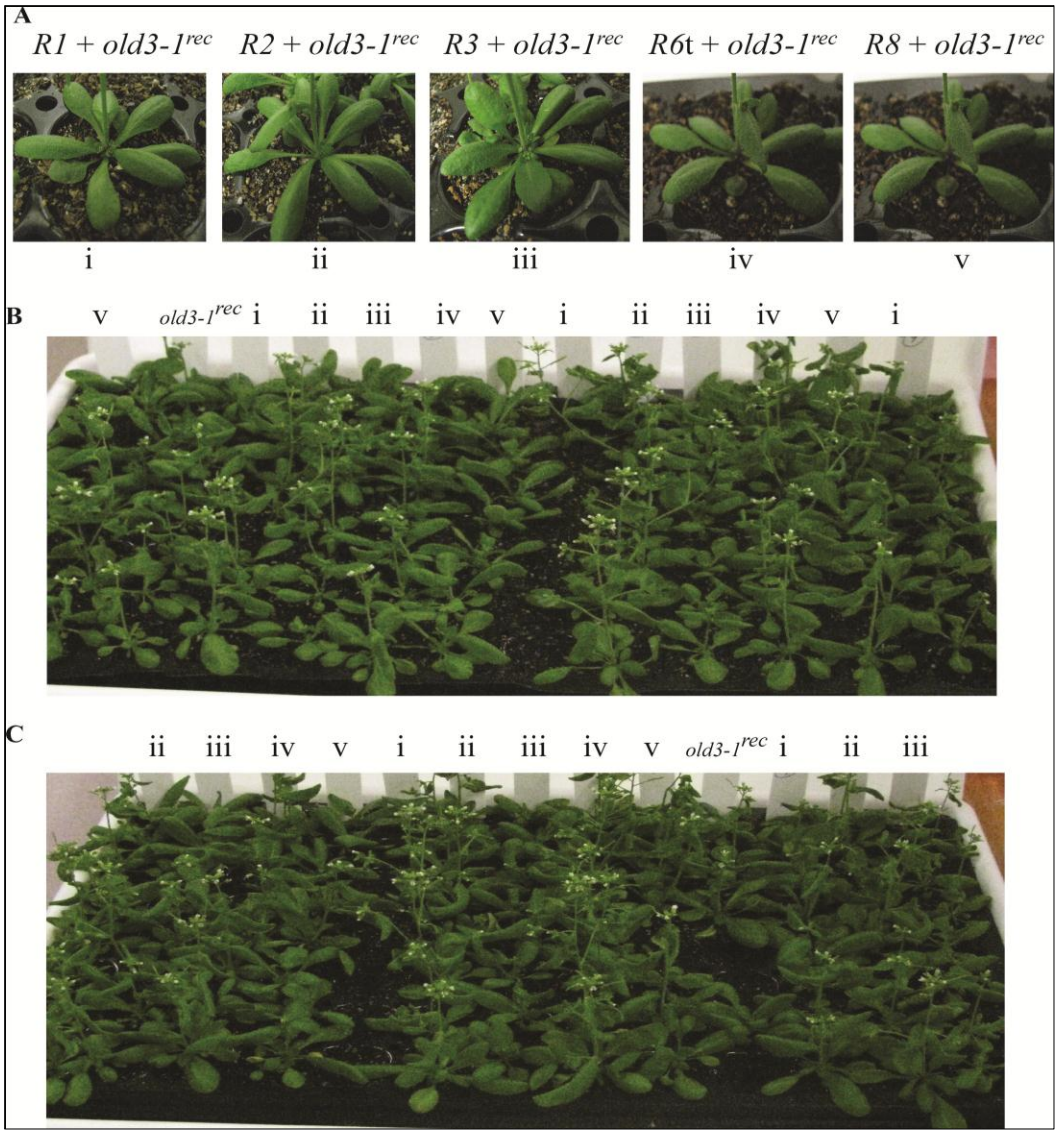

Figure 4.12. Complementation of various *RPP1*-like *R* genes from the *odd-ler* region in the *old3-1*^{rec} line. *RPP1*-like *R* genes were cloned into *old3-1*^{rec}lines. A) At least seven lines were selected for the expression of each *R* gene and screened for the necrosis phenotype at 21ºC. Figures are representative pictures of the lines. Further the segregating (B) T2 and (C) T3 population from at least seven lines was also screened for the necrosis phenotype at 21 ºC. Figures are representative pictures of the lines.

In parallel to the complementation approach of *R* genes, the RNAi-tool was also employed as an alternative strategy to identify the candidate *R* gene(s). The putative coding regions of full-length *R* genes in the L*er*-0 BAC (FJ446580) are already predicted (Alcázar et al., 2009). Due to high homology between the coding regions of *RPP1* genes, it was however difficult to target specific *R* genes for effective RNAi. Therefore, the non-coding mRNA regions were analysed for the identification of polymorphic sequences. However putative *R* genes sequences lacked this information (Alcázar et al., 2009). Therefore, *RPP1*-like *R* genes from the *odd-ler* region were first re-annotated with the various gene prediction programs (including Fgenesh, Gene Scan and Augusts) to identify putative 5′ and 3′ un-translated regions (UTRs) of the *R* genes. Using Agustus Gene prediction software, putative 5 and 3′ UTRs were identified in all *R* genes (detail of gene models in Appendix 9).

To target the putative 5′ UTR, four different RNAi constructs were designed, each targeting a different combination of *R* genes (Appendix 10). In contrast, different combinations were available for the 3′ UTR and four different RNAi constructs were designed to target the 3' UTR regions (Appendix 10). In this way a total of 8 different constructs targeting different combinations of *R* genes were prepared (Appendix 10) and cloned individually in the *old3-1* mutant. It is to be noted that the targeted region may or may not be the part of the transcribed region.

Targeting the putative 5′ UTR region, only two constructs were able to rescue the phenotype i.e., targeting *R3*, *R4*, *R5*, *R7* and *R8* or *R1*, *R2*, *R3*, *R4*, *R5* and *R7* (Figure 4.13A). Whereas the other two constructs targeting the putative 5′ UTR region of *R2* and *R8* or *R5* and *R8* did not rescue the mutant phenotype (Figure 4.13A).

Targeting the region in 3′ UTR , RNAi mediated knock down using a unique sequence present in the putative 3′ end of *R4*, *R7* and *R8* only rescued the *old3-1* phenotype (Figure 4.13B). The other three RNAi constructs, targeting putative 3′ UTR of *R1* or *R2* and *R5* or *R3* were not able to rescue the *old3-1* mutant phenotype (Figure 4.13B).

To test that the rescue of the phenotype is consistent with suppression of the targeted *R* genes, the rescued lines achieved by targeting the putative 3′ UTR of *R4*, *R7* and *R8* were analysed. Results showed a significant correlation of suppression of *R7* to the rescued phenotype as compared to the two other targeted genes *R4* and *R8* in multiple lines (Figure 4.14; Appendix 11). Transcript abundance of non-targeted full-length *R* genes was also not reduced in the rescued lines in comparison to the *old3-1* mutant (Appendix 12). The results suggest that *RPP1*-like *R7* is a candidate gene involved in autonecrosis and this requires further confirmation. Nevertheless, the possibility that other *R* genes may contribute to this genetic interaction cannot yet be conclusively ruled out.

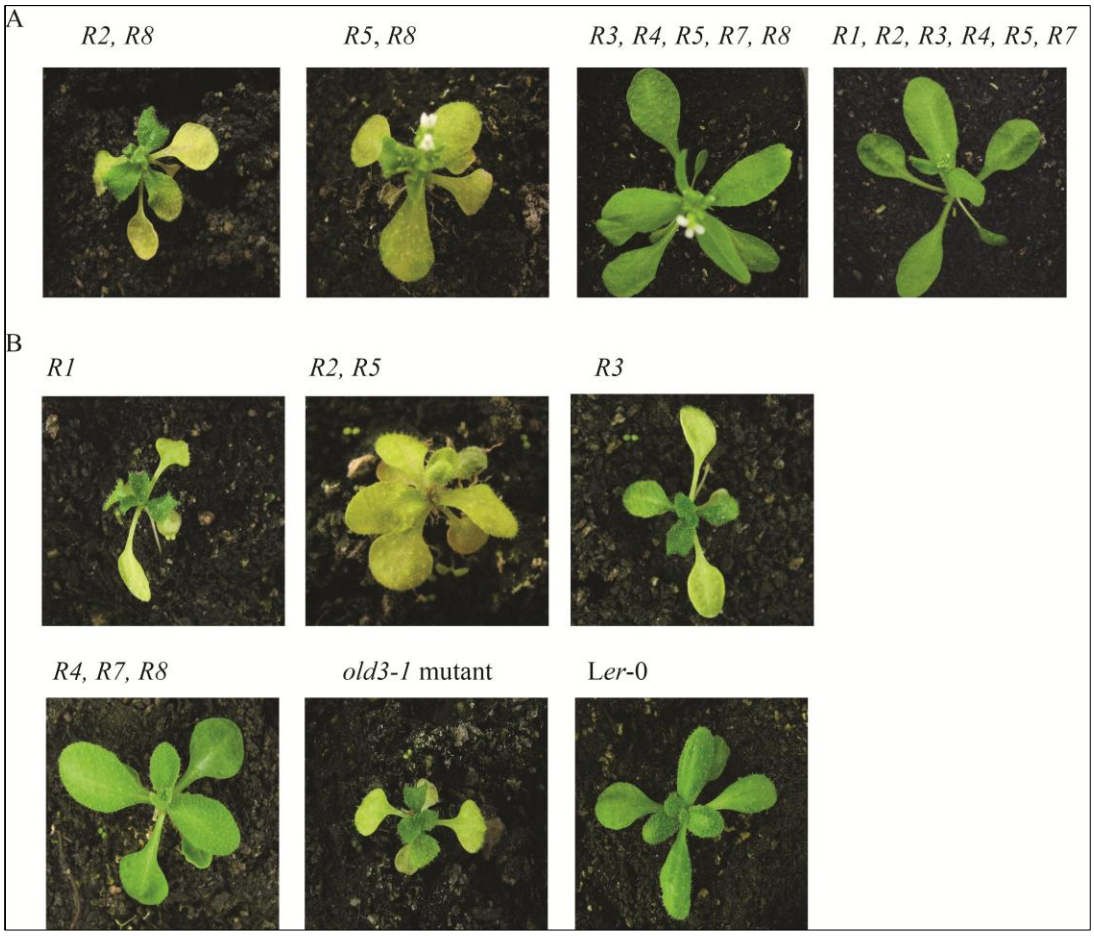

Figure 4.13. RNAi-medated suppression of specific *R* genes targeting the putative 5 and 3' UTR regions. RNAi constructs targeting the putative (A) 5' UTR and (B) 3' UTR of the specific *R* genes were transformed into the *old3-1* mutants. At least 5 transgenic lines were selected for each constructs, grown at 28 ºC and then transfered to 21 ºC to analyse the onset of chlorosis. Representative figures of the lines are shown. R gene targets of the RNAi constructs are indicated above each panel.

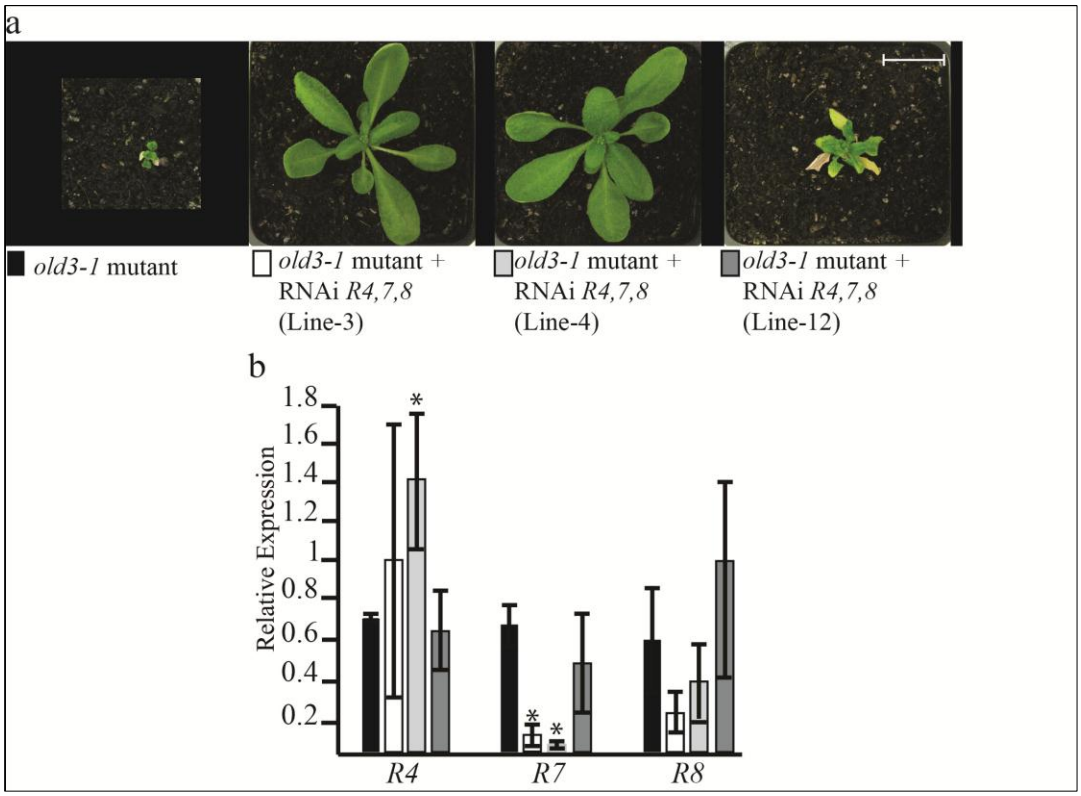

Figure 4.14. RNAi-mediated suppression of *RPP1*-like *R7* rescues autonecrosis.(A) Phenotypes of the *old3-1* mutant and 3 transgenic *old3-1* mutant + RNAi *R4,7,8* plants (Line 3, 4 and 12) containing an RNAi cassette targeting the putative 3' UTR of *R4*, *R7* and *R8*. Plants were grown for one week at 28 °C and then for 16 days at 21 °C. (B) Relative expression of *RPP1*-like genes *R4*, *R7* and *R8*. Black (*old3-1* mutant), white (Line 3), light-grey filled (Line 4) and dark-grey filled (Line 12) bars are in serial order as shown in (A). The expression values are relative to *Actin*2. Data represent the mean value of three biological replicates. Error bars represents standard deviation of the mean. * indicates statistically significant differences in mean value of each *R* gene expression within the transgenic line in comparison to the *old3-1* mutant using Student's *t* test ($P < 0.05$).

Discussion

Plant immune components and autoimmunity

The cytosolic OASTL-A1 contributes a major proportion to total OASTL activity and was found to be essential in providing resistance to oxidative stress, heavy metal and herbicide pollutant toxicity (Barroso et al., 1999; Domínguez-Solís et al., 2001; Noji et al., 2001; Dominguez-Solis et al., 2004; Lopez-Martin et al., 2008; Shirzadian-Khorramabad et al., 2010). This suggests a function of OASTL-A1 under stress conditions possibly due to increased sequestration of cysteine in various pathways involved in abiotic stress and possibly biotic stress responses as well. *RPP1*-like *R* activated autonecrosis in response to *old3-1* highlights that OASTL-A1 possibly interacts with innate immune signalling and likely *R*-driven immunity.

Immunity provides various levels of resistance against diseases by detecting agents/molecules from pathogens. The ability to detect foreign molecules is gained by continuous evolution of the immune system to detect non-self (Dubery et al., 2012). In plants, the immune system is broadly defined into two modes (Dangl and Jones, 2001; Jones and Dangl, 2006); in the first mode, the immunity can be activated upon detection of PAMPs or MAMPs via plant-based PRR proteins. This response is generally termed as PAMPS/**M**AMPs-**T**riggered **I**mmunity (P/**MTI**) and provides resistance against a number of host-specific and non-host specific pathogens which acts as a basal level of defence in plants. To counter the PTI, pathogens have evolved with the strategy of deploying a number of effector molecules/proteins through the Type-III secretion system (TTSS) inside the plant cell. Effectors can intercept and suppress P/MTI signalling or functions of other plant proteins which are involved in basal immunity and therefore manipulate host metabolism to cause susceptibility. This keeps an evolutionary selection pressure on plants to develop counter measures against effector weaponry system. Plants have therefore evolved with R proteins that can sense effector-induced changes in the host system and initiate a very strong immune response known as **ETI**. ETI activates HR and cell death at the site of host-infection, upon detection of specific effector signatures, which helps in halting pathogen growth. Although many pathogen effector molecules are released inside plant cell, detection of a single effector signature by its cognate R protein would be sufficient to activate ETI. The function of

pathogen-effector and R-mediated resistance can drive a co-evolutionary arms race between plants and pathogens which results in the evolution of plant immune system as described by the zig-zag model (Jones and Dangl, 2006).

Aberrant activation of immune response in the absence of pathogens is termed as autoimmunity. In this phenomenon, an immune system fails to differentiate between the self and non-self (Dubery et al., 2012). The phenomenon of autoimmunity is present in various organisms including mammalian species, in which the immune system is relatively more complex as compared to those of others. In mammals, autoimmunity is observed in various organs and can be chronic and life threatening (Cañas and Cañas, 2012), whereas autoimmunity in plants is observed in the whole plant and results in early death of the seedlings or leaves (Bomblies et al., 2007). Previously Bomblies et al. (2007) identified cases of dosage-dependent autonecrosis in hybrids of *Arabidopsis* accessions. Hybrids of Uk-1 and Uk-3 showed temperature-dependent autoimmune response and dwarfism. The cause of autonecrosis was revealed to be a negative epistatic interaction between an *R* gene in the Uk-3 accession with an unknown allele at the *DM2* locus in the Uk-1 accession, which was mapped to a region that includes the *odd* region on chromosome 3 (Bomblies et al., 2007). In an analogous study, a QTL3 locus that overlaps the *odd-ler* region was detected as an incompatible locus. QTL3 was found to cause a range of cell death phenotypes and autoimmunity, in the L*er*-0 × Kas-2 and L*er*-0 x Kond hybrid progenies, in combination with distant loci on chromosome 4 and 5 (Alcázar et al., 2009). Thus *RPP1* genes have been already implicated in negative epistatic interaction with the other genes from distant loci. In this study the genetic interaction which sets the basis of the *old3-1* mediated negative epistasis was dissected. The disease resistance *RPP1*-like *R* gene(s) were identified to be the second locus involved in the antagonism. RPP1-like R protein(s) auto-activate temperature-dependent innate immune responses which is the cause of cell death and oxidative burst in the *old3-1* mutants that coincides with the onset of autonecrosis. However, why RPP1 proteins activate immune response due to old3-1 remained elusive. The genetic basis of autoimmune syndrome, during intra and inter-specific hybridization in different plant species, has now pinpointed plant proteins which modulate basal defence and interact with *R*-gene innate immune signalling (Yang and Hua, 2004; Alcázar et al., 2009; Jeuken et al., 2009; Alcazar et al., 2010a; Yamamoto et al., 2010). These results support the view that *R*-mediated resistance can be based

on interaction with other host proteins (Dangl and Jones, 2001). *RPP1*-like *R7*-activated autonecrosis in response to *oastl-a1/old3-1* highlight that OASTL-A1 interacts with innate immune signalling.

RPP1 gene evolution and pathogen resistance

RPP1 alleles were initially identified in the Ws accessions of *Arabidopsis* for conferring resistance against *H. arabidopsidis* (Botella et al., 1998; Rehmany et al., 2005). *H.arabidopsidis* belongs to *Peronosporaceae* family of oomycetes which adopts an obligate parasitic life style i.e., they feed on host to complete the life cycle. Most of the pathogens from *Peronosporaceae* family cause downy mildew in major commercial crops including grapevines and tobacco. The oomycete *H.arabidopsidis* develops pathogenic relationship with *Arabidopsis* in wild and therefore provides the opportunity to study a model of co-evolutionary changes during plant-pathogen interaction (Baxter et al., 2010; Coates and Beynon, 2010). Previously it is shown that different *RPP1* alleles are involved in recognition of different avirulence effectors from *H.arabidopsidis* and activating resistance (Botella et al., 1998; Rehmany et al., 2005). Since host-pathogen interactions drive co-evolutionary selection pressures for both resistance and virulence, new *R* alleles are also evolved in plants to provide resistance against the relatively faster evolving effector molecules in pathogens (Figure 2.15) (Dangl and Jones, 2001; Jones and Dangl, 2006). The genome map of *H.arabidopsidis* is recently drafted and shows that it encodes for ~ 134 putative effector proteins i.e., containing the cell entry signal determined by effector-specific RxL motifs (Baxter et al., 2010). Interestingly a few of these effector proteins are known to cause disease in *Arabidopsis* including *Atr1* and *Atr13* against which *RPP1* alleles have been identified to provide HR resistance (Rehmany et al., 2005; Coates and Beynon, 2010). The phylogenetic analysis of the *RPP1* alleles indicates the birth/death and complex evolution of *RPP1* alleles in these accessions. Whether the evolution of *RPP1* haplotype at the *odd-ler* region is involved in active resistance against diverse virulence effector weaponry in various *H.arabidopsidis* isolates or other pathogens is yet to be investigated. Regardless, the extended haplotype *RPP1* gene family at the *odd-ler* region in contrast to Ws and Col-0 suggest selection for diverging and distinct alleles as well as conservation of a few highly similar *RPP1* homologues among these accessions.

The heterogeneity of *R* alleles at the *odd-ler* region was found to be largely in the nucleotide sequences of the gene regions encoding the LRR domain rather than the TIR and NBS-encoding regions, similar to what has been reported previously (Meyers et al., 2003; Meyers et al., 2005). Within the LRR domains, *R7* and *R8* are more like the Col-0 *RPP1*-like genes (Alcázar et al., 2009), while those of *R1, R2, R3, R4 and R5* are more diverse. The results further highlight that during genomic recombination events, polymorphism and differentiation in the LRR domains of these *R* genes is favoured. Since TIR, NBS and LRR domains are shared by a single gene, a positive selection has likely occurred for the "de-differentiation" in the TIR and NBS domains during such recombination events. This correlates well with the evolutionarily conserved role of TIR domains in downstream signalling for the activation of immune response (Staal et al., 2008; Bernoux et al., 2011). The nature of polymorphism observed within the LRR domain of RPP1 proteins from Ws was previously suggested to be correlated with recognition specificity for divergent effectors from *H.arabidopsidis* isolates and therefore translates into active resistance by *RPP1* alleles (Botella et al., 1998; Krasileva et al., 2010). Results indicate that the polymorphism observed at the LRR domain in *RPP1* alleles set the basis of evolutionary divergence in the *RPP1* gene cluster at the *odd-ler* region. Polymorphism within the LRR domain of RPP1 proteins at the *odd-ler* region may therefore be linked with different recognition specificities against divergent effector molecules.

Expansion of the immunity gene family and negative epistatic interactions-implications in the process of reproductive isolation

New species evolve once an inter-breeding population becomes reproductively isolated as a result of a physical or biological barrier. The Dobzhansky and Muller incompatibility model (DM) proposes that inviable hybrids of the two inter-breeding population appear due to negative epistatic interactions between at least two genes from the two populations (Coyne and Orr, 2004). Genes involved in DM type negative epistasis in model organisms including *Saccharomyces cerevisiae, Drosophila melanogaster* and *Arabidopsis thaliana* have been shown to exhibit faster evolutionary rates at the nucleotide level (Presgraves et al., 2003; Bikard et al., 2009; Tang and Presgraves, 2009). *RPP1* haplotypes from the *odd* region are implicated in

multiple DM-type incompatibilities in the *Arabidopsis* population (Bomblies et al., 2007; Alcázar et al., 2009; Alcazar et al., 2010a). The results here support the notion that the *odd-ler* region has evolved as a hotspot for genetic incompatibilities within the *Arabidopsis* species. It is therefore tempting to speculate that the evolution of *R* alleles at the *odd* genomic region is the cause of the incompatibility in the intra-specific hybrid lethality cases identified by Bomblies *et al*. (2007) and Alcazar *et al*. (2009), but this would need to be experimentally confirmed. The pleiotropic effects of faster evolutionary rates and new haplotypes at *R* loci, as a result of selective pressure during plant-pathogen arms race (Bomblies et al., 2007) appear to cause some of these loci to evolve DM type incompatibilities during inter- and intra-specific crosses (Krüger et al., 2002; Jeuken et al., 2009; Alcazar et al., 2010a; Mizuno et al., 2010; Yamamoto et al., 2010; Mizuno et al., 2011; Takumi and Mizuno, 2011). In this study the comparison of the *R* alleles at the *odd-ler* region suggests complex patterns of recombination and rearrangements in their genetic structure, similar to other *R* genes (Meyers et al., 2003). These genes contain diverse rearrangements in the GSB regions encoding for TIR-NBS-LRR (TNL) domains. Complex evolution of TNL domains, which may have resulted due to unequal crossing-over and gene conversions (McDowell and Simon, 2006, 2008), yielded a pool of hybrid *RPP1*-like *R* genes at the *odd-ler* region which can be categorized as a Type-I evolving *R* gene cluster (Kuang et al., 2004; Kuang et al., 2008). Whether Type-I evolving *R* gene clusters may acts as potential hot-spots to restrict gene flow in *Arabidopsis* is the next question. Regardless the inter and intra-specific hybrids of various species including rice, lettuce, tomatoes, *Arabidopsis* and wheat also showed temperature-dependent autonecrosis and implicated the involvement of disease resistance *R* genes (Krüger et al., 2002; Jeuken et al., 2009; Alcazar et al., 2010a; Mizuno et al., 2010; Yamamoto et al., 2010; Mizuno et al., 2011; Takumi and Mizuno, 2011).

Extreme genetic polymorphism is detected at the major histocompatibility locus (MHC) which encodes recognition receptors involved in innate and adaptive immune system in mammals. MHC alleles have been identified in autoimmune diseases as well (Penn and Potts, 1999; Candore et al., 2002). Extreme haplotype of MHC alleles are thought to be associated with the host-pathogen co-evolutionary arms race indicating that the nature of genetic changes and recombination events associated with haplotypes also generates autoimmunity in mammals (Penn and Potts, 1999; Candore et al., 2002). The phenomenon of autoimmunity is linked to

faster evolutionary rates of immunity genes in plants and mammals and it appears that autoimmunity has emerged as an unwanted by-product of fitness in a co-evolving host-pathogen system (Bomblies et al., 2007; Cañas and Cañas, 2012). However autoimmunity also acts as a mechanism of restricting gene flow (Bomblies et al., 2007; Cañas and Cañas, 2012) and therefore can cause reproductive isolation in plants (Krüger et al., 2002; Jeuken et al., 2009; Alcazar et al., 2010a; Mizuno et al., 2010; Yamamoto et al., 2010; Mizuno et al., 2011; Takumi and Mizuno, 2011). Since DM incompatibility sets the genetic basis of the speciation process (Coyne and Orr, 2004), autoimmunity can contribute to punctuated events which may lead to onset of reproductive isolation.

The temperature and light dependent control of autoimmunity

The effect of the temperature on the onset of autonecrosis is notable. Cases of D-M associated hybrid necrosis across species (Bordenstein and Drapeau, 2001), and in plants implicate *R* genes as D-M loci (Krüger et al., 2002; Bomblies et al., 2007; Alcázar et al., 2009; Jeuken et al., 2009; Alcazar et al., 2010a; Mizuno et al., 2010; Yamamoto et al., 2010; Mizuno et al., 2011; Takumi and Mizuno, 2011) and were shown to be temperature-sensitive. High temperature was shown to be linked with the suppression of plant defence gene expression and normal growth (Yang and Hua, 2004). The results in this study showed that within hours after induction of autonecrosis by temperature shift, expression of defence-related markers and *R* genes increased. Thus high temperature-mediated rescue may be linked to the suppression of *R* and other defence-related genes. This is consistent with previous suggestions that increased expression of *R* genes resulted in autoactivation of immune responses that also negatively affected the plant growth (Oldroyd and Staskawicz, 1998; Yi and Richards, 2007). Moreover, findings from a recent study implicates modifications , such as histone methylation, of the genomic DNA as a causal factor for an abnormally increased expression of the *R* genes and autoimmunity. This indicates that chromatin remodelling can act as a key element impacting innate immunity (Palma et al., 2010). In contrast, reduced expression of the *R* genes can result in loss of function of the R-mediated active resistance against the specific pathogen and consequently the onset of risk to disease (Eulgem and Somssich, 2007). Thus a balanced *R* gene expression must be evolutionary required to off-set the hazardous consequences associated with the autoimmunity and lack of immunity.

In contrast, an NB-LRR protein SNC1 was recently suggested to be the main component in the defence signalling pathway mediating temperature sensitivity in disease resistance (Zhu et al., 2010). The authors showed that temperature-mediated regulation of autoimmunity is controlled by specific protein conformational changes in the SNC1 R protein. Mutation in the SNC1 R protein resulted in the autoactivation of immune response even at higher temperature. This suggests that high temperature suppresses a specific signal, which is associated with the R protein conformation, required for launching the autoimmunity. The role of temperature in various cases suggests that relatively high temperatures act as "bridles" to the R-mediated signalling in plant immunity. This raises important questions such as why relatively high temperatures are evolutionary netted with off-setting various R-mediated autoimmune phenomenon among different plant species and how it impacts the evolution of plant-pathogen interaction.

In addition to temperature, day length is also an important environmental factor that modulates immunity in plants (Roden and Ingle, 2009). Results in this study show that R-mediated autonecrosis and dwarfism was far more suppressed in SD as compared to LD. As R protein(s) activate an immune response in the *old3-1* mutant, rescue at SD may be due to dampening of the plant immune responses. This is highlighted in another study, which shows that SD conditions suppress constitutive accumulation of defence-related SA and Camalexin in an *Arabidopsis* lesion-mimic mutant in contrast to LD (Chaouch et al., 2010). This is consistent with another finding which shows that SA is the required signal in causing autonecrosis and dwarfism during hybrid necrosis (Alcázar et al., 2009).

Blank Page

Chapter 5

OASTL-mediated cysteine metabolism and stress defence in *Arabidopsis*

Introduction

Cysteine acts as a key metabolite in oxidative stress and aging in mammals (Droge, 2005). However the role of cysteine metabolism and BSAS isoforms in aging and senescence of plants is yet unclear. The cytosol is a major site for cysteine biosynthesis and mutation in the cytosolic OASTL-A1 enzyme has been shown to be detrimental to plant cellular redox balance likely due to lower total cysteine (Cys) and glutathione (GSH) levels (Lopez-Martin et al., 2008). Furthermore, the transcriptomic analysis of the *oas.a1.1* mutant, lacking functional OASTL-A1, showed that genes associated with oxidative stress, senescence and phosphate starvation are also up regulated, when grown under normal growth conditions. Along with this, the expression of *R* genes, cytochrome P450, glutathione S-transferase, oxido-reductase and peroxidase encoding genes are also induced in the *oas.a.1.1* mutant (Lopez-Martin et al., 2008). These results already implicate the role of OASTL-A1 as an important component in stress signalling. Interestingly, contrary to such implications about the role of OASTL-A1, others have shown that the lack of OASTL-A1 did not severely reduce the total Cys and GSH levels as well as growth of the mutant plants is without any defects in comparison to wild-type plants (Heeg et al., 2008; Watanabe et al., 2008a). It is perhaps eminently conceivable that contrasting observations may have been related to differing growth conditions in distant research facilities.

It is hypothesized that *old3-1* is inactive *in vivo* and may alter cysteine metabolism (Shirzadian-Khorramabad et al., 2010). Lack of functional OASTL-A1 therefore could results in activation of R-mediated immune response and autonecrosis. This is already suggestive of the indispensability of OASTL-A1 function in specific accessions. To test this hypothesis, two strategies were designed in this study. In the first approach, the basis of R-mediated immune response in *old3-1* mutant was investigated by performing a genetic analysis on the *OASTL-A1* locus. In the second approach, metabolic analysis of the *old3* mutants was performed at different temperatures to identify the changes associated with different mutations in *OASTL-A1*. Moreover, the findings in the previous chapter highlight the role of OASTL-A1 in plant immunity. Therefore the plants lacking functional *OASTL-A1* were subjected to disease resistance assay to identify any changes in disease susceptibility or pathogen virulence. Finally, the microarray data available at the public database Genevestigator was investigated to identify any significant correlation between various abiotic and biotic stress treatments and transcriptional activation of other *BSAS* genes in *Arabidopsis*.

Results

5.1 Lack of functional OASTL-A1 does not cause autonecrosis in L*er*-0 genetic background

The autonecrosis phenotype could be the result of reduced enzyme activity in combination with the *odd-ler* allele. To test this possibility, two approaches were taken. As the OASTL-A1 T-DNA knock-out line was unavailable in L*er*-0, a recombinant *OASTL-A1* functional knock out line was generated in the first approach. This was achieved by crossing L*er*-0 with the *OASTL-A1* T-DNA KO mutant *old3-2*, which is identical to the previously described lines *oas.a1.1* and *bsas1;1* (Lopez-Martin et al., 2008; Watanabe et al., 2008a). The F1 progeny samples were genotyped for the *old3-2* and the *odd-ler* locus and plants were selected. These plants were raised at high temperature i.e, 28 ºC and scored for necrosis. Plants were then shifted to low temperature to observe any changes in phenotype. No necrosis was observed in the F1 population at both temperatures (data not shown). From the F2 population of the cross, more than four different seedlings were identified which were homozygous for both the *old3-2* and *odd-ler* alleles. These lines are referred to here as *old3-2 odd-ler* lines and have a mixed L*er*-0/Col-0 genetic background. The *old3-2 odd-ler* lines did not show the autonecrosis phenotype when grown at 21 ºC (Figure 5.1). The lines were also grown at 14 ºC but no necrosis phenotype was apparent in these lines (data not shown). Two of the lines were also analysed for the expression of the two *R* genes at the *odd-ler* region and the absence of the *OASTL-A1* gene expression (Figure 5.1). Thus, lack of OASTL-A1 in an *odd-ler* background is not the cause of autonecrosis. To further confirm these results in a pure genetic background, *OASTL-A1* gene silencing was attempted in L*er*-0, using an RNAi approach. To avoid the homology of the target sequences with other OASTLs, cytosolic OASTL-A1 specific sequence was chosen for RNAi. Results show that silenced L*er*-0 lines with up to 97% reduced *OASTL-A1* transcript levels also do not result in the development of autonecrosis (Figure 5.2). Thus, lack of functional *OASTL-A1* does not cause autonecrosis in the *odd-ler* genetic background.

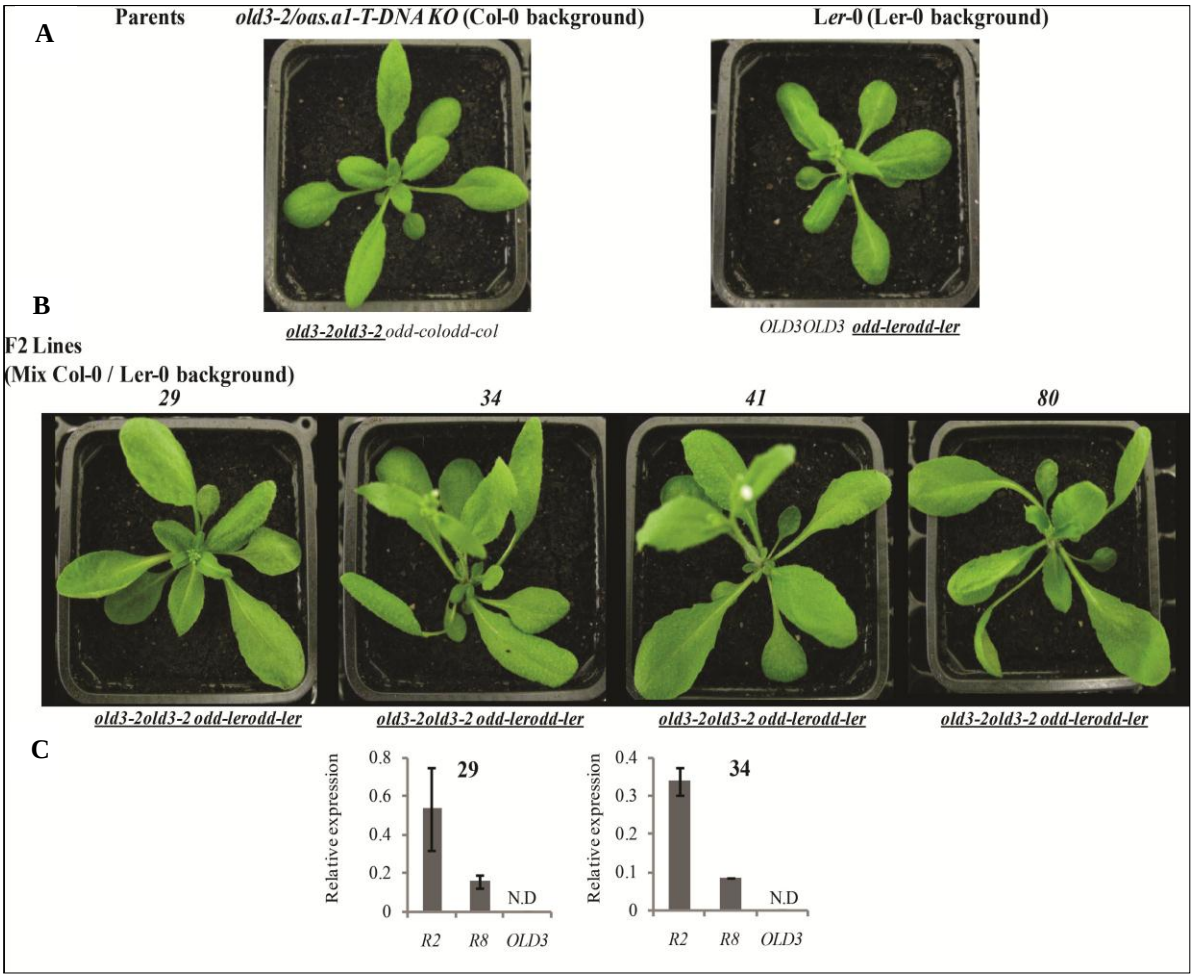

Figure 5.1. Characterization of *old3-2 odd-ler* lines at 21 °C. Figure shows A) *old3-2* and L*er*-0 plants and B) four lines homozygous for *old3-2 and odd-ler* region from F2 population when grown at low temperature of 21 ºC. F3 progenies of these genotypes and parents (*old3-2* and L*er*-0) were grown at 21 °C in L.D. condition for four weeks. C) Two of the *old3-2 odd-ler* lines (34 and 29) were also tested for expression of 2 *R* genes in the *RPP1* cluster and *OASTL-A1*/*OLD3*. Expression is relative to *Actin2* and is mean of two biological replicates. Error bar represents standard deviation. N.D. is non-detectable.

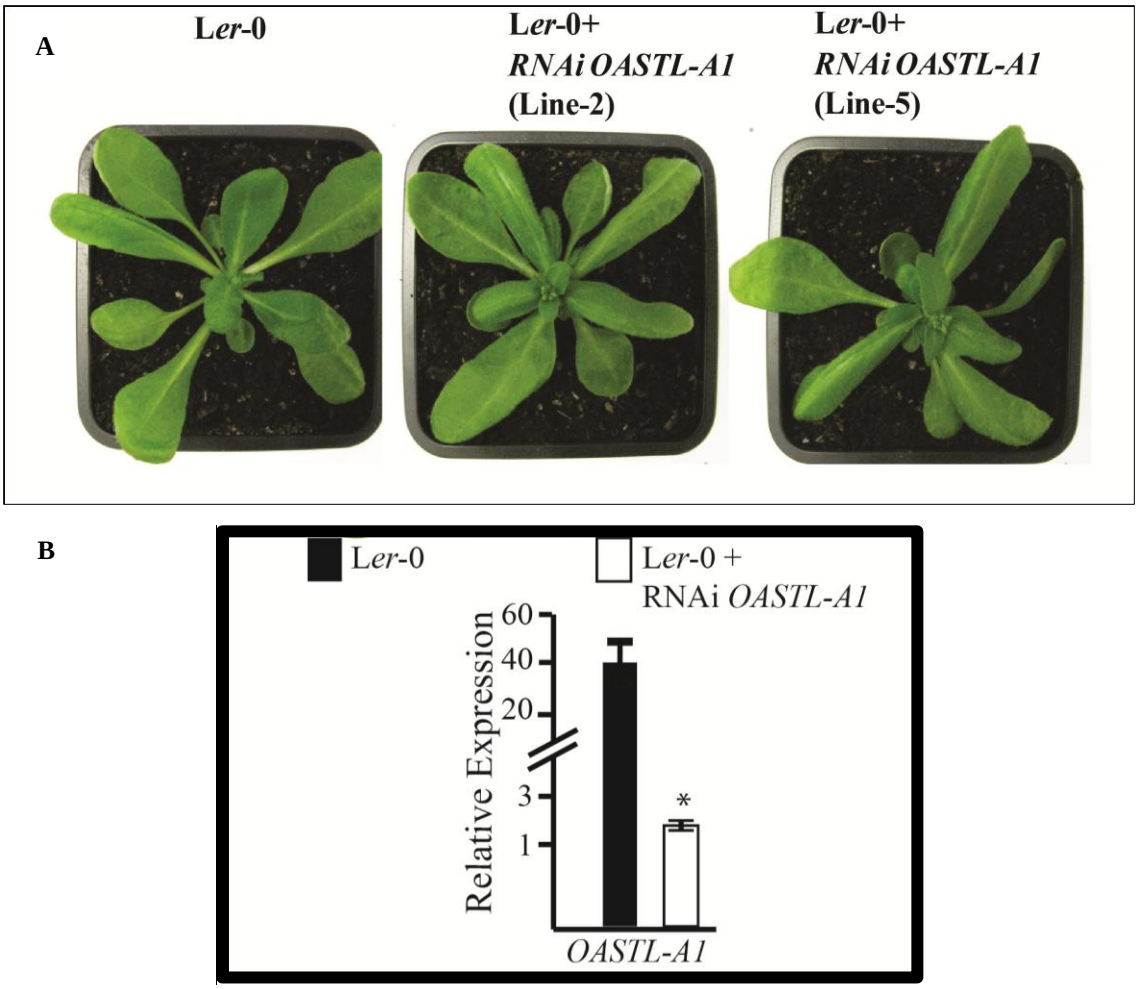

Figure 5.2. Lack of functional *OASTL-A1* does not cause autonecrosis. A) Representative pictures of L*er*-0 and L*er*-0 + RNAi *OASTL-A1* lines and B) relative expression of *OASTL-A1* is presented. Wild type and RNAi lines were grown for 1 week at 28°C and then for three weeks at 21 °C. Expression of *OASTL-A1* was measured in the wild-type and RNAi-Line-2. Expression values are relative to *Actin2*. Error bar represents standard deviation. Values represent mean within two biological replicates. * indicates statistically significant differences in the mean value of the gene expression in between wild-type and RNAi line using Student's *t* test ($P < 0.01$).

5.2 The mutation in OASTL-A1 activates *RPP1*-like *R* mediated autonecrosis

The result in this study indicates that specifically the *old3-1* mutation causes the autonecrosis phenotype in combination with *R* genes from the *odd-ler* region. To test this further, *old3-1* gene silencing was attempted in the *old3-1* mutants using the *OASTL-A1* specific RNAi construct, explained above. The autonecrosis phenotype was completely rescued in all the transformants, consistent with the reduction in *old3-1* expression levels (Figure 5.3). Thus, the G/E substitution at residue 162 of the OASTL-A1 results in the activation of autoimmunity concomitant to the presence of *R* gene(s) at the *odd-ler* region.

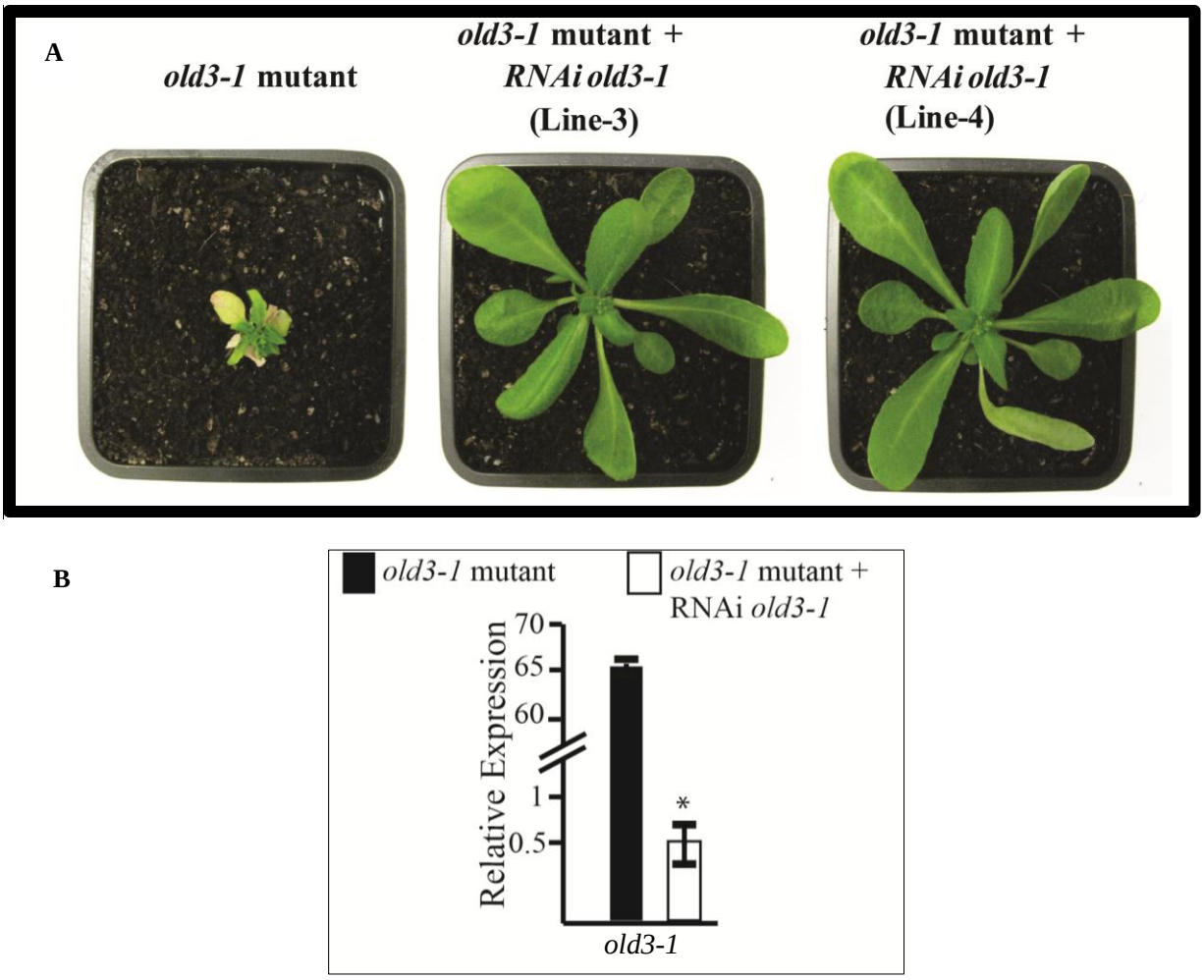

Figure 5.3. A mutation in OASTL-A1 activates *R*-mediated autonecrosis. A) Representative pictures of the *old3-1* mutant and *old3-1* mutant + RNAi *old3-1* lines and B) relative expression of *old3-1* is presented. Mutant and RNAi lines were grown for 1week at 28°C and then for three weeks at 21 °C. Expression of *OASTL-A1* was measured. Expression values are relative to *Actin2*. Error bar represents standard deviation. Values represent mean within two biological replicates. * indicates statistically significant differences in the mean value of the gene expression in between wild-type and RNAi line using Student's *t* test ($P < 0.01$).

5.3 Mutations in the *OASTL-A1* gene cause a major reduction in total OASTL activity *in planta* but not a reduction in total SERAT activity and cysteine and glutathione levels

The availability of cysteine for the production of thiols and other metabolites in plant cells is linked to the OASTL and SERAT enzymatic machinery (Figure 5.4). Therefore the OASTL and SERAT enzyme activity of *old3* mutants was first investigated. To characterise the effects of mutations affecting OASTL-A1 function *in planta*, initially the five genotypes described in Figure 5.4 were used: the *old3-1* mutant with its wild type parent L*er*-0, the *OASTL-A1* T-DNA KO mutant *old3-2* and its Col-0 wild-type parent, and finally, to analyse the effect of *old3-1* in the absence of the haplotype *RPP1*-like *R* genes from the *odd-ler* region, *old3-1*^{rec} is also used in this experiment.

The *old3-1* phenotype is rescued at high temperature and therefore all lines were grown under LD condition on soil at 28 $^{\circ}$C (permissive temperature) for 16 days. One experimental set of plant lines was subsequently grown for an additional 5 days at 28 $^{\circ}$C to suppress autonecrosis in *old3*-1 mutant, while another set was transferred to 20 $^{\circ}$C after which only the *old3-1* mutant exhibited autonecrosis within 5 days (Figure 5.4). In contrast, the *old3-2* and *old3-1*^{rec} lines were indistinguishable from wild-type plants in both temperatures (Figure 5.4). Enzymatic activities were analysed at 0, 2 and 5 days in the temperature shift experiment in both the sets (Figure 5.4; for detailed layout see Appendix 13).

The *old3-2* mutant showed a significant reduction i.e., up to 40-80% in total OASTL activity in comparison to its wild-type Col-0, under different growth temperature (Figure 5.5). Similar to *old3-2*, *old3-1* and *old3-1*^{rec}mutants also had significantly reduced total OASTL activity i.e., up to 40-60% in comparison to the wild type L*er*-0 and Col-0 plants (Figure 5.5). The total SERAT activity remained unaltered in the *old3-1* mutant compared to L*er*-0 in either of the growth temperatures, but showed significant reduction in *old3-2* and *old3-1*^{rec} plants when shifted to low temperature (Figure 5.5). As OASTL-A1 is also implicated to possess β-cyanoalanine synthase (CAS) activity, which is involved in cyanide detoxification (Watanabe et al., 2008a), the CAS activity was also tested in all the lines. A consistently significant reduction in total CAS activity

was observed in *old3-2* at both temperatures but not in the *old3-1* mutant and wild-types (Appendix 14) suggesting that CAS activity is not affected due to the *old3-1* mutation. The *old3-1*^{rec} mutant, instead, showed consistently significant reduction in total CAS activity in both temperatures as compared to Col-0 and L*er*-0. This is in contrast to the results obtained from the *old3-1* mutant (Appendix 14). This difference could be due to the effects of a mixed genetic background. Thus a comparable reduction in OASTL activity was seen in all *old3* mutant lines, regardless of growth temperature and the presence of the autonecrosis phenotype.

To identify the effects of reduced OASTL activity on sulfur assimilation, the sulfate, O-acetylserine (OAS), cysteine (Cys) and glutathione (GSH) levels were analysed (Figure 5.6). Total cellular sulfate, OAS, Cys and GSH levels were not significantly affected in the *old3-2* and *old3-1*^{rec} mutant in comparison to the wild-type Col-0 at both high and low temperatures. Only, *old3-2* mutant showed a significant reduction in total GSH level at the 5th day of temperature change but not at 28 ºC. These metabolites were not reduced in the *old3-1* mutant at either temperature as compared to L*er*-0 (Figure 5.6). The total Cys, OAS and sulfate levels were, however, increased in the *old3-1* mutant within 2 days after shift to low temperature (Figure 5.6). GSH levels however were not significantly altered as compared to L*er*-0 (Figure 5.6). Cumulatively, these results show that there is no severe reduction of cysteine in the *old3-1* mutant and this is similar to the other *old3* lines. However, autonecrosis coincided with increased cysteine, OAS and sulfate levels in the *old3-1* mutant.

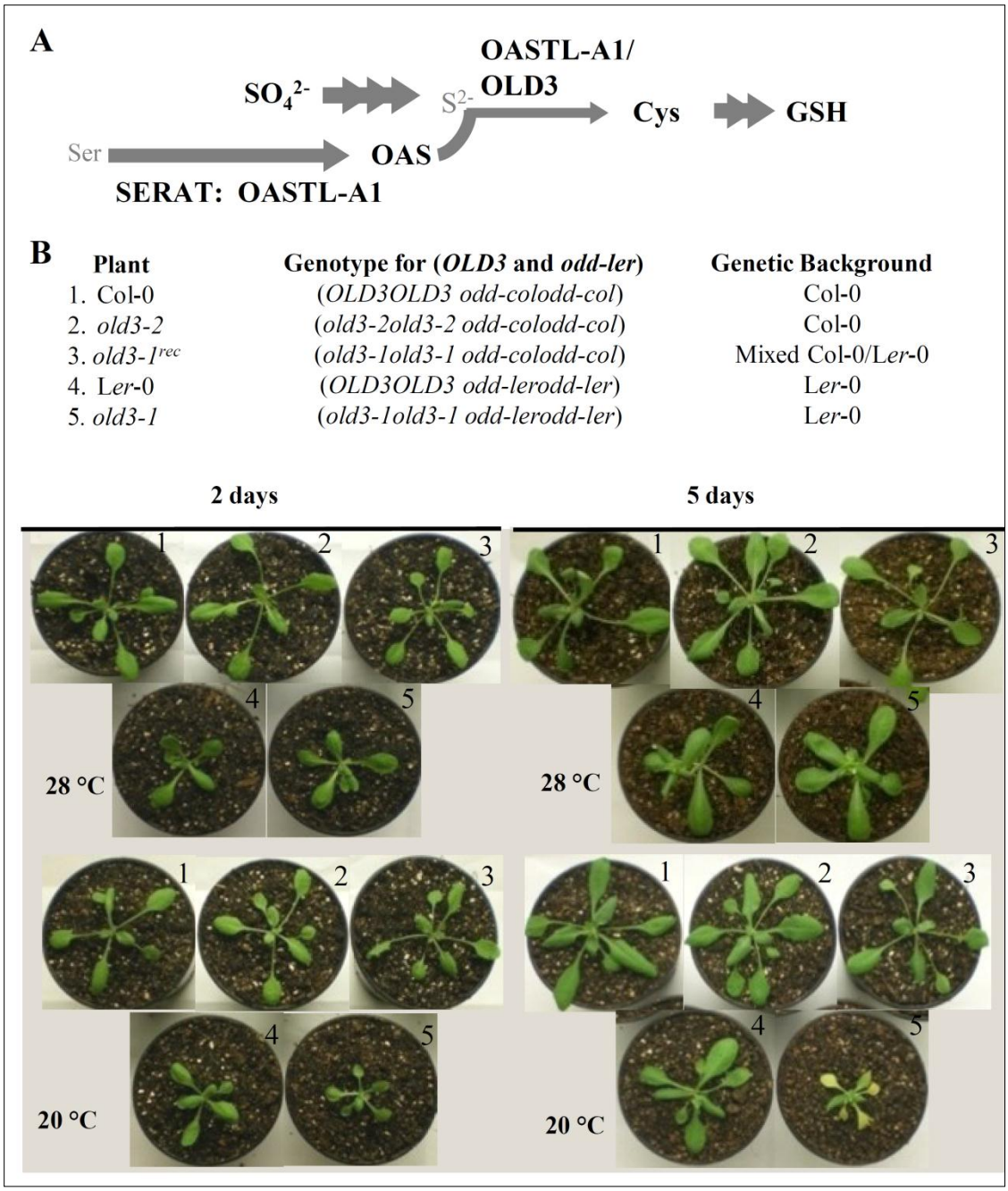

Figure 5.4. Characterisation of *old3* lines in the temperature shift experiment. A. Schematic representation of the sulfur assimilation pathway. Not all steps are shown as indicated by multiple arrows. B. Five different plant lines and their corresponding genotypes are described. Plants were first grown at 28 °C for 16 days to suppress necrosis in the *old3-1* mutant in long-day conditions (16 h of light / 8 h of dark). One experimental set of plant lines was kept at 28 °C, while another set was transferred to 20 °C and plants were then grown for an additional 5 days. Pictures of representative plants grown for 2 and 5 day after temperature shift are shown.

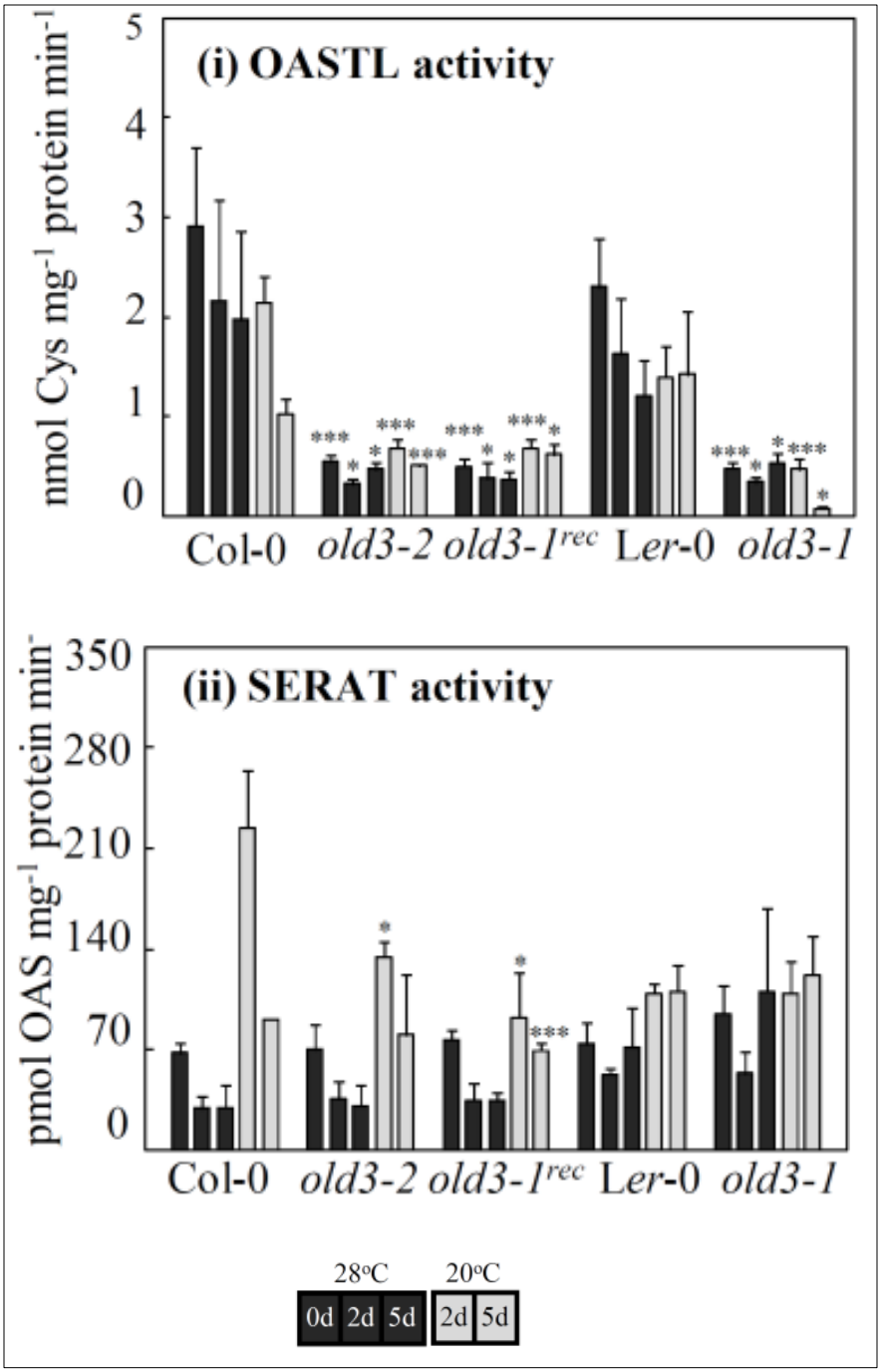

Figure 5.5. Enzymatic activities of (i) OASTL and (ii) SERAT in five genotypes. Black bars indicate data for plants grown at 28 °C for 16, 16+2 days and 16+5 days. Grey bars indicate data for plants grown for 16+2 days and 16+5 days at 20 °C, after temperature shift at day 16 from 28 °C. Data represents the mean of three biological replicates. Statistically significant differences in the values between the mutants and the respective wild-types, using Student's *t* test are shown by * at $P < 0.05$, ** at $P < 0.01$ and *** at $P < 0.005$. *old3-1rec* is a mixed L*er*-0/Col-0 background and the levels of metabolites in this line were statistically analysed against those of Col-0.

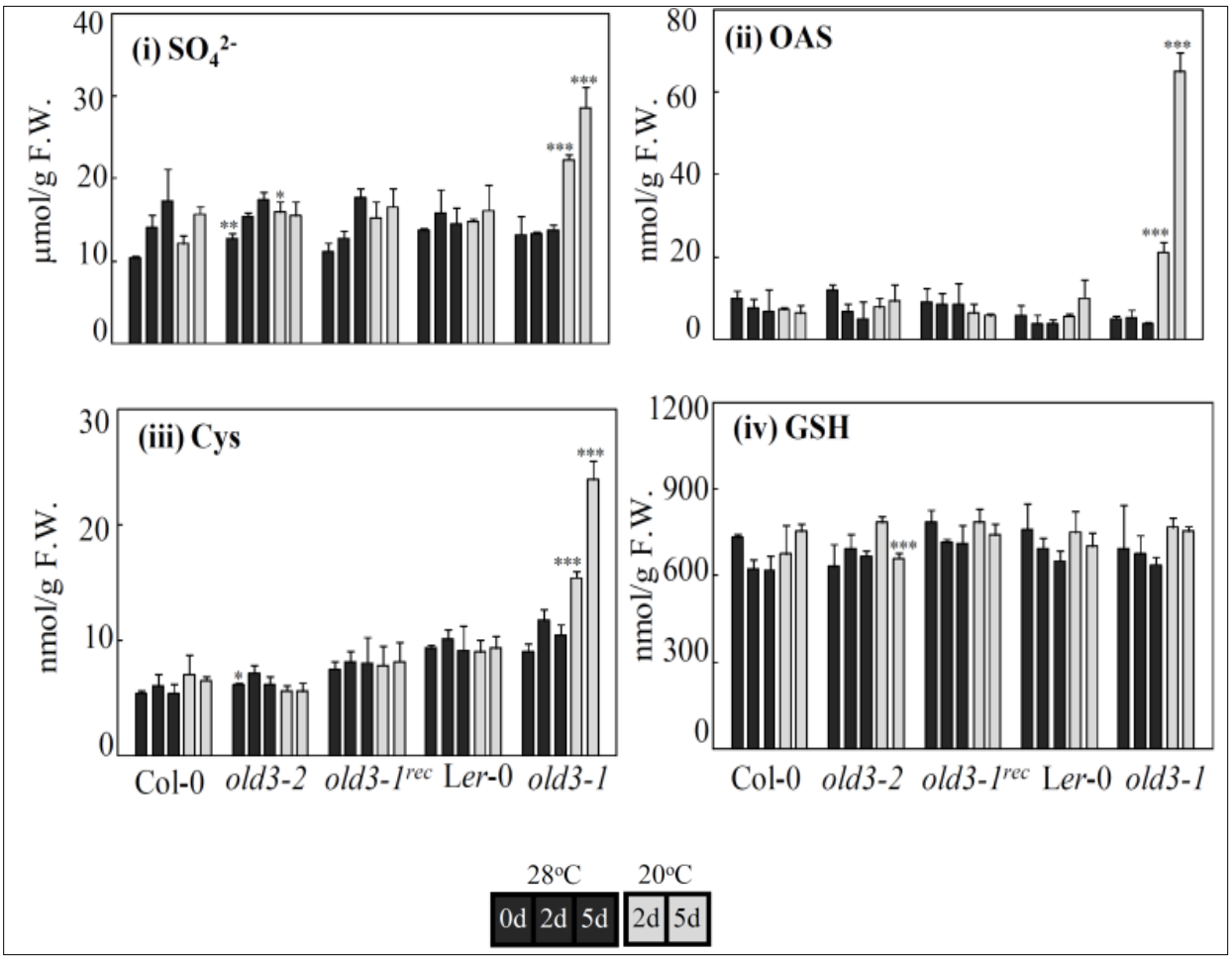

Figure 5.6. Levels of (i) SO_4^{2-}, (ii) OAS, (iii) Cys and (iv) GSH in all five genotypes. Black bars indicate data for plants grown at 28 °C for 16, 16+2 days and 16+5 days. Grey bars indicate data for plants grown for 16+2 days and 16+5 days at 20 °C, after temperature shift at day 16 from 28 °C. Data represents the mean of three biological replicates. Statistically significant differences in the values between the mutants and the respective wild-types, using Student's *t* test are shown by * at $P < 0.05$, ** at $P < 0.01$ and *** at $P < 0.005$. *old3-1rec* is a mixed L*er*-0/Col-0 background and the levels of metabolites in this line are statistically analysed with those of Col-0.

5.4 Metabolic profiling of *old3* mutants

It is apparent from the preceding data that cysteine metabolism is affected in the *old3-1* mutant at low temperature. To further characterize the different effects of *old3* mutation, metabolic profiling was opted for *old3* mutants as it would provide a global overview of the changes in a large number of metabolites. Furthermore, the data generated could assist in understanding the basis of phenotypic variation among the *old3* mutants, caused by genetic variation between the two accessions together with the effect of different *old3* mutations in variable temperatures. Therefore, all five genotypes were characterised by targeted metabolic profiling of over 60 metabolites at 0, 2 and 5 days in the temperature shift experiment. Hierarchical clustering analysis (HCA) was performed to monitor variation in biological replicates within each genotype in two different temperature regimes (Appendix 15).

(i) The *old3-1* mutant shows delayed degradation of total chlorophyll content and sharp changes in levels of anions before the development of necrosis.

Results obtained show that the *old3-1* mutant exhibited significantly lower levels of chlorophyll *a* when grown at high or low temperature, as compared to wild type L*er*-0 (Figure 5.7). However, chlorophyll *b* content was not reduced at either temperature, except for day 0 at high temperature. The degradation for chlorophyll *a* content was not observed in *old3-1*^{rec} and *old3-2* mutant as compared to wild-type (Figure 5.7). These results suggest that lack of functional OASTL-A1 or the presence of *old3-1* alone is not responsible for reduced chlorophyll *a* content. Lower chlorophyll *a* levels in the *old3-1* mutant may be linked with the effect of *old3-1* in a pure L*er*-0 background. However, there remains the possibility that this reduction is linked with negative epistatic interaction between *old3-1* and *R* gene(s) products. Regardless, the *old3-1* mutant plants specifically exhibited reduction in total chlorophyll levels only at day 5 of temperature change consistent with enhanced leaf chlorosis (Figure 5.7). The data also reflects the effect of temperature on the chlorophyll content. Overall, high or low temperature did not affect the total chlorophyll content among all genotypes that do not show autonecrosis. However, when compared to high temperatures, low temperatures result in a decrease in chlorophyll *b* content in all genotypes (Figure 5.7).

When grown at high temperature, results show that no significant differences appeared for total nitrate levels in all genotypes, except that the *old3-1*^{rec} plants showed slightly higher levels of nitrate at day 0. However, total nitrate concentrations were significantly lowered only in the *old3-1* mutant during the onset of autonecrosis at low temperature (Figure 5.8). This decrease was significant at 2 days, which is well before the onset of chlorophyll degradation that is observed on the 5th day of temperature shift (Figure 5.8). Regardless, nitrate levels increased across genotypes over time at both temperatures. In contrast to nitrate, total phosphate levels were increased during the onset of autonecrosis and these changes were significant after 2 days of temperature shift (Figure 5.8). This is similar to the pattern observed for changes in total sulfate levels in the *old3-1* mutant as shown in the section above. Overall, changes in temperature and genetic background did not result in any variation in the total nitrate and phosphate levels between wild-type and other *old3* mutants.

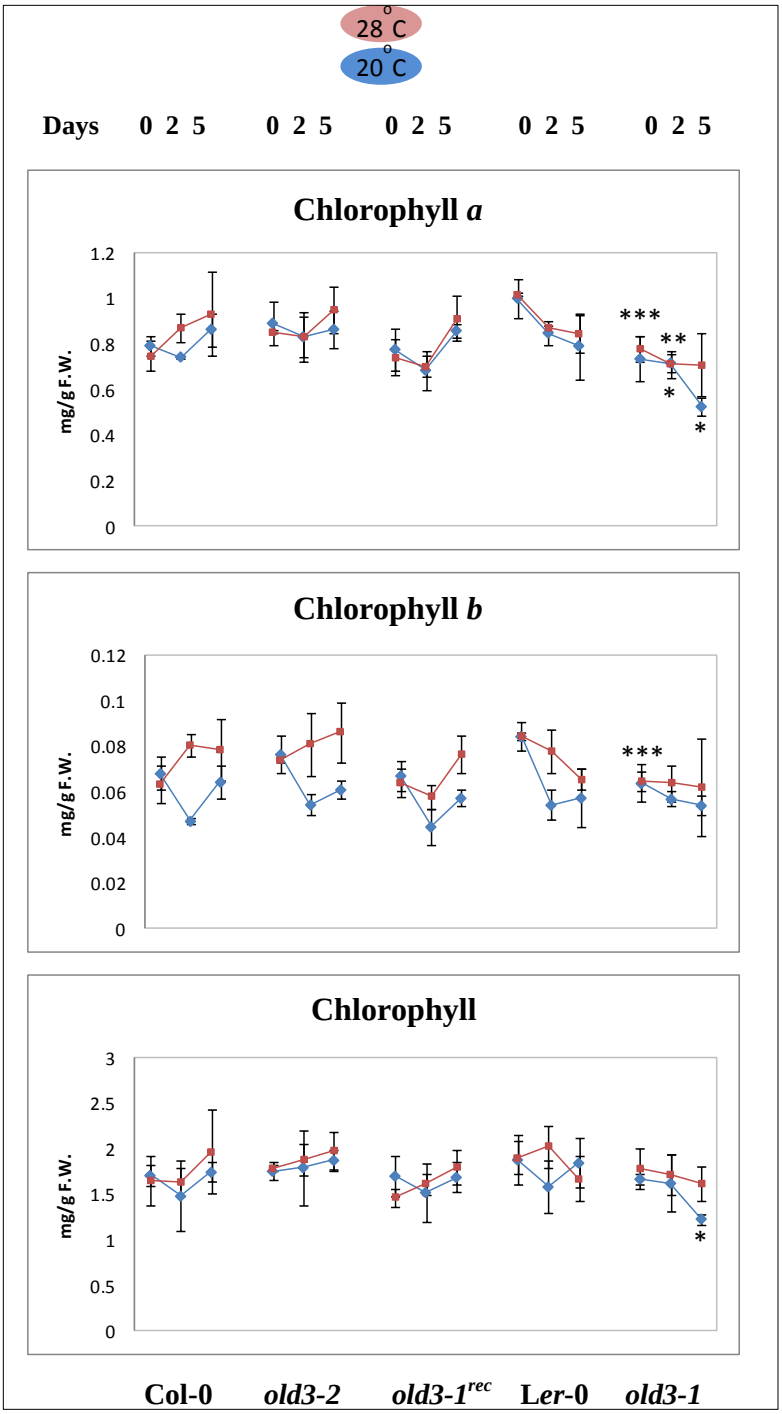

Figure 5.7. Changes in chlorophyll contents in *old3* mutants. Red dots indicate data for plants grown at 28 °C for 16 (0), 16+2 days (2 days) and 16+5 days (5 days). Blue dots indicate data for plants grown for 16+2 days (2 days) and 16+5 days (5 days) at 20 °C, after temperature shift at day 16 from 28 °C. The data in blue dots at 0 days, is soon after shift to 20 °C at day 16 from 28 °C. Data represents mean of three biological replicates. Error bar represents standard deviation. Statistically significant differences in the values between the mutants and the respective wild-types, using Student's *t* test are shown by * at $P < 0.05$, ** at $P < 0.01$ and *** at $P < 0.005$. Asterisks above the dots are for the data at 28 ºC and asterisks below the dots are for the data at 21 ºC. In *old3-1*^{rec}, the values are statistically analysed against the data from Col-0.

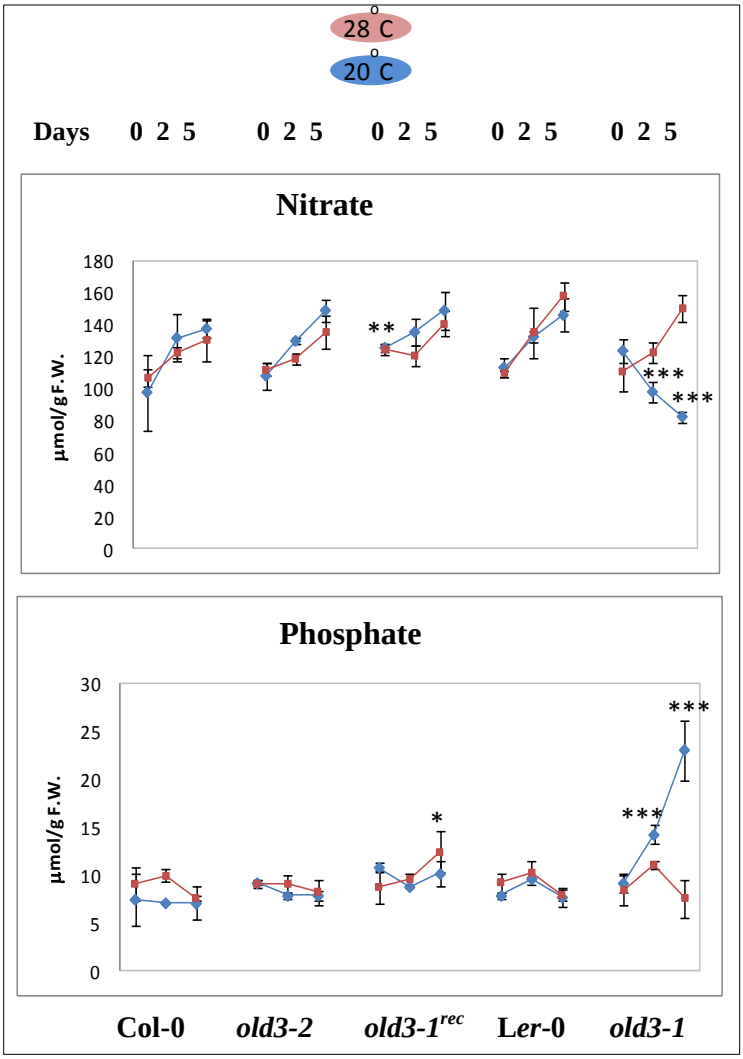

Figure 5.8. Changes in the level of anions in the *old3* mutants. Red dots indicate data for plants grown at 28 °C for 16 (0), 16+2 days (2 days) and 16+5 days (5 days). Blue dots indicate data for plants grown for 16+2 days (2 days) and 16+5 days (5 days) at 20 °C, after temperature shift at day 16 from 28 °C. The data in blue dots at 0 days, is soon after shift to 20 °C at day 16 from 28 °C. Data represents mean of three biological replicates. Error bar represents standard deviation. Statistically significant differences in the values between the mutants and the respective wild-types, using Student's *t* test are shown by * at $P < 0.05$, ** at $P < 0.01$ and *** at $P < 0.005$. In *old3-1*^{rec}, the values are statistically analysed against the data from Col-0.

(ii) Perturbations in primary and secondary metabolism in the *old3-1* mutant

a. Amino acids, sugars and their precursors

The synthesis of amino acids and sugars links the assimilation pathways of nitrogen and carbon and other secondary metabolisms. The carbon skeleton of amino acids is derived from CO_2, which is assimilated during photosynthesis in the form of carbohydrate products. The carbohydrates are further metabolised in the cytosol through glycolysis to release energy, and subsequently broken down into various metabolites, including glyceraldehyde 3-phosphate (3PGA), phosphoenoylpyruvate (PEP) and pyruvate, which in turn, act as precursors to many amino acids and other metabolites (Figure 5.9). Results show that the levels of pyruvate are specifically increased in the *old3-1* mutant as compared to wild-type at day 2 of temperature shift (Figure 5.10). However, pyruvate concentration decreases at day 5 of temperature shift. In contrast, pyruvate levels were not largely affected in *old3-2* mutant and Col-0 at either temperature. Interestingly the levels of amino acids derived from pyruvate, including alanine and the branched-chain amino acids leucine, valine and isoleucine, were significantly increased in the *old3-1* mutant as compared to wild-type L*er*-0 at day 2 of temperature shift (Figure 5.10). The concentration of valine, isoleucine and leucine was massively increased in the *old3-1* mutant at day 5 of temperature shift. The level of these amino acids was not increased in other *old3* mutants and wild-types (Figure 5.10).

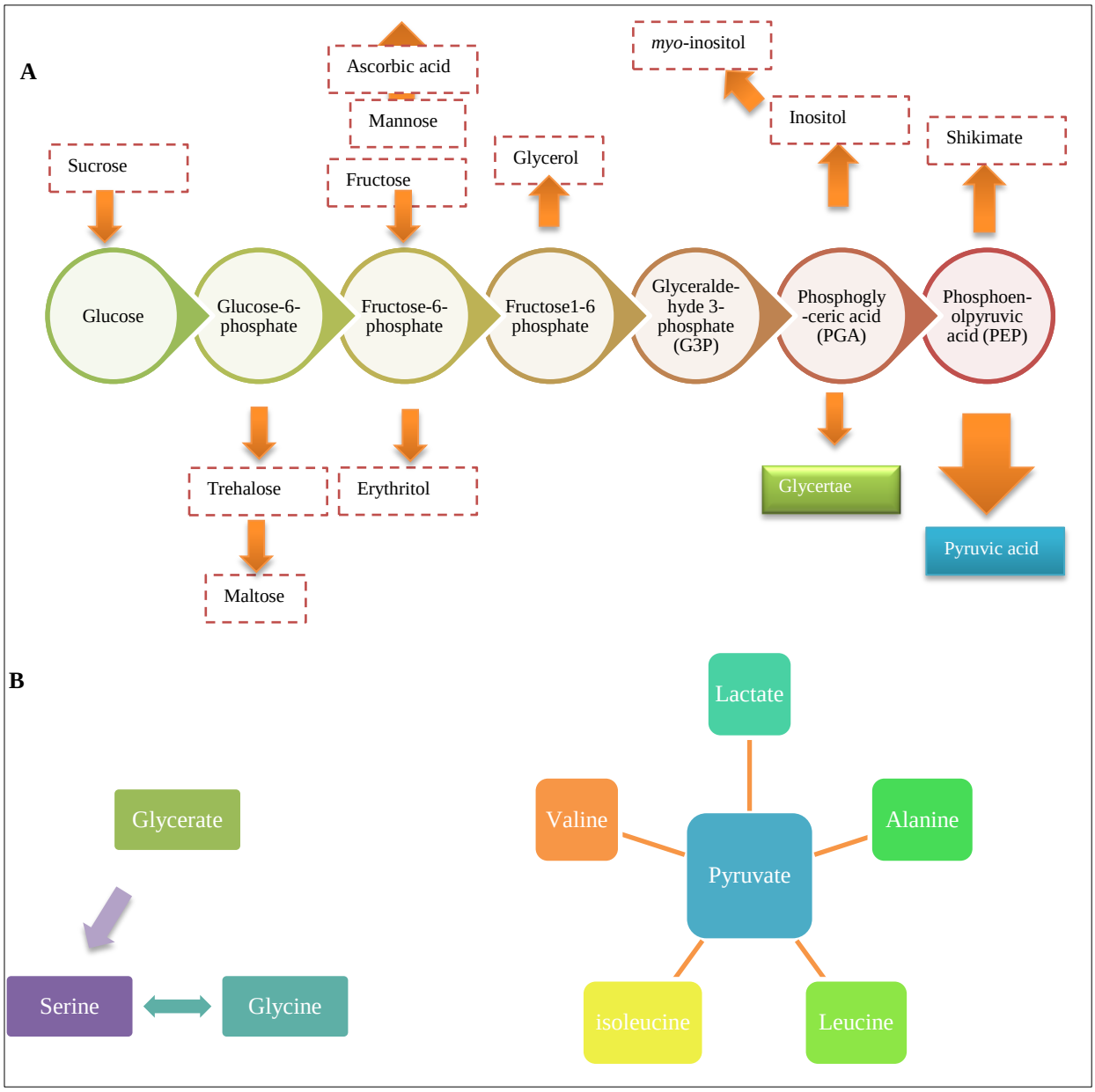

Figure 5.9. Glycolysis and incorporation of its intermediate and end metabolites in synthesis of amino acids, secondary metabolites, sugars and lipids. A) shows the process of glycolysis and use of its intermediates in synthesis of sugars, lipids and other metabolites. B) shows synthesis of different amino acids from glycerate and pyruvate.

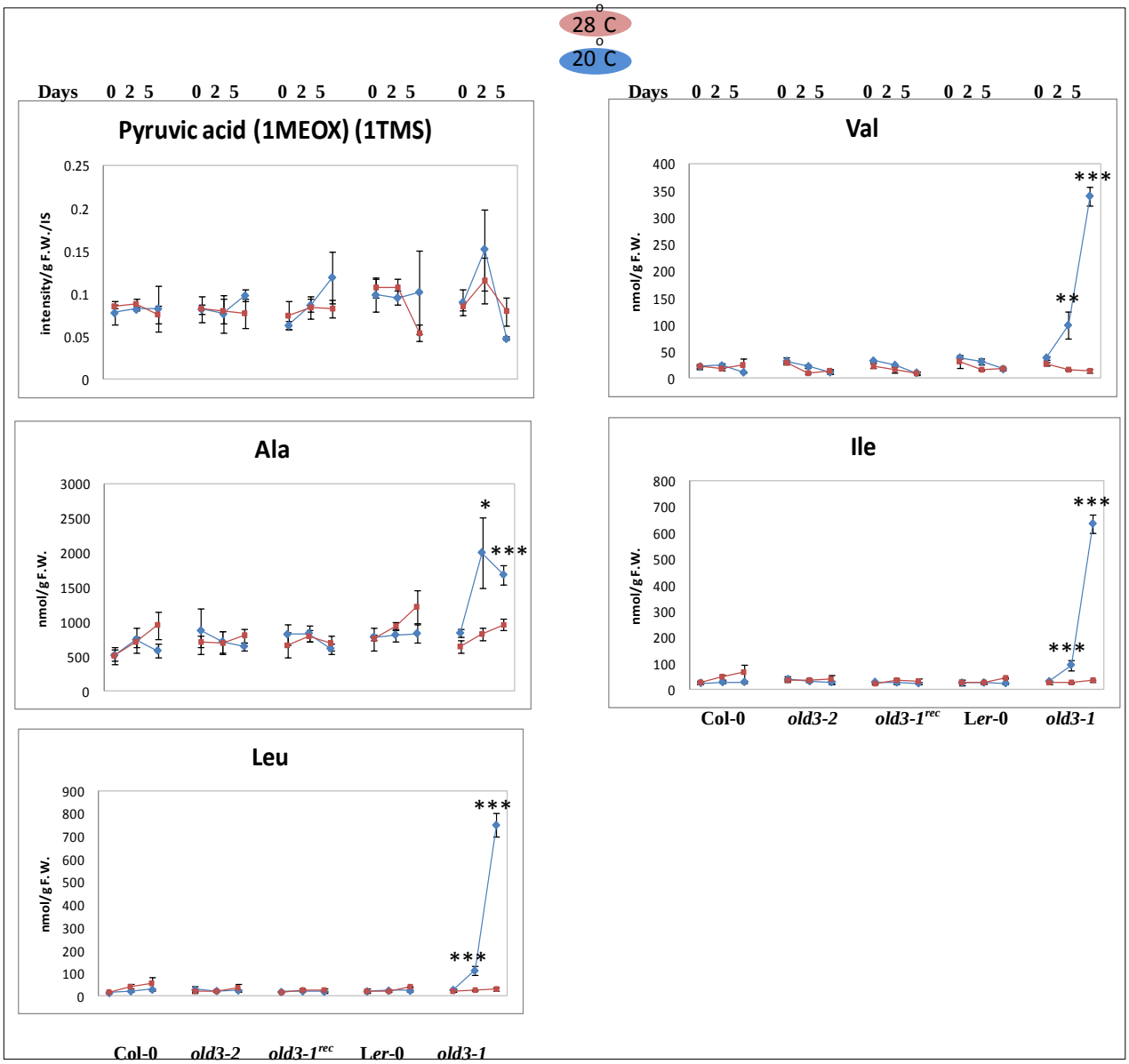

Figure 5.10. Changes in pyruvate-driven amino acid concentrations in the *old3* mutants. Red dots indicate data for plants grown at 28 °C for 16 (0), 16+2 days (2 days) and 16+5 days (5 days). Blue dots indicate data for plants grown for 16+2 days (2 days) and 16+5 days (5 days) at 20 °C, after temperature shift at day 16 from 28 °C. The data in blue dots at 0 days, is soon after shift to 20 °C at day 16 from 28 °C. Data represents mean of three biological replicates. Error bar represents standard deviation. Statistically significant differences in the values between the mutants and the respective wild-types, using Student's *t* test are shown by * at $P < 0.05$, ** at $P < 0.01$ and *** at $P < 0.005$. In *old3-1*^{rec}, the values are statistically analysed against the data from Col-0.

Pyruvate is further fed into the tricarboxylic acid (TCA) cycle or Krebs' cycle in the mitochondria, where it is fed into the synthesis of other amino acids as well as secondary metabolites (Figure 5.11). Results show that most of the TCA metabolites including malic acid, fumaric acid and succinic acid were accumulated in the *old3-1* mutant at low temperature only as compared to wild-type, but not at high temperature (Figure 5.12). The level of these metabolites was not significantly altered in other *old3* mutants as compared to wild-type lines (Figure 5.12). Glutamate is an important amino acid synthesised from the TCA intermediate α-ketoglutarate. The levels of glutamate were significantly increased in the *old3-1* mutant by day 5 of temperature shift, as compared to wild-type. Glutamate acts as a precursor to other amino acids including glutamine, histidine, proline and also to arginine, via the urea cycle. Results show that levels of these amino acids were also increased in the *old3-1* mutant as compared to wild-type L*er*-0 at 20 ºC. None of these however showed accumulation in other *old3* mutants at 20 ºC or 28 ºC as compared to wild-type (Figure 5.12).

Aspartate is another amino acid which is derived from the TCA cycle intermediate oxaloacetate and acts as a precursor to other amino acids including asparagine, β-alanine, lysine, methionine and threonine (Figure 5.13). The level of these amino acids that are produced from aspartate in the metabolic pathway were found to be significantly accumulated in the *old3-1* mutant as compared to wild-type at day 2 and day 5 of temperature shift (Figure 5.13). During the onset of autonecrosis, only the levels of methionine were significantly reduced at day 2 in the *old3-1* mutant, but remained significantly higher at day 5 of temperature shift (Figure 5.12). Some of these amino acids did show temperature-dependent regulation in all the lines, but none of them were significantly altered in other *old3* mutants as compared to wild-type.

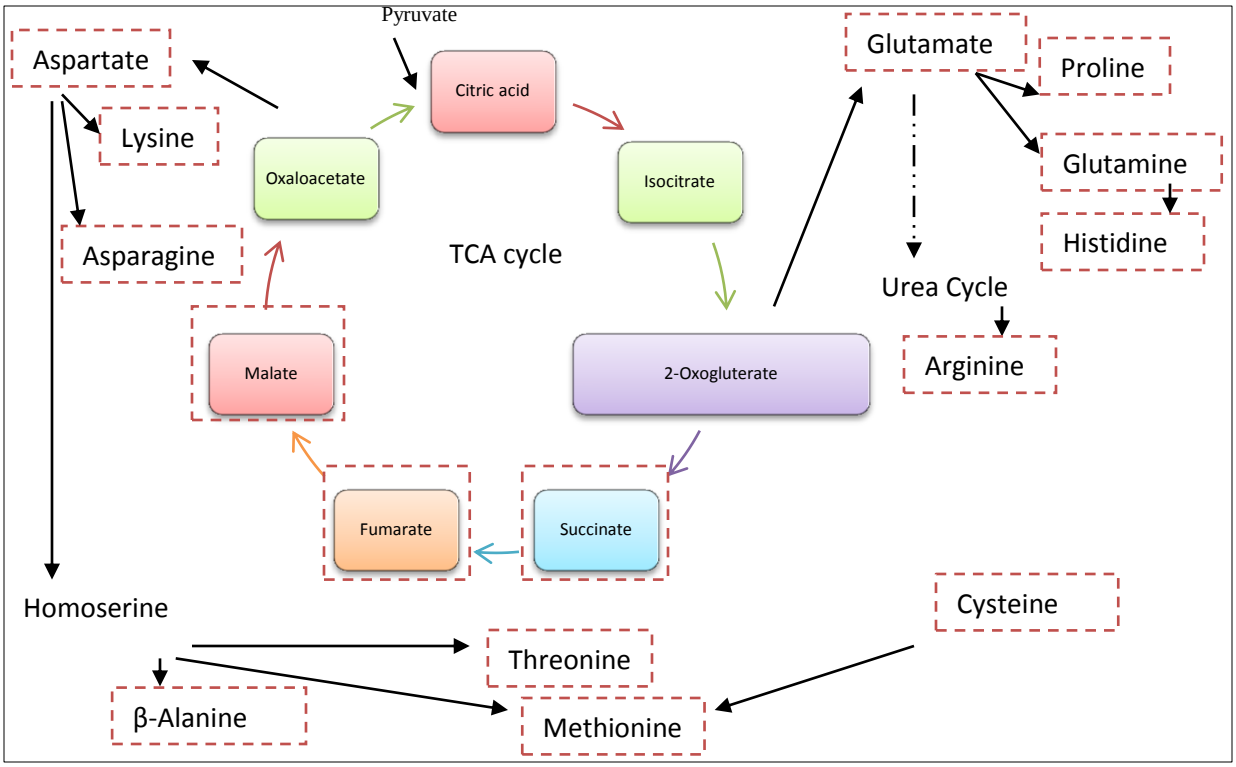

Figure 5.11. TCA cycle and pathways of synthesis of amino acids. Metabolites of TCA cycle are highlighted in colour whereas amino acids generated from these compounds are highlighted in red dashed outline box. Metabolites and amino acids highlighted in red dashed outline box were measured in all the lines.

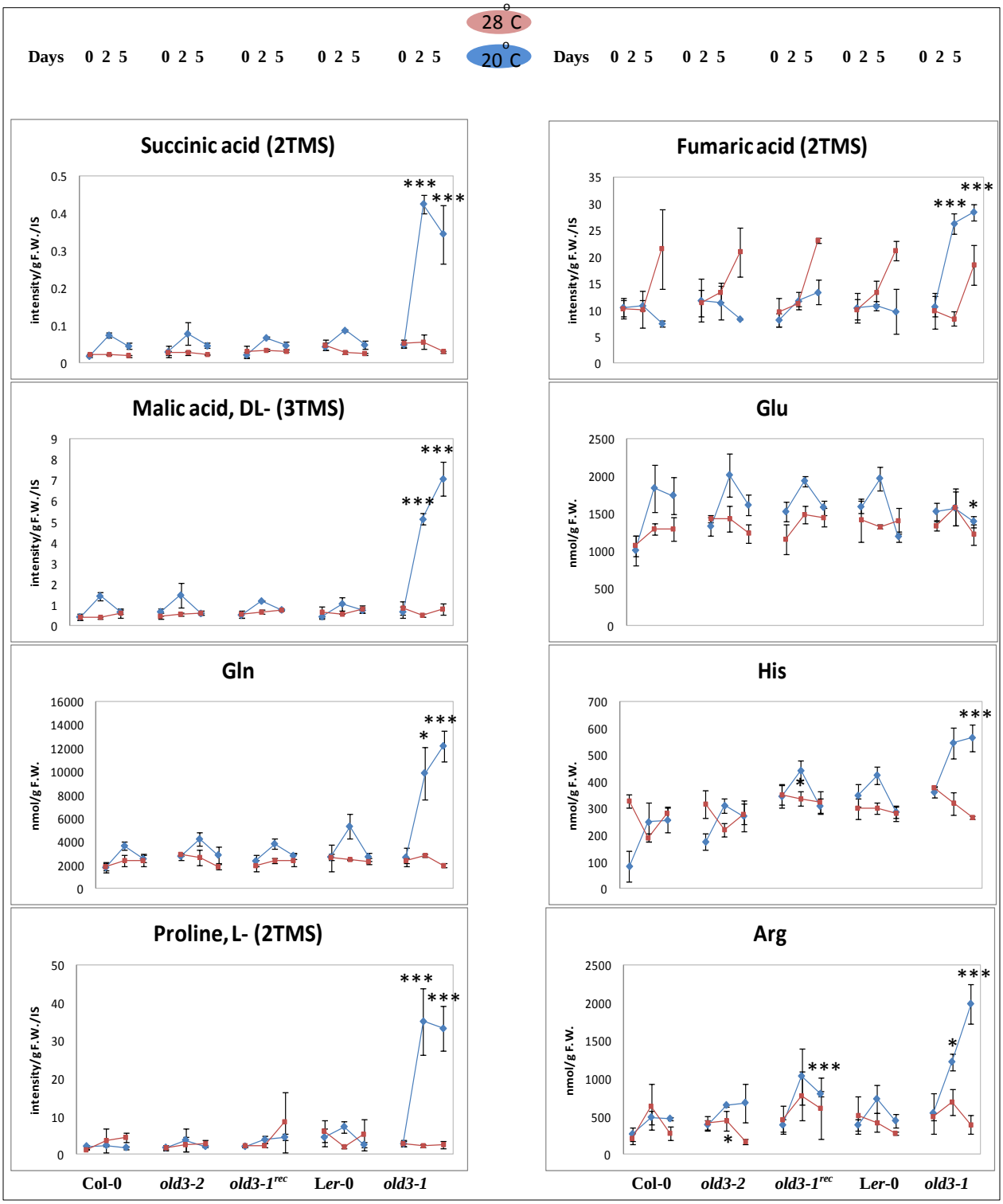

Figure 5.12. Changes in the level of TCA intermediates and amino acid concentrations in the *old3* mutants. Red dots indicate data for plants grown at 28 °C for 16 (0), 16+2 days (2 days) and 16+5 days (5 days). Blue dots indicate data for plants grown for 16+2 days (2 days) and 16+5 days (5 days) at 20 °C, after temperature shift at day 16 from 28 °C. The data in blue dots at 0 days, is soon after shift to 20 °C at day 16 from 28 °C. Data represents mean of three biological replicates. Error bar represents standard deviation. Statistically significant differences in the values between the mutants and the respective wild-types, using Student's *t* test are shown by * at $P < 0.05$, ** at $P < 0.01$ and *** at $P < 0.005$. In *old3-1*^{rec}, the values are statistically analysed against the data from Col-0.

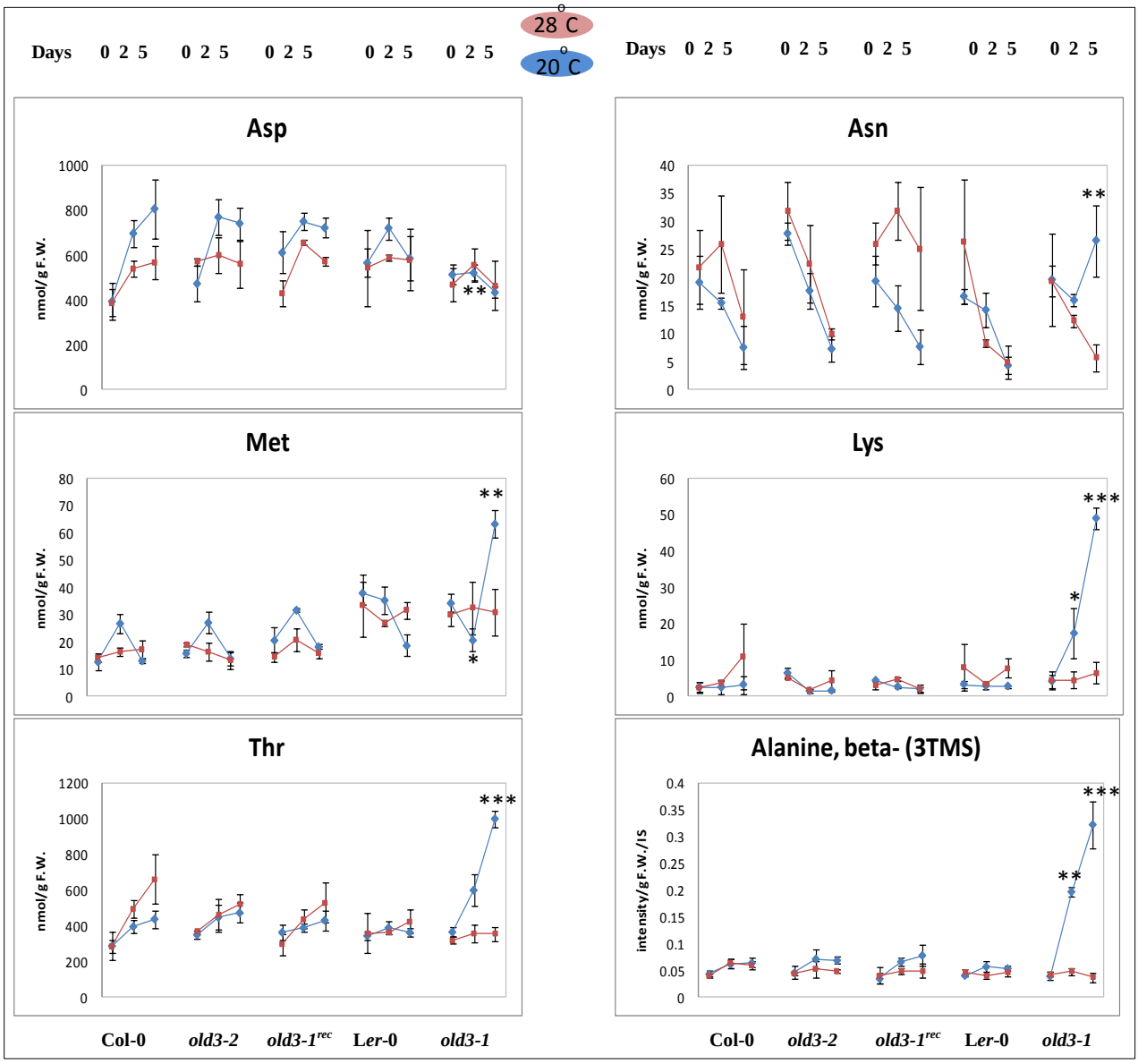

Figure 5.13. Changes in the level of other amino acids in the *old3* mutants. Red dots indicate data for plants grown at 28 °C for 16 (0), 16+2 days (2 days) and 16+5 days (5 days). Blue dots indicate data for plants grown for 16+2 days (2 days) and 16+5 days (5 days) at 20 °C, after temperature shift at day 16 from 28 °C. The data in blue dots at 0 days, is soon after shift to 20 °C at day 16 from 28 °C. Data represents mean of three biological replicates. Error bar represents standard deviation. Statistically significant differences in the values between the mutants and the respective wild-types, using Student's *t* test are shown by * at $P < 0.01$, ** at $P < 0.005$ and *** at $P < 0.001$. In *old3-1*^{rec}, the values are statistically analysed against the data from Col-0.

Phosphoenoylpyruvate (PEP), which is the precursor of pyruvate, also acts as the precursor of a key metabolite, shikimate, which drives the synthesis of three different aromatic amino acids; tryptophan, tyrosine and phenylalanine. Results show that all three amino acids are accumulated in the *old3-1* mutant as compared to wild-type at 20 ºC (Figure 5.14). However the level of these amino acids was non-significantly altered in other *old3* mutants and wild-type. Similarly, levels of other amino acids including serine and glycine were specifically higher in the *old3-1* mutant as compared to wild-type during the shift to low temperature (Figure 5.14). Thus in conclusion, amino acids and their precursor metabolites emerging from the TCA cycle, the glycolysis/glycogenesis and the Shikimate pathway were highly accumulated before the development of autonecrosis.

Total soluble protein levels were also measured from all the lines including the *old3-1* mutant. The total protein levels were not significantly altered in the *old3-1* mutant as compared to wild-type at 28 ºC (Figure 5.14). However a slight but significant reduction was observed in total protein levels at 20 ºC, at day 2, in the *old3-1* mutant as compared to L*er*-0 (Figure 5.14). No protein degradation was observed in other *old3* mutants and wild-type. Thus, protein degradation may contribute to the pattern of an increase in the level of amino acids during autonecrosis.

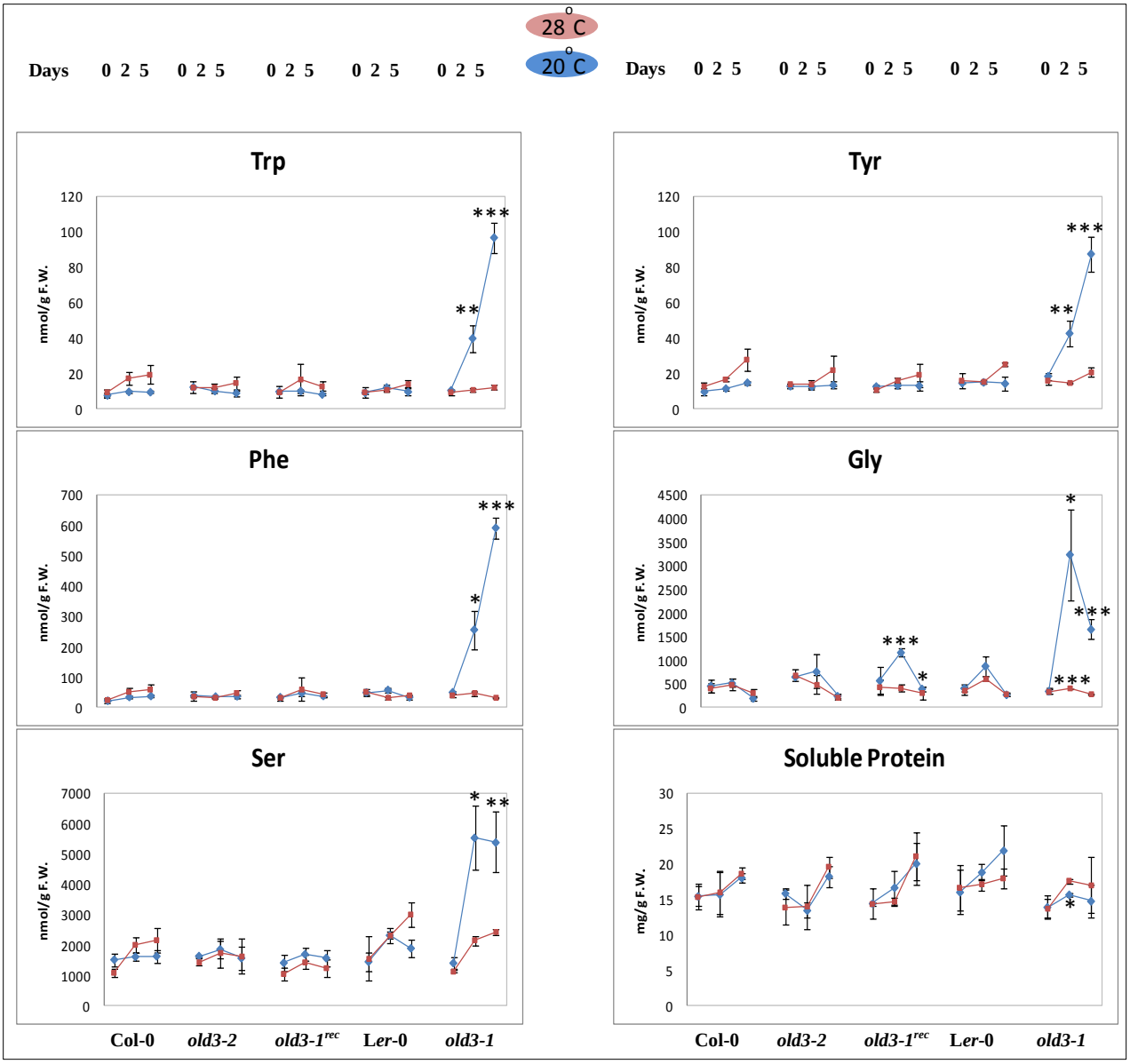

Figure 5.14. Changes in the level of amino acids in shikimate pathway, Ser/Gly metabolism and total soluble protein in the *old3* mutants. Red dots indicate data for plants grown at 28 °C for 16 (0), 16+2 days (2 days) and 16+5 days (5 days). Blue dots indicate data for plants grown for 16+2 days (2 days) and 16+5 days (5 days) at 20 °C, after temperature shift at day 16 from 28 °C. The data in blue dots at 0 days, is soon after shift to 20 °C at day 16 from 28 °C. Data represents mean of three biological replicates. Error bar represents standard deviation. Statistically significant differences in the values between the mutants and the respective wild-types, using Student's *t* test are shown by * at $P < 0.01$, ** at $P < 0.005$ and *** at $P < 0.001$. In *old3-1*^{rec}, the values are statistically analysed against the data from Col-0.

As most of the precursors for the amino acids are derived from metabolites in glycolysis/glucogenesis pathway, sugar metabolism was also analysed. Results obtained indicates that the total level of sugars including glucose, sucrose and fructose were also increased in the *old3-1* mutant as compared to wild-type at 20 ºC while their levels were unaltered at 28 ºC (Figure 5.15). Consistent with these changes in sugar metabolism, maltose concentration was also increased specifically in the *old3-1* mutants as compared to L*er*-0 at 20 ºC (Appendix 15). In contrast, the total starch levels were not significantly affected in the *old3-1* mutant as compared to wild-type at 20 ºC or 28 ºC (Figure 5.15). Similarly, the level of starch was not significantly affected in other lines at both 20 and 28 ºC. In conclusion, the results showed that higher levels of sugars and its derivatives were accumulated in the *old3-1* mutant without affecting total starch levels.

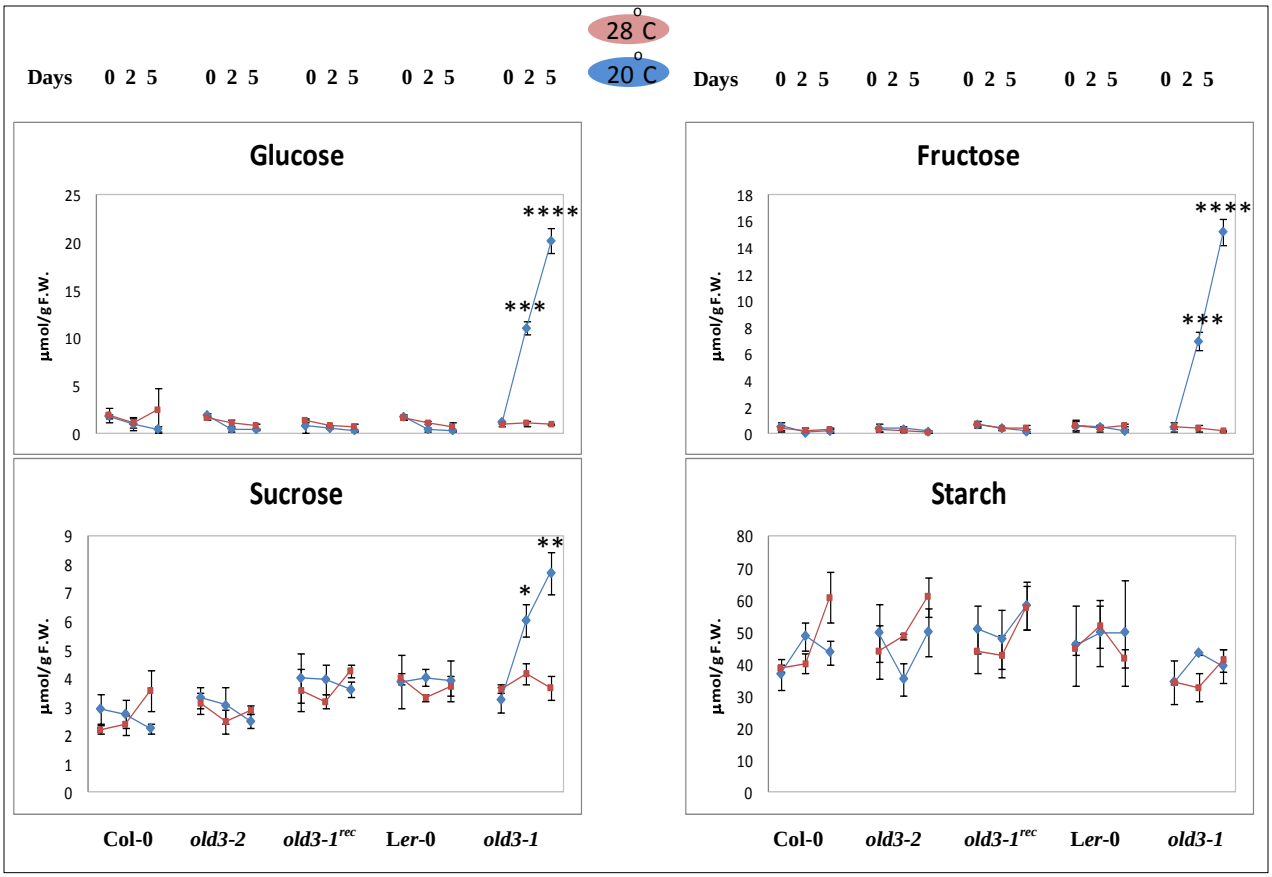

Figure 5.15. Changes in the sugars and starch levels of the *old3* mutants. Red dots indicate data for plants grown at 28 °C for 16 (0), 16+2 days (2 days) and 16+5 days (5 days). Blue dots indicate data for plants grown for 16+2 days (2 days) and 16+5 days (5 days) at 20 °C, after temperature shift at day 16 from 28 °C. The data in blue dots at 0 days, is soon after shift to 20 °C at day 16 from 28 °C. Data represents mean of three biological replicates. Error bar represents standard deviation. Statistically significant differences in the values between the mutants and the respective wild-types, using Student's *t* test are shown by * at $P < 0.01$, ** at $P < 0.005$, *** at $P < 0.001$ and **** at $P < 0.0005$. In *old3-1*^{rec}, the values are statistically analysed against the data from Col-0.

b. Secondary metabolites involved in abiotic stress response and disease resistance

Primary metabolism further branches out into secondary metabolism and, therefore, secondary metabolites derived from key amino acids and sugars were specifically targeted in metabolic profiling among all the lines. The TCA-derived glutamate acts as a precursor to various secondary metabolites, including ornithine, putrescine, γ-aminobutyric acid (GABA) and pyroglutamic acid which are associated with abiotic and biotic stress defence (Ye et al., 1997; Shelp et al., 1999; Sharma and Dietz, 2006; Jang et al., 2009; Alcazar et al., 2010b; Gill and Tuteja, 2010). Results from this study showed that these metabolites were highly accumulated in the *old3-1* mutant as compared to the wild-type, when grown at 20 ºC (Figure 5.16). This is consistent with the accumulation of proline in the *old3-1* mutant, which is also involved in abiotic stress-defence, as described earlier. These metabolites were not significantly affected in *old3-2* as compared to Col-0 under the same growth conditions (Figure 5.16). However, significant variation was observed in their levels in the *old3-1* mutant as part of autonecrosis. Thus, lack of OASTL-A1 itself does not activate stress-defence in *Arabidopsis* under permissive growth conditions.

Sugar metabolism is involved in the synthesis of some important compounds and metabolites that regulate stress signaling and cell death. These include the disaccharide, trehalose, which is involved in stress defence signalling (Avonce et al., 2004), *myo*-inositol, which negatively regulates cell death (Meng et al., 2009; Donahue et al., 2010), and ascorbic acid which acts as an important antioxidant (Valpuesta and Botella, 2004). Results from the analysis here indicate that trehalose and ascorbic acid are significantly accumulated in the *old3-1* mutant at 20 ^{o}C only (Figure 5.16; Appendix 15). In contrast, levels of *myo*-inositol decreased in the *old3-1* mutant at 20 ^{o}C, consistent with activation of cell death in the *old3-1* mutant. These metabolites were not significantly altered in other *old3* lines (Figure 5.16).

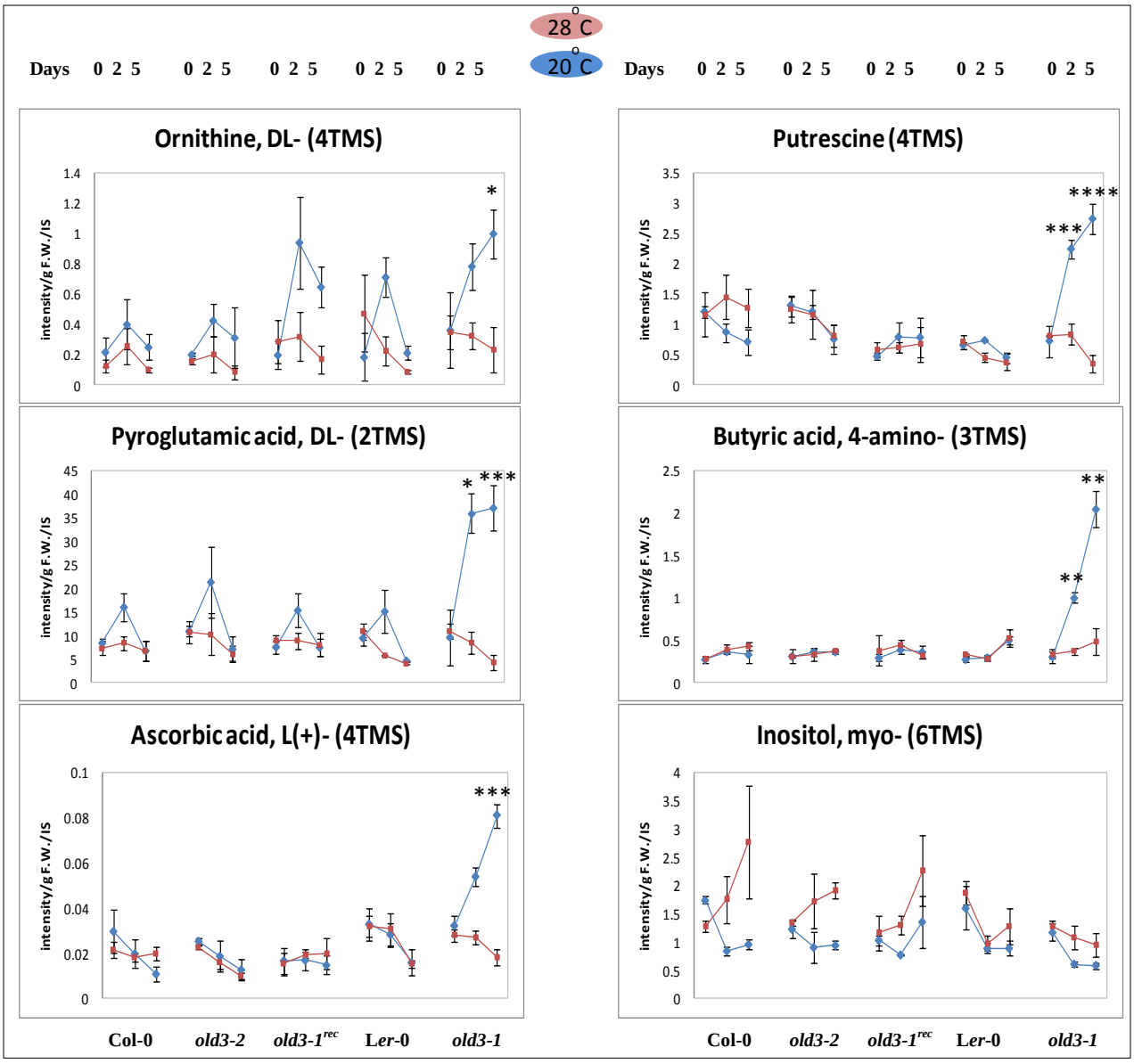

Figure 5.16. Changes in the level of metabolites of abiotic stress defence in the *old3* mutants. Red dots indicate data for plants grown at 28 °C for 16 (0), 16+2 days (2 days) and 16+5 days (5 days). Blue dots indicate data for plants grown for 16+2 days (2 days) and 16+5 days (5 days) at 20 °C, after temperature shift at day 16 from 28 °C. The data in blue dots at 0 days, is soon after shift to 20 °C at day 16 from 28 °C. Data represents mean of three biological replicates. Error bar represents standard deviation. Statistically significant differences in the values between the mutants and the respective wild-types, using Student's *t* test are shown by * at $P < 0.01$, ** at $P < 0.005$, *** at $P < 0.001$ and **** at $P < 0.0005$. In *old3-1*^{rec}, the values are statistically analysed against the data from Col-0.

The indole-glucosinolates, phenylpropanoids, flavonoids, phytoalexins and other disease resistance compounds are derived from the aromatic amino acids, tyrptophan and phenylalanine, via the shikimate pathway. A selection of key representatives of these metabolites was also tested in all the lines. The results from this investigation indicated that camalexin, which is synthesized *de novo* upon perception of pathogen-derived elicitors or toxins (Bednarek et al., 2009), accumulated specifically in the *old3-1*mutant at 20 ^{o}C but was not detected in the other plant lines at both temperatures or in the *old3-1* mutant when grown at 28 ^{o}C (Figure 5.17). Levels of tryptophan-driven indole-glucosinolates, including indole-3-yl-methyl (I3M) and 4-methoxy-indol-3-ylmethyl-glucosinolate (4MI3M), which contribute to basal immunity and disease resistance upon pathogen infection (Bednarek et al., 2009; Clay et al., 2009) and aphid feeding (Kim et al., 2008), were also significantly increased in the *old3-1* mutant only (Figure 5.17). These changes coincided with an increase in the hormone, salicylic acid (Figure 5.17), which is derived from the chorismate-shikimate pathway and is intricately involved in disease resistance responses (Vlot et al., 2009).

In contrast to these changes, metabolites, including benzoic acid, phenylpropanoids and flavonoids, which are involved in stress defence (Treutter, 2006), were not significantly altered in the *old3-1* mutant and other lines at 20 or 28 ºC (Appendix 15). Thus, only those compounds in the shikimate metabolic pathway which are involved in disease resistance were specifically accumulated in the *old3-1* mutant. These changes were not observed in *old3-2* or *old3-1*^{rec}. Aliphatic glucosinolates, which are derived from methionine and are also implicated in resistance against insect herbivory (Beekwilder et al., 2008), were also tested in all the lines. The results from this examination indicate that these glucosinolates were largely unaffected in all *old3* mutants as compared to respective wild-type lines (Appendix 15). Overall, metabolomic studies at both temperatures suggest that some, yet not all, metabolic pathways involved in diverse stress responses, are up regulated during autoimmune syndrome.

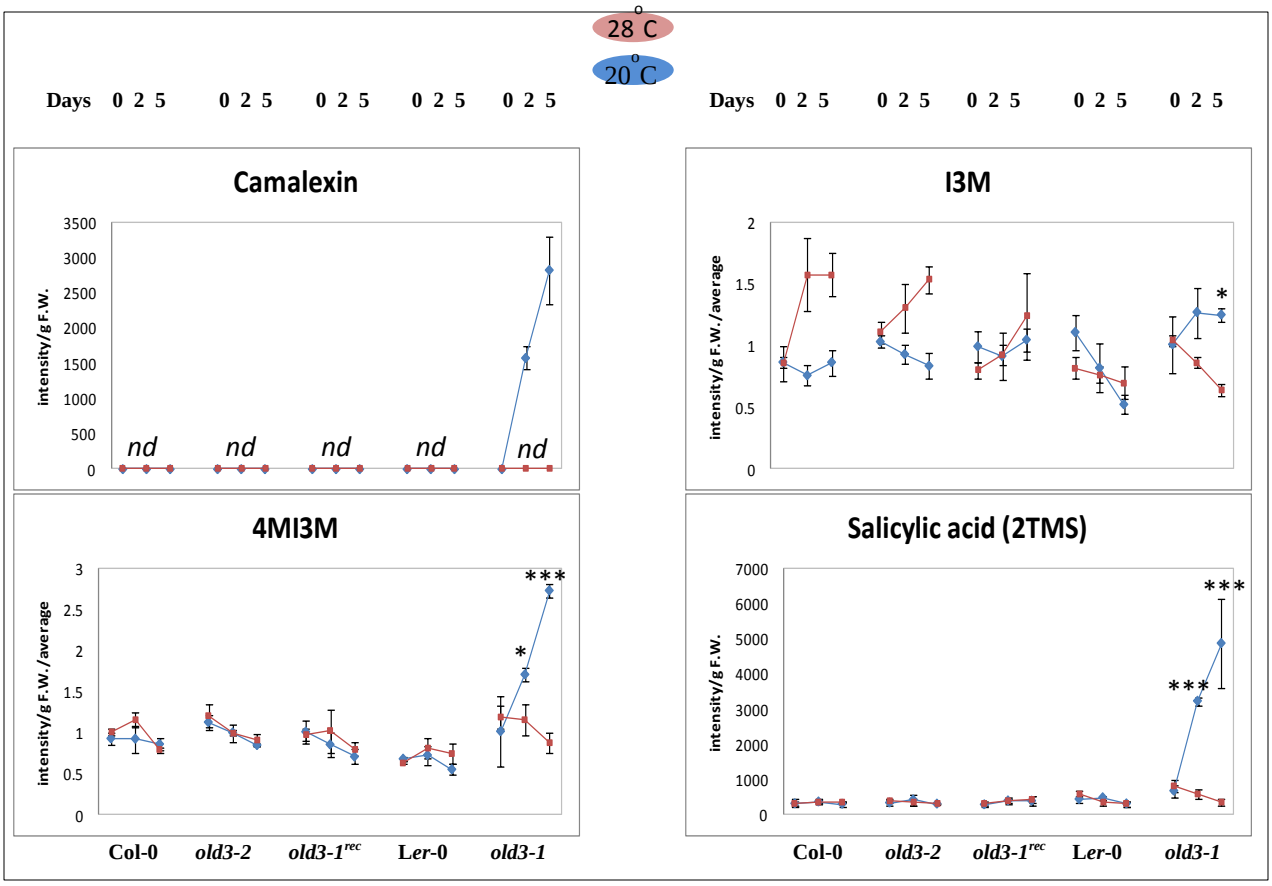

Figure 5.17. Analysis of compounds associated with innate and basal immunity in *old3* mutants. Red dots indicate data for plants grown at 28 °C for 16 (0), 16+2 days (2 days) and 16+5 days (5 days). Blue dots indicate data for plants grown for 16+2 days (2 days) and 16+5 days (5 days) at 20 °C, after temperature shift at day 16 from 28 °C. The data in blue dots at 0 days, is soon after shift to 20 °C at day 16 from 28 °C. Data represents mean of three biological replicates. Error bar represents standard deviation. Statistically significant differences in the values between the mutants and the respective wild-types, using Student's *t* test are shown by * at $P < 0.01$, ** at $P < 0.005$, *** at $P < 0.001$ and **** at $P < 0.0005$. In *old3-1*^{rec}, the values are statistically analysed against the data from Col-0.

c. Changes in primary metabolism due to growth temperature

Some key differences were observed in the metabolic profile of all the lines that show the effects of the natural genetic background and variation in growth temperature at the level of metabolites. These show that levels of some amino acids including glutamine and aspartate were only lower, at high temperature, as compared to when grown at low temperature. However, other amino acids and sugars were not affected due to growth temperature or natural variation. Similarly, the levels of metabolites from cysteine metabolism including OAS, Cys, GSH and sulfate were also not affected by the environment or variation in the genotype.

d. Variation in secondary metabolites due to differences in genetic background and growth temperature

In contrast to metabolites of primary metabolism, many secondary metabolites appeared to be affected between the L*er*-0 and Col-0 plants. The levels of almost all methionine glucosinolates were found to be naturally higher in Col-0 as compared to L*er*-0 background (Appendix 15). Methionine-glucosinolates were previously shown to be involved in resistance against insect herbivory (Beekwilder et al., 2008). Interestingly, as L*er*-0 is also found to be more susceptible to Diamondback Moth feeding in comparison to another *Arabidopsis* accession, Cvi (Collins et al., 2010), it is possible that reduced methionine-glucosinolates level may be the cause of susceptibility to herbivory in L*er*-0. Furthermore, the metabolic profiling also indicated that in Col-0, levels of methionine glucosinolates were higher when grown at high temperature as compared to low temperature (Appendix 15). Thus, high temperatures can increase the accumulation of insect defence-related compounds. Consistent with this, the pathogen defence-related indole-glucosinolate i.e, indole-3-yl-methyl (I3M) was also found to be accumulated at high temperature only in Col-0 as compared to L*er*-0 (Appendix 15), indicating the role of higher temperature in affecting biotic stress defence pathways as well as higher level of defence activation in Col-0.

Similarly, level of metabolites from the phenylpropanoid pathway including sinapoyl esters and flavonoids also differed between Col-0 and L*er*-0 genotype and these levels were further affected due to temperature changes (Appendix 15). Levels of sinapoyl-malate, which is implicated to

function in UV protection and male fertility (Ruegger and Chapple, 2001), were found to be higher in Col-0 when grown at low temperature as compared to when grown at high temperature. Furthermore, natural levels of sinapoyl-malate were higher in Col-0 as compared to L*er*-0, which is consistent with the previous observations (Ruegger and Chapple, 2001). Similarly, levels of all flavonoids including anthocyanins, quercetins and kaempferols were increased after shifting to low temperature as compared to when grown at high temperature in Col-0 but not in L*er*-0 (Appendix 15). These results implicate that growth temperature may significantly affect the biosynthesis and /or homeostasis of flavonoids depending upon the genotype.

Levels of secondary metabolites including glyceric acid and ornithine were found to be increased in L*er*-0 but not in Col-0, when shifted to low from high temperature (Figure 5.16 and Appendix 15). On the other hand, levels of fumaric acid, which is an intermediate in TCA cycle, was also increased in both genotypes at high temperature but no other TCA metabolites such as succinic or malic acid under the same growth conditions (Figure 5.12). Similarly, levels of erythritol, a ROS scavenging sugar, were also found to be increased in Col-0 at high temperature only (Appendix 15). Another metabolite *myo*-inositol, which is involved in suppressing cell-death activation (Meng et al., 2009; Donahue et al., 2010), was also increased in Col-0 at high temperature (Figure 5.16).

5.5 Mutations in OASTL-A1 affect disease resistance against the pathogen *Pseudomonas syringae* pv. *tomatoDC3000*

The results in this study suggested a possible relationship between OASTL-A1 and immunity. Therefore the disease resistance in *Arabidopsis* plants lacking OASTL-A1 was assessed against the pathogen *Pseudomonas syringae* pv. *Tomato DC3000*. *Pst DC3000* causes effector-triggered susceptibility (ETS) by releasing effector molecules that dampen PAMP-Triggered Immunity (PTI) (Katagiri et al., 2002). *Arabidopsis* furthermore lacks an ETI response against *Pst DC3000*, rendering this pathogen virulent. *Arabidopsis* L*er*-0 plants in which *OASTL-A1* expression was suppressed using RNAi and the *old3-2* mutant, together with their respective wild-types, were infiltrated with *Pst DC3000*. Subsequent to infection, mutants lacking functional OASTL-A1 in two different genetic backgrounds showed enhanced infection rate at day 2, concomitant with higher bacterial counts/CFU as compared to their wild types (Figure 5.18 and Appendix 16). Thus, OASTL-A1 contributes in resistance against a virulent pathogen in *Arabidopsis*.

To identify, whether OASTL-A1 is involved in a PTI-driven resistance phenotype in plants, the resistance response of *old3* mutants was determined for a non-virulent *Pst* strain. For this purpose the *Pst* DC3000, *hrpA*$^{-}$ strain was used for infections, which lacks the ability to deliver effector molecules inside plant cells to cause ETS. Therefore, *Arabidopsis* successfully triggers PTI against this strain without showing disease-induced chlorosis (Roine et al., 1997; Wei et al., 2000). Results demonstrated that upon infiltration or spray inoculation of *Pst hrpA*$^{-}$, *old3-2* mutants showed development of enhanced disease-induced chlorosis as compared to wild-type Col-0 plants (Figure 5.19). *old3-1*-RNAi-*RPP1/ B40-12* line, in which expression of the *RPP1*-like *R* genes was suppressed, was also included in the analysis. Both *old3-2* and *old3-1*-RNAi-*RPP1* plants showed enhanced chlorosis as compared to L*er*-0 (Figure 5.19). These results highlight a novel role of OASTL-A1 in a specifically PTI-driven disease resistance response in both accessions and indicate that the function of cytosolic OASTL-A1 is indispensable in plant defence.

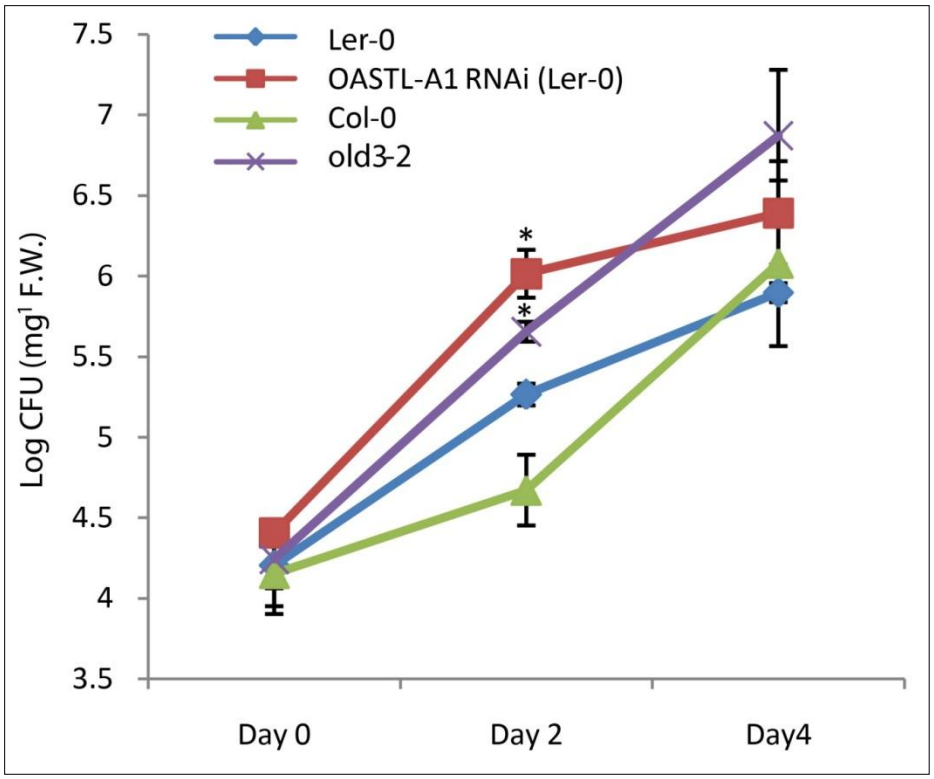

Figure 5.18. Disease susceptibility of *old3* mutants and wild-type *Arabidopsis* during infection with virulent *Pst DC3000*. Colony Forming Units (CFU) for *Pst D3000* were measured in all the lines at day 0, 2 and 4 post-infection. Data represents mean values of three biological replicates for each line. For each biological replicate, tissues were pooled from six to seven leaves. Mean counts from three biological replicates for each line per time point is represented. Error bars represent standard deviation of the mean. * indicates statistically significant differences in values between the mutant and their respective wild-type at similar time point using Student's *t* test ($P < 0.05$). The experiment was performed twice and similar results were obtained.

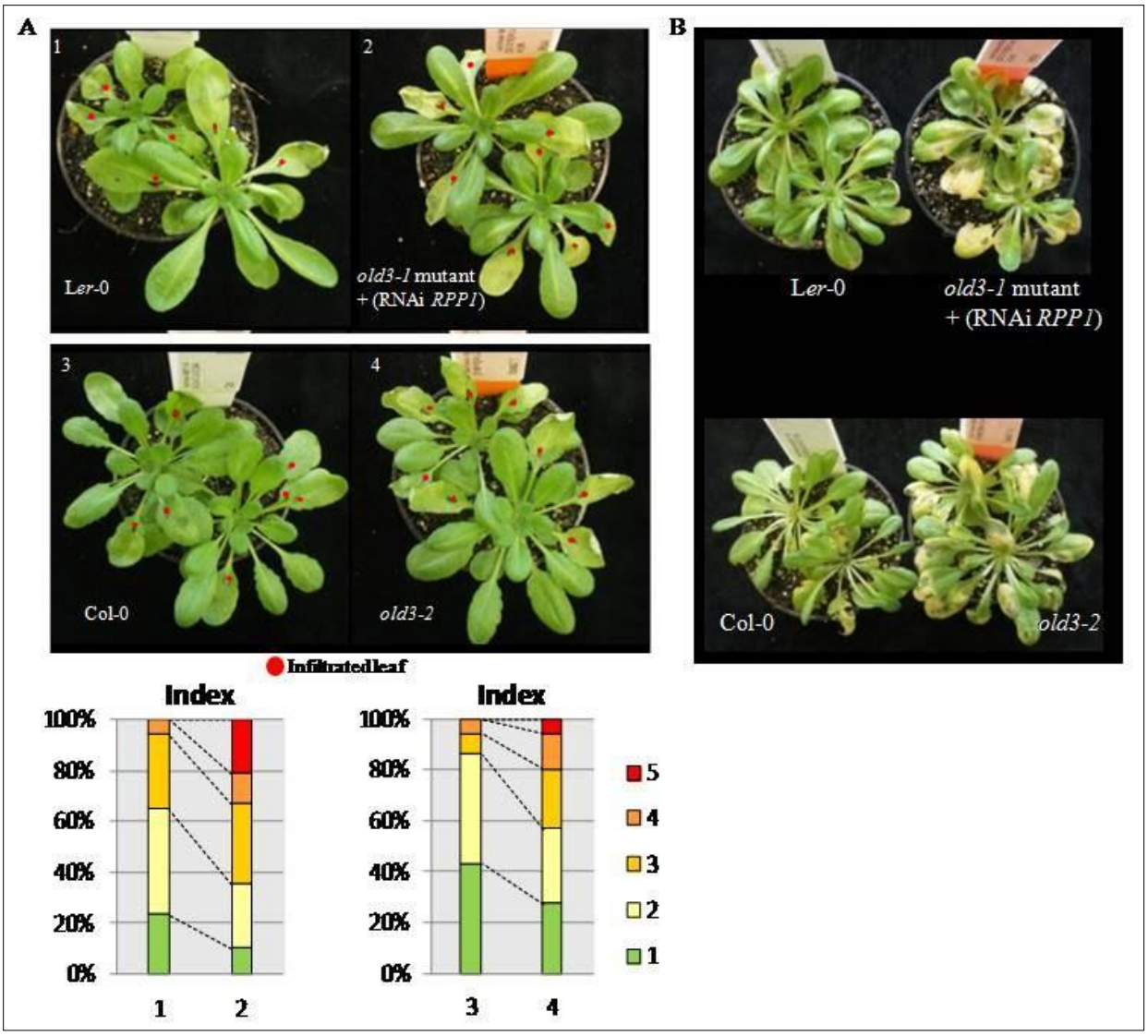

Figure 5.19. *OASTL-A1* contributes in basal resistance.(A) shows phenotypes and disease resistance score in *Arabidopsis* plant lines against infection by *Pst DC3000* (*hrpA*$^-$). (1) L*er*-0, (2) *old3-1* mutant rescued with RNAi-*RPP1/B40-12*, (3) Col-0 and (4) *old3-2* that were infected with *Pst*. Syringe inoculation of *Pst* (1 x 10^4 cfu/mL) was performed on plants grown for 6 weeks under SD (8 h day/16 h night; 20 °C/16 °C). Disease index was scored after 3 days of infection on n=51 leaves from 14 plants for each genotype. Disease levels, 1 (no visible symptoms) to 5 (complete water-soaking chlorosis) were scored to generate the index for each genotype. In a Student's *t*-test for the disease index scores, the *P*-value is 4 x 10^{-5} for L*er*-0 and *old3-1 odd-ler* rescued with RNAi *RPP1*and 2 x 10^{-3} for Col-0 and *old3-2*. All mock inoculated leaves (10 mM $MgCl_2$) showed absence of any visible lesions. (B) shows L*er*-0, *old3-1 odd-ler* rescued with RNAi *RPP1/B40-12*, Col-0 and *old3-2* infected with *Pst DC3000* (*hrpA*$^-$). Spray inoculation of *Pst* (1 x 10^8 cfu/mL) was performed on plants grown for 7 weeks under SD (8 h day/16 h night; 20°C/16°C) conditions. Representative plants, 7 days after spray inoculation are shown.

5.6 Transcript accumulation of *BSAS* genes in different treatments and stress conditions

The findings in this study have pinpointed the link between the function of an OASTL enzyme in cysteine metabolism and disease resistance. Also, the role of other BSAS enzymes in mitigating stress in *Arabidopsis* has been comprehensively reviewed in Chapter 2. Together these observations supports the process of "Sulfur-Induced Resistance" (SIR) or Sulfur Enhanced Defence (SED) in plants as proposed previously (Rausch and Wachter, 2005; Bloem et al., 2007; Kruse et al., 2007). Concomitantly, it would not be surprising if various stress signals may regulate *BSAS* gene expression in plants. The gene transcript accumulation of *BSAS* isoforms is well studied in plant shoots and roots under normal growth conditions (Watanabe et al., 2008a). However, very little information is available on the effects of various external signals on the transcriptional regulation of specific *BSAS* genes. This may provide interesting information on putative cross-talks between the function of different *BSAS* genes under a diverse set of environments and signals.

In this study, the data from various microarray experiments carried out on *Arabidopsis* plants was obtained from the Genevestigator IV tool (Hruz et al., 2008). Microarray experiments with various growth conditions provided the opportunity to obtain a detailed view of transcriptional response of the *BSAS* genes in *Arabidopsis* in response to various abiotic and biotic signals. Nevertheless, use of the public microarray database from the Genevestigator tool comes with some limitations. It has to be taken into account that the expression spectrum presented here is based on individual treatments, plant lines and different growth conditions that may differ between different research groups. Moreover, the gene expression changes cannot predict the changes in enzyme activities of these isoforms. Irrespective of these limitations associated with the Genevestiagtor output, the differential expression of specific *BSAS* genes in response to a particular change in environment or stress is still a positive indicator of potential cross-talks between the signal and the functionality of the genes being activated or repressed.

Initially, the expression of *BSAS* genes was analysed in specific organs and tissues of *Arabidopsis* during various stages of development (Figure 5.20). The data obtained suggest

differential transcript accumulation of all the *BSAS* genes in various aerial parts and tissues during different stages of development (Figure 5.20 and Figure 5.21). Results showed that globally, the *OASTL-A1*, *OASTL-B* and *β*-CAS transcripts were highly abundant as compared to *OASTL-C* and *CysD1* and *CysD2*. The lowest transcript abundance was recorded for the *DES* and *CS26*.

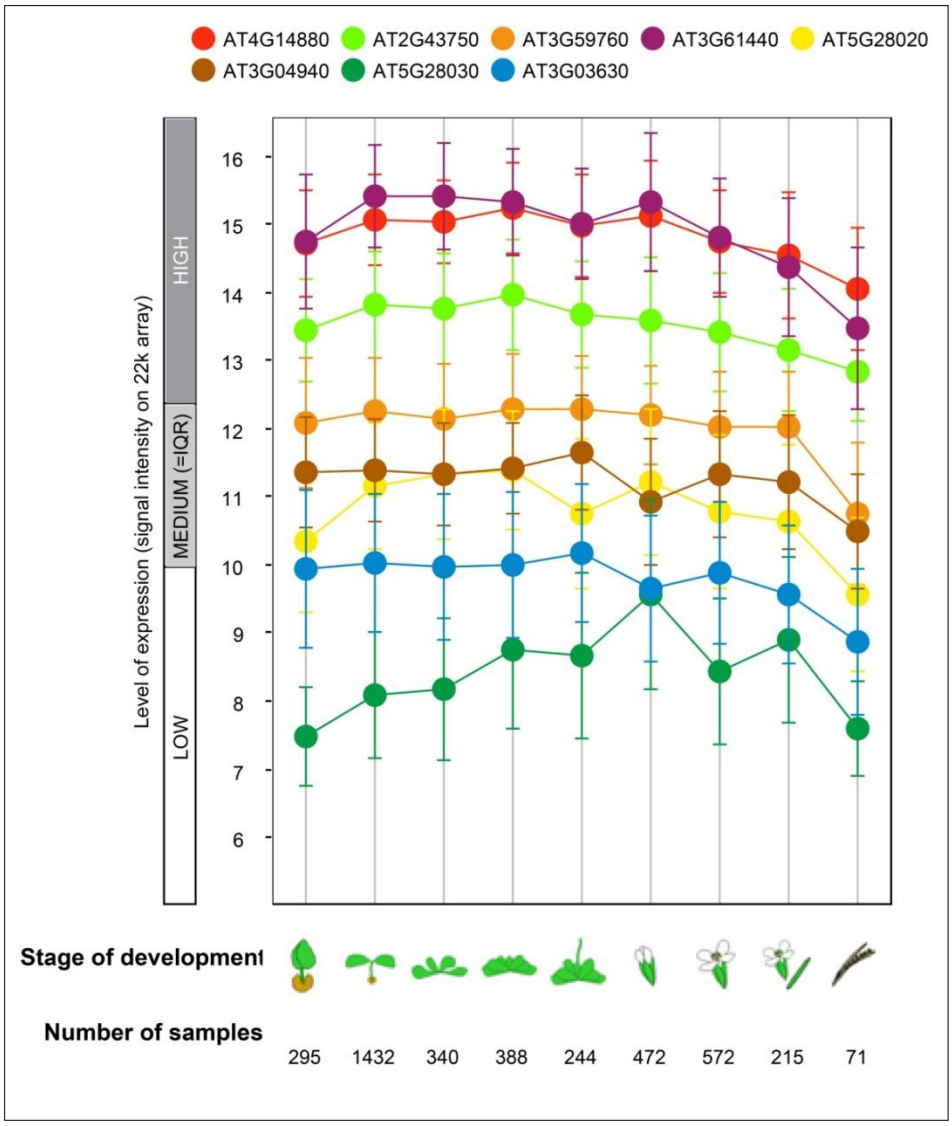

Figure 5.20. Transcript abundance of *BSAS* genes in various aerial parts of *Arabidopsis* during different stages of development.

AT4G14880 is *OASTL-A1*, AT2G43750 is *OASTL-B*, AT3G59760 is *OASTL-C*, AT3G61440 is *CysC1/β-CAS*, AT5G28020 is *CysD2*, AT3G04940 is *CysD1*, AT5G28030 is *DES1* and AT3G03630 is *CS26*. Data and figure obtained from Genevestigator VI .

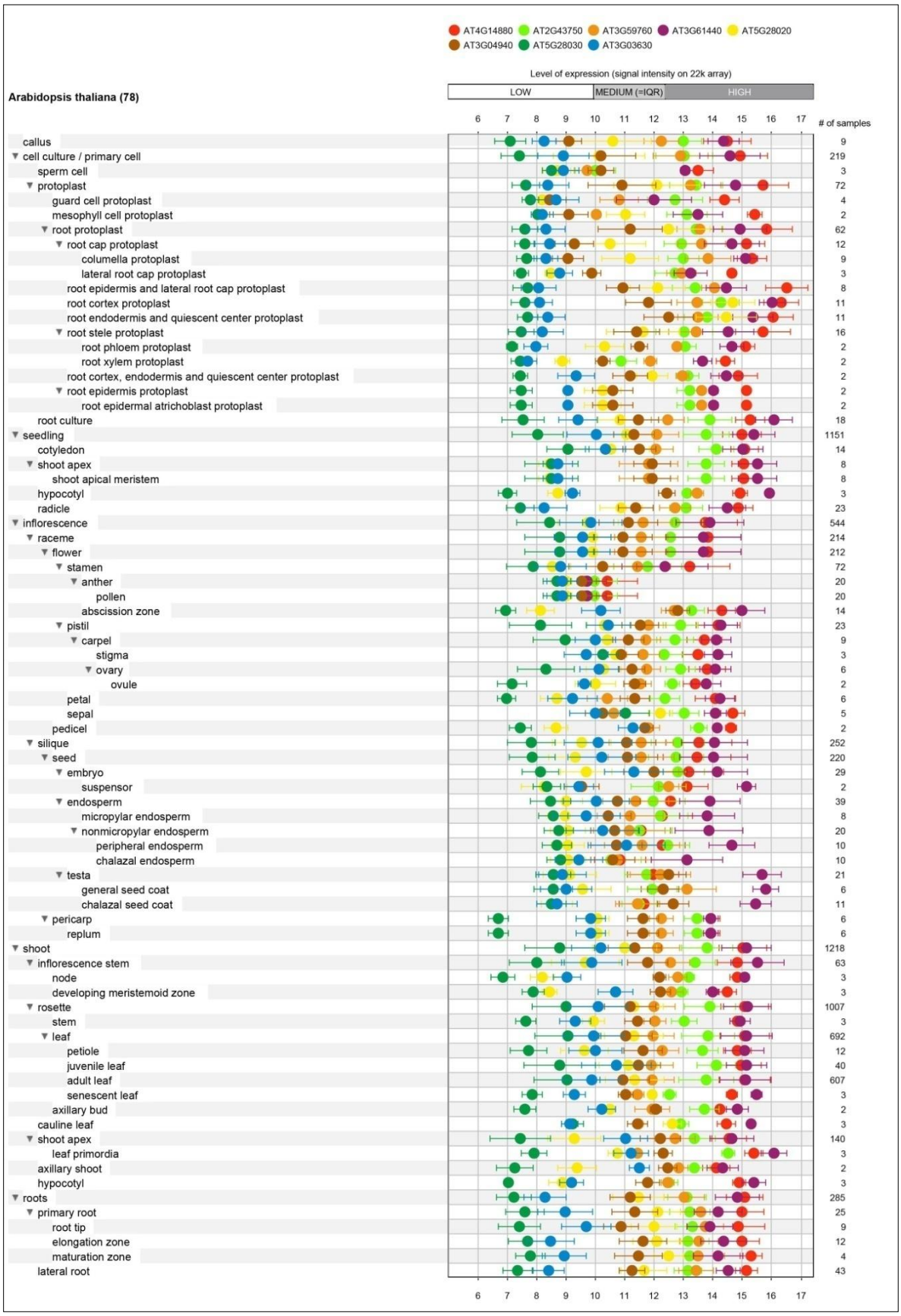

Figure 5.21. Transcript abundance of *BSAS* genes in various tissues in the major organs of *Arabidopsis* during different stages of development. AT4G14880 *is OASTL-A1*, AT2G43750 is *OASTL-B*, AT3G59760 is *OASTL-C*, AT3G61440 is *CysC1/β-CAS*, AT5G28020 is *CysD2*, AT3G04940 is *CysD1*, AT5G28030 is *DES1* and AT3G03630 is *CS26*. Data and figure obtained from Genevestigator. VI

The Genevestigator tool provides the opportunity to identify significant changes in gene expression in plant tissues under various growth conditions. Therefore from thousands of treatments those were filtered which were able to induce ≥2 fold change in the expression of *BSAS* genes and were statistically significant at cut-off value $P \leq 0.05$. Not all the *BSAS* genes were found to be differentially expressed at the criterion used for filtering the data. Abundance of the the *BSAS* gene transcripts varied in response to the different external abiotic and biotic signals or treatments. Therefore these treatments were divided into three groups: (i) pathogens and elicitors, (ii) hormones and (iii) abiotic stress treatments.

(i) Pathogens and elicitors

Pseudomonas syringae (*Pst*) strains have been identified as virulent pathogens of *Arabidopsis* and are widely used to study plant-pathogen interactions. To infer the response of *BSAS* genes expression in pathogen assay, experiments involving infections with various *Pst* strains, including, *P. syringae pv. tomato, P. syringae pv. maculicola* and *P.syringae pv.phaseolicola,* were analysed using the Genevestigator toll. Results showed that infection of *Arabidopsis* with these strains suppressed the transcript accumulation of the *OASTL-B, Cys-D1, Cys-D2, DES* and *CS26* gene (Figure 5.22). However transcript abundance of the *OASTL-A1, OASTL-C* and *β-CAS* gene was found not to be significantly affected during these experiments. From those which were negatively affected during biotic stress, *DES* was found to be the only gene whose transcript abundance was also negatively affected upon infection with the fungus *Golovinomyces cichoracearum* (Figure 5.22). Infection of *Arabidopsis* plants with the *Blumeria graminis* fungus, which causes powdery mildew, was found to specifically suppress the expression of the *CysD1* and *CS26* genes (Figure 5.22).

The ability of plants to trigger a defence response to pathogens is based on their detection system. The Patteren Recognition Receptors (PRRs) in plants can detect Microbe-Associated Molecular Patterns (MAMPs) and initiate a basal defence called PAMPS or **M**AMPs-**T**riggered **I**mmunity (**P/MTI**). Bacterial flagellin Flg22 and the Elongation Factor-Tu (EF-Tu), which are conserved pathogen MAMPS, are commonly used elicitor in the studies to detect basal defence response and disease resistance. Treatments with the flagellin Flg22 and EF-Tu peptides were

found to negatively affect the transcript accumulation of *CysD1* and *CysD2*, *DES* and *CS26*, although the expression of *OASTL-B* was differentially affected as well (Figure 5.23).

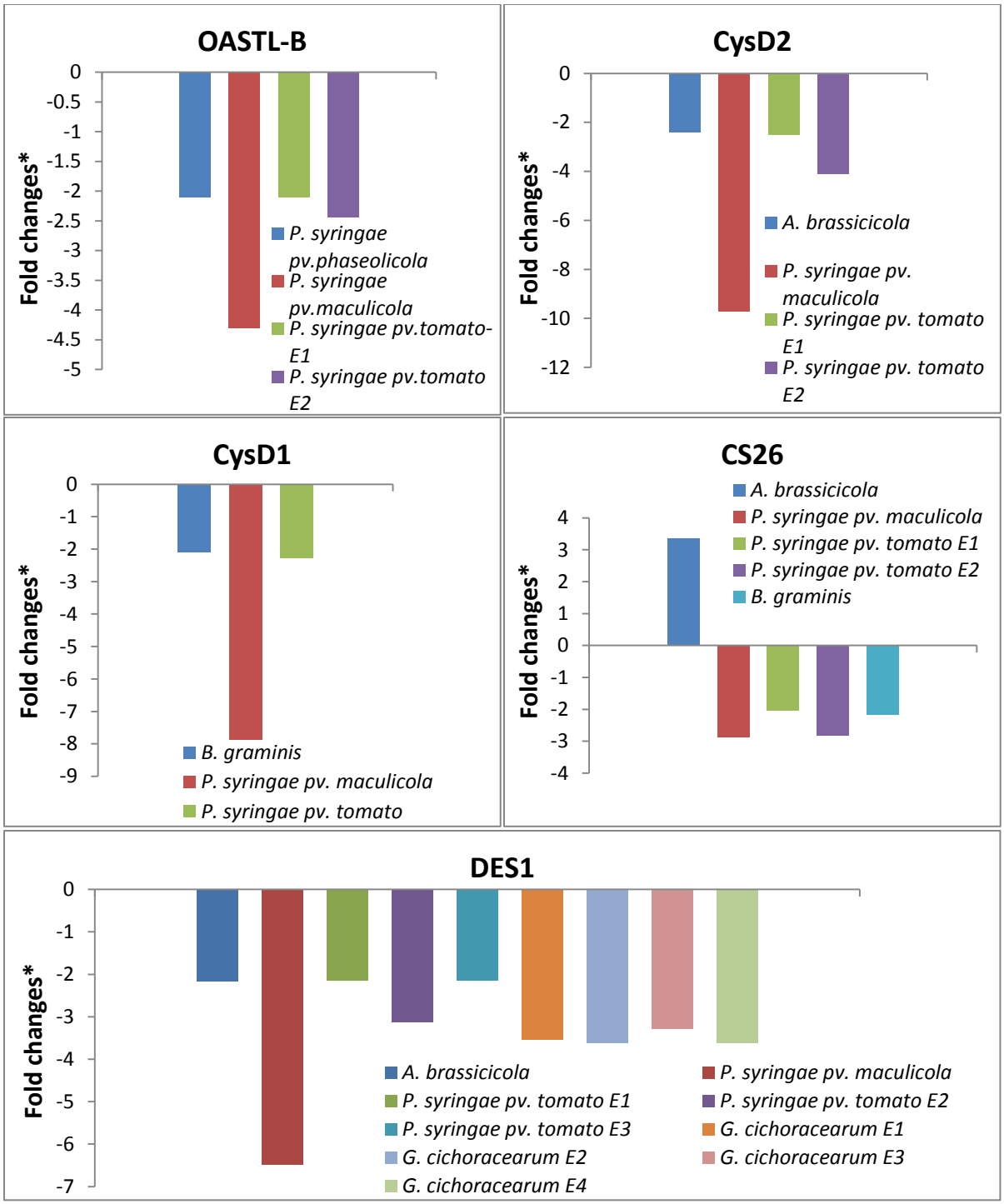

Figure 5.22. Fold changes in the abundance of *BSAS* genes transcripts in *Arabidopsis* post- infection with different pathogens. Figure represents changes in the expression of various *BSAS* gene in *Arabidopsis* in response to different pathogen infections including *Pseudomonas syringae (P.syringae)*, *Alternaria brassicicola (A. brassicicola*), *Blumeria graminis* (*B. graminis*), *Golovinomyces cichoracearum* (*G. cichoracearum*).Those treatments were selected which were able to induce ≥2 fold change in the expression of the *BSAS* genes. The values were statistically significant at $P \leq 0.05$. Not all the *BSAS* genes were found to be affected at the criterion used for filtering the data. Data represents changes between 0-36 h post-infection/treatment. *E1..En* represents different number of experiments..

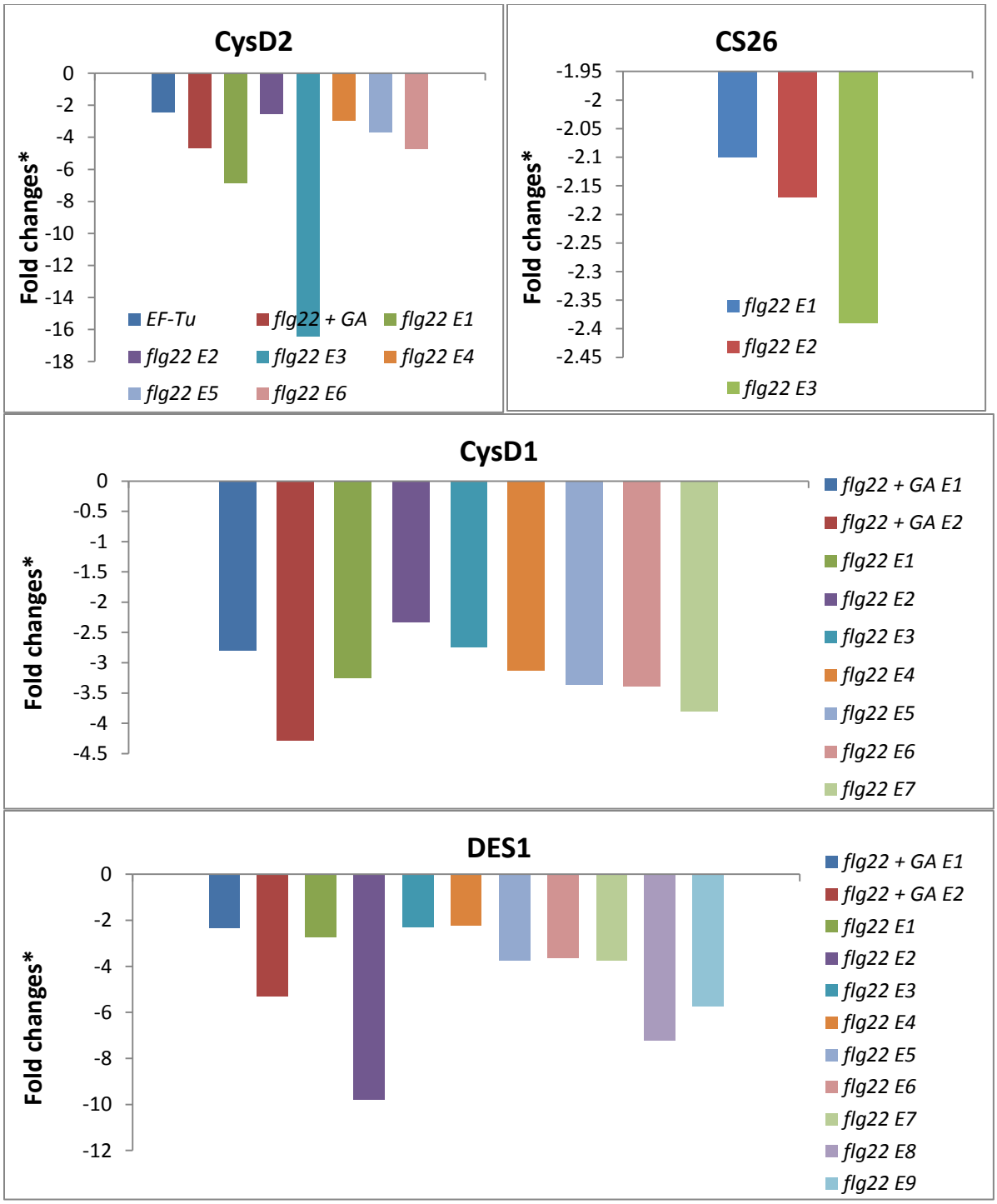

Figure 5.23. Fold changes in the abundance of *BSAS* genes transcripts in *Arabidopsis* post-treatment with the microbial peptides EF-Tu and flg22. Figure represents changes in the expression of various *BSAS* genes in *Arabidopsis* in response to treatment with the bacterial elongation factor (EF-Tu) and flagellum-specific protein (flg22). Those treatments were selected which were able to induce ≥2 fold change in the expression of the *BSAS* genes. The values were statistically significant at $P \leq 0.05$. Not all the *BSAS* genes were found to be affected at the criterion used for filtering the data. Data represents changes between 0-36 h post-infection/treatment. *E1..En* represents different number of experiments.

(ii) Hormones

The functions of plant hormones are diverse and linked to various mechanisms of plant development. From treatments with different hormones, Brassinolide, which is a Brassinosteroid and involved in plant growth and cell division, was found to strongly affect all the *BSAS* genes, except *DES1*, *CysD2* and *OASTL-A1*. Treatments with Brassinolide were found to enhance the transcriptional activity of the *CysD1*, *β-CAS*, *CS26* and *OASTL-B*. However the expression of the *OASTL-C* gene was negatively affected by treatment with the Brassinolide in various experiments.

Various hormonal treatments, specifically those which are involved in biotic stresses were found to affect the transcript accumulation of *BSAS* genes. Methyl-Jasmonates (MeJa) are involved in plant defence against insect attack and herbivory. Treatment of *Arabidopsis* with MeJa was found to negatively affect the transcript accumulation of *CysD1*, *CysD2*, *DES* and *β-CAS* only (Figure 5.24 and 5.25). However the plastid and mitochondrial localised BSAS encoding genes, *OASTL-B* and *CS26* and the *OASTL-C*, respectively, showed increased accumulation in response to MeJa application (Figure 5.24 and 5.25). Further the role of Salicylic acid (SA), which is directly involved in resistance against t pathogens, was also investigated. It was identified that treatment with SA negatively affected the transcript accumulation of the *DES* and *CS26* only, but not the other *BSAS* genes (Figure 5.24 and 5.25). Furthermore the role of abscisic acid (ABA) in regulating BSAS transcripts was also explored. Interestingly abscisic acid (ABA), which is involved in resistance against abiotic stress, was found to suppress the transcript abundance of the *β-CAS*, *CS26* and *CysD1* only (Figure 5.25).

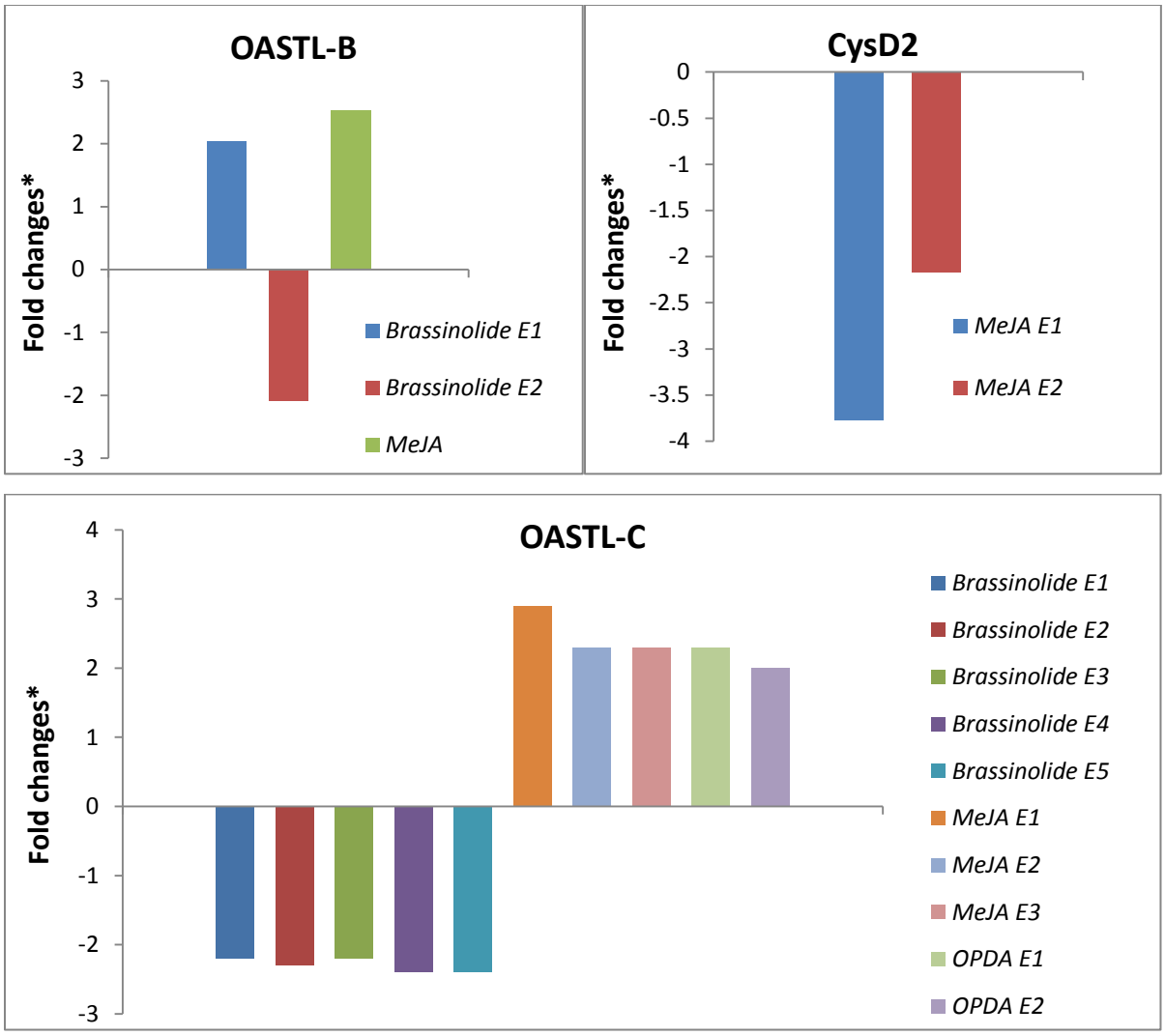

Figure 5.24. Fold changes in the abundance of *BSAS* genes transcripts in *Arabidopsis* upon treatment with different hormones. Figure represents changes in the expression of various *BSAS* genes in *Arabidopsis* in response to treatment with different hormones, including Brassinolide, Methy-Jasmonate (MeJA), and 12-oxo-phytodienoic acid (OPDA). Those treatments were selected which were able to induce ≥2 fold change in the expression of the *BSAS* genes. The values were statistically significant at $P \leq 0.05$. *E1..En* represents different number of experiments..

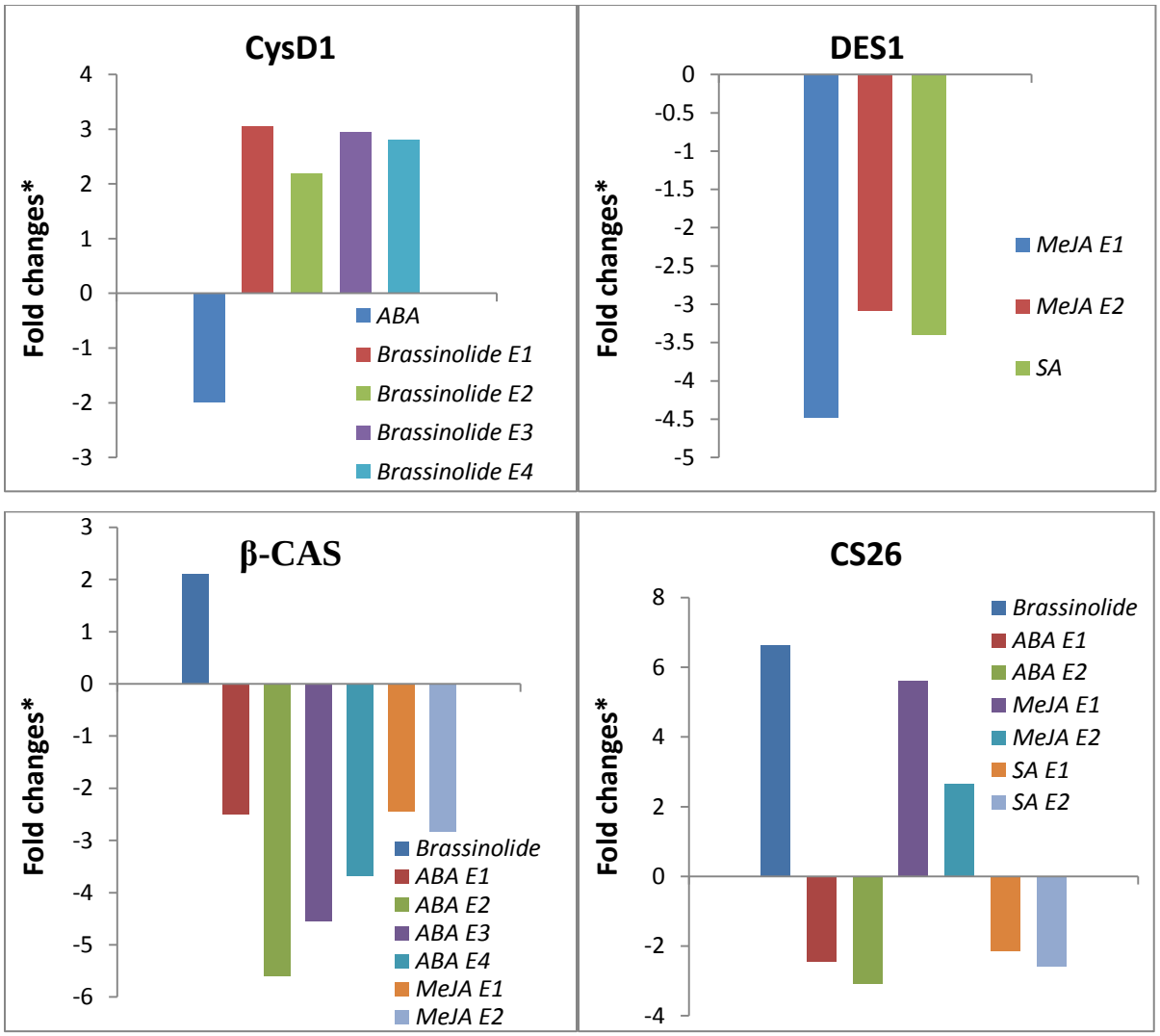

Figure 5.25. Fold changes in the abundance of *BSAS* genes transcripts in *Arabidopsis* upon treatment with different hormones. Figure represents changes in the expression of various *BSAS* genes in *Arabidopsis* in response to treatment with different hormones, including Brassinolide, Methy-Jasmonate (MeJA), Abscisic acid (ABA) and Salicylic acid (SA). Those treatments were selected which were able to induce $\geq$2 fold change in the expression of the *BSAS* genes. The values were statistically significant at $P \leq 0.05$. *E1..En* represents different number of experiments. Data obtained from Genevestigator VI.

(iii) Abiotic stress

BSAS genes transcripts were found to be differentially accumulated in *Arabidopsis* plants when exposed to different abiotic stress treatments (Figure 5.26 and 5.27). Light and temperature are two important signals that regulate plant growth and development. Data from various experiments in Genevestigator indicated that the transcript abundance of the *OASTL-B*, *β-CAS*, *CysD2* and *DES* genes was suppressed under high light conditions (Figure 5.26 and 5.27). In contrast high light intensity resulted in the accumulation of the *CS26* gene only. However in a shift to L.D. from S.D, the *CysD2* transcript specifically accumulated in comparison to the other *BSAS* genes (Figure 5.27). Furthermore, the experiments involving temperature reduction highlighted that the *CysD2* transcripts were specifically suppressed in cold treatments as compared to the other *BSAS* genes (Figure 5.27). In contrast, heat treatments resulted in relatively high transcript accumulation of the *CysD2, CysD1* and *DES* genes only but had a negative impact on the accumulation of the *OASTL-C* and *β-CAS* gene transcripts (Figure 5.26 and 5.27).

Experiments involving sulfur deficiency were found to induce expression of the *CysD1* and *CS26* genes but did not significantly affect the expression of other *BSAS* genes (Figure 5.26 and 5.27). Similarly nitrate starvation suppressed the *CysD2* and *CS26* gene expression (Figure 5.27). Exposure of plants to saline conditions was also found to negatively affect the *CysD2* and *DES* transcript accumulation (Figure 5.26 and 5.27). Similarly hypoxia treatments were specifically found to negatively affect the abundance of the *DES* and *CS26* genes as well as the accumulation of mitochondrial *OASTL-C* (Figure 5.26 and 5.27).

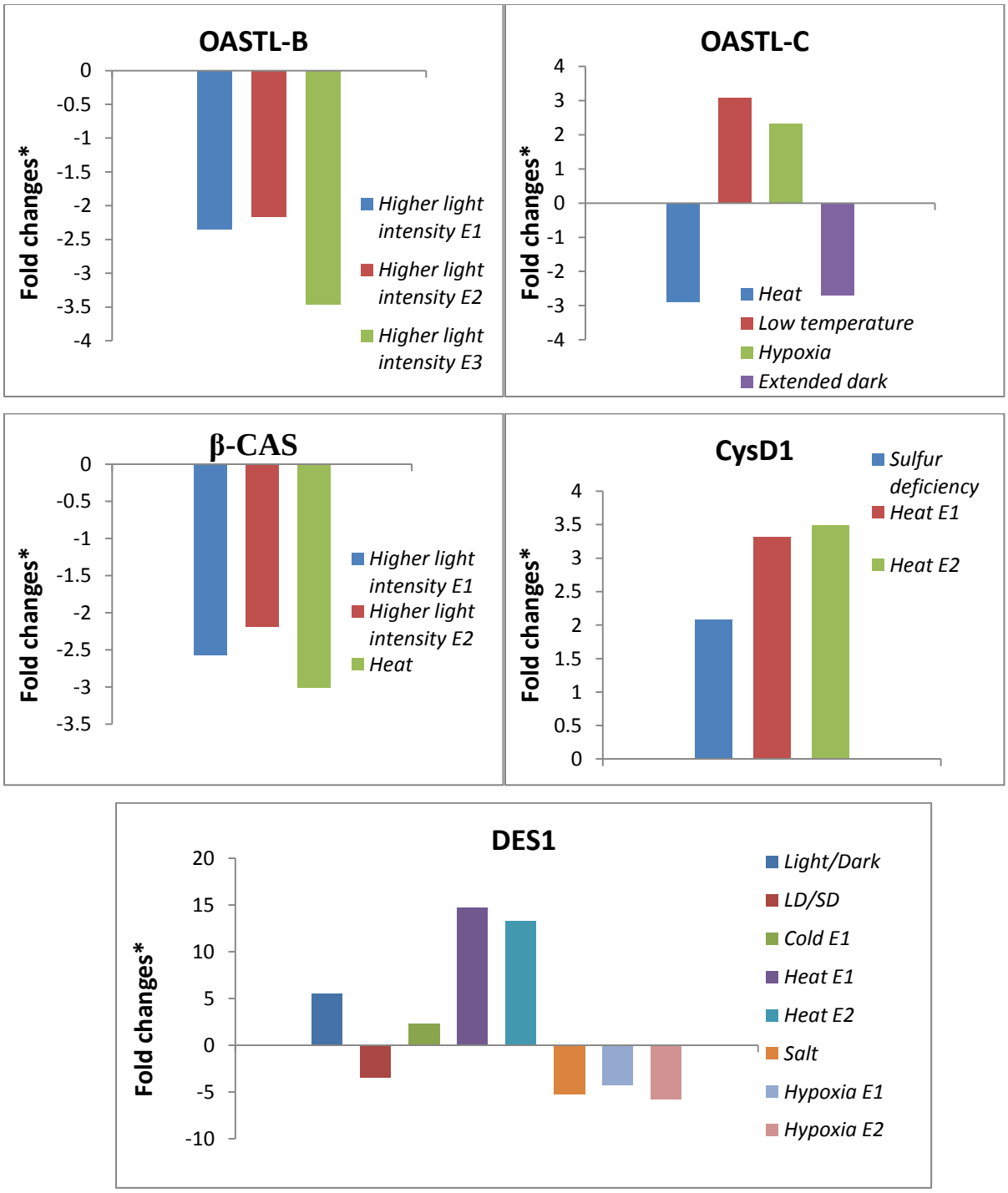

Figure 5.26. Fold changes in the abundance of *BSAS* genes transcripts in *Arabidopsis* under different growth conditions. Figure represents changes in the expression of various *BSAS* genes in *Arabidopsis* in response to different growth conditions. Those treatments were selected which were able to induce ≥2 fold change change in the expression of the *BSAS* genes. The values were statistically significant at $P \leq 0.05$. *E1..En* represents different number of experiments.

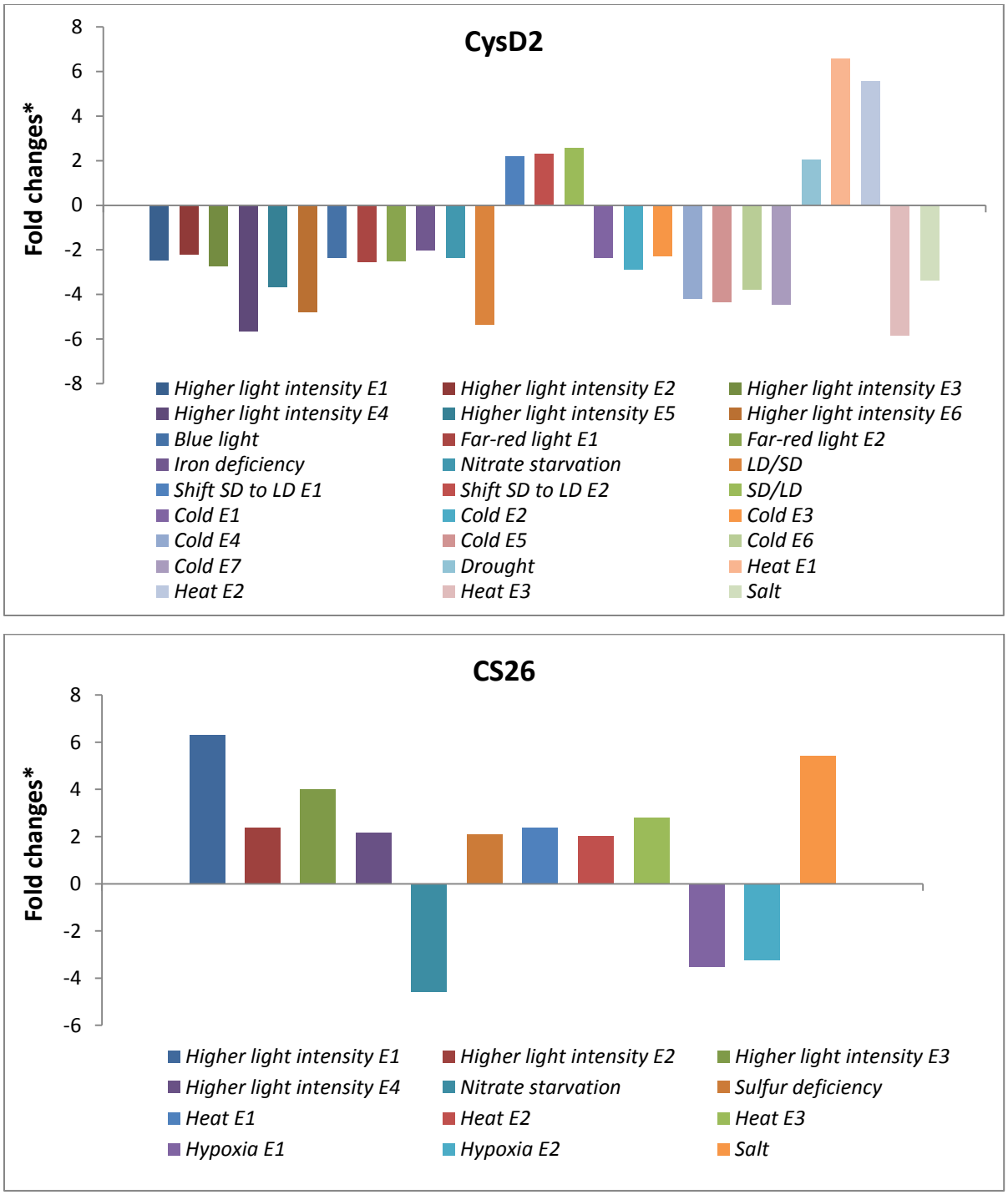

Figure 5.27. Fold changes in the abundance of *BSAS* genes transcripts in *Arabidopsis* under different growth conditions. Figure represents changes in the expression of various *BSAS* genes in *Arabidopsis* in response to different growth conditions. Those treatments were selected which were able to induce ≥2 fold change change in the expression of the *BSAS* genes. The values were statistically significant at $P \leq 0.05$. *E1..En* represents different number of experiments.

Discussion

Cysteine metabolism in the *oastl-a1/old3* mutants

The effect of the *old3-1* mutation is detrimental to OASTL activity in plants. It is important to note that the *old3-1* mutation, G/E^{162}, is located near the PLP interacting His^{157}residue. The total SERAT activity was not reduced in the *old3-1* mutant. However, a significant reduction was observed in the *old3-2* mutant. Although this reduction was observed at a time point at low temperature, the results indicated that growth temperature shows a regulatory effect on total SERAT activity but not on the total OAS or cysteine levels. Regardless, the results also suggest that OASTL-A1 contributes to *β*-CAS activity and that old3-1 may still possess the *β*-CAS activity as it was not significantly reduced in the *old3-1* mutant. Thus old3-1 may be functional with respect to the OASTL-SERAT interaction and *β*-CAS activity but this needs further investigation *in vivo* and *in planta*.

The results show that lack of a functional cytosolic OASTL-A1 have largely neutral effects on plant phenotype, cysteine levels and metabolites of stress-defence pathways in *Arabidopsis*, when grown under permissive growth conditions. Remarkably, while mean OASTL activity dropped by ~45-50 % among *old3* mutants, no significant difference in cysteine levels were found. Similarly, anti-sense suppression of OASTL genes in potato caused reduced OASTL activity without a reduction in cysteine levels (Riemenschneider et al., 2005). Nevertheless, it was earlier reported that *Arabidopsis oastl-a1/old3-2* mutants had reductions in cysteine levels ranging from 15-28% (Heeg et al., 2008; Watanabe et al., 2008a). The reduced cysteine levels were reported to coincide with the absence of growth phenotype (Heeg et al., 2008; Watanabe et al., 2008a), while others noted an ~34% reduction in cysteine levels, coinciding with lesions resulting from increased oxidative stress (Lopez-Martin et al., 2008). These differences can be attributed to variations in growth media, day length and age. Indeed, a significant reduction in GSH levels was detected at day 5 after temperature shift in *old3-2* only, which indicates that altering growth conditions or age may affect thiol levels. Thus, while cytosolic-specific cysteine levels might have been affected in *old3* mutants, the results are consistent with the suggestion

that facilitated diffusion of cysteine between sub-cellular compartments likely contributes in maintenance of the total cysteine and GSH levels, at least under non-stressed growth conditions (Heeg et al., 2008; Watanabe et al., 2008a; Krueger et al., 2009).

Upon activation of autoimmunity in the *old3-1* mutants, amino acid levels including cysteine increased markedly, despite the reduced total OASTL activity. The increase in cysteine and other amino acids may result from protein degradation as total protein levels decreased during autoimmunity. However, it cannot be excluded that cysteine is synthesised *de novo* as a result of remaining functional OASTL activity in plastids and mitochondria. Indeed, the *oastl-ab* mutant lacks functional OASTL-A1 and B but accumulates significantly higher cysteine levels, likely because of residual OASTL activity (Heeg et al., 2008). The *oastl-ab* mutant displays growth retardation and the higher cysteine accumulation in this mutant may be part of a stress-response.

Since SERAT activity depends on the interaction with OASTLs, cytosolic SERAT activity may be lower in *old3* mutants. However, lack of functional OASTL-A1 did not affect total SERAT activity in the *old3* mutant lines in different genetic backgrounds. This is consistent with a previous observation (Heeg et al., 2008), but an approximately 30% increase in SERAT activity was found by others (Lopez-Martin et al., 2008). Unchanged total SERAT activity coincided with unaltered total OAS levels as reported here, under permissive growth conditions and by Heeg *et al*., (2008). The observed higher OAS concentration, during the autoimmune response, in the *old3-1* mutant is likely the result of the functional SERAT-OASTL partners in plastids and mitochondrial compartments. Indeed, the *oastl-ab*, but not *oastl-c* mutant, has previously been shown to accumulate higher OAS levels (Heeg et al., 2008). This suggests that OAS levels can increase during stress provided the presence of functional mitochondrial OASTL-C. This is consistent with the finding that not cytosol but mitochondria are the major site of OAS production (Heeg et al., 2008; Watanabe et al., 2008a; Krueger et al., 2009). Higher OAS concentration furthermore coincided with higher sulfate and cysteine levels in the *old3-1* mutants during autoimmunity.

Metabolic changes in *R*-triggered autoimmunity

Autoimmunity involves activation of immune responses and previous studies indicate that synthesis of immune compounds including salicylic acid is required and/or associated with the autoimmune phenotypes in plants (Alcázar et al., 2009; Takumi and Mizuno, 2011) .The accumulation of plant defence compounds including phytoalexin camalexin from the shikimate pathway and the hormone SA was associated with the autonecrosis in the *old3-1* mutant and appears to be the hallmarks of autoimmunity.

Accumulation of SA and camalexin is associated with the accumulation of 4MI3M glucosinolate, a compound which is involved in disease resistance (Bednarek et al., 2009; Clay et al., 2009), in the *old3-1* mutant. These changes were not observed in *old3-2* and *old3*^{rec} indicating that the lack functional OASTL is not responsible for accumulation of these metabolites. However increased levels of OAS and sulfate, as identified in the *old3-1* mutant, may be responsible or necessary for higher 4MI3M concentration since metabolites in the sulfur assimilation pathway are involved in the regulation of glucosinolate biosynthesis (Mugford et al., 2009; Yatusevich et al., 2010; Moldrup et al., 2011).

The metabolic changes in the *old3-1* mutant include *de novo* accumulation of sugars and amino acids despite a major reduction in starch levels. These changes represent a state of disorder and metabolic stress, in comparison to wild-type, as it couples with the accumulation of stress-defence compounds. Increase in free sugars and amino acids, during the immune response against pathogen infection, has been reported across species, likely as a consequence of plant-pathogen interaction (Scharte et al., 2005; Swarbrick et al., 2006). Furthermore sugars can act as precursors for the carbon skeleton in amino acids. As amino acids were shown to be precursors of plant defence compounds (Halkier and Gershenzon, 2006; Stuttmann et al., 2011), the execution of a constitutive stress response implies a fitness cost, likely resulting from an altered central metabolism (Bolton, 2009). Regardless, the basis of the sugar accumulation during autoimmune response remains unexplainable and it's possible that these changes are part of hypersensitive (HR) immune response i.e., R-mediated Programmed Cell Death (PCD). In

contrast, the levels of Met-glucosinolates and other metabolites in the phenylpropanoid pathway, including flavonoids and anthocyanins, were not significantly accumulated during autoimmunity.

Role of OASTL-A1 in disease resistance and R-triggered immunity

The role of cytosolic OASTL-A1 has been already highlighted in resistance to oxidative stress and metal and pollutant toxicity (Barroso et al., 1999; Domínguez-Solís et al., 2001; Noji and Saito, 2002; Heeg et al., 2008; Lopez-Martin et al., 2008; Shirzadian-Khorramabad et al., 2010). This suggests OASTL-A1 as a major BSAS enzyme involved in regulating stress tolerance. In this study, mutations in *OASTL-A1* were found to enhance disease susceptibility against a virulent pathogen. This is consistent with a recent finding which shows that the *oas.a1.1* (*old3-2)* mutant exhibits an impaired ETI response (Alvarez et al., 2012b). Further, the results indicate a novel role of OASTL-A1 in basal defence, as wild-type *Arabidopsis* successfully establishes PTI against *Pst DC3000, hrpA*$^{-}$ (Wei et al., 2000). Thus, the recent evidence and findings presented here suggest that the cytosolic OASTL machinery is important in *Arabidopsis* immunity.

The *old3-2*/*oas.a1.1* mutant has an oxidised cellular redox state (Lopez-Martin et al., 2008) and reduced total OASTL activity. Emerging evidence indicates that cytosolic redox status modulates defence reprogramming in the nucleus and cysteine-derived metabolites including GSH, glucosinolates and camalexin are involved in basal defence (Parisy et al., 2007; Tada et al., 2008; Bednarek et al., 2009; Clay et al., 2009). Thus the impaired disease resistance response in *old3-2/oas.a1.1* mutants may be linked to reduced cysteine availability in the cellular system during biotic stress conditions (Alvarez et al., 2012b). Hence OASTL-A1 may contribute to plant fitness during both abiotic and biotic stress.

In contrast, the *old3-1* mutation in OASTL-A1 causes activation of plant defence and autonecrosis, in certain accessions. These findings are reminiscent of those observed for *ACCELERATED CELL DEATH6* (*ACD6*), which is involved in plant fitness and disease resistance but genetic variation at this locus activate immune responses and later onset of necrosis in specific *Arabidopsis* accessions (Todesco et al., 2010). The *old3-1* mutation in OASTL-A1 activates an innate immune response due to a novel genetic interaction with disease

resistance *RPP1*-like *R* gene(s). The rescue of autonecrosis via RNAi-mediated suppression of *OASTL-A1* or *RPP1*-like genes in the *old3-1* mutant (Chapter 4) furthermore demonstrated that *R*-mediated autoimmune response is caused by the mutation in OASTL-A1 in combination with the R protein(s) and not because of lower cysteine biosynthesis. The absence of noticeable differences between the *old3-1*^{rec} and *old3-2* metabolome (i.e., in the absence of the *odd-ler* allele) shows that old3-1 itself does not cause major metabolic disturbances and suggest that old3-1 is not involved in the synthesis of compounds that activate immune responses. If old3-1 does have an ectopic activity, then an RPP1-like protein(s) is required for this activity to be detected. The functional basis of R mediated epistatic interactions however remains obscured in many cases (Alcázar et al., 2009; Yamamoto et al., 2010). The genetic basis of negative epistasis linked with *R* mediated autoimmune syndrome in different plant species, has now pinpointed plant proteins which modulate basal defence and interact with *R*-mediated innate immune signalling (Alcázar et al., 2009; Jeuken et al., 2009). These results support the view that *R*-mediated resistance can be based on interaction with other host proteins (Dangl and Jones, 2001).

BSAS gene expression under different abiotic and biotic stress signals

The gene expression mining study using the Genevestigator tool (Hruz et al., 2008) was successful in identifying key signals that account for differential expression spectrum of *BSAS* genes in *Arabidopsis*. Higher expression levels of the *OASTL-A1*, *OASTL-B* and *β*-CAS gene transcripts across different developmental stages in *Arabidopsis* suggest that during evolution the roles of these genes may have become very important for growth. This is consistent with the notion that OASTL-A1 and OASTL-B are the major isoforms in regulating cysteine biosynthesis (Heeg et al., 2008; Watanabe et al., 2008a; Krueger et al., 2009). However this does not negate the significance of the role of other BSAS isoform encoding genes, the *OASTL-C*, *CysD1*, *CysD2*, *DES* and *CS26*, in the plant life cycle. This is well-supported by the concept proposed in Chapter 2 that the BSAS isoforms work as biological router in cysteine biosynthesis and homeostasis system, based on various recent studies (Heeg et al., 2008; Lopez-Martin et al., 2008; Watanabe et al., 2008a; Krueger et al., 2009; Alvarez et al., 2010; Bermúdez et al., 2010b; Shirzadian-Khorramabad et al., 2010; Alvarez et al., 2012b; Alvarez et al., 2012a; Birke et al., 2012). Moreover enhanced *BSAS* gene expression in response to the Brassinolide hormone

treatment is further suggestive of the putative involvement of BSAS isoforms in plant growth and development.

The effect of the pathogen and effector treatments on the transcriptional activity of specific *BSAS* genes, including *OASTL-B*, *CysD1*, *CysD2* and *DES1*, is notable. The expression of the *DES1* encoding gene was specifically affected under various bacterial and fungal pathogen treatments. Recent findings have also shown that the lack of the *DES1* gene results in constitutive systemic acquired immunity and disease resistance against fungal and bacterial pathogens (Alvarez et al., 2012b). Thus the function of the *DES1* and other *BSAS* genes including *OASTL-B*, *CysD1* and *CysD2* may be crucial in immune signalling during plant-pathogen interaction. It is notable that the *OASTL-A1* transcript abundance was unchanged under most treatments and experimental conditions. There were however, a few chemical treatments (data not shown), which were able to induce significant fold changes in its transcript abundance.

The interaction between different disease and pest resistance-related plant hormones and *BSAS* transcriptional response is intriguing. Methyl-Jasmonate treatments were found to activate the expression of the major *OASTL-B* and *OASTL-C* genes as well as *CS26*. It is currently not well-understood how jasmonic acid integrates with the cysteine and sulfur metabolism. However cysteine-driven glutathione biosynthesis and sulfur metabolism is part of the glucosinolates biosynthesis pathway which fuels herbivory resistance in *Arabidopsis* (Mugford et al., 2009). Since JA also plays a significant role in insect herbivory, transcriptional control of the *BSAS* genes by JA treatment therefore warrants investigation how JA may be modulating plant cysteine biosynthesis and homeostasis for herbivore resistance. Treatment with JA and the other disease resistance hormone SA was found to suppress the expression of the *DES1* gene. *DES1* has already been implicated in disease resistance (Alvarez et al., 2010; Alvarez et al., 2012b) and its suppression due to SA treatment is further suggestive of possibly a negative role during disease and pest resistance response. As DES is involved in the degradation of cysteine, its suppression can enrich the cellular cysteine-thiol pool (Alvarez et al., 2010; Alvarez et al., 2012b). These changes could directly affect the cellular redox conditions which has been now shown to play a central role in plant immunity (Spoel et al., 2003; Spoel et al., 2010; Spoel and Loake, 2011; Alvarez et al., 2012b). In conclusion these findings implicate novel cross-talk between post-

infection basal defence signalling and transcriptional changes in specific *BSAS* genes, most of which play a very minor role in cysteine biosynthesis.

The effect of abiotic elements on the expression of different *BSAS* genes was also notable. *β-CAS*, which is associated with the cyanide detoxification and therefore can successfully contribute to abiotic stress-defence, was found to be suppressed with ABA treatments. ABA is already known to mitigate stress development in plants. It was therefore surprising why ABA negatively affect the expression of *β-CAS* which degrades the un-wanted by-product, the cyanide, of the stress-induced compound. The specific suppression of *β-CAS* transcripts with the hormone treatments including MeJa and ABA would be worth further investigating to better understand how stress-related hormones regulate other stress-mitigating enzymes. The effects of temperature and light specifically on *CysD2* transcript profile in comparison to the other genes warrants the biochemical and physiological characterisation of the *cysd2* mutants in various temperature and light growth conditions. This may further help in understanding its cross-talk with stress-related responses. On the other hand salt treatment has been shown to induce *CS26* transcripts, likely because CS26 is involved in the synthesis of S-sulfocysteine which is implicated in redox control in the chloroplast (Bermúdez et al., 2010b). Overall, the stress factors-induced regulation of *BSAS* transcriptional activity provides new insights on possible functional aspects of those isoforms whose roles are not clearly demonstrated in cellular cysteine biosynthesis or homeostasis. This includes the *CysD1* and *CysD2* which are also the true OASTLs.

Blank Page

Chapter 6

Functional characterization of structural variations in OASTL-A1

Introduction

PLP is required as a co-factor to various enzymes, among prokaryotes and eukaryotes, that carry out diverse biochemical reactions. Protein structure of the PLP-dependent enzymes including threonine synthase in *Arabidopsis* plant as well as enzymes from distant species including *S. typhimurium* tryptophan synthase β-subunit and *Sacchromyces cerevisiae* threonine synthase and the *Hansenula saturnus*1-aminocyclopropane-1-carboxylate deaminase are well characterised (Hyde et al., 1988; Yao et al., 2000; Thomazeau et al., 2001; Garrido-Franco et al., 2002). The *Arabidopsis* plant OASTL-A1 enzyme carries out cysteine biosynthesis using PLP as a co-factor and shows high homology to other PLP dependent enzymes in its α/β-domain structure (Bonner et al., 2005). Diversification, regarding substrate binding and the nature of the enzymatic reaction among PLP-dependent enzymes, is associated with the sequence variations in the residues that bind to PLP (Bonner et al., 2005).

OASTL-A1 carries out the substitution of the acetyl-moiety in OAS with the sulphide and generates cysteine and acetyl-coA. PLP binding to the Lys^{46} residue of OASTL-A1 via Schiff base linkage is pre-requisite to this reaction and determines the OASTL activity (Daum et al., 2002). The residues Asn^{77} and Gln^{147} are active in binding to the substrate O-acetylserine and therefore set the basis of substrate specificity in OASTLs. The Thr^{74} and Ser^{75} residues are further implicated into sulfate binding, as mutation in these residues affected the K_m value for sulfide. A detailed structural analysis of OASTL-A1 has already been performed in previous

studies to understand the role of various residues involved in the catalytic activity of OASTL (Bonner et al., 2005).(also described in detail in Chapter 2). OASTL interacts with the enzyme SERAT and makes a hetero-oligomeric complex. In this interaction the SERAT activity increases which yields *O*-acetylserine, whereas OASTL activity becomes significantly reduced (Saito et al., 1995; Droux et al., 1998). The complex of SERAT-OASTL protein comprises of a SERAT hexamer of ~180 kD and two OASTL dimers, each of ~70 kD (Kredich et al., 1969; Saito et al., 1995). Active sites involved in the OASTL activity also determines the interaction of OASTL with the SERAT and this is confirmed by various protein-protein interaction studies (Bogdanova and Hell, 1997; Wirtz et al., 2001; Bonner et al., 2005; Francois et al., 2006; Zhao et al., 2006; Kumaran et al., 2009).

The *old3-1* mutation has highlighted a novel genetic interaction between an enzyme involved in cysteine metabolism and immune-related R protein(s) which resist pathogen virulence. It is therefore important to understand the relevance between the R-triggered immunity and active sites of OASLT-A1 required in major functions associated with OASTL-A1 i.e., cysteine biosynthesis and SERAT interaction. The *old3-1* mutation resides in an important motif, TTGPEIW in α5 helix, which is evolutionary conserved among all the BSAS isoforms in *Arabidopsis* as well as the cysteine synthase gene in bacteria (Bonner et al., 2005; Heeg et al., 2008; Watanabe et al., 2008a). However, the function of the residues in this motif is not well-established among BSAS isoforms. That said, the *old3-1* mutation is first to indicate the role of this motif in OASTL activity (Shirzadian-Khorramabad et al., 2010). The question arises whether mutations at other residues in OASTL-A1, affecting the OASTL activity and/or SERAT interaction also show negative epistatic interaction with R proteins. To answer this question, previously characterised and uncharacterised residues in OASTL-A1 were targeted for modification with an aim to test the effect of altered OASTL function on R-triggered immunity. As true OASTL also interacts with SERAT via the OASTL-SERAT complex, it was also identified how the *old3-1* mutation affected the evolutionary conserved interactions with the SERAT enzyme

Results

6.1 Selection of the target residues for mutagenesis in OASTL-A1

A detailed structural analysis of OASTL-A1 is already published (Bonner et al., 2005). Using the crystal structure information, key amino acids were identified in OASTL-A1 for mutagenesis. The characteristics of these mutations are listed in Table 6.1. Most of these mutations were designed with an aim to affect the OASTL activity and SERAT interactions. Further, a few mutations were also designed in close proximity of residue Gly^{162}, which is the position of *old3-1* mutation, to identify the role of this region both in OASTL activity and R-triggered immunity. Third, mutations were also designed to affect the homodimerisation of OASTL-A1 protein and therefore these mutations target dimer interface residues (Table 6.1). In this way, various spots were selected in the OASTL-A1 protein for mutagenesis (Figure 6.1).

Site-directed mutagenesis was carried on OASTL-A1, using the SLIM protocol (see methods), to induce the candidate mutations. In total 11 different mutations were induced separately, each resulting in a single amino acid substitutions per protein-coding gene model (Table 6.1; Figure 6.1). The substitutions were designed to significantly change the properties of the targeted wild-type amino acid residues which includes the size, charge and/or polarity of the amino acid (Table 6.1; Figure 6.1). The mutations were initially labelled as *JT106* to *JT116* and re-named here as *old3-3* to *old3-14* (Table 6.1; Figure 6.1).

To test the impact of the mutation on the OASTL activity of the old3 proteins, an *in vivo* approach was employed. This involves the use of plant OASTL protein to complement the growth of the *E. coli* bacteria-NK3 strain which is lacking its native OASTL, the *CysK* protein. The NK3 lack CysK and therefore exhibit cysteine autotrophy. Expression of a true OASTL from plants has been shown to rescue the growth of NK3 on Cys minimal medium, indicating that a functional plant OASTL can substitute the bacterial CysK function in bacteria(Yamaguchi et al., 2000). Furthermore it has been also shown that mutations abolishing the activity of the

plant OASTL protein *in vitro* do not rescue the cysteine auxotrophy in NK3 ,thereby suggesting NK3 as a preliminary system for determining functionality of the OASTL.

Table 6.1. Characteristics of site-directed mutations in OASTL-A1.

Parameters of site-directed mutagenesis in OASTL-A1	Label	Name	Nucleotide mutation and positions in CDS	Amino acid substitutions					
				Location and position	Targeted wild-type a.a	Properties of wild-type a.a	Significance of the residue	Substituted a.a	Substituted a.a properties
Random (Control)	JT105	*old3-1*	G**G**A > G**A**A	α5 helix, 162	TT**G**PEI	Neutral, hydrophobic, small	not determined	TT**E**PEI	Negatively charged, polar, large
OASTL Activity	JT106	*old3-3*	**A**AA > **G**AA, 136	α1 helix, 46	SSV**K**DRK	Positively charged, polar, large	PLP cofactor binding	SSV**E**DRK	Negatively charged, polar, large
OASTL Activity	JT107	*old3-4*	**A**AA > **GC**A, 136-137	α1 helix, 46	SSV**K**DRK	Positively charged, polar, large	PLP cofactor binding	SSV**A**DRK	Neutral, hydrophobic, small
OASTL Activity and SERAT interaction	JT108	*old3-5*	A**C**A > A**A**A, 221	Loop between β3-sheet and α2 helix, 74	P**T**SGNT	Neutral, polar, medium	Substrate and SERAT binding	P**K**SGNT	Positively charged, polar, large
SERAT interaction	JT109	*old3-6*	**AA**G > **GC**G, 649-650	Loop between β8-sheet and β9-sheet, 217	GG**K**PG	Positively charged, polar, large	SERAT binding	GG**A**PG	Neutral, hydrophobic, small
OASTL activity	JT110	*old3-7*	**TC**A > **AA**A, 805-806	α8 helix, 269	VGI**S**SG	Neutral, polar, small	PLP interacting residue	VGI**K**SG	Positively charged, polar, large
In close proximity of *old3-1* mutation	JT111	*old3-8*	C**T**T > C**G**T, 578	α6 helix, 193	KY**L**KE	Neutral, hydrophobic, large	Not determined	KY**R**KE	Positively charged, polar, medium
In close proximity of *old3-1* mutation	JT112	*old3-9*	G**A**G > G**G**G, 491	α5 helix, 164	TTGP**E**I	Negatively charged, polar, large	Not determined	TTGP**G**I	Neutral, hydrophobic, small
Homodimerisation	JT113	*old3-10*	G**A**A > G**G**A, 941	α9 helix, 314	TRK**E**A	Negatively charged, polar, large	Not determined	TRK**G**A	Neutral, hydrophobic, small
Homodimerisation	JT114	*old3-11*	G**C**T > G**A**T, 776	α7 helix, 259	QL**A**LKE	Neutral, hydrophobic, small	Not determined	QL**D**LKE	Negatively charged, polar, medium
Homodimerisation	JT115	*old3-12*	G**C**T > G**A**T, 332	α3 helix, 111	ILL**A**FG	Neutral, hydrophobic, small	Not determined	ILL**D**FG	Negatively charged, polar, medium
Homodimerisation	JT116	*old3-13*	G**C**T > G**A**T, 260	α2 helix, 87	TA**A**AK	Neutral, hydrophobic, small	Not determined	TA**D**AK	Negatively charged, polar, medium

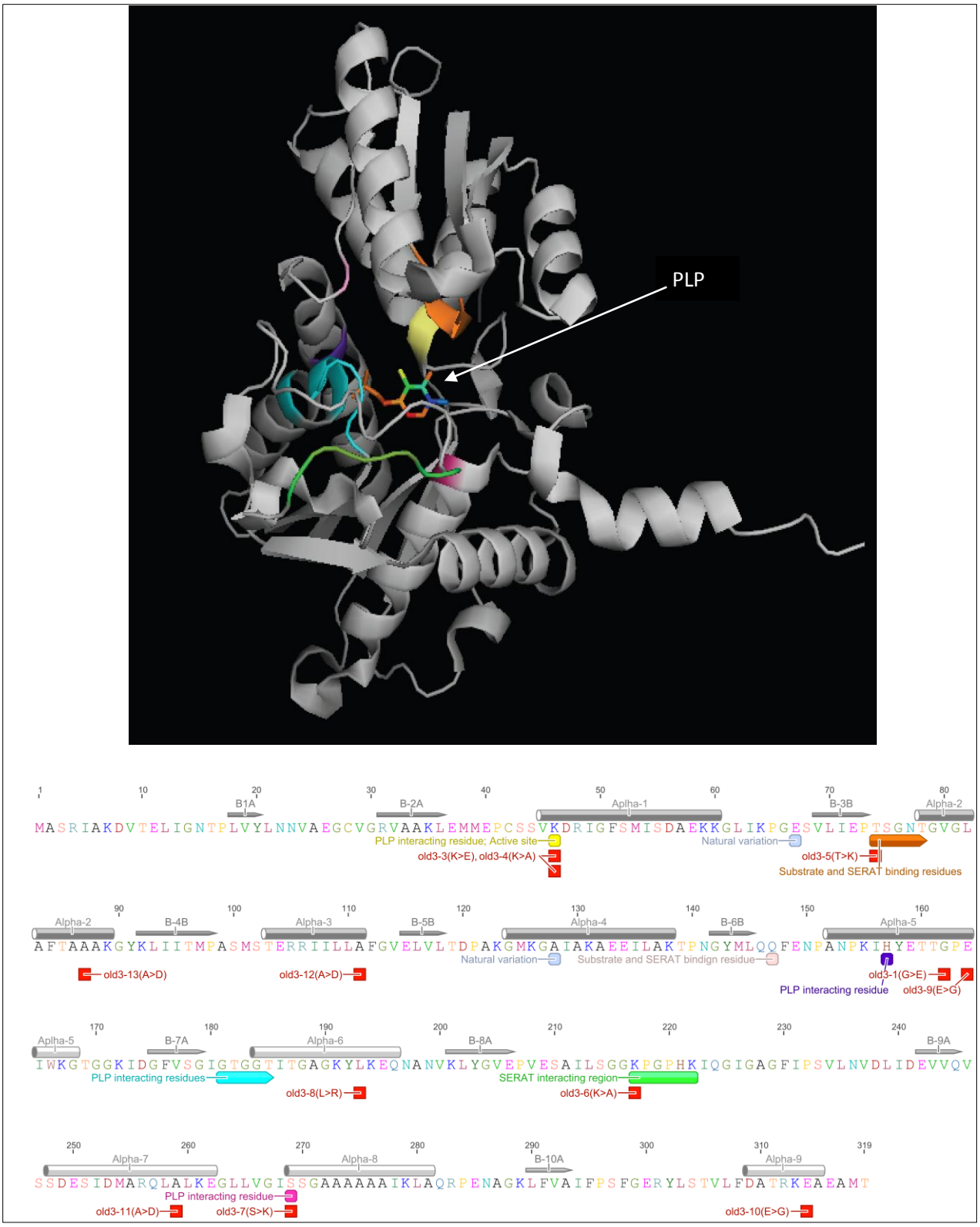

Figure 6.1. Map of the functional residues in the 3D structure of OASTL-A1 and location of the site-directed mutations in the protein sequence.

6.2 Mutations in the PLP co-factor, substrate and SERAT binding region of OASTL-A1 and their role in complementing cysteine auxotrophy

Initially the old3-1, OASTL-A1 and the empty vector were transformed into the NK3 strain and were tested for cysteine auxotrophy. Only OASTL-A1 rescued NK3 on the Cys minimal medium in contrast to old3-1 (Figure 6.2) or empty vector (Appendix 17), consistent with the findings that old3-1 is inactive *in vitro* (Shirzadian-Khorramabad et al., 2010) and *in planta*. The *old3-1* substitution is positioned in a conserved region in α5 helix nearby the His^{157} residue which interacts with the PLP binding site. Moreover, the old3-1 mutation is 4-6 Å away from other conserved residues, including Ala^{189}, Tyr^{192} and Leu^{193} as well as those residues which interact with PLP from 181-184 in the parallel α6 helix (Figure 6.2). Substitution of the G with the E amino acid at residue 162 shows that old3-1 mutation induces a significant change in size and charge of the molecule which can affect the helical arrangements and likely the cause of disturbance in the PLP catalytic activity (Shirzadian-Khorramabad et al., 2010).

To obtain other mutations targeting the OASTL activity, the *old3-3* and *old3-4* were specifically designed at the Lys^{46} residue, which is the binding site for the PLP co-factor and is crucial for enzyme activity. *old3-3* results in the substitution of the positively charged, polar and large molecule of Lys(K) with a negatively charged Gly(E) residue (Figure 6.3). On the other hand, *old3-4* brings in a neutral, hydrophobic and small amino acid, Ade (A), in place of Lys (Figure 6.3). Results indicate that these substitutions negatively affect the ability of OASTL-A1 to complement the growth of NK3 in Cys minimal medium (Figure 6.3) and this is consistent with previous studies (Bonner et al., 2005). Similarly *old3-7* was designed in the α8 helix and target an PLP interacting Ser^{269} residue . *old3-7* causes substitution of a neutral, polar and small amino acid with a positively charged and large size polar residue of Lys(K) (Figure 6.4). Like *old3-3 and 4*, *old3-7* was also unable to rescue the growth of NK3 on Cys minimal medium.

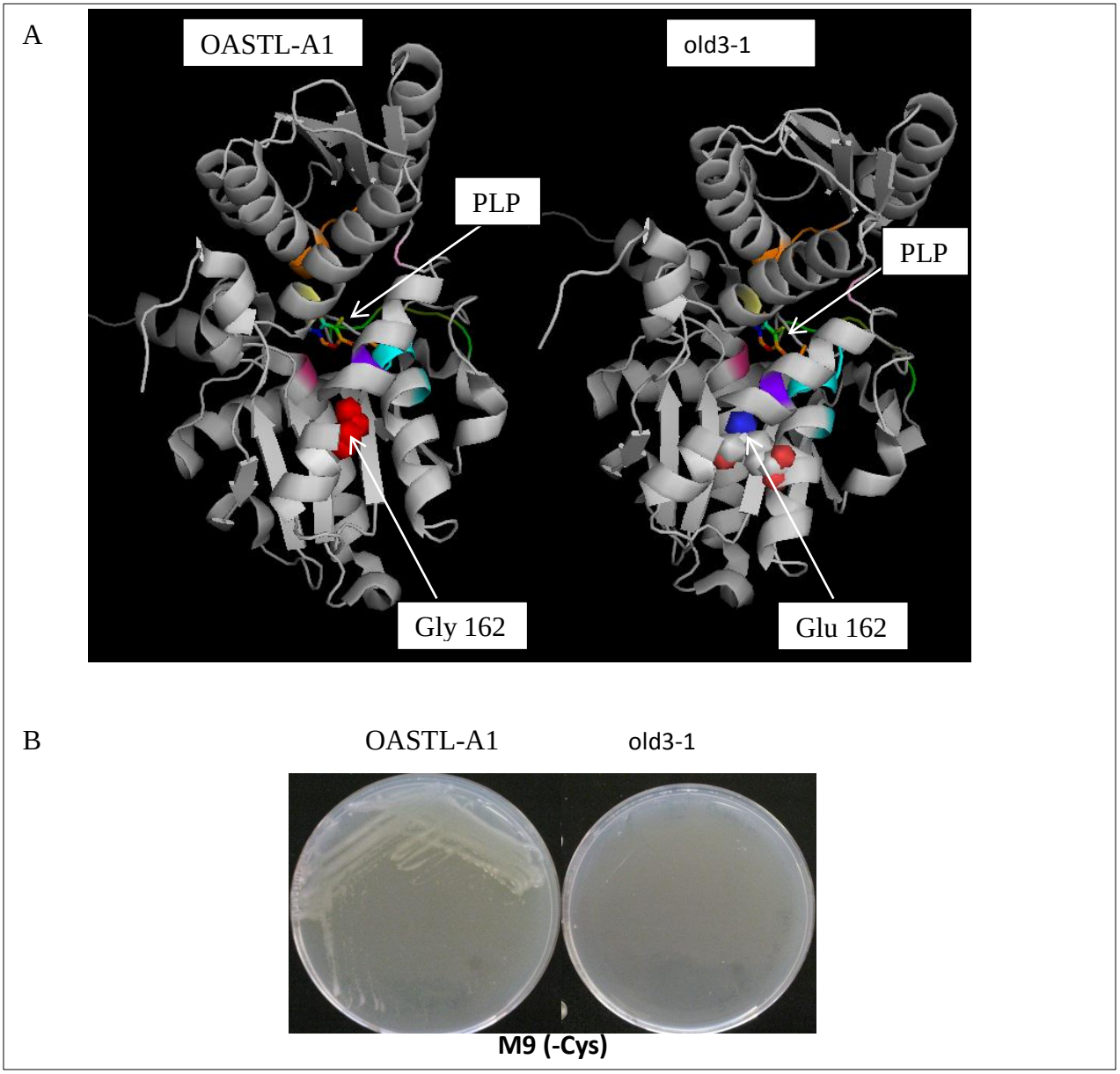

Figure 6.2. *old3-1* mutation and its effect on cysteine auxotrophy in *NK3*. A) shows 3D structure of OASTL-A1 and old3-1 highlighting the position of old3-1 mutation and its effect on the structure of the enzyme. NK3 strain carrying OLD3 and old3-1 were grown on M9 minimal medium containing cysteine. A single colony from these plates was re-streaked at the M9 minimal medium without cysteine supplementation (M9 -Cys). These plates were kept at 37 °C for 24 hr and then photographed.

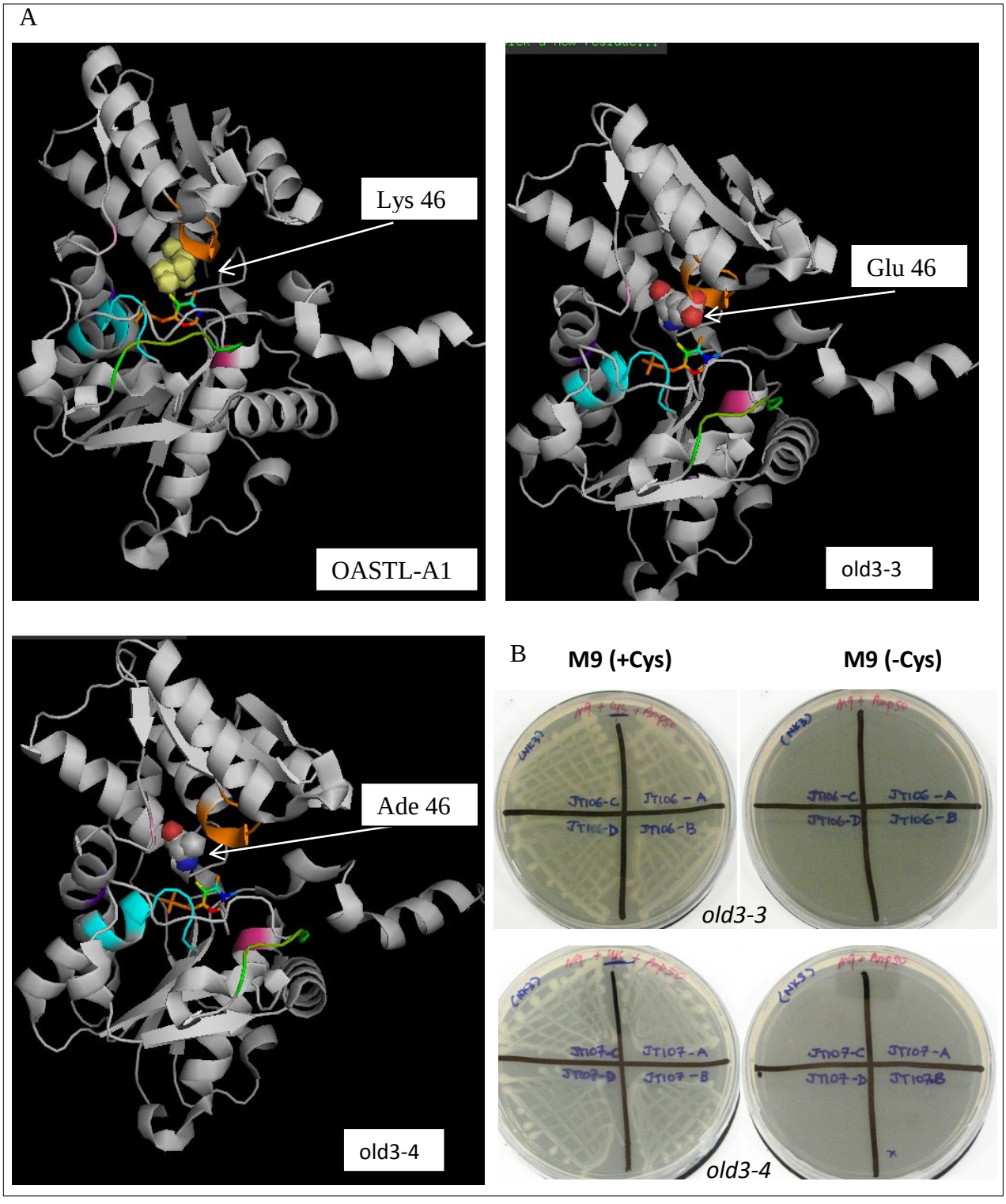

Figure 6.3. Effects of *old3-3* and *old3-4* mutation on cysteine auxotrophy in *NK3*. A) 3D structure of OASTL-A1, *old3-3* and *old3-4* highlighting the position of the mutations and their effect on the structure. B) Growth of NK3 strain carrying old3-3 and old3-4 on M9 minimal medium with or without cysteine, after 24 hr at 37 °C

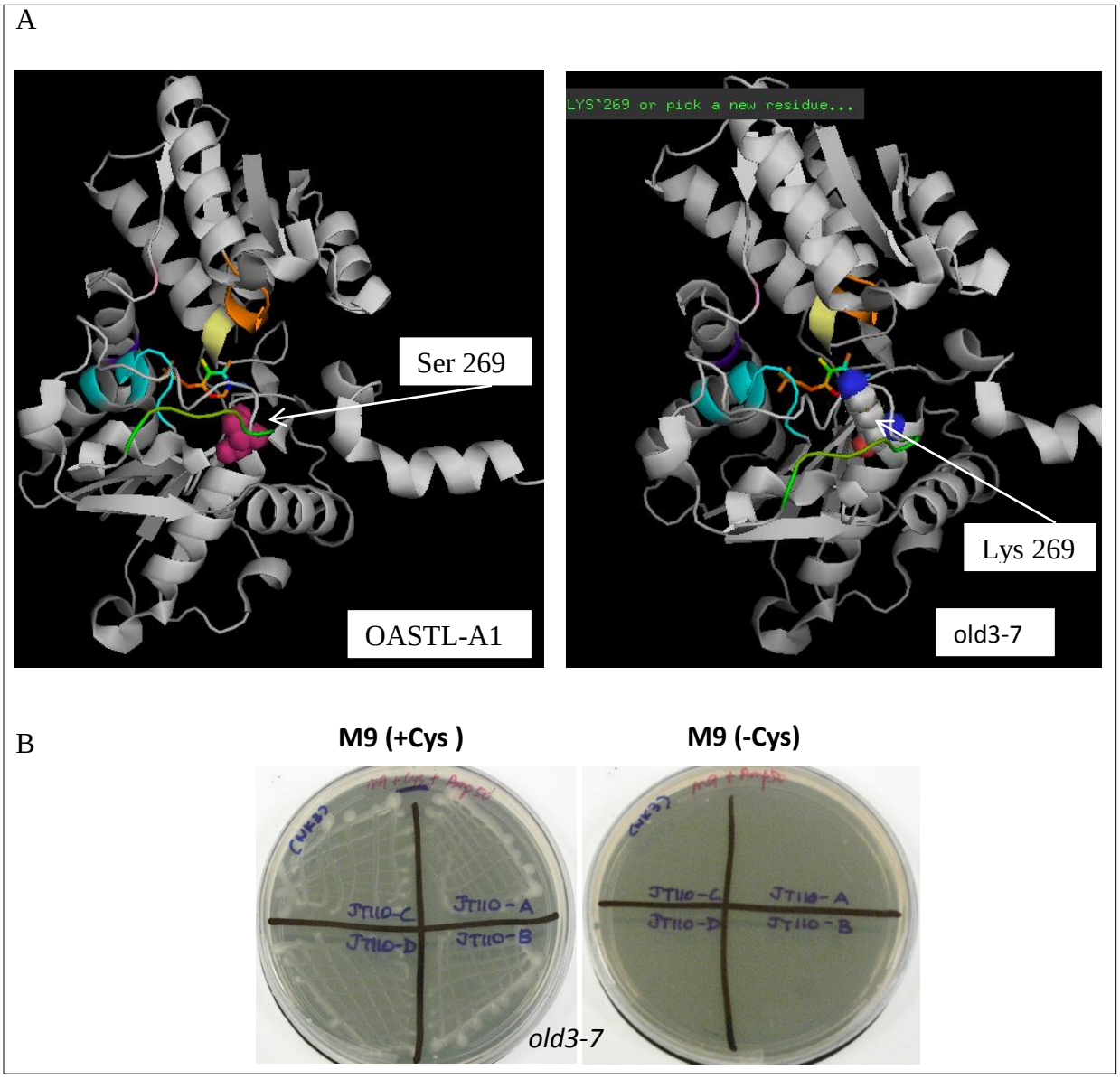

Figure 6.4. Effects of *old3-7* mutation on cysteine auxotrophy in *NK3*. A) 3D structure of OASTL-A1 and *old3-7* highlighting the position of the mutation and its effect on the structure. B) Growth of NK3 strain carrying old3-7 on M9 minimal medium with or without cysteine, after 24 hr at 37 °C .

The loop of residues between β3 sheet and α2 helix, T74-SGN-T78, makes a conserved motif among BSAS isoforms which is involved in binding with the substrate as well as it also interacts with the SERAT enzyme. Mutation in this motif has been previously shown to negatively affect both the OASTL activity and OASTL-SERAT complex formation (Bonner et al., 2005; Francois et al., 2006). The *old3-5* targets a conserved residue in this motif, the Thr^{74} and replaces it with the positively charged, polar and large amino acid of Lys^{74} (Figure 6.5). Results indicate that *old3-5* did not rescue the growth of NK3 on Cys minimal medium affirming that *old3-5* is likely a null oastl with respect to the catalytic activity (Figure 6.5). In contrast, *old3-6* specifically targets the SERAT binding Lys^{217} residue in the loop between β8 and β9 sheet (Figure 6.6). The old3-6 replace Lys^{217} with A^{217} (Figure 6.6). Results show that *old3-6* was able to rescue the NK3 on Cys minimal medium suggesting that old3-6 is still an active OASTL (Figure 6.6).

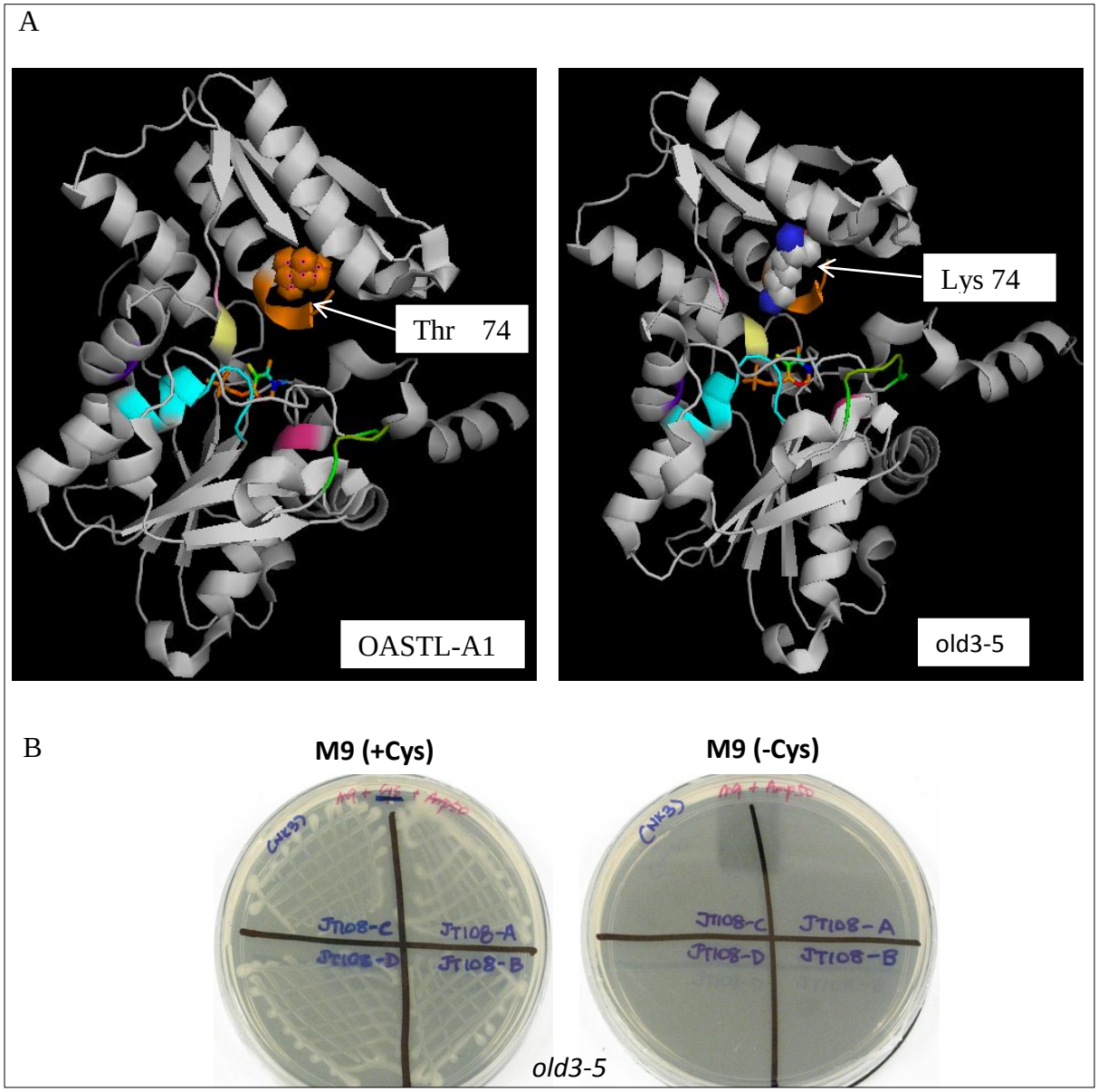

Figure 6.5. Effects of *old3-5* mutation on cysteine auxotrophy in *NK3*. A) 3D structure of OASTL-A1 and *old3-5* highlighting the position of the mutation and its effect on the structure. B) Growth of NK3 strain carrying old3-5 on M9 minimal medium with or without cysteine, after 24 hr at 37 °C .

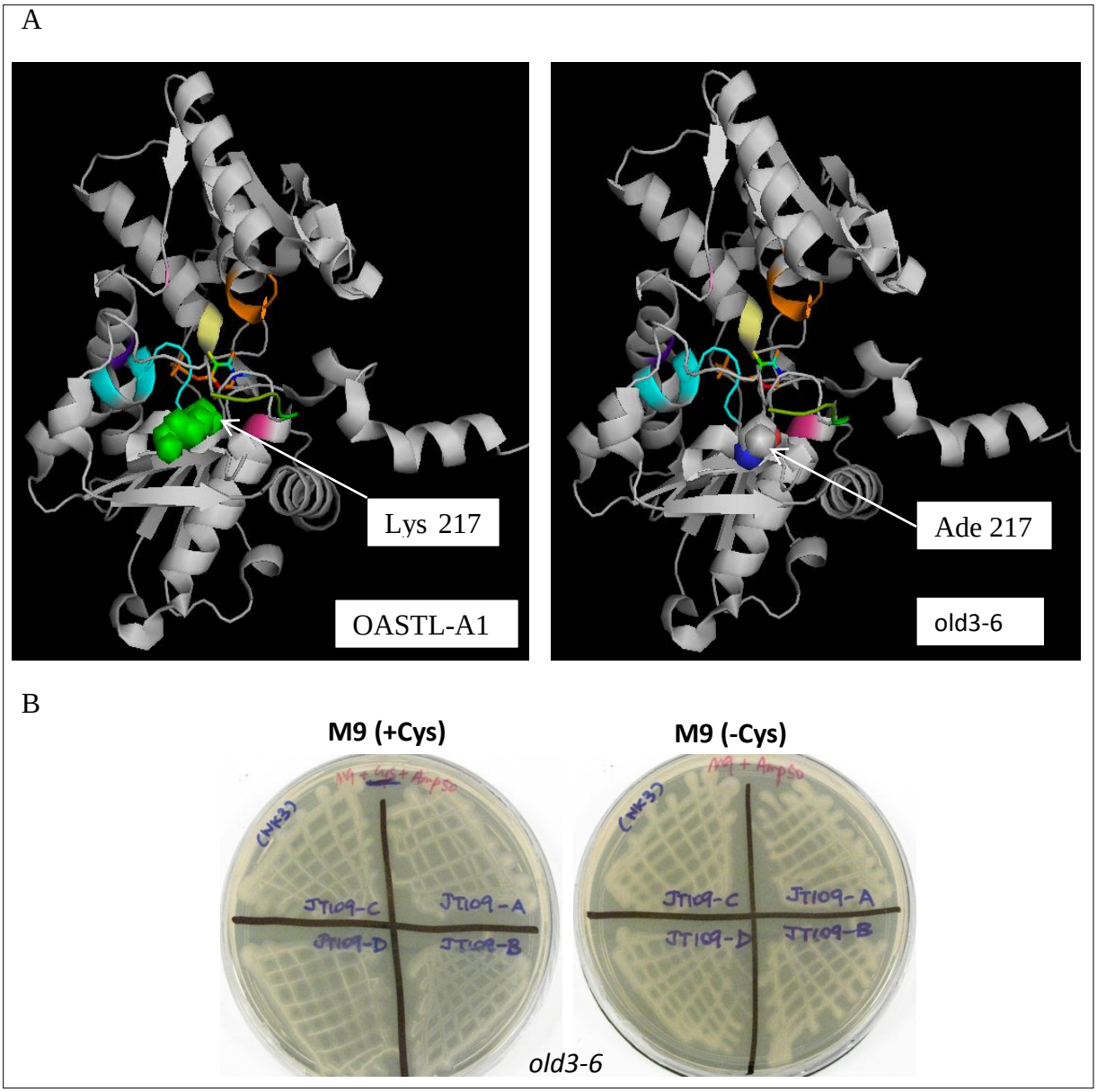

Figure 6.6. Effects of *old3-6* mutation on cysteine auxotrophy in *NK3*. A) 3D structure of OASTL-A1 and *old3-6* highlighting the position of the mutation and its effect on the structure. B) Growth of NK3 strain carrying old3-6 on M9 minimal medium with or without cysteine, after 24 hr at 37 °C .

6.3 Evolutionary conserved residues in the α5 and α6 helices of OASTL-A1

Various residues in the α-helices are invariant among BSAS isoforms in *Arabidopsis* and may play an important function regarding the structure and activity of this PLP-dependent enzyme family. Some of these residues were targeted for mutagenesis in this study. Two novel mutations were designed in the α6 and α5 helices in close proximity of Gly^{162}, where the *old3-1* mutation was identified. The *old3-8* is located in the α6-helix, in parallel to Gly^{162} and results in the substitution of the conserved neutral and hydrophobic Leu^{193} molecule with a positively charged and polar residue of Arg^{193} (Figure 6.7). Results indicate that the cysteine auxotrophy was retained in the NK3 strain carrying *old3-8* (Figure 6.8).

The *old3-9* mutation causes the substitution of Glu^{164} into Gly^{164}, which resides in a conserved TTGP**E**I motif. old3-9 was not able to rescue the NK3 growth on Cys minimal medium (Figure 6.7 and 6.8). It is important to note that *old3-9* /$164^{E/G}$ is present in the same motif, where *old3-1* /$162^{G/E}$ was previously identified (Figure 6.8). The results suggest that these residues and the motif in α6 and α5 helices are essential for the catalytic activity of OASTL-A1 which further confirms the importance of these interfaces in the function of OASTL-A1.

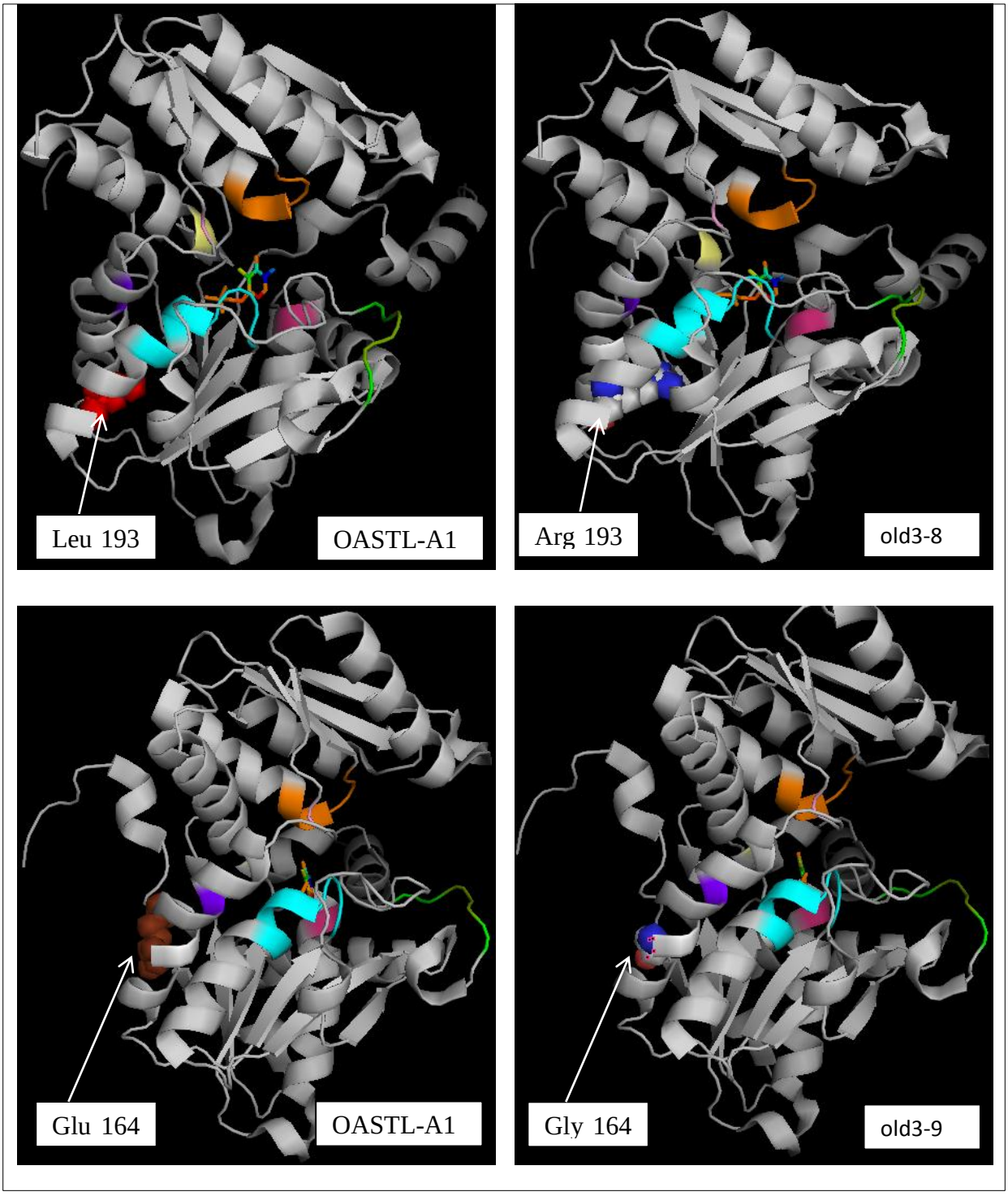

Figure 6.7. The 3D structure of OASTL-A1, *old3-8* and *old3-9* highlighting the position of the mutation and its effect on the structure.

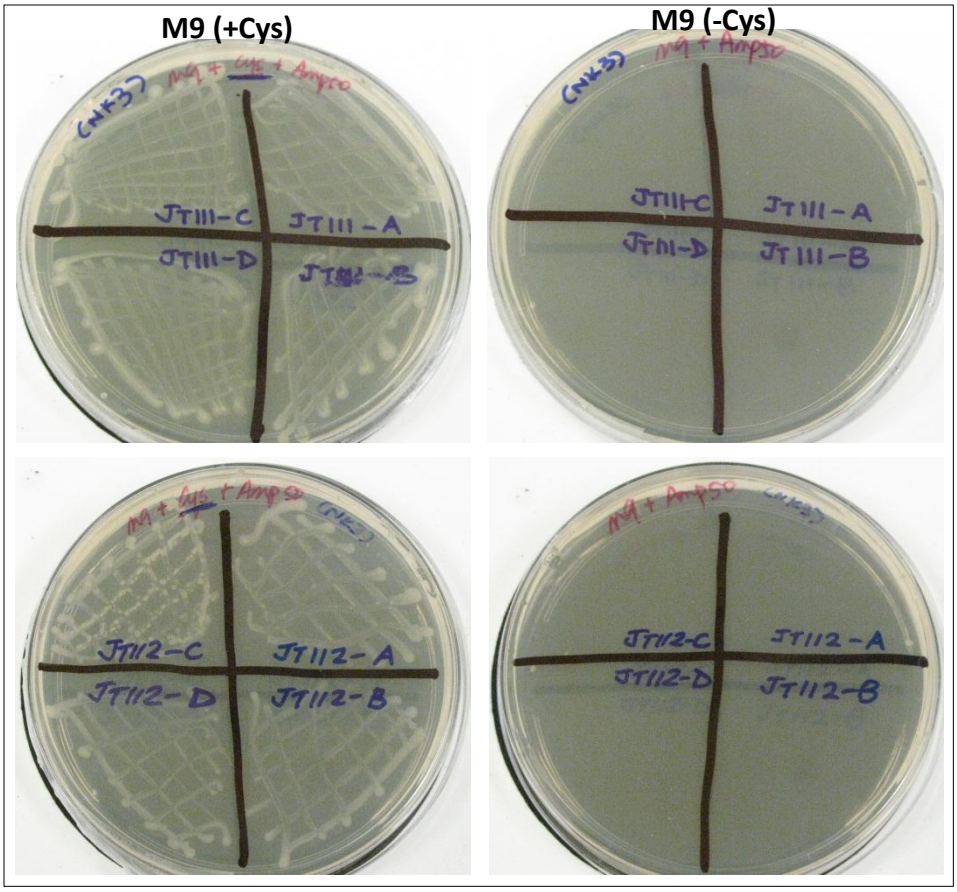

Figure 6.8. Effects of *old3-8* and *old3-9* mutation on cysteine auxotrophy in *NK3*. Growth of NK3 strain carrying old3-8 and old3-9 on M9 minimal medium with or without cysteine, after 24 hr at 37 °C .

6.4 Residues involved in homodimerization of OASTL-A1 and cysteine biosynthesis function

OASTL-A1 makes a homodimer which play an important role in the OASTL activity (Bonner et al., 2005). In this study, residues in the dimer interface were also targeted with an aim to disrupt the homodimerzation of OASTL-A1 and check its effect in cysteine biosynthesis and later interaction with R-triggered immunity. Four novel mutations, *old3-10*, *old3-11*, *old3-12* and *old3-13*, were induced individually in the OASTL-A1 at different positions of the putative dimer interface (Bonner et al., 2005). These mutations resulted in the substitution of the neutral and hydrophobic molecules with the negatively charged and polar residues or vice versa (Figure 6.9-6.12). The *old3-10 to -13* mutations were targeted in α helices, 9, 7, 3 and 2, respectively.

Results show that *old3-10*, *old3-11* and *old3-13* were not able to rescue the cysteine autotrophy in NK3 (Figure 6.9, 6.10 and 6.12). However, the NK3 strain carrying *old3-12* showed reduced cysteine auxotrophy (Figure 6.11). This suggests that *old3-10*, *old3-11* and *old3-13* likely affected the OASTL activity of the protein, whereas the OASTL activity of *old3-12* may have been negatively affected but is not abolished.

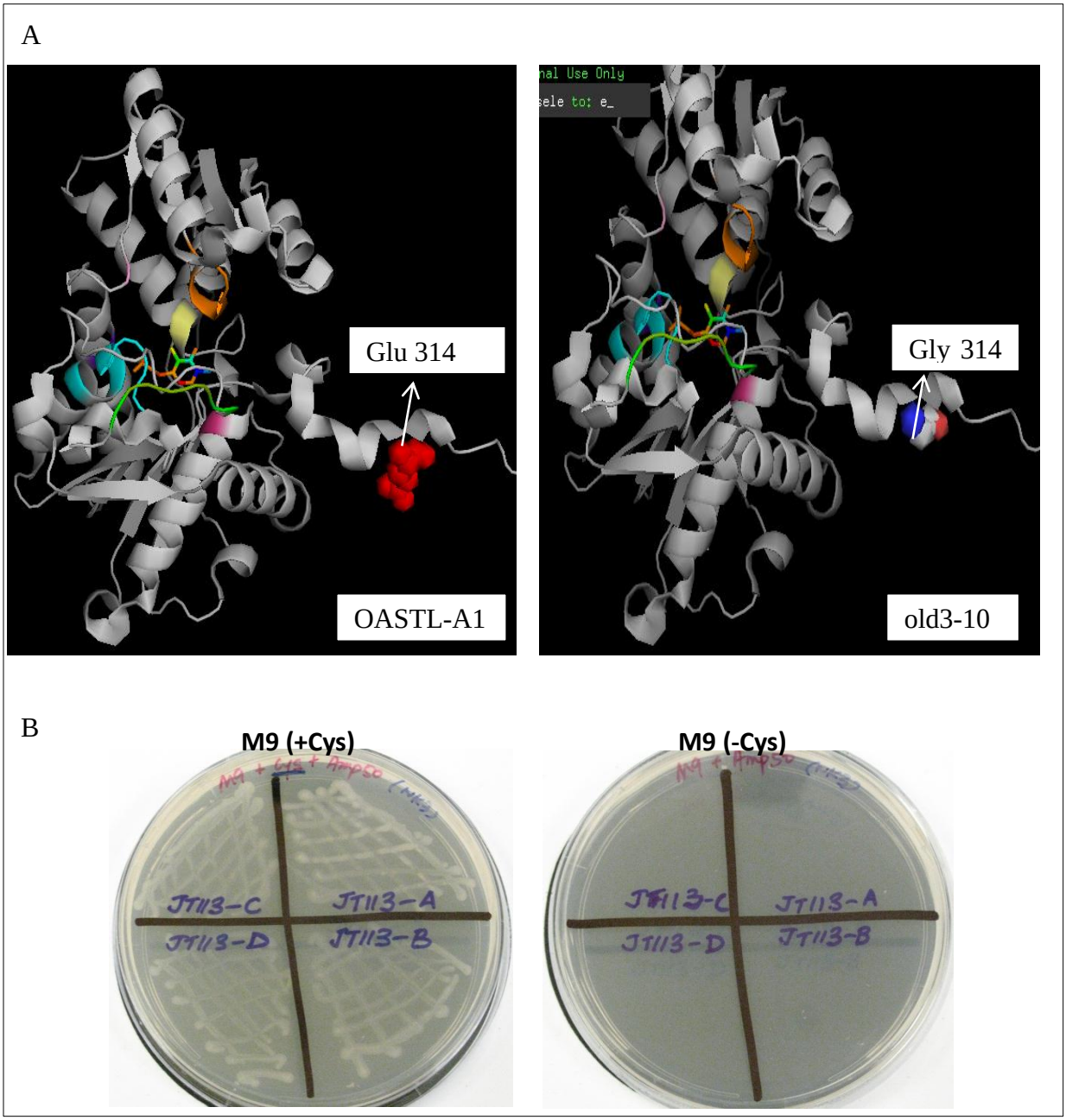

Figure 6.9. Effects of the *old3-10* mutation on cysteine auxotrophy in *NK3*. A) 3D structure of OASTL-A1 and *old3-10* highlighting the position of the mutation and its effect on the structure. B) Growth of NK3 strain carrying old3-10 on M9 minimal medium with or without cysteine, after 24 hr at 37 °C.

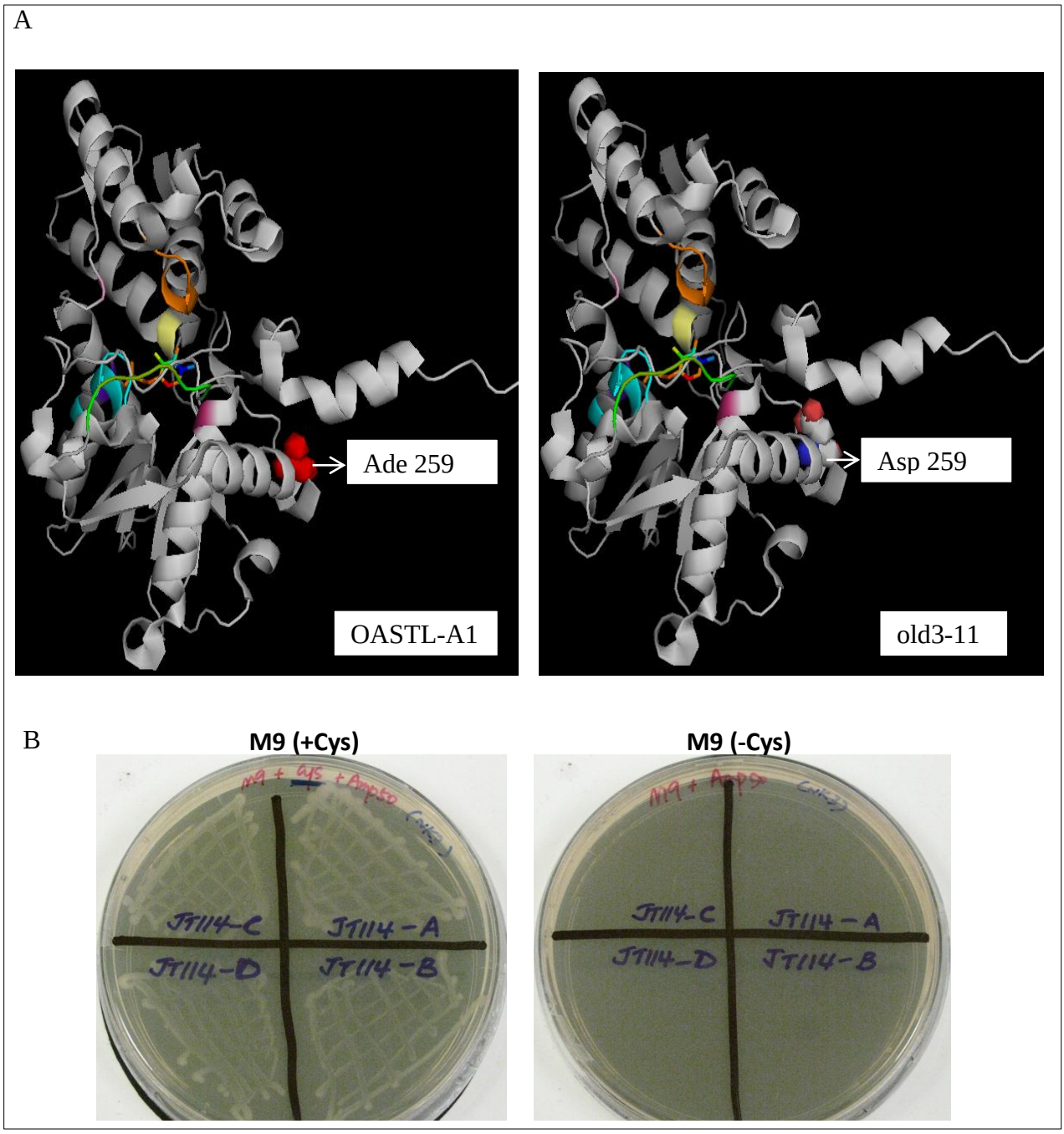

Figure 6.10. Effects of *old3-11* mutation on cysteine auxotrophy in *NK3*. A) 3D structure of OASTL-A1 and *old3-11* highlighting the position of the mutation and its effect on the structure. B) Growth of NK3 strain carrying old3-11 on M9 minimal medium with or without cysteine, after 24 hr at 37 °C.

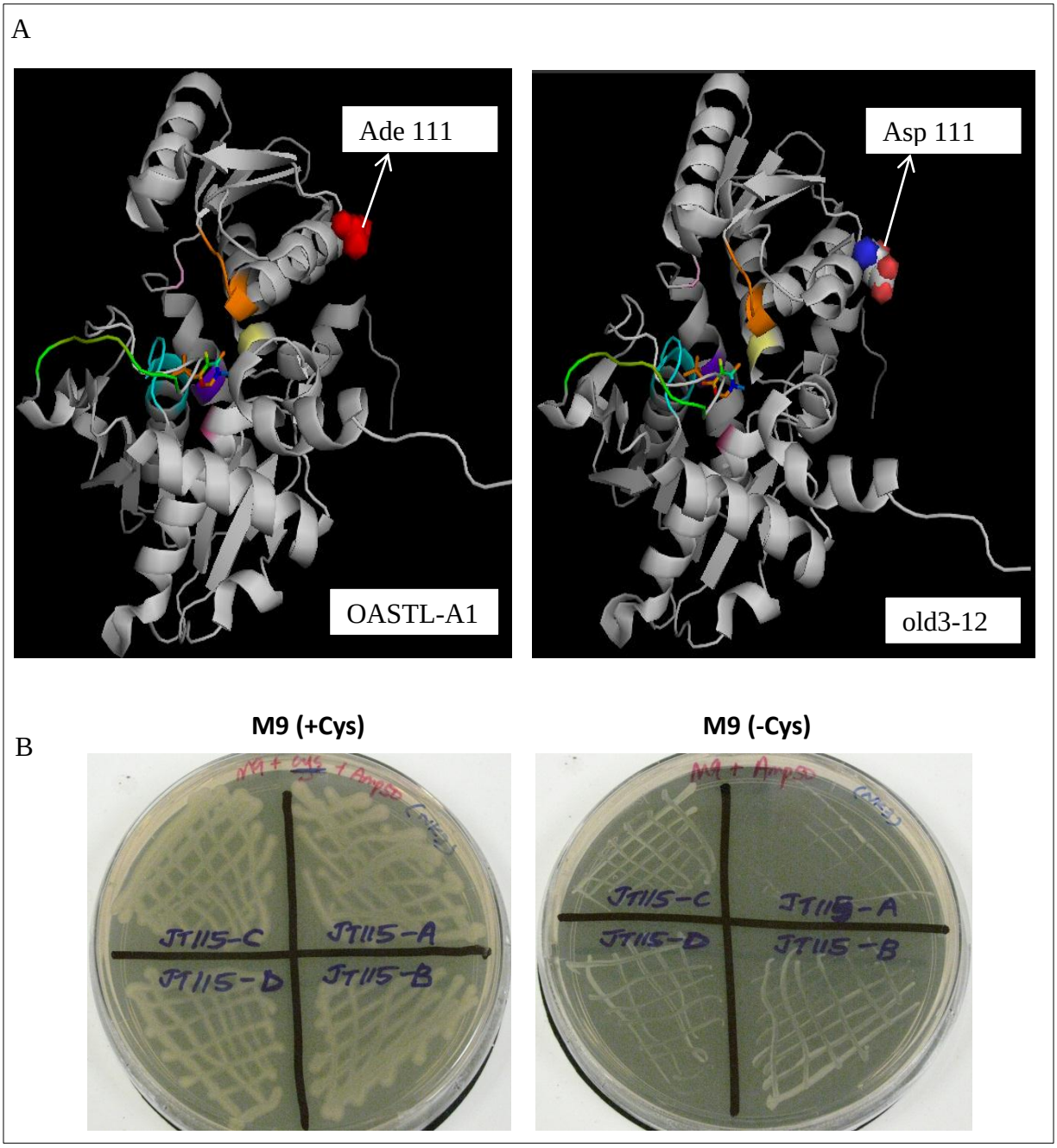

Figure 6.11. Effects of *old3-12* mutation on cysteine auxotrophy in *NK3*. A) 3D structure of OASTL-A1 and *old3-12* highlighting the position of the mutation and its effect on the structure. B) Growth of NK3 strain carrying old3-12 on M9 minimal medium with or without cysteine, after 24 hr at 37 ℃.

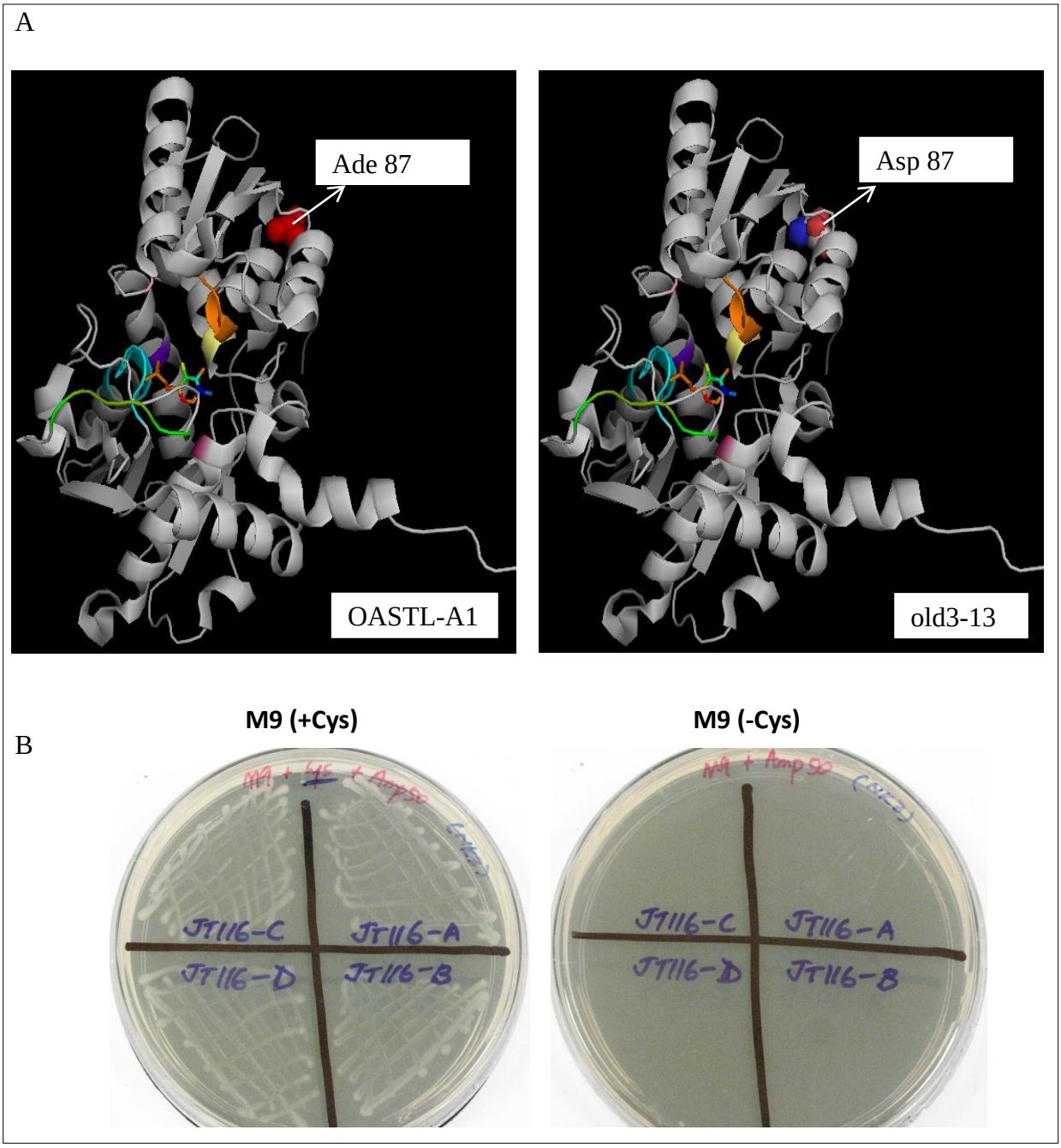

Figure 6.12. Effects of *old3-13* mutation on cysteine auxotrophy in *NK3*. A) 3D structure of OASTL-A1 and *old3-14* highlighting the position of the mutation and its effect on the structure. B) Growth of NK3 strain carrying old3-14 on M9 minimal medium with or without cysteine, after 24 hr at 37 °C.

6.5 Stable and transient expression of oastl-a1/old3 variants in the *odd-ler* background

To test the effect of various mutations in OASTL-A1 on epistatic interaction with *RPP1*-like *R* genes in the *odd-ler* background, old3 mutants were aimed to be expressed in *old3-2 odd-ler* recombinant plant lines. For this purpose *old3* mutants were overexpressed under the CaMV 35S promoter and transformed into the *Agrobacterium* strains GV3101. Since complementation of the *old3-1* allele in L*er*-0 has been previously shown to causes necrosis and death of plants (Shirzadian-Khorramabad et al., 2010), a transient expression approach was initially employed to observe the effects of old3 mutants in activating cell death. Presence of the *old3-1* in combination with the *odd-ler R* gene was expected to result in the development of HR and necrotic spots in the infected leaves. As *old3-2 odd-ler* is a mixed genetic background, L*er*-0, Col-0 and *old3-2 odd-ler* leaf infiltrations were performed initially with the *Agrobacterium* strains carrying OASTL-A1, old3-1 or no vector.

Results indicate that upon infiltration with the wild-type *Agrobacterium* strain *GV3101*, chlorosis developed in the leaf tissues of L*er*-0 but not Col-0 accession (Appendix 18). This suggested that the laboratory-specific *Agrobacterium* strain *GV3101* is virulent in the L*er*-0 genetic background but not in Col-0. Transformation of the L*er*-0 with the *Agrobacterium* strain *GV3101* containing OLD3 or old3-1 also resulted in chlorosis. In addition a varying degree of necrosis was also observed in the leaves infiltrated with OASTL-A1 and old3-1. Necrosis of the infiltrated tissues is an indicator of HR-induced cell death development (Zhang et al., 2004) and this is consistent with the incompatibility induced by *old3-1* and *odd-ler RPP1* gene interaction. However why infiltration with OLD3 resulted in necrosis in some tissues remained obscured. Infiltration with the wild-type *Agrobacterium* strain resulted in chlorosis in the *old3-2 odd-ler* lines as well; however no chlorosis appeared in the *old3-2 odd-ler* lines when infiltrated with the strains carrying OLD3 or old3-1. Nevertheless collapse of leaf tissues and necrosis was detectable in some tissues infiltrated with old3-1. In conclusion two different genetic backgrounds affected the phenotypes of *old3-2 odd-ler* leaves infiltrated with the transgenic *Agrobacterium* strains carrying old3-1 or OASTL-A1/OLD3 (Appendix 18). Since *old3-2 odd-ler* is a mixed Col-0/ L*er*-0 genetic background, and not a near-isogenic line (NIL), the transient expression approach

of old3 mutants in L*er*-0 or *old3-2 odd-ler* did not emerge as a suitable test of the genetic interaction. Therefore the constructs were directed for stable transformation in the *old3-2 odd-ler* lines. Currently the stable transformation for the *old3-1* up to *old3-13* variants is in process and therefore the genetic interaction between *old3* variants and *odd-ler* awaits the phenotypic characterisation of the stably transformed *old3-2 odd-ler* lines.

6.6 Loss of interaction of old3-1 with the SERAT *in vivo*

It was shown previously that mutations which negatively affect the OASTL activity may or may not interfere with the OASTL-SERAT interaction (Bonner et al., 2005; Francois et al., 2006). This is because of the two different SERAT binding sites in OASTL-A1. Since old3-1 abolishes the OASTL activity, it remained unknown whether it also affected the interaction of old3-1 with the SERAT. OASTL-A1 interacts with its cytosolic SERAT1.1/SAT5 partner *in vivo*, as shown by the yeast-2-hybrid system and co-immunoprecipiation studies (Bogdanova and Hell, 1997; Jost et al., 2000; Heeg et al., 2008; Wirtz et al., 2010). Therefore the interaction between the mutant old3-1 protein and its cytosolic SERAT1.1 enzyme partner was studied using the protein-protein interacting system in yeast. For this purpose the yeast 2-hybrid system was employed. The old3-1 and OASTL-A1 were used as bait against the SERAT enzyme as prey.

Results show that in contrast to the wild type OASTL-A1, there is a loss of interaction between the old3-1 mutant protein and the SERAT1;1 (Figure 6.14 and Appendix 19). This suggest that the mutant old3-1 protein does not interact with the cytosolic SERAT1;1 *in planta* either. However, it remains possible that the mutant protein behaves differently in the plant as compared to yeast.

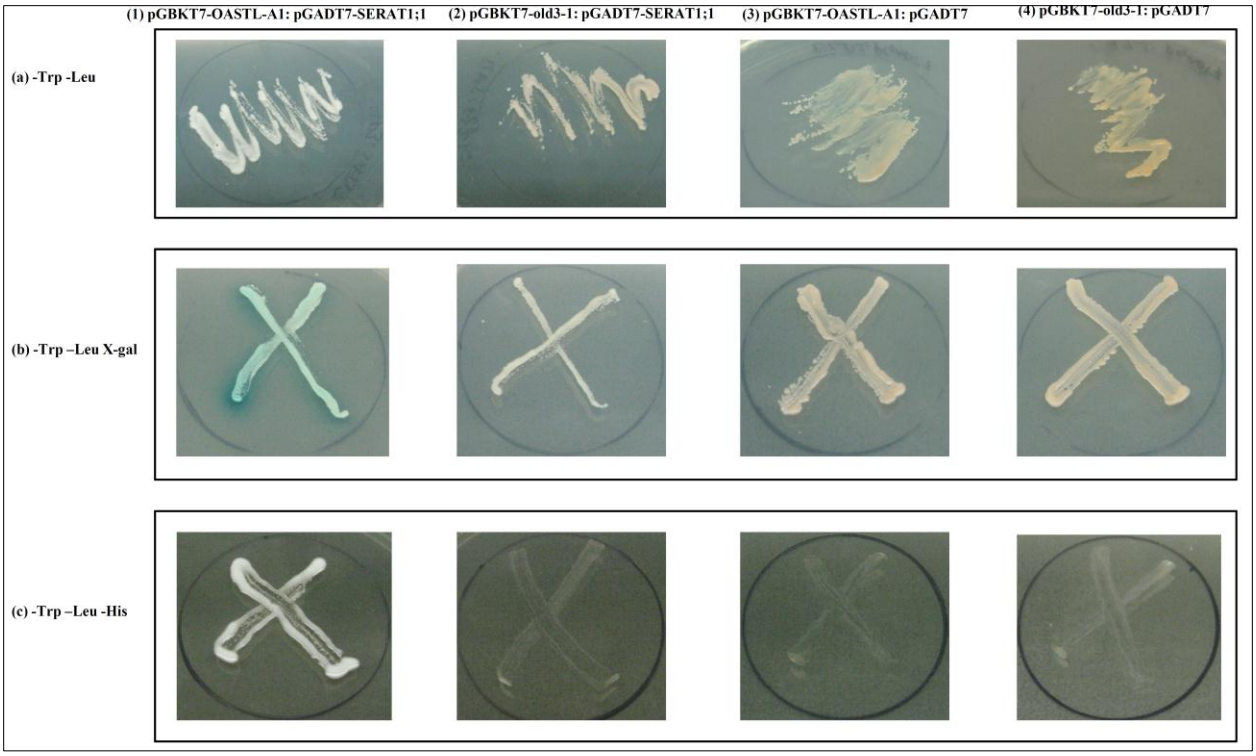

Figure 6.13. Analysis of protein-protein interaction of cytosolic OASTL-A1 and old3-1 with cytosolic SERAT1;1/SAT5 in yeast. Figure shows a Yeast-2-hybrid test for protein-protein interaction between OASTL-A1/OLD3 and old3-1 and cytosolicSERAT1;1/SAT5. AH109 yeast strains carrying the (1) OASTL-A1or (2) old3-1 cDNA fused with GAL4 binding domainin the bait vector pGBKT7 were transformed with the prey vector pGADT7 containing SERAT1;1/SAT5 cDNA fused with the GAL4 activation domain (1 and 2) or empty pGADT7vector(3 and 4), as a control. After transformation colonies were re-streaked at the SD media:(a) -Trp-Leu to confirm the presence of both vectors,(b)-Leu-Trp, Xα-gal and (c)-His-Leu-Trp, plates to test the activation of reporter gene. Development of blue colour in plates in (b) and growth on nutritional selection medium in (c) are indicator of positive protein-protein interaction. Streaked plates were kept at 30°C for two days and then photographed. Plates photographed at day 11 of growth are shown in Appendix 19.

Discussion

Site-directed mutagenesis was performed in OASTL-A1 to identify the effects of different mutations on the OASTL activity and activation of R-mediated immunity. OASTL activity of these proteins was not measured *in vitro* or *in vivo*, and cysteine auxotrophy of NK3 *E. coli* strain was employed as a preliminary approach to detect the effects of various mutation on OASTL mediated cysteine biosynthesis. Results indicate that the mutations which were designed to target the residues associated with the PLP activity and substrate binding region negatively affected the catalytic activity of OASTL-A1 and this is consistent with previous findings (Bonner et al., 2005; Francois et al., 2006). Results also suggest that disruption of the SERAT interacting residue seems to exert neutral effects on the OASTL activity and this is also consistent with the previous data (Bonner et al., 2005; Francois et al., 2006).

Mutations were also induced in the putative dimer interface of OASTL-A1 and results suggest that most of these mutations exert a negative impact on the catalytic activity of OASTL-A1. However it remains unknown whether these mutations actually affect the homodimersitation of OASTL-A1 *in vivo* or *in planta*. Previously, mutations in the residues of dimer interface of bacterial OASTL has been shown to negatively affect the homodimerisation of the protein but this did not affect the catalytic activity of the OASTL/CysK (Liszewska et al., 2005). Regardless, plant OASTL-A1 could behave differently as compared to bacterial OASTL in terms of homodimerization and catalytic activity.

Results further indicate that the *old3-1* mutation negatively affects the interaction with SERAT. It was previously reported that old3-1 mutation could bring a significant change in α5 helix arrangement (Shirzadian-Khorramabad et al., 2010). The Gln^{147} residue, which is positioned on the top of the α5 helix in the OASTL-A1, is pivotal for interacting with the C-terminus peptide of the SERAT as well as the OAS (Francois et al., 2006). Therefore old3-1 induced helical disturbance may have affected proper orientation of the closely associated SERAT + substrate interacting region. This can negatively affect the SERAT interaction as well as the OASTL activity and this is now consistent with the enzymatic properties of old3-1.

Results further suggest that the *old3-8* and *old3-9* mutation which targeted the residue in close proximity of old3-1 i.e., in α5 and α6 helix seems to negatively affect the OASTL activity. These mutations brought significant changes in the size and charge of the molecule which can have a disturbing effect on the helical arrangements. Other residues in the start of α5 and α6 helices were previously shown to be involved in interacting with PLP. It is therefore possible that any disturbance in helical structure or arrangement caused by *old3-8* and *old3-9* may have adversely affected the interaction between PLP interacting residues from these helices and the co-factor PLP. It is further possible that old3-8 and old3-9, which are mutated at the key residues in α6 and α5 helices and seems to negatively affect the OASTL activity, also affects the interaction with the SERAT enzyme. Since the residues affected in *old3-1*, *old3-8* and *old3-9* mutations seems to emerge as major regulatory points for OASTL activity and likely SERAT interaction, this may be a reason for these residues to be highly invariant among BSAS isoforms in *Arabidopsis*. The relation between the functions of these residues with the activities of the divergent or non-true OASTLs therefore demands investigation as well. Nevertheless what remains an interesting question is the role of these mutations in the activating *R*-mediated autoimmunity.

Blank Page

Chapter 7

Final discussion, conclusions, questions and outlook

The emerging role of OASTL-A1 in basal defence

The results in this study have shown that lack of cytosolic OASTL-A1 enhances disease susceptibility and impairs basal defence/MTI/PTI in *Arabidopsis* suggesting that cytosolic OASTL activity and cysteine biosynthesis has an important role in plant immunity. Recent studies have unravelled an important role of redox status and cysteine and sulfur metabolism in basal defence (Spoel et al., 2003; Parisy et al., 2007; Bednarek et al., 2009; Clay et al., 2009; Mugford et al., 2009; Spadaro et al., 2010; Spoel et al., 2010; Moore et al., 2011; Spoel and Loake, 2011; Yun et al., 2012). SA is a key hormone involved in the disease resistance against a wide range of pathogens by activating an array of defence related gene expression including *WRKYs*, and *PATHOGENESIS RELATED* genes (Vlot et al., 2009). SA mediated plant defence responses are largely associated with an important component known as a Non-expresser of Pathogenesis Related 1(NPR1) protein. The NPR1 acts downstream of the defence hormone SA and directs the expression of pathogenesis related genes in the nucleus (Spoel et al., 2003; Blanco et al., 2009; Zhang et al., 2010). NPR1 protein normally resides in an oligomeric state in the cytosol and its localisation from cytosol to the nucleus determines the activation of defence. The localisation of NPR1 from cytosol to the nucleus is mediated by SA driven redox changes in the cytosol (Tada et al., 2008). SA induces an increase in GSH levels as compared to GSSH which results in reduced cytosolic conditions (Spoel and Loake, 2011; Alvarez et al., 2012b)(Spoel and Loake, 2011; Alvarez et al., 2011). This allows the reduction of the disulphide

bridges present at key cysteine residues in the NPR1 protein. Reduction of the di-sulphide bridges results in monomerisation of the NPR1 protein which aids in its translocation into the nucleus to activate the expression of defence genes in association with the specific transcription factors (Tada et al., 2008). SA mediated changes in the redox status in cytosol also indicates that SA likely affect the activity of the enzymes involved in cysteine and glutathione biosynthesis. Consistent with this, SA has been shown to cause accumulation of OAS and cysteine and glutathione production, likely by modulating the OASTL and SAT mediated cysteine metabolism (Freeman et al., 2005). Moreover requirement of cysteine-derived metabolites including GSH has been also highlighted in synthesis of defence metabolites including phytoalexin and indole-glucosinolates (Zook, 1998; Rausch and Wachter, 2005; Bednarek et al., 2009; Bottcher et al., 2009; Clay et al., 2009). Consistent with this the role of GSH was found to be indispensable in basal defence (Parisy et al., 2007; Maughan et al., 2010). These observations support the role of cysteine-thiol biosynthesis and OASTL-A1 in innate immunity in plants.

The Guard hypothesis and function of OASTL-A1 in R-mediated innate immunity

R proteins are involved in activation of an HR response known as ETI, in response to pathogen effector-induced virulence. R-mediated innate immunity is activated mostly upon sensing modifications in specific host proteins . The Guard hypothesis suggests that R protein(s) “guard” against modifications in the host/“guardee” proteins when targeted by the pathogen effectors to promote effector triggered susceptibility (ETS) (Dangl and Jones, 2001; Jones and Dangl, 2006). To promote virulence, various proteins are host-targets of pathogen effectors, but this results in activation of ETI, only when the guarding *R* gene(s) is present in the genetic background (Krüger et al., 2002; Mackey et al., 2003; Belkhadir et al., 2004; Bernoux et al., 2008). Therefore avirulence (avr) effector-induced changes in various host-proteins are sensed directly or indirectly by guarding/cognate R proteins which trigger ETI to provide resistance against the attempted virulence (Jones and Dangl, 2006). Absence or modification of the host proteins via mutations is proposed to mimic effector-induced modifications which autoactivates R-mediated immune response (Krüger et al., 2002; Belkhadir et al., 2004; Yang and Hua, 2004; Jeuken et al.,

2009; Alcazar et al., 2010a). For example amino acid changes in a cysteine protease RCR3, in tomato causes autonecrosis which is activated by an R Cf-R protein encoded in the parent genetic background (Krüger et al., 2002). Cysteine proteases contribute to resistance against pathogen infection as they can degrade cysteine rich pathogen effectors. To promote virulence, cysteine protease RCR3 is a host-target of pathogen effector(s), but this result in activation of ETI, by the guarding R protein Cf-R. oastl.a1/old3-1 may therefore mimic "effector-induced modified-self" for the RPP1-like R protein encoded in the parent genetic background which therefore activates ETI-like response. OASTL-A1/OLD3 may therefore be "guarded" directly or indirectly by the RPP1-like R protein(s) from a haplotype-*R* gene cluster against an unknown pathogen virulence activity.

Pathogen effectors were previously shown to target *Arabidopsis* enzymes to either modify the function of the host enzyme or use the host-enzyme as a protein partner in enhancing virulence (Bernoux et al., 2008; Zhou et al., 2011). For example the plant cysteine protease RD-19 is used as a chaperone by the pathogen effector Pop2 to travel in the plant nucleus and cause virulence. This activity is detected by the RPS-R1 protein which activates ETI. Moreover, it was recently shown that bacterial CysK protein *O*-acetylserine sulfhydrylase, is targeted by a foreign bacterial effector protein (Diner et al., 2012). The foreign tRNase/CdiA protein complexes with the host CysK protein and activate the foreign nuclease, resulting in growth inhibition of the targeted host. Thus, the bacterial OASTL is targeted to suppress growth. Whether any pathogen effectors, that are close homologues of tRNase, promote virulence by modifying/targeting cytosolic OASTL-A1 enzyme in plants however remains to be established.

Further the results in this study are in line with the recent findings which show that the OASTL-A1 is required in *RPM1 R*-mediated ETI against the virulence activity of an *avrRpm1* molecule which targets and modify the plant RIN4 protein (Alvarez et al., 2012b). RIN4 protein is involved in plant disease resistance and affects basal defence. RPM1 guards RIN4 against modifications and can auto-activate ETI due to mutations in the *RIN4* encoding gene (Belkhadir et al., 2004). The finding by Alvarez *et al*. (2012) suggests that *RPM1* driven resistance against *avrRmp1*-targting-RIN4 can be indirectly dependent on the cytosolic cysteine production driven by OASTL-A1. As *RPM1* and the *RPP1*-like *R* genes are differently evolved *R* gene sub-classes,

recent data and the findings in this study suggest that cytosolic OASTL machinery acts as an important component in both PTI/MTI and ETI. It is furthermore important to note that from a genetic point of view, OASTL-A1 is not a negative regulator of *R*-mediated immunity, as knock-down or knock-out of OASTL-A1 in the *odd-ler* background does not cause autonecrosis. This is reminiscent of that between disease resistance *Cf-R* genes and allelic variation in cysteine protease encoding *RCR3* genes in tomato (Krüger et al., 2002). Autonecrosis in tomato *Rcr3* allelic lines is associated with non-synonymous substitutions in Rcr3 protein and is mediated by Cf-R, while lack of functional Rcr3 in the *rcr3-3/4* mutant (encoding truncated protein) does not activate *Cf-R*-dependent autonecrosis (Krüger et al., 2002). In contrast some protein coding genes in *Arabidopsis* can negatively regulate *R*-triggered immunity. For example, *R*-gene mediated autonecrosis is activated by the absence of *RPM1 interacting protein 4* (*RIN4*) or *BON1* (Belkhadir et al., 2004; Yang and Hua, 2004). However, it still may be possible that RPP1-like protein(s) guard or interact with multiple cytoplasmic OASTLs and the R protein(s) do not detect absence of a single OASTL, but rather an altered OASTL conformation resulting from a point mutation and/or effector-induced modification. In this scenario, OASTLs together may still act as negative regulator of R-mediated innate immunity.

Recently it is shown that the RPM1 protein which senses modification in the host or "guardee" RIN4 protein and activates ETI, actually perceives phosphorylation-induced modification of the RIN4 protein (Chung et al., 2011; Liu et al., 2011). A phosphomimic mutant of RIN4 autoactivates the RPM1-mediated ETI in the absence of pathogen effector unravelling the molecular basis of modified self-required in activating R-mediated immunity. The *old3-1* mutation is in an important motif TTGPEIW, which is invariant among all the BSAS isoforms in *Arabidopsis* as well as among the cysteine synthase gene in prokaryotes (Bonner et al., 2005; Heeg et al., 2008; Watanabe et al., 2008a). The threonine residues in the motif are suggestive of this as a phosphorylation site. Although phosphorylation of OASTLs has not been shown yet *in vitro*, it may be required or involved in modification or signalling *in planta*. On the other hand multiple sub-species of OASTL-A1 have been also identified but the nature of their modification remains elusive (Heeg et al., 2008; Wirtz et al., 2010). In this regards, it is possible that the old3-1 mutation might have affected any post-translational modification process or signalling associated with the OASTL-A1 *in planta* which affects the intra-molecular interaction of the

RPP1 protein and causes autoactivation of ETI like response which demands further investigations.

Questions and Outlook

Nevertheless, important questions remain to be addressed to further understand the role of OASTL-A1 in plant-pathogen interactions. For example *RPP1* genes have been characterised in different *Arabidopsis* accessions to provide resistance against effector molecules from the isolates of obligate biotrophic oomycete *H. arabidopsidis* (Botella et al., 1998; Rehmany et al., 2005; Coates and Beynon, 2010). Therefore, the role of OASTL-A1 is needed to be explored in *RPP1*-mediated ETI against *avr/vir* effectors. Similarly it is unknown how cytosolic cysteine production affects various pathways in innate and basal immunity against pathogen. Addressing these questions will also extend our insight into the evolution of *R* genes and their interaction with components of basic plant metabolism.

The findings that a mutation in a BSAS isoform activates RPP1-mediated autoimmunity provide a novel example of genetic epistatic interaction between *R* genes of the plant innate immune system and sulfur-cysteine metabolism. Recently mutations in the BSAS encoding *DES* and *CS26* genes were shown to cause auto-activation of immune and biotic stress responses (Alvarez et al., 2010; Bermúdez et al., 2010a; Alvarez et al., 2012b). *DES* and *CS26* are involved in cysteine degradation and synthesis of S-sulfocysteine in the cytosol and plastids, respectively. However, the mechanism underlying constitutive immune and biotic stress response in these *BSAS* mutants is currently unclear. Therefore it is tempting to speculate that these BSAS isoforms may interact with components of plant immunity as well. The study highlights the role of cysteine metabolism and OASTL in immunity and this is consistent with the emerging evidence in other species across kingdoms (Soutourina et al., 2010; Ghezzi, 2011; Diner et al., 2012).

Blank page

Appendices

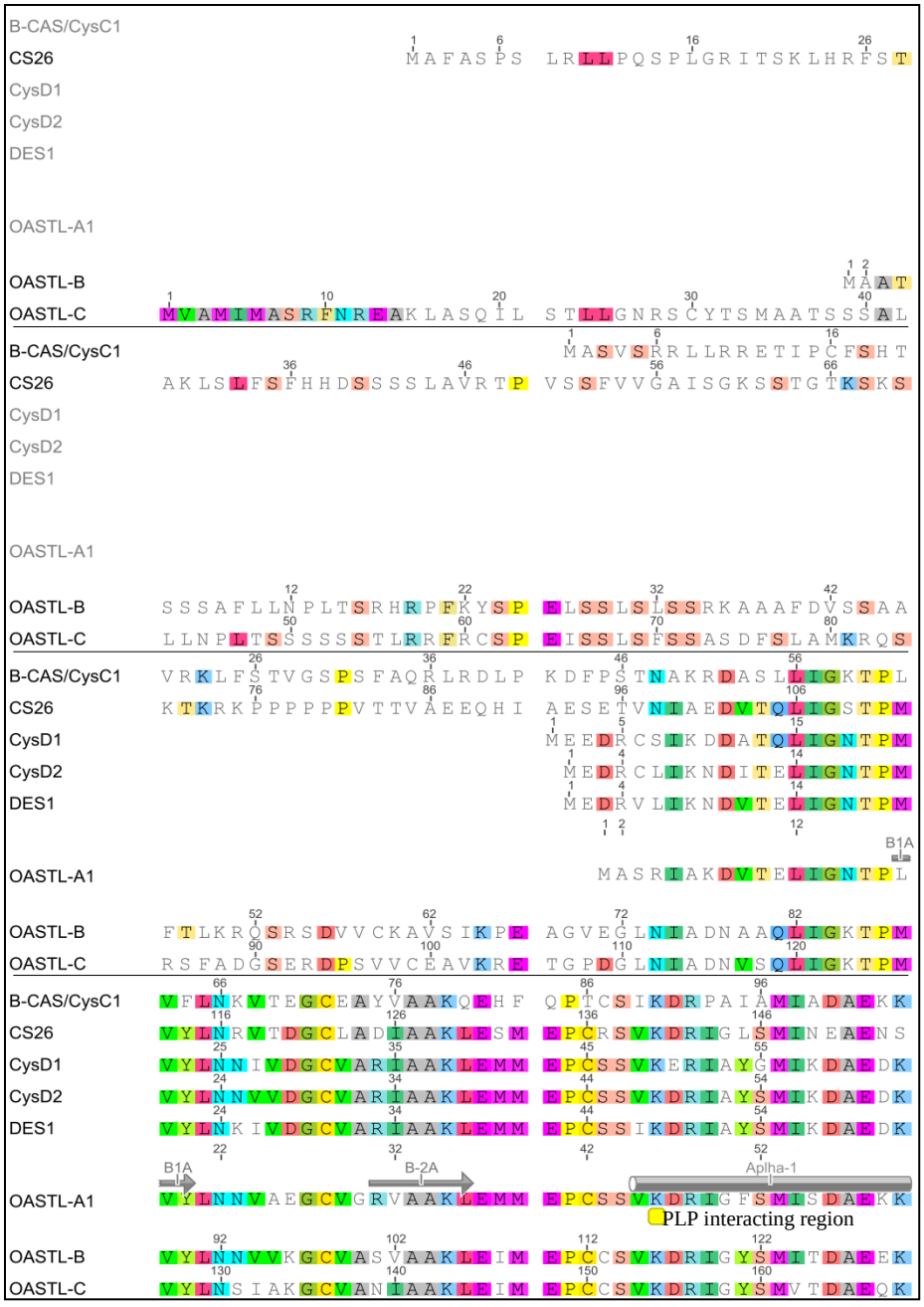

Appendix 1. Protein sequence alignment of all eight functional BSAS isoforms. Protein sequences of all the isoforms were aligned using Geneious alignment. The OASTL-A1 sequences shows annotations for its α and β domain structures.

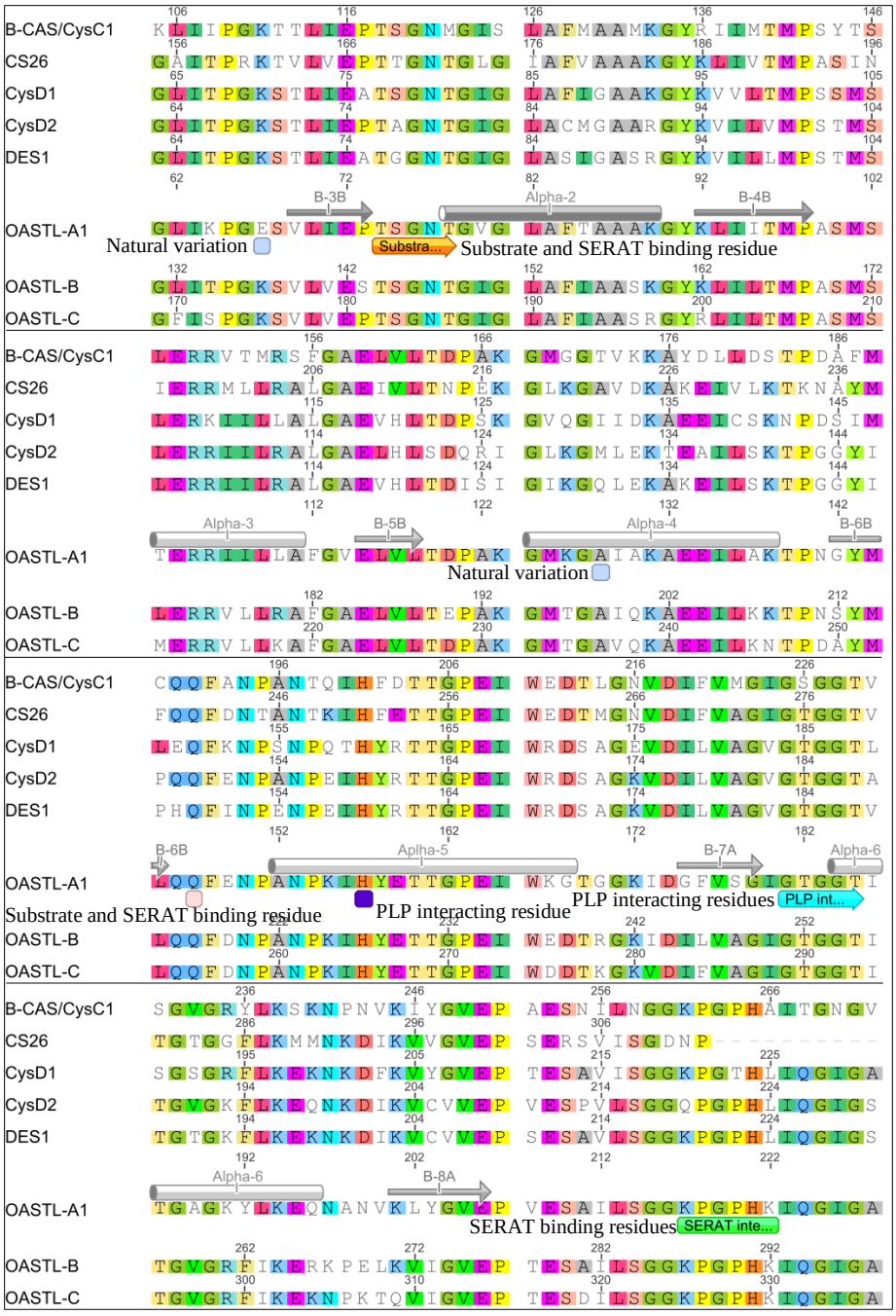

Appendix 1 *contd*. Protein sequence alignment of all eight functional BSAS isoforms. Protein sequences of all the isoforms were aligned using Geneious alignment. The OASTL-A1 sequences shows annotations for its α and β domain structures.

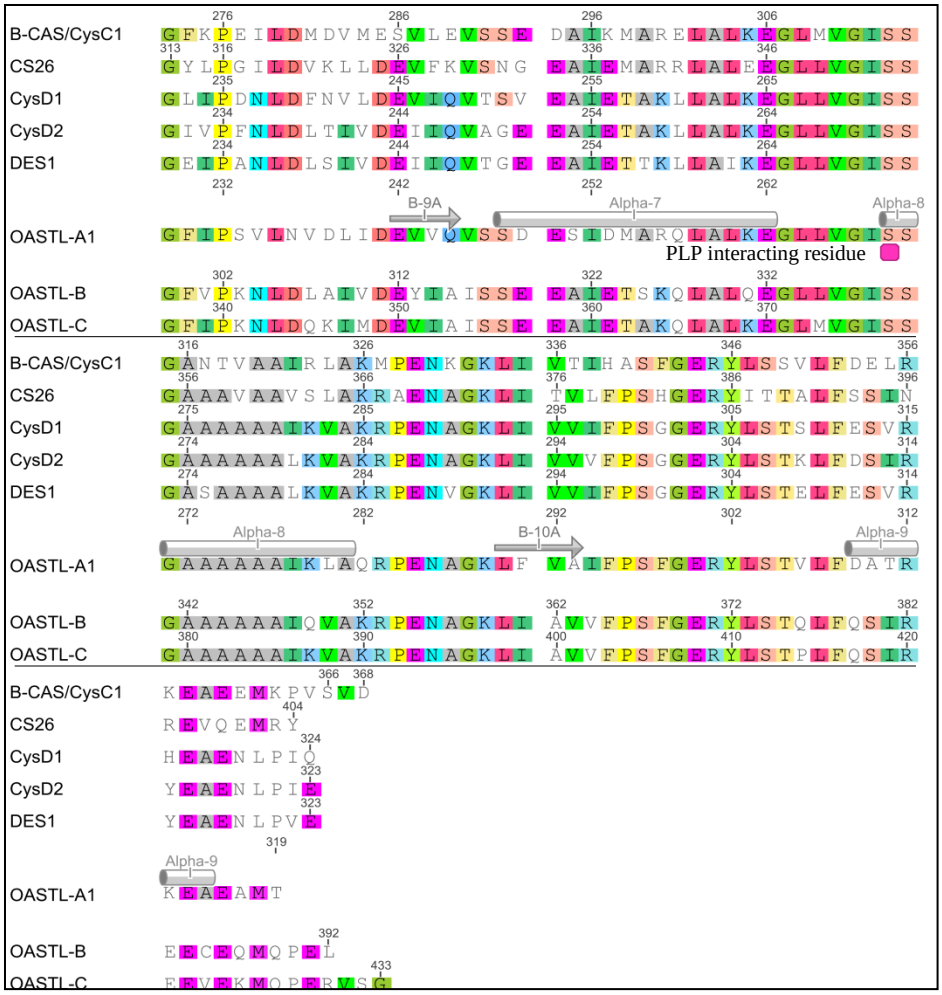

Appendix 1 *contd*. Protein sequence alignment of all eight functional BSAS isoforms. Protein sequences of all the isoforms were aligned using Geneious alignment. The OASTL-A1 sequences shows annotations for its α and β domain structures.

Appendix 2. Analysis of protein-coding gene models of all eight functional BSAS.

Cytosolic OASTL isoforms

(i) OASTL-A1

Multiple splicing patterns are available for the OASTL-A1/At4g14880, however all encodes for one standard protein coding gene model (figure adapted from TAIR 2012).

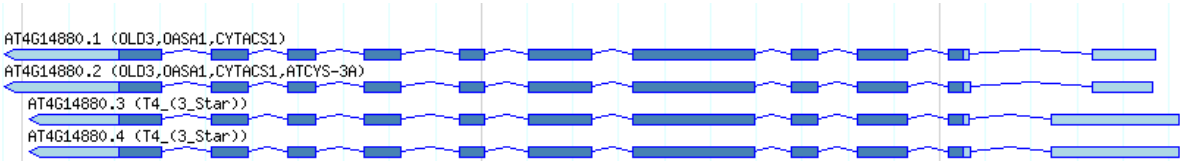

Localisation predictions of the protein sequence:

iPSORT Prediction: Predicted as: not having any of signal, mitochondrial targeting, or chloroplast transit peptides;_Predicted by Neural Nets- Chloroplast with score = 2.9; Chloroplast Transit peptide 1-29 is found; Integral Prediction of protein location: Membrane bound Chloroplast with score = 6.8; Predicted by PredSL cTP score = 0.552; mTP score = 0.5522; Secretion protein = 0.41

(ii) CysD1

A single protein encoding gene model is available for CysD1/At3g04940 (figure adapted from TAIR 2012).

Localisation predictions of the protein sequence:

iPSORT Prediction: Predicted as: not having any of signal, mitochondrial targeting, or chloroplast transit peptides;

Predicted by Neural Nets - Chloroplast with score = 2.8; Chloroplast Transit peptide 1-32 is found; Integral Prediction of protein location: Membrane bound Chloroplast with score = 8.8; Predicted by PredSL cTP score = 0.00635; mTP score = 0.0; Secretion protein = 0.21.

(iii) CysD2

Multiple splicing patterns are available for the CysD2/At5g28020 which results in two different protein coding gene models (figure adapted from TAIR 2012).

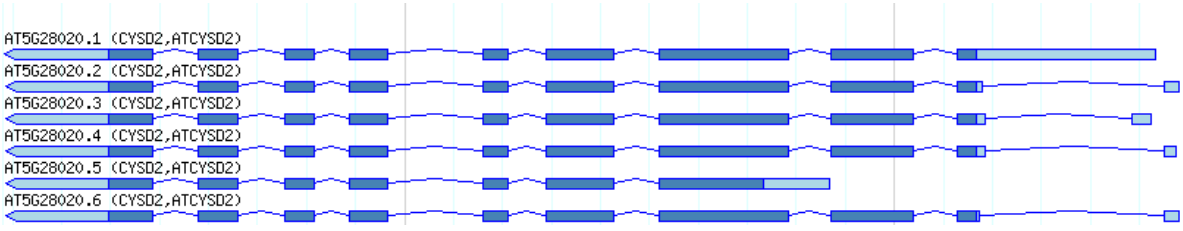

Localisation predictions of the protein sequence:

iPSORT Prediction: Predicted as: not having any of signal, mitochondrial targeting, or chloroplast transit peptides;

Predicted by Neural Nets - Cytoplasmic with score = 2.7; Integral Prediction of protein location: Cytoplasmic with score = 9.7. Predicted by PredSL cTP score = 0.002; mTP score = 0.002; Secretion protein = 0.21.

(iv) DES1

Two different splicing patterns are available for DES1/At5g28030 but encode for one protein coding gene model only (figure adapted from TAIR 2012).

Localisation predictions of the protein sequence:

iPSORT Prediction: Predicted as: not having any of signal, mitochondrial targeting, or chloroplast transit peptides;

Predicted by Neural Nets - Chloroplast with score = 1.8; Chloroplast Transit peptide 1-31 is found; Integral Prediction of protein location: Membrane bound Chloroplast with score = 5.8; Predicted by PredSL cTP score = 0.0014; mTP score = 0.0; Secretion protein = 0.02.

Plastidic OASTL isoforms

(i) OASTL-B

Two different splicing patterns are available for OASTL-B/At2g43750 but encode for one protein coding gene model only (figure adapted from TAIR 2012).

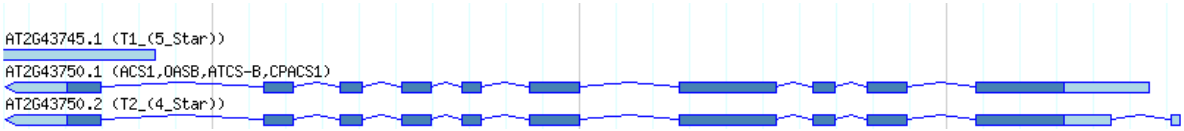

Localisation predictions of the protein sequence:

iPSORT Prediction: Predicted as: having a chloroplast transit peptide; Predicted by Neural Nets - Chloroplast with score = 2.4; Integral Prediction of protein location: Membrane bound Chloroplast with score = 5.0; Predicted by PredSL cTP score = 0.99; mTP score = 0.0; Secretion protein = 0.0.

(ii) CS26

One protein coding gene model is available for CS26/At3g03630 (figure adapted from TAIR 2012).

Localisation predictions of the protein sequence:

iPSORT Prediction: Predicted as: having a chloroplast transit peptide; Predicted by Neural Nets - Chloroplast with score = 3; Chloroplast Transit peptide 1-17 is found; Integral Prediction of protein location: Membrane bound Chloroplast with score = 9.0; Predicted by PredSL cTP score = 0.99; mTP score = 0.02; Secretion protein = 0.0.

Mitochondrial OASTL isoforms

(i) OASTL-C

Three different splicing patterns are available for OASTL-C/At3g59760 which encode for three different protein-encoding gene models (figure adapted from TAIR 2012). However all these three models contain comparable N-terminal sequences and varies in C-terminal only.

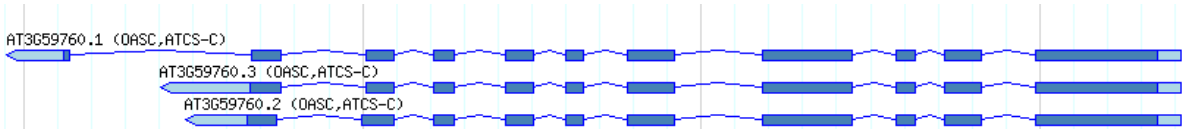

Localisation predictions of the protein sequence:

iPSORT Prediction: Predicted as: having a mitochondrial transit peptide; Predicted by Neural Nets - Chloroplast with score = 2.6; Chloroplast Transit peptide 1-7 is found; Integral Prediction of protein location: Membrane bound Chloroplast with score = 5.3; Integral Prediction of protein location in Mitochondria = 4.36; Predicted by PredSL cTP score = 0.99; mTP score = 0.02; Secretion protein = 0.0.

(ii) *β*-CAS

Three different splicing patterns are available for *β-CAS*/At3g61440 which encode for three different protein-encoding gene models (figure adapted from TAIR 2012). All these three models contain divergent N-terminal sequences and overlapping 5′ UTR and 1st and 2nd exon regions, however are invariant in the C-terminal region. As the N-terminal region, ranging from 1-17 a.a reisdues, contain the mitochondrial localisation signal, the splice variant At3g61440.3 and At3g61440.2 lacks this signal and consequently may not be targeted to the mitochondrion.

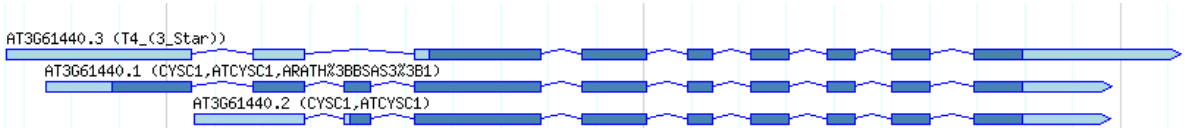

Localisation predictions of the protein sequence:

iPSORT Prediction: Predicted as: having a mitochondrial transit peptide; Predicted by Neural Nets - Chloroplast with score = 1.8; Chloroplast Transit peptide 1-14 is found; Integral Prediction of protein location: Membrane bound Chloroplast with score = 9.4; Integral Prediction of protein location in Mitochondria = 0.34; Predicted by PredSL cTP score = 0.04; mTP score = 0.99; Secretion protein = 0.0.

Appendix 3. Variation in OASTL-A1 protein coding sequence in the *Arabidopsis* accessions.

From *Arabidopsis* accession database (1001genomes.org/datacenter, Weigel D, Mott R (2009) Genome Biol 10:107) AT4G14880 protein coding sequences were extracted and aligned in reference to the OASTL-A1/AT4G14880 coding sequence of the reference accession Col-0, using Clustal W in Geneious. Based on the alignment of the sequences, the sequences from the accessions that showed non-synonymous substitutions are listed in the table. Those that are 100% conserved to the reference OASTL-A1/OLD3/AT4G14880 coding sequence from Col-0 accession, are: Aa; Abd; Aedal(-1,-3); Ag(-0); Agu(-1); Ale(Stenar-44-4,56-14); Algutsrum; Alst(-1); Altai(-5); Amel(-1); An(-1); Ang(-0); Anholt(-1); Ann(-1); Anz(-0); App1(-12,14,16); Appt(-1); Ba(-1); Baa-1; Baa1(-2); Baa4,5(-1); BaK(-2,-7); Bch-1; Bd-0; Benk-1; Ber; Bik-1; Bil(-5,-7); Bl-1; Bla-1; Boot-1; Bor-1; Bor-4; Br-0; Broesarp-34-145; Broet-1-6; Bs-1; Bsch-0; Bu-0; Bur-0; C24; Ca-0; Cal-0; Cdm-0; Cerv-1; Chat-1; Chi-0; Cnt-1; Co-1; Col-TAIR; Cvi-0; Da1-12; Db1; Del-10; Di-G; Dja-1; Do-0; Doer-10; Dog-4; Don-0; Dr-0; Dra-0; Dra2-1; Dra3-1; Durh-1; Eden(-1,-2,-7); Eden(-9); Edes(-1,-9); Ei(-2); El-0; Ema-1; En-2; En-D; Er-0; Es-0; Est-1; Est; Et-0; Etna-2; Ey15-2; Fei-0; Fi-0; Fjae(1-5,2-4); Fjae1-1; Fjae1-2; Fly2(-1,-2); Fr2; Fri-2; Ga-0; Gel-1; Gie-0; Gifu-2; Got-7; Gr-1; Gre-0; Gro-3; Groen(-5,-12,-14); Gu-0; Gy-0; Ha-0; Had(-1,-2); Hag-2; Hal-1; Ham-1; Hau-0; Hel-3; Hey-1; Hh-0; HKT2.2; Hn-0; Hola(-1-1,-1-2,-2-2); Hov(3-2,4-1); Hov1-10; Hov1-7; Hov3-5; Hovdala-2; Hs-0; ICE(-107-111-112-119); ICE(-120-130-138-163-212-213-226,228-29); ICE(-127-134-150-152-153); ICE(-169-173); ICE(-21-181-216); ICE(-71-72-73-75-79); ICE-(91-92-93-97-98); ICE-1; ICE-102; ICE-104; ICE-106; ICE-33; ICE-36; ICE-49; ICE-50; ICE-60; ICE-61; ICE-7; ICE-70; In-0; Is-0; Istisu-1; Je-0; Jl-3; Jm-0; Kaevlinge-1; Kar_1; Kas_1; Kastel-1; Kelsterbach_4; Kia-1; Kil_0; Kin_0; Kl_5; Kni-1; Knox_18; Ko_2; Koch-1; Kondara; Kor-3; Kro-0; Kro_0; Krot_0; Kru-3; Kulturen-1; Kyoto; Kz_9; La_0; Lag2.2; Lan-1; Lan_0; Le_0; Leo-1; Ler-0; Ler-1; Ler-1; Lerik1-3; Li_2:1; Liarum; Lilloe-1; Lip_0; Lis-2; Lis-3; Litva; Lm_2; Lom1-1; love-1; love-5; Lp2_2; Lu-1; Lund; Mer-6; Mnz_0; Ms_0; Mz_0; Naes-2; Nc_1; Nemrut-1; Neo_6; Nie1-2; Nok_3; Np_0; Nw_0; Nyl(-13-2-7); Ob_0; Oede-2; Oemoe1-7; Oer-1; Old_1; Omn(-1-5); Ove_0; Ped-0; Per_1; Pi_0; Pla_0; Pna(_10_17); Pog_0; Pra-6; Pro_0; Pt_0; Pu2_23; Pu2_7; Puk-2; Qar_8a; Qui-0; Ra_0; Ragl_1; Rd_0; Rennes_1; Rev-1; Rev-2; Rld_1; Rmx_A02; Roed-17-319; Rome_1; Rou_0; RRs_10; RRS_7; Rubeznhoe_1; Rue3-1-31; San-2; Sanna-2; Se_0; Seattle; Sei_0; Sg_1; Sha; Si_0; Sim-1_; Sorbo; Sp_0; Sparta-1; Spr1-2; Spr1-6; Spro-1; Spro-3; Sq_8; Sr:3; Sr:5; St-0; Star-8; Ste-2; Ste-3; Ste-4; Stu1-1; Stw_0; Su_0; Sus_1; T1000; T1020; T1070; T1080; T1090; T1110; T1130; T1160; T460; T470; T480; T530; T540; T550; T570; T710; T720; T740; Ta_0; TAA-04; TAA-14; TAA-18; TAAD-01; Tamm-2; Tamm_2; TBO-01; TDr-1; TDr-13; TDr-16; TEDEN-02; TEDEN-03; TFAE-06; TFAE-07; Tgr-01; Tha_1; Ting_1; Tny-04; Tol_0; TOM-04; TOM-06; Tomegap-2; Tottarp-2; TRAE-01; Ts_1; Tscha_1; Tsu-1; Tu_0; TueSB30-3; Tuescha9; TueV13; TueWa1-2; Tul_0; Tur-4; TV-10; TV-22; Ty_0; Uk_1; UllA-1; Ull2-3; Ull2-5; Uod_1; Utrecht; Vaar-1; Vaar2-1; Vaar2-6; Vaestervik; Van_0; Vash-1; Ven_1; Vie-0; Vimmerby; Vind_1; Vinsloev; Wa_1; WalhaesB4; Wc_1; Wei_0; Westkar_4; Wl_0; Ws_2; Xan-1; Yeg-1; Yo_0; Yst-1; Zal_1; Zdr_1

Conserved 99.9%	Substitution position
OLD3-Rhen_1.SALK	E>V/67
OLD3-Mc_0.SALK	A>S/128
OLD3-Ak(-1)-SALK	A>T/275
OLD3-Kal-2.GMI	I>V/278
OLD3-Com-1.SALK	P>L/284
OLD3-HR-5.SALK	P>L/284
OLD3-Spro-2.GMI	P>L/284
OLD3-Wt_5.SALK	P>L/284
OLD3-Mh_0.SALK	A>S/293

Appendix 4. Supplemental methods.

Details of the supplemental methods include the genetic maps of the vectors (Appendix 4.1-4.5) and the primers (Appendix 4.6) used in the study. These details are provided as follow;

Appendix 4.1. Genetic map of the pGreen 0229vector.

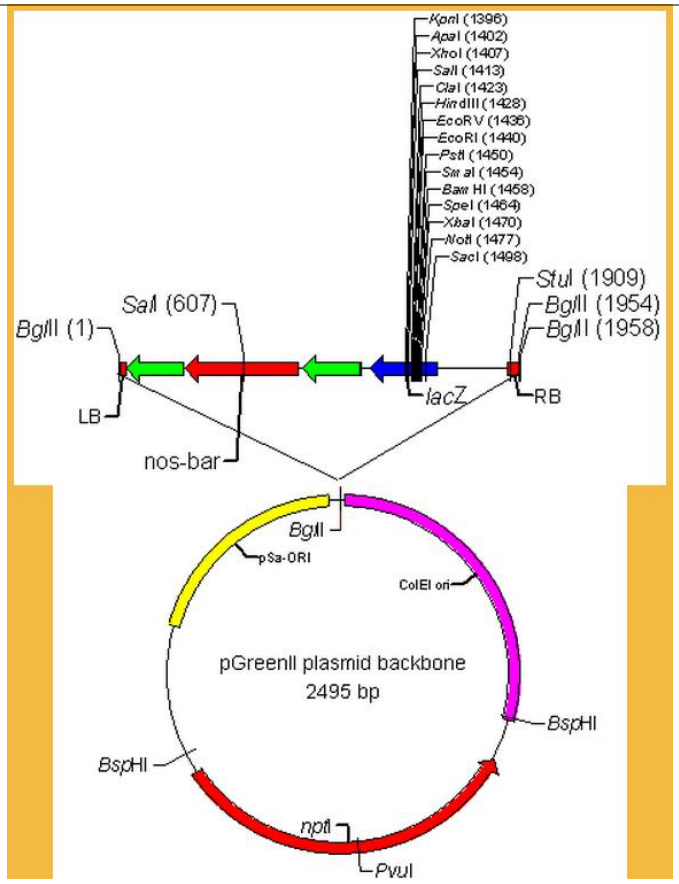

pGreen 0229 (figure adapted from www.pgreen.ac.uk/JIT/pG0229.htm)

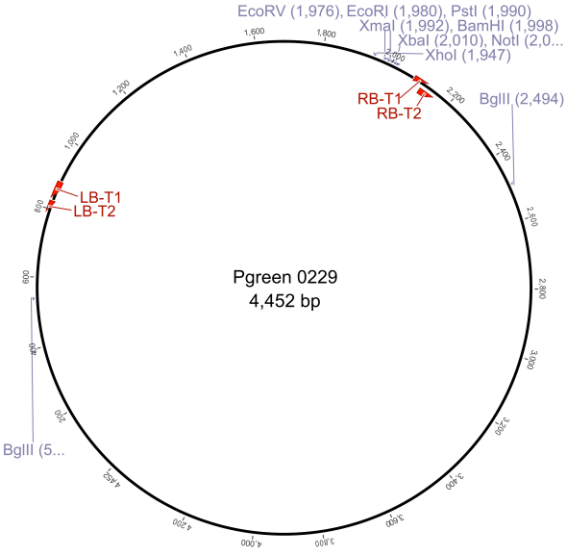

pGreen 0229

Appendix 4.2. Genetic map of the pGreen0229 vector.

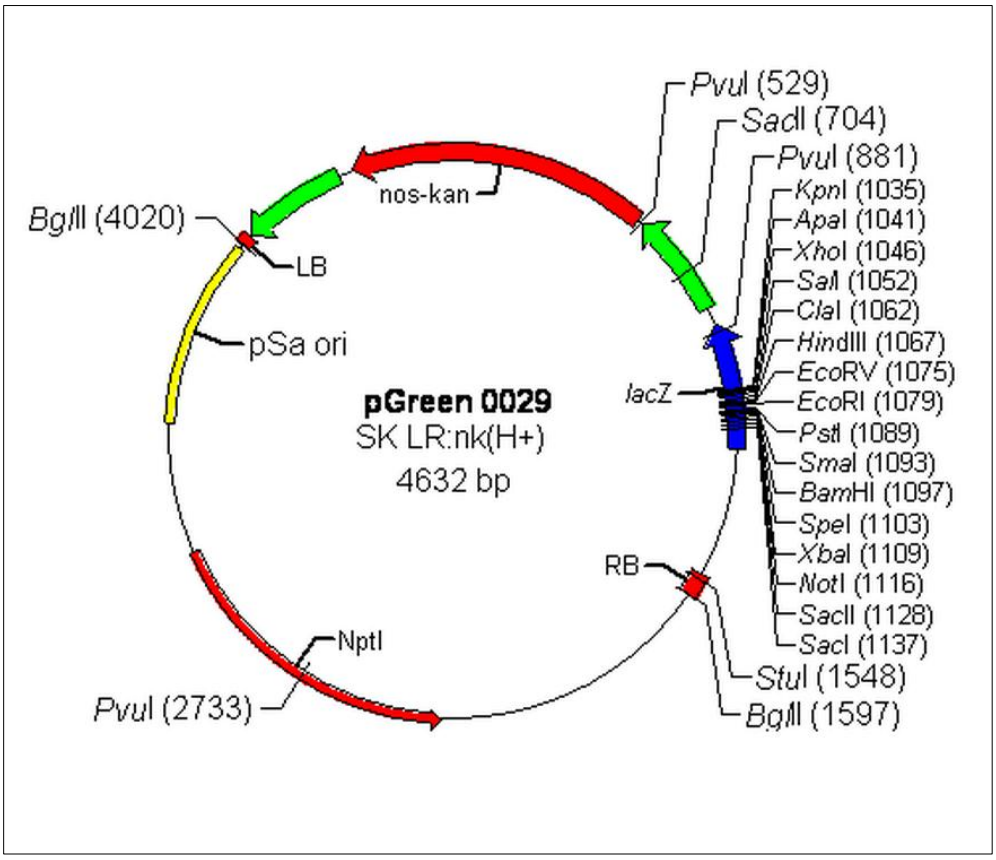

pGreen 0029 (figure adapted from www.pgreen.ac.uk/JIT/pG0029.htm)

Appendix 4.3. Genetic map of the pART7 vector.

pART7 (figure adapted from Gleave, 1992)

Appendix 4.4. Genetic map of the pDAH2 vector.

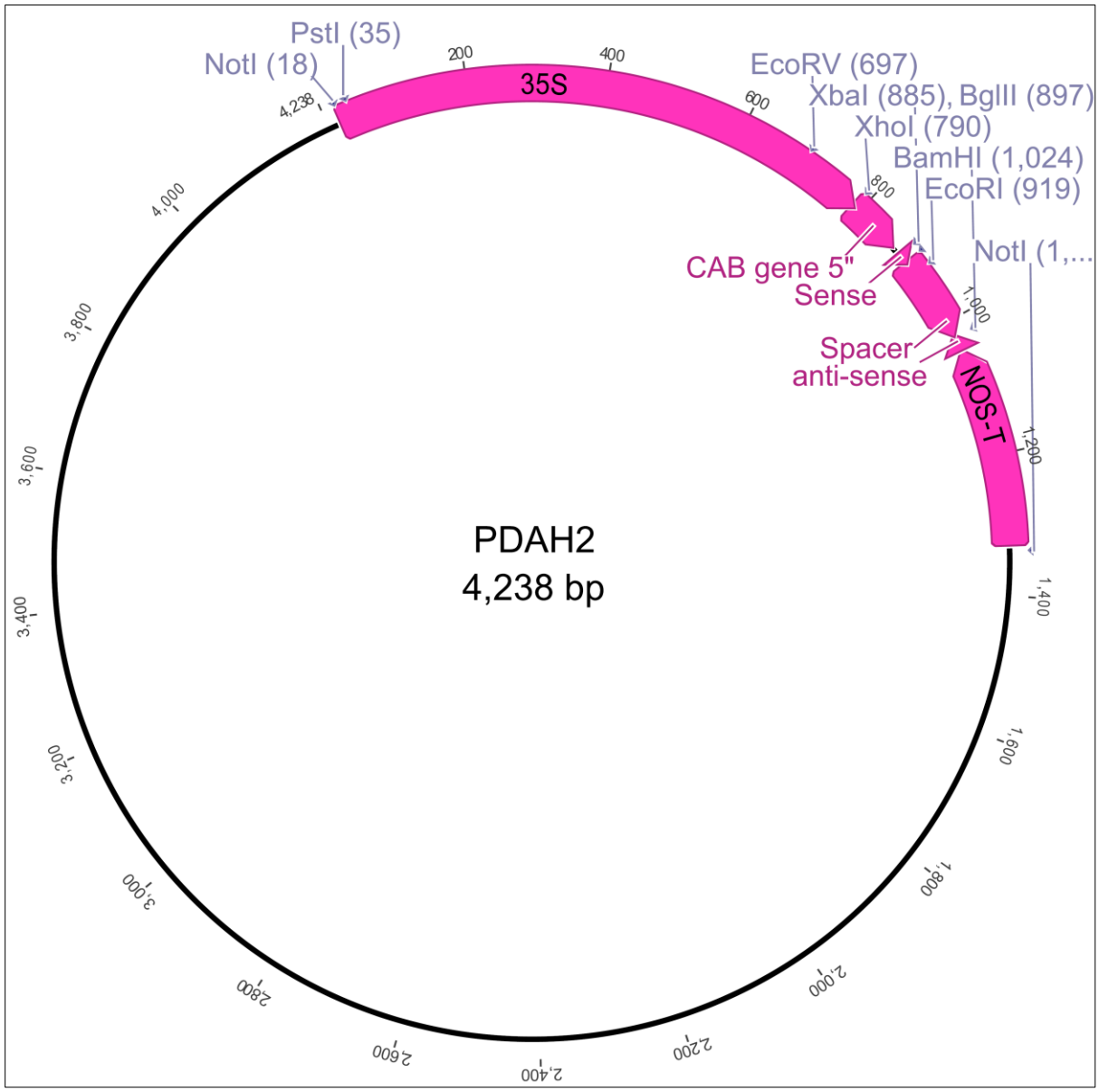

pDAH2 (*AmpR* in the backbone)

Appendix 4.5. Genetic map of the pET32 vector.

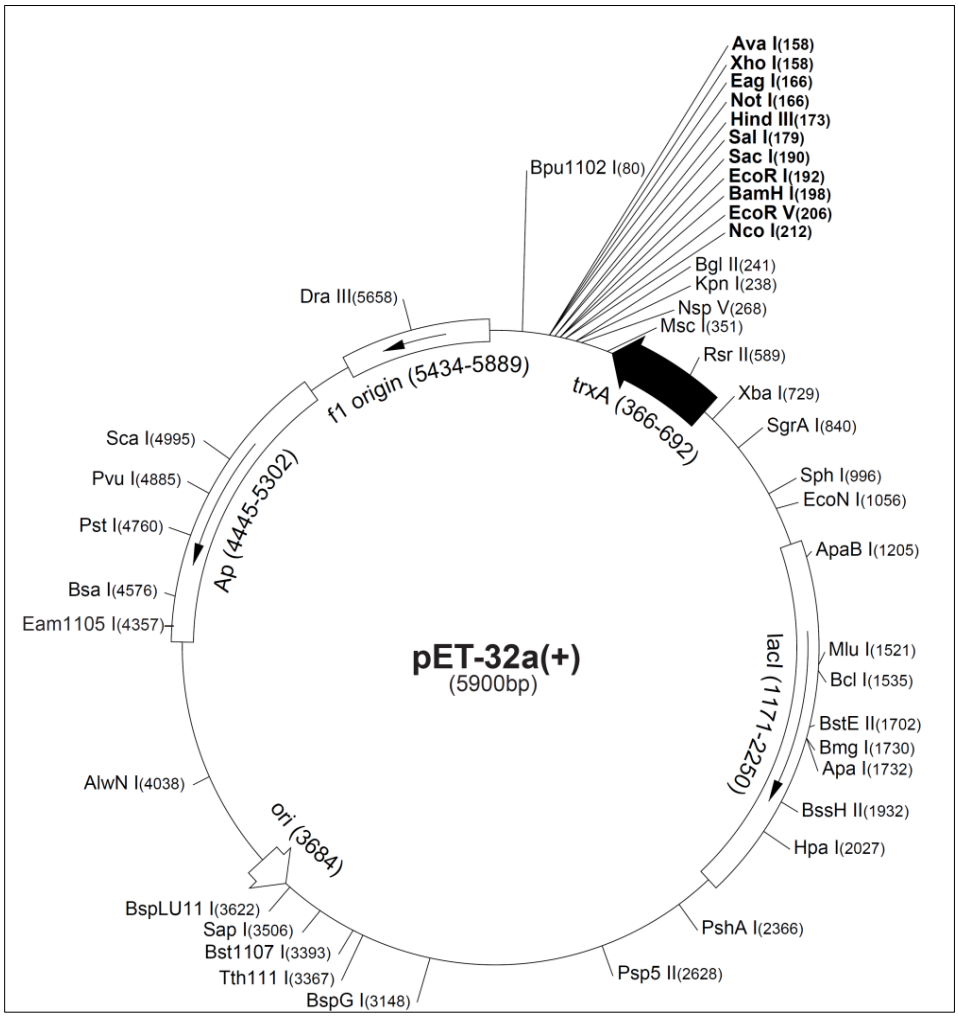

pET32 (adapted from Novagen, https://wasatch.biochem.utah.edu/chris/links/pET32.pdf)

Appendix 4.6. List of the primers used in the study.

Gene	Sense-primer	Anti-sense primer
Genotyping		
*(T-DNA-**OASTL-A1/OLD3**)*		
old3-2	*TGGTTCACGTAGTGGGCCATCG*	*TACACCAATGGAGTGTTCCCAATCA*
odd-specific marker		
odd- marker1	*ACCTCGTGATAATCAATTGTTCCAGCGGAAT*	*GAATGAACCGTGAGCTGATGGTGCTGGTGTTA*
odd- marker2	*GGCATGATTACGAGGAGGTAT*	*AAATTGTTGTATGATGTGAGA*
Genome walking of *odd-ler*		
AT3G44610	*TCTCAGTAGATCGGAAAATGGA*	*AATAATAGTCGACATGGGTTTCC*
AT3G44620	*ATCCATTGCAAGAATGAGATCAA*	*CCGATGCAGATAAGAAGGTTAAG*
AT3G44630		
P1	*TGTGTGGACGTGAAGTGTTG*	*CTGATCAAATCAATATTTACAATCAAA*
P2	*TGTGTGGACGTGAAGTGTTG*	*TTAGCTTGCCAAATCCGACT*
P3	*TGTGTGGACGTGAAGTGTTG*	*TCCAAAGATTGTTGGCAGTTC*
P4	*TGTAGGTCGTGTTCGTTTGC*	*TTGCTTATTTGTTCAGTTGGATG*
P5	*TGTGGACGTGAAGTGTTGTTG*	*TGTGTGGACGTGAAGTGTTG*
P6	*TGTGTGGACGTGAAGTGTTG*	*AAAGCCCTCGTCATTTGATGG*
P7	*GAGGAAAGCAACGAGTCAGG*	*CCTCTCAAACAGTGGTCCTAGC*
P8	*CCGATCAAGGCATCTGATTT*	*CACACCTGAAACCCATTAGGA*
P9	*CATGCTCAACAAACGATGCT*	*AACCCGTCGAAATCTCTTGA*
BAC end-sequencing		
T7	*TAATACGACTCACTATAGGG*	
SP6	*ATTTAGGTGACACTATAG*	

Appendix 4.6 *contd.* List of primers used in the study.

Gene	Sense-primer	Anti-sense primer
RNAi of candidate genes		
R genes		
RPP1-A;	*GCCTCTAGAGCC TTAAATCTCAAGGTTGTACGAAG*	*CGCGGATCCCATCATGCACACATCAACTCG*
RPP1-B-	*GCCTCTAGACCGCAGCTTTTACAAAATTCA*	*CGCGGATCCGATCGACTTACCCCTCTCCA*
AT3G44620	*GCCTCTAGACGGCTTCTCTAACAATCCCTTC*	*CGCGGATCCGCTGGACTCCGACAAATGTT*
AT3G44610	*GCCTCTAGACTCGCGAGCTCCTTTTTATC*	*CGCGGATCCAGCTTTACATCAGCCGGAAC*
OASTL-A1/OLD3	*GCCTCTAGATTCGATGCGACAAGGAAAG*	*CGCGGATCCGATGGAAGCAAAGACGCAAT*
UTR specific RNAi of *R* genes		
5′ UTR specific		
R2, R8	*CTTCAACTCTCTGGAGATTTC*	*CTCATTGCAGAACCCATGAGAACT*
R5, R8	*TTGCTGATCTTAATGGTTTAATTG*	*CAGAACCCATTGAATATTCACTGCAGC*
R3, R4, R5, R7, R8	*TTAAGAACTAGCCTCGACGGAA*	*TATGAGAGATTTCTGAGCTAATATGT*
R1, R2, R3, R4 R5, R7	*ATTGAGCTTCTCATGCTCACAGGA*	*TTGACCCATGGAGGAACTTCTTGT*
3′ UTR specific		
R1	*GGCATGATTACGAGGAGGTATT*	*AAATTGTTGTATGATGTGAGAG*
R2, R5	*TTTATGATGATTATGTGT*	*TTTCTCCTATGATATGTCTC*
R3	*GTCTTTGCTGCACGGTATCATAAC*	*CAAATTTATAATATTGCTGAGTCC*
R4, 7, 8	*GTCTCATGGATTGGTTAATGAATC*	*CACAGCTAATTCCCATTCACACA*

Appendix 4.6 *contd.* List of primers used in the study.

Gene	Sense-primer	Anti-sense primer
Over-expression of OASTL-A1 in plants (cDNA including UTR)		
OASTL-A1, old3-1	*GCCTCTAGATAAATTGATAGCGTGTGCCATGT*	*CGCGGATCCATGTTGGTTTAGTTTTGATCATGAA*
Over-expression of OASTL-A1 in NK3-strain (cDNA)		
OASTL-A1, old3-1	*ggaattccatATGGCCTCGAGAATTGCTAAAGATGTG*	*cgcggatccTCAAGCCTCGAAGGTCATGGCTTC*
Site directed mutagenesis of OASTL-A1		
Mutations		
old3-3/JT106	*TCGAAGACAGGATTGGTTTTAG*	*TTCGACGCTAGAGCACGGTTC*
old3-4/JT107	*CGTCGCAGACAGGATTGGTTTTA*	*TCTGCGACGCTAGAGCACGGTT*
old3-5/JT108	*AAAAAGTGGAAACACTGGAGTTG*	*TTTTTGGCTCAATCAGCACACTC*
old3-6/JT109	*TGGGGCGCCAGGTCCTCACAAGA*	*TGGCGCCCCACCGGATAGAATA*
old3-7/JT110	*ATAAAATCCGGTGCAGCAGCTG*	*GGATTTTATTCCCACAAGAAGA*
old3-8/JT111	*TCGTAAAGAACAGAACGCAAACGTCA*	*TACGATACTTCCCAGCACCTGTAA*
old3-9/JT112	*TGGGATATGGAAAGGCACTGGTG*	*TCCCAGGTCCCGTAGTCTCATAG*
old3-10/JT113	*AGGAGCGGAAGCCATGACCTTCG*	*CTCCTTTCCTTGTCGCATCGAAA*
old3-11/JT114	*TGATCTTAAAGAAGGTCTTCTTG*	*GATCAAGCTGCCTTGCCATGTCA*
old3-12/JT115	*AGATTTTGGAGTTGAGTTGGTTT*	*AATCTAAGAGAATGATTCTTCT*
old3-13/JT116	*AG**A**TGCCAAAGGCTACAAGCTTA*	*CA**T**CTGCCGTGAATGCTAACCC*
Primers for complementation of *R* genes in *old3-1*^{rec}		
R1	*ACAACTTGATCGGAGCGAAAC*	*ATTGAGAACGTTAATAGGAGAATTTGA*
R2	*GTTATCAAATTGTCTTTAACCGAACAC*	*AACTCGTCTTACCATCTAATTCAGTTC*
R3	*GATGGAGGAGGTATTGAAATTCTCTG*	*CAACATTTTCACAAATCAGAAACATAA*
R4	*CTTCTTGGAAAGTTCTTGGATGTG*	*AAGATAGGGAATCGGAAAGTTGTG*
R5	*CCGTTAAATTGTTGATATCATTACAAA*	*TTGTCCATTAGTATCTTGTTGTTTCAG*
R6	*GAGATATTTGCAAACCAAACTAGAGAC*	*ACCATGTCGTATTACAATCGATCC*
R7	*TGACGTAAATTAACTAACCTTCCT*	*ATTTCACCAAACAAACACCAAGAG*
R8	*ACAATGATGAGAAAGTGTACAAAAGAG*	*CAATAATTTTCTGCCAAAACTCTTAAA*

Appendix 4.6 *contd.* List of primers used in the study.

Gene	Sense-primer	Anti-sense primer
Expression of plant genes in yeast		
OASTL-A1/old3-1	*GGAATTCGCCTCGAGAATTGCTAA*	*CGGGATCCAGCCTCGAAGGTCAT*
SERAT	*TGTGAATTCATGCCACCGGCCGGAGAACTCCGA*	*GCGGGATCCTTATATGATGTAATCTGACCATTCCGAGAT*
BASTA-resistance gene		
BAR	*GAAGTCCAGCTGCCAGAAAC*	*TCGTCAACCACTACATCCAGAC*
Transcriptional analysis through Real-time PCR		
EDS1	*GTTGAACCGTGTTCAGTTTCCTTG*	*TACTCCTCACAGCCATTTCCACAG*
PAD4	*AGATACGCGAGCACAACGCAAG*	*TTTCTCGCCTCATCCAACCACTC*
ICS1/SID2	*GCTTGGCTAGCACAGTTACAGC*	*CACTGCAGACACCTAATTGAGTCC*
WRKY18	*TGGACGGTTCTTCGTTTCTCGAC*	*TCGTAACTCACTTGCGCTCTCG*
PR-1	*ACACGTGCAATGGAGTTTGTGG*	*TTGGCACATCCGAGTCTCACTG*
B-Tubulin	*ACCACTCCTAGCTTTGGTGATCTG*	*AGGTTCACTGCGAGCTTCCTCA*
Actin2	*TCCCTCAGCACATTCCAGCAGAT*	*AACGATTCCTGGACCTGCCTCATC*
R1	*AACTGCTTCACTTCAAGATTATACA*	*AGCTCCACTAAACTTGAGCAACG*
R2	*ATGCTGGAACAATTGTTGCGCCAT*	*GTTTTGTAGTTGCAATTGTGCACTGCG*
R3	*TCATGGGATCAATCATGTTTACAAGGTC*	*GGGAGTTCACCAGCAAGGTAGG*
R4	*CTGCATGTATGTTTGATCGGT*	*ATCTTGTAGTTTCAATTGTGCGT*
R5	*GCGTTTTATAGGGATTATACT*	*ATCTTTTGAGAATGATGAAGG*
R7	*TTCAAACATGTTGGATTTATC*	*TAGGCGCAACAATTGTTCCGTCCTTT*
R8	*TGCCTTTTTAAAGACGAATTAT*	*AAAAGGAATTCTCATCAATGGA*
OASTL-A1/OLD3	*ACAGAACGCAAACGTCAAGCTG*	*GCTTCCCACCGGATAGAATAGCAC*

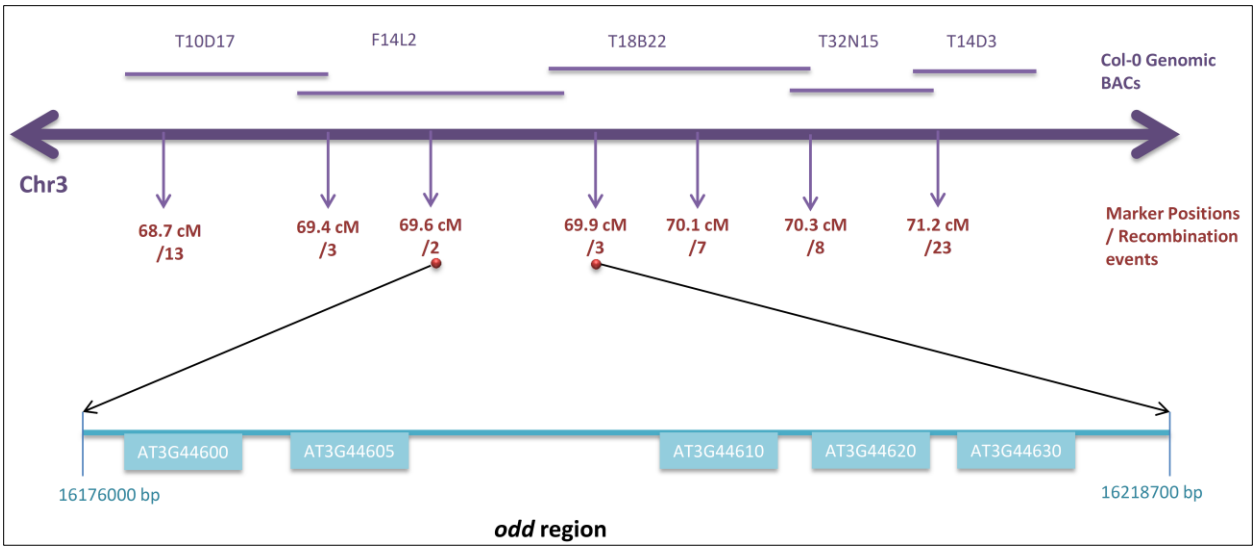

Appendix 5. Map of the *odd-col* region. Diagram showing map-based cloning of the *odd* region on Chr 3, in Col-0. The BACs in Col-0 spanning the mapped regions are shown. The tested SNP markers are shown by their positions on the Lister & Dean RI map and on the physical map. The position of the marker and number of recombination events flanking the region is shown. The predicted genes in the *odd* region are indicated with blue bars.

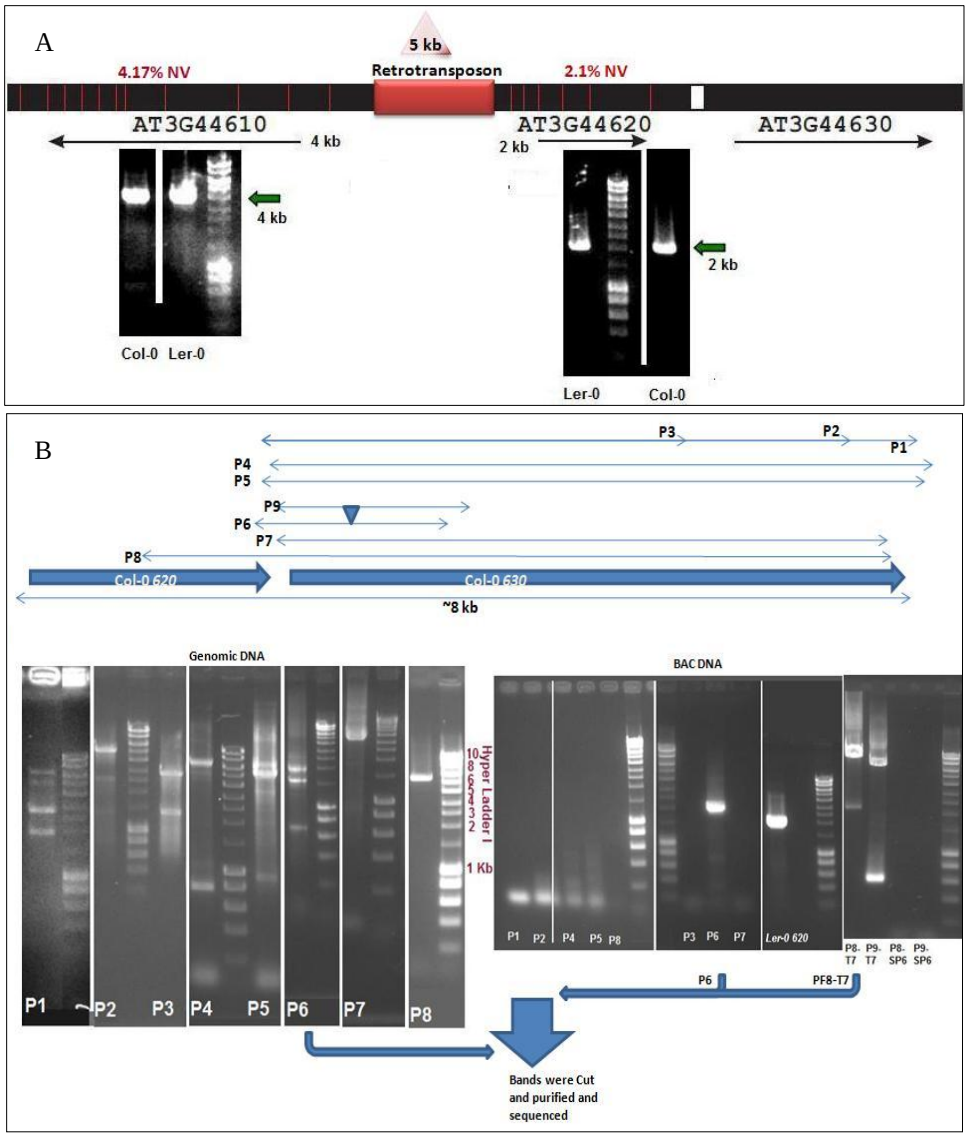

Appendix 6. Nucleotide variation of the At3g44610,At3g44620 and *R* gene polymorphism in the *odd-ler* region. (A) Non-scaled map of Ler-0 genes adjacent to retrotransposon insertion with mutation percentage based on total substitutions and InDels. The bands in the gels show the unchanged gene size of the corresponding genes in both the accession.(B) shows the model for rigorous primer designing for L*er*-0 At3g44630 based on Col-0's sequence information. On the left-side, figure shows the PCR results employing primers over genomic DNA that provided unexpected band sizes and multiple bands, which were individually cut, cloned an end-sequenced but revealed NBS-LRR sequence polymorphic to Col-0. On the right side, figure shows that no amplification was rendered employing these primers on 10G16 BAC DNA, where a Ler-0 At3g44620 amplification works as a control. Only one primer set P6 was able to amplify the target sequence from BAC DNA.

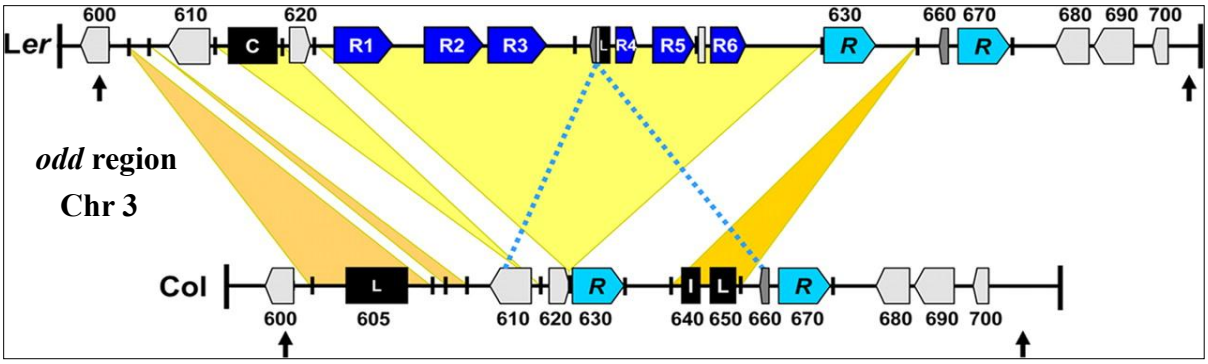

Appendix 6 *contd*. Nucleotide variation of the At3g44610, At3g44620 and *R* gene polymorphism in the *odd-ler* region. Figure adapted from Alcazar *et al*., 2009. Comparison of the genetic architecture in QTL 3 (L*er*-0 BAC FJ446580) between L*er*-0 and Col. Compared with the compatible Col-0 haplotype, the L*er*-0 sequence contains a genomic insertion of 65 kb between At3g44620 and At3g44630 that has 5 genes encoding TIR-NB-LRR proteins (*R1–R5)* with sequence similarities to *RPP1*-like genes, and 1 gene that is truncated with a predicted TIR- domain (*R6*). Together with the *RPP1*-like At3g44630 and At3g44670 homologs in L*er* (*R7* and *R8*) a polymorphic cluster of 8 *TIR-NB-LRR* genes is evolved in L*er*-0 compared with the 2 *TIR-NB-LRR* genes in Col.

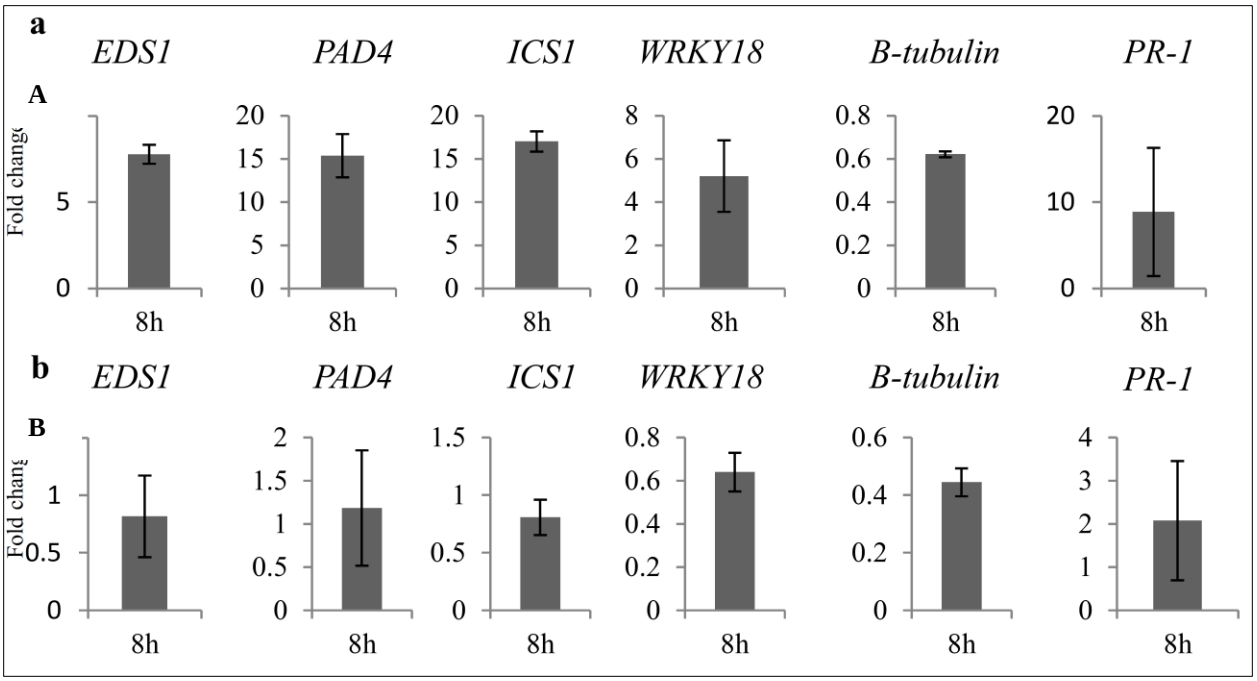

Appendix 7. Transcriptional changes in the defence markers in *old3-1* and L*er*-0 within 8 h of change in temperature. Immune response in the *old3-1* mutant and wild-type L*er*-0 after 8 h of temperature shift. Transcriptional analysis was performed for defence related markers in the *old3-1* mutant and L*er*-0 tissues within 8 h of temperature shift from 28 to 21 °C. Fold-change in expression of *EDS1, PAD4, ICS1, WRKY18* , *β-tubulin* and *PR-1* genes in the (a) *old3-1* mutant and (b) L*er*-0 after temperature shift. Expression values at both time points were first calculated relative to *Actin2* and then fold-changes were calculated at 8 to 0 h. Data represent the mean value of three biological replicates for each time point. Error bars represents standard deviation.

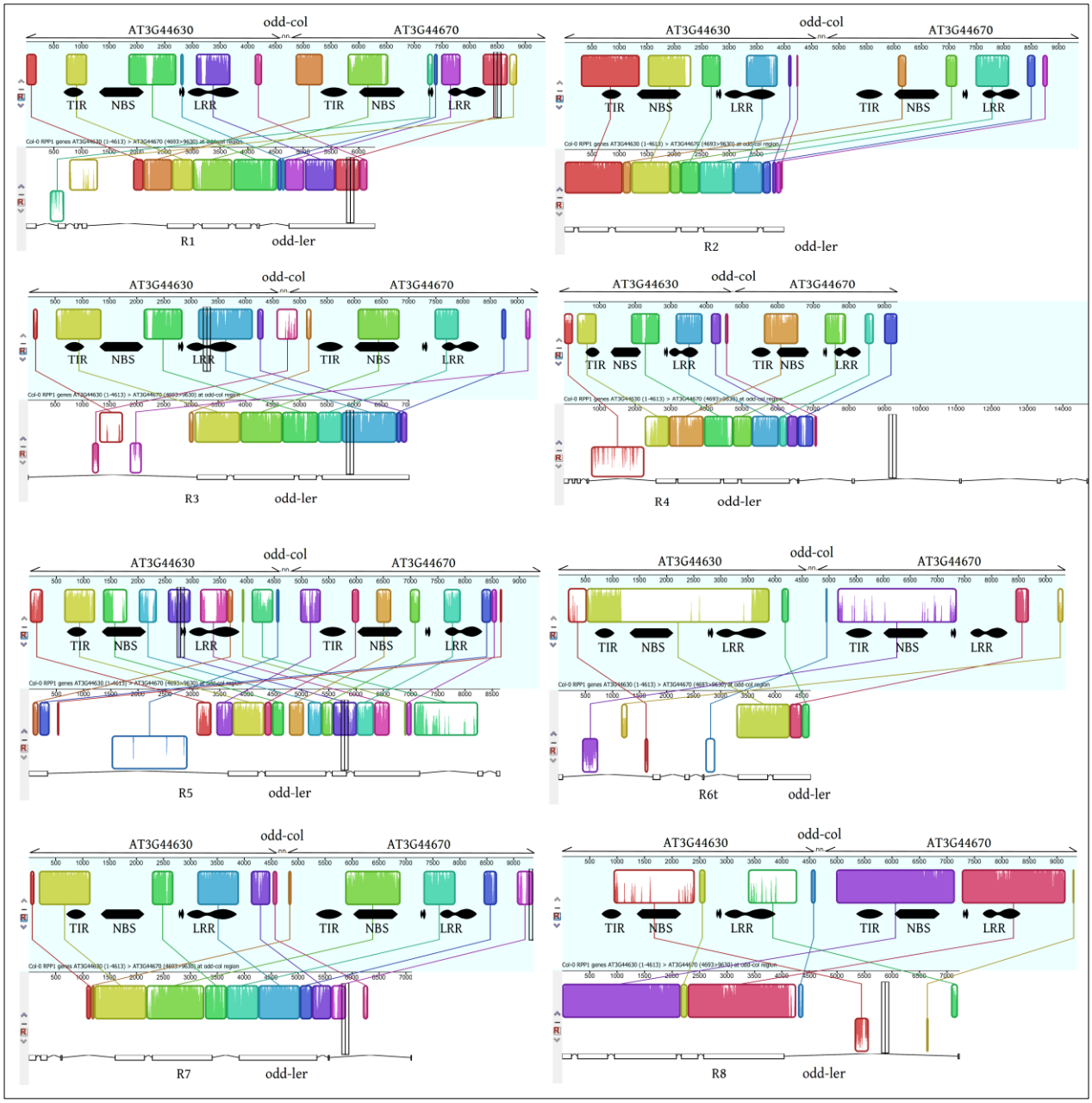

Appendix 8. Genetic rearrangements in *RPP1*-like *R* genes. The Col-0 genomic sequences of 2 *RPP1*-like *R* genes in *odd-col* region were analysed for sequence homology with each *RPP1*-like *R* genes in the *odd-ler* region. Employing an algorithm in *progressivemauve* software that identifies collinear blocks, homologous regions were identified in the alignments between each *R* gene from the *odd-ler* region in comparison to *R* genes in *odd-col*. *RPP1* genes in Col-0 are annotated for putative TIR-NBS-LRR domains based on Swissprotein database. Putative *RPP1*-like R gene annotations in the cluster are obtained from Alcazar, R., Garcia, A.V., Parker, J.E., and Reymond, M. (2009). Incremental steps toward incompatibility revealed by Arabidopsis epistatic interactions modulating salicylic acid pathway activation. Proc. Natl. Acad. Sci. USA 106: 334-339.

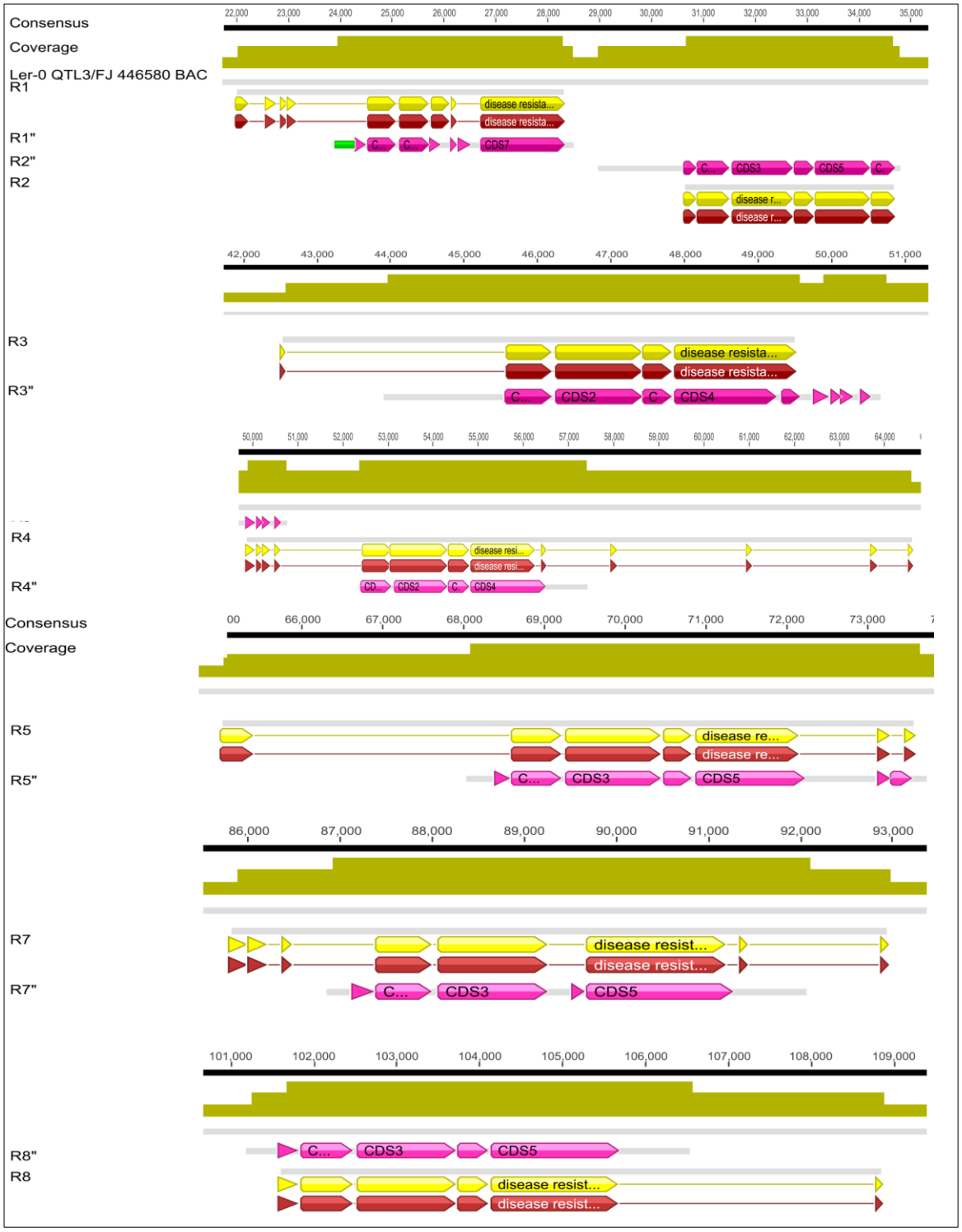

Appendix 9. Details of *RPP1*-like *R* gene models using the Augusts gene prediction tool. The figure shows the alignment of the gene models (*R1-R8*, excluding *R6t*) predicted by Alcazar et al., 2009 and those (*R1"-R8"*) predicted by the Agustus gene prediction tool. It is to be noted that the prediction of new *R"* gene models overlaps the previous models as predicted by Alcazar et al., 2009, but unlike previously these models also indicate 5 and 3′ regions.

Appendix 10. Various combinations of *R* genes for RNAi, through selecting a homologous region in the putative 5′ and 3′ un-translated regions (UTRs).

Group of *R* genes showing significant homology in a region in the putative 5′ UTR.

1	*R2, R8*
2	*R5, R8*
3	*R3, R4, R5, R7, R8*
4	*R1, R2, R3, R4, R5, R7*

Group of *R* genes showing significant homology in a region in the putative 3′ UTR.

1	*R1*
2	*R2, R5*
3,	*R3*
4	*R4, R7, R8*

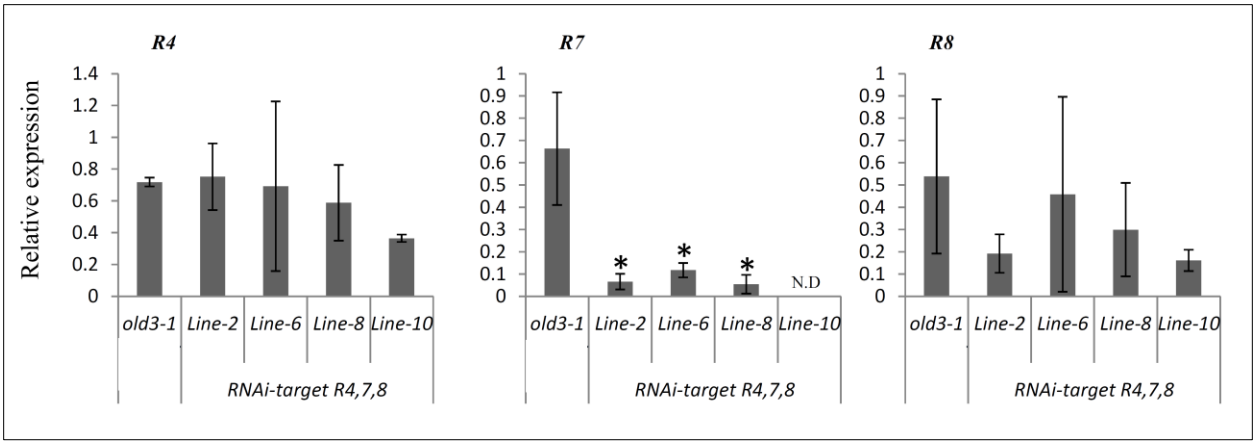

Appendix 11. Expression of *R4, R7* and *R8* in the *old3-1* mutant and the *old3-1* mutant transgenic lines carrying RNAi-cassette targeting a putative 3' UTR region of *R4, R7, R8*.

Data for line-3, line-4 and line-12 is shown in main manuscript. Expression values are relative to *Actin2*. Values represents mean of three biological replicates. Error bar represents standard deviation. * indicates statistically significant differences in mean value of each *R* gene expression within the transgenic line in comparison to the *old3-1* mutant using Student's *t* test ($P < 0.05$). N.D is not detected.

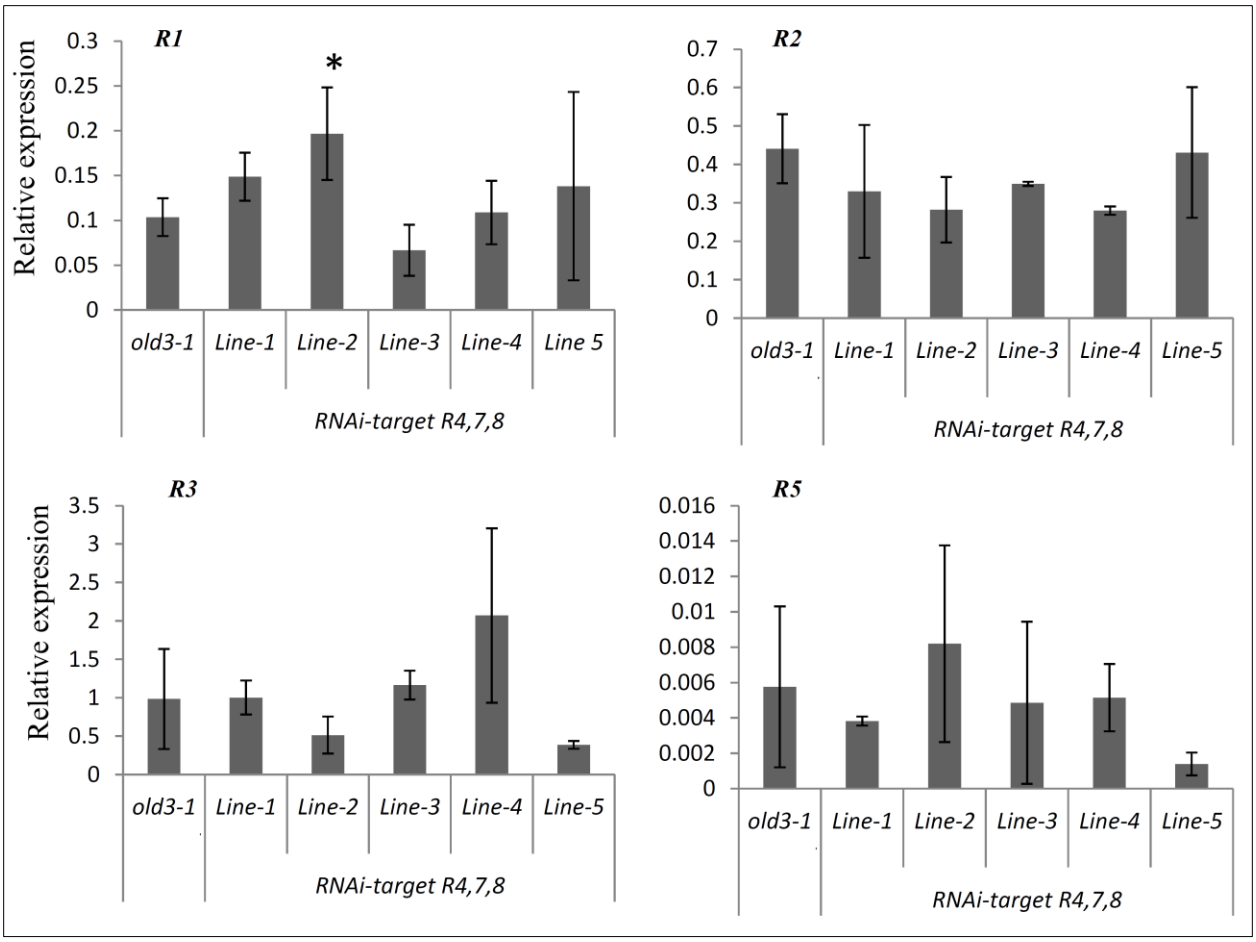

Appendix 12. Expression of non-targeted full-length *R* genes in the *old3-1* mutant and the *old3-1* mutant transgenic lines carrying RNAi-cassette targeting putative 3' UTR region of *R4, R7, R8*. Expression values are relative to *Actin2*. Values represents mean of three biological replicates. Error bar represents standard deviation. Statistically no significant differences in mean value of each *R* gene expression within the transgenic line in comparison to the *old3-1* mutant were found using Student's *t* test ($P < 0.05$).

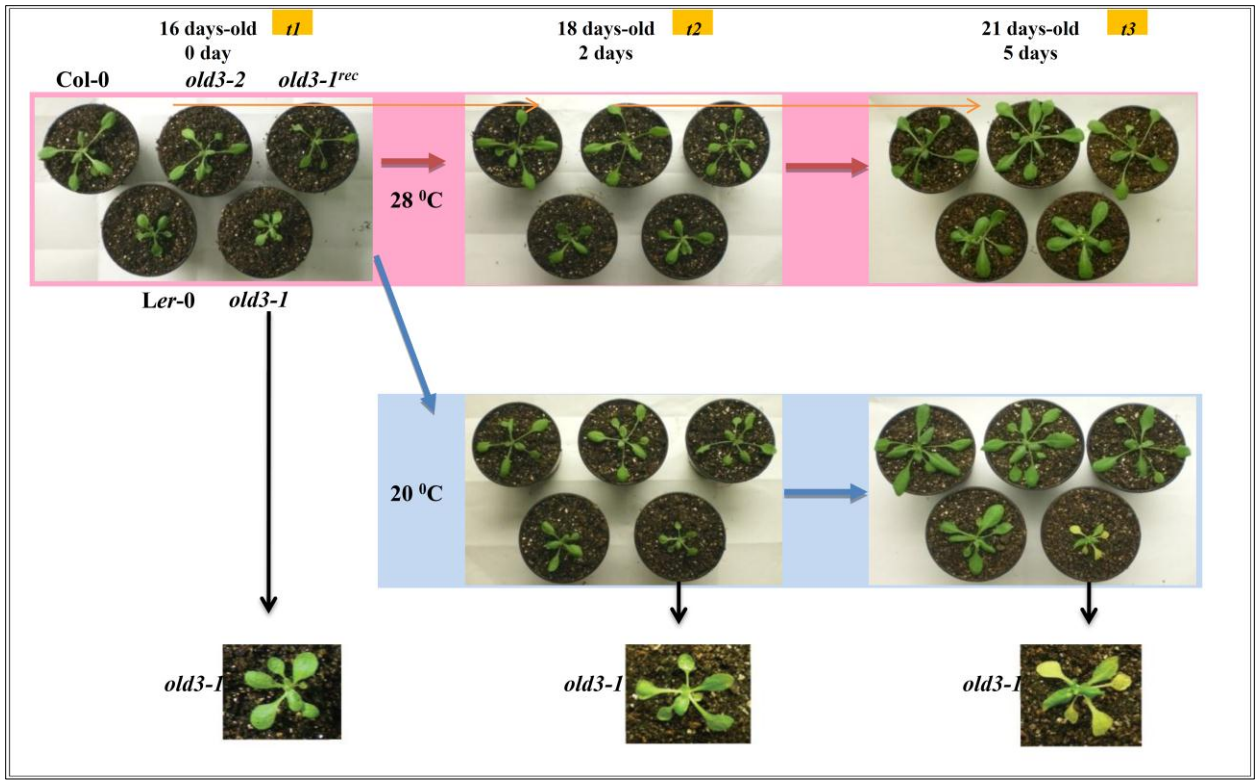

Appendix 13. Experimental layout for the temperature shift experiment for five genotypes.

Plants were cultured on soil (type GS-90 Einheitserde', Gebrueder Patzer, Germany) in a L.D. condition in growth chamber (16 h day, 140-160 µmol m-2 s-1, 28 °C; 8 h night, 28 °C) for 16 days (*t1*) and transferred to either 20 °C or kept at 28 °C and grown for additional days. Plants were harvested at time points *t1*, *t2* and *t3* in both temperatures for measurements of enzymatic activities and metabolic profiling in all five lines.

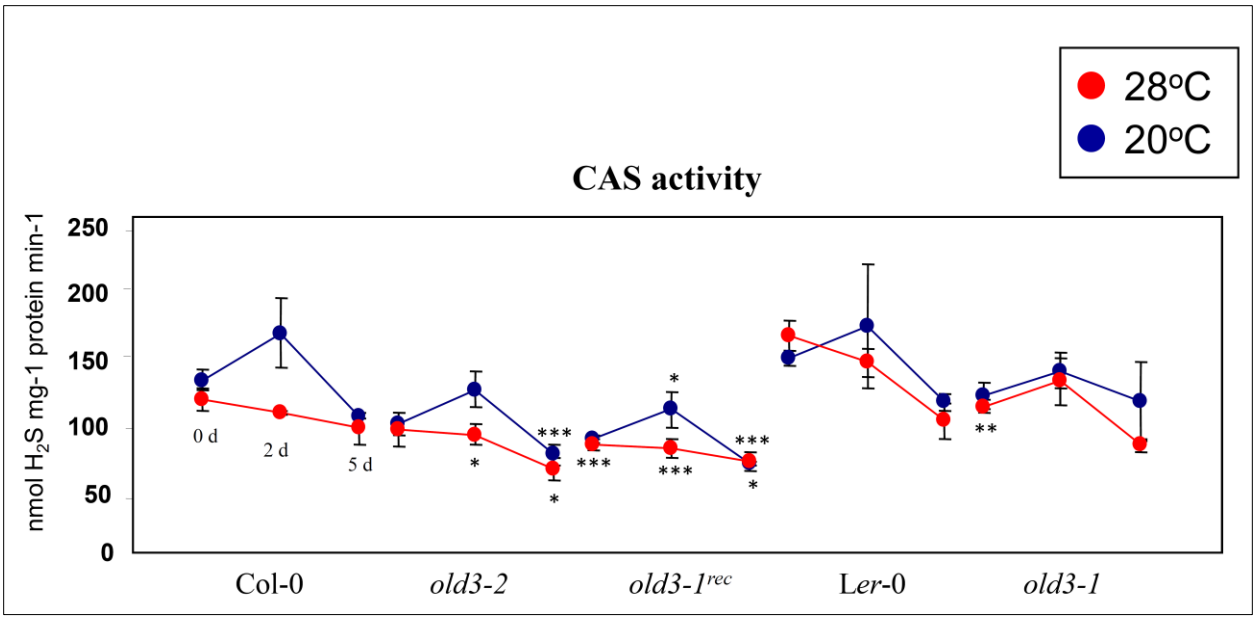

Appendix 14. Activity of the mitochondrial enzyme *β*-cyanoalanine synthase in five genotypes in the temperature shift experiment. Measurements in red colour is for 28 °C and blue for 20 °C grown plants at 0, 2 and 5 days of temperature shift. Data represents mean of three biological replicates. Error bar represents standard deviation. Statistically significant differences in the values between the mutants and the respective wild-types, using Student's *t* test are shown by * at $P < 0.05$, ** at $P < 0.01$ and *** at $P < 0.005$. Data for *old3-1rec* is statistically analysed against the values of those of Col-0.

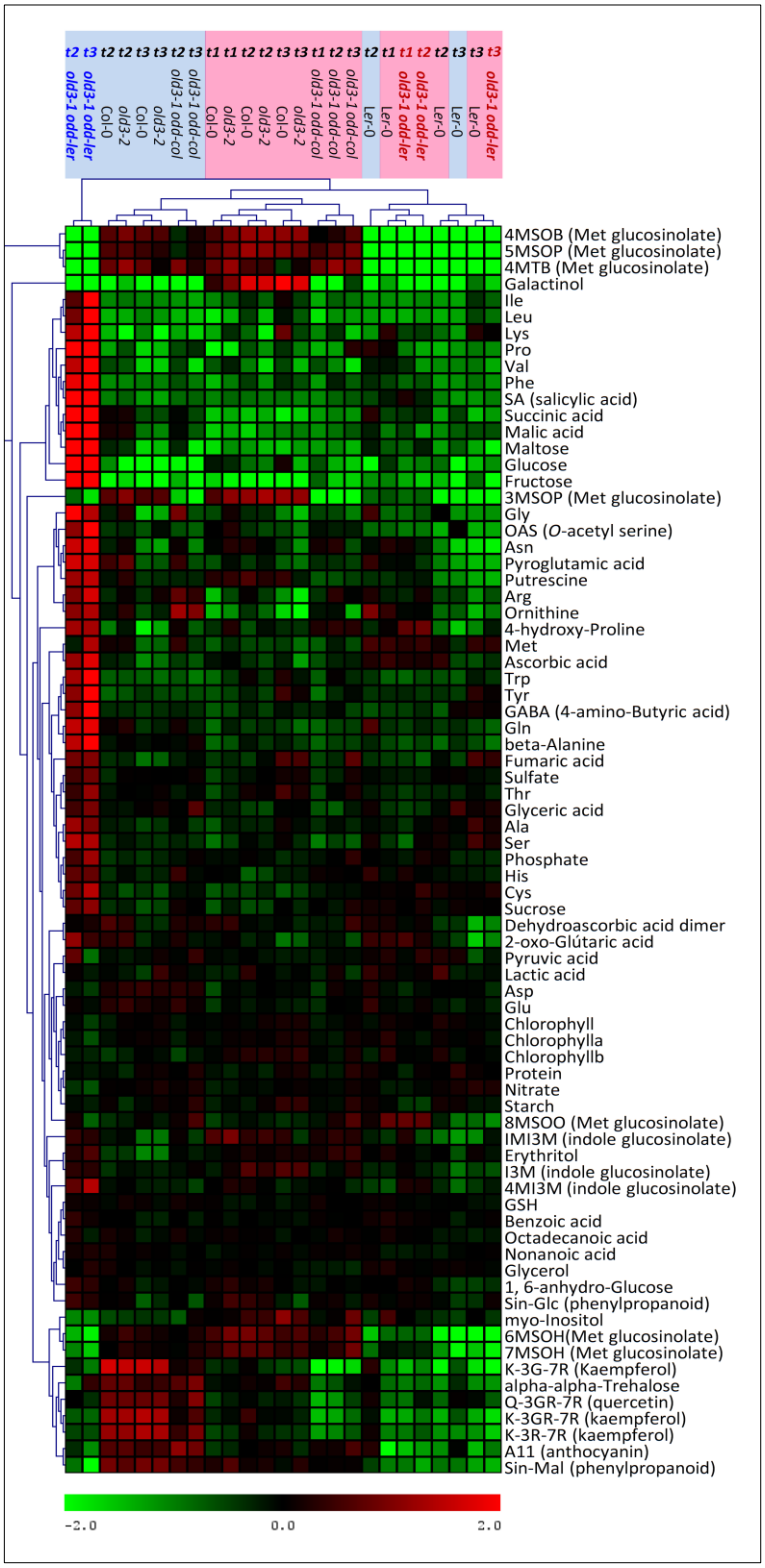
t2 t3 t2 t2 t3 t3 t2 t3 t1 t1 t2 t2 t3 t3 t1 t2 t3 t2 t1 t1 t2 t2 t3 t3 t3
old3-1 odd-ler
old3-1 odd-ler
Col-0
old3-2
Col-0
old3-2
old3-1 odd-col
old3-1 odd-col
Col-0
old3-2
Col-0
old3-2
old3-1 odd-col
old3-1 odd-col
old3-1 odd-col
Ler-0
old3-1 odd-ler
old3-1 odd-ler
Ler-0
Ler-0
Ler-0
old3-1 odd-ler
4MSOB (Met glucosinolate)
5MSOP (Met glucosinolate)
4MTB (Met glucosinolate)
Galactinol
Ile
Leu
Lys
Pro
Val
Phe
SA (salicylic acid)
Succinic acid
Malic acid
Maltose
Glucose
Fructose
3MSOP (Met glucosinolate)
Gly
OAS (O-acetyl serine)
Asn
Pyroglutamic acid
Putrescine
Arg
Ornithine
4-hydroxy-Proline
Met
Ascorbic acid
Trp
Tyr
GABA (4-amino-Butyric acid)
Gln
beta-Alanine
Fumaric acid
Sulfate
Thr
Glyceric acid
Ala
Ser
Phosphate
His
Cys
Sucrose
Dehydroascorbic acid dimer
2-oxo-Glútaric acid
Pyruvic acid
Lactic acid
Asp
Glu
Chlorophyll
Chlorophylla
Chlorophyllb
Protein
Nitrate
Starch
8MSOO (Met glucosinolate)
IMI3M (indole glucosinolate)
Erythritol
I3M (indole glucosinolate)
4MI3M (indole glucosinolate)
GSH
Benzoic acid
Octadecanoic acid
Nonanoic acid
Glycerol
1, 6-anhydro-Glucose
Sin-Glc (phenylpropanoid)
myo-Inositol
6MSOH(Met glucosinolate)
7MSOH (Met glucosinolate)
K-3G-7R (Kaempferol)
alpha-alpha-Trehalose
Q-3GR-7R (quercetin)
K-3GR-7R (kaempferol)
K-3R-7R (kaempferol)
A11 (anthocyanin)
Sin-Mal (phenylpropanoid)
-2.0
0.0
2.0

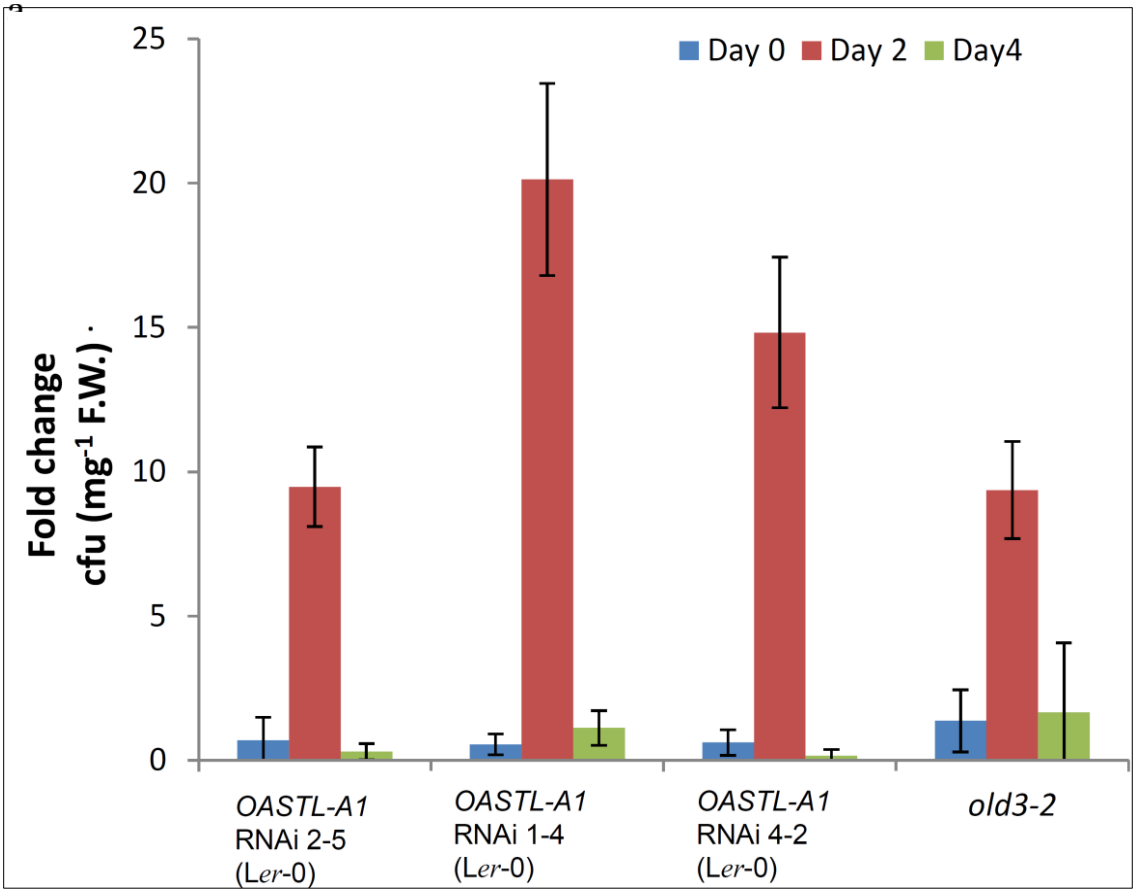

Appendix 16. *OASTL-A1* contributes in resistance to infection by the *Pst DC3000*. Colony Forming Units (CFU) for *Pst D3000* were measured in all the lines at day 0, 2 and 4 post-infection. Data represents mean of fold change value in CFU counts in *old3* mutant as compared to the wild-type at each specific time point. Three biological replicates were harvested from each line per time point and for each biological replicate, tissues were pooled from six to seven leaves from which counts were obtained. At each time point fold change in CFU value was calculated between each biological replicate of the mutant as compared to the wild-type. Mean of three fold-change values from three biological replicates is presented here. Error bar represent standard deviation of the mean. The data are representative of one experiment.

Appendix 15. Hierarchical Clustering Analysis (HCA) of metabolite data for the temperature shift experiments. Heat map of the metabolite pools of the five genotypes, Col-0, (*OLD3OLD3 odd-colodd-col*); *old3-2* (*old3-2old3-2 odd-colodd-col*); *old3-1rec(old3-1old3-1 odd-colodd-col*); L*er*-0 (*OLD3OLD3 odd-lerodd-ler*); *old3-1* mutant (*old3-1old3-1 odd-lerodd-ler*) at *t1*, *t2* and *t3* at two different temperatures (blue =20 ^{o}C and pink=28 ^{o}C). Each row represents one metabolite and each column represent one genotype. Data was normalized and metabolites with high abundance are presented by dark-red coloured cells of value 2 and metabolites showing lower abundance are presented as cells with dark-green colour of value -2. The scale of the heat-map is presented on the right side. The data was submitted to Hierarchical Clustering Analysis (HCA) using Euclidian distance to identify clusters of similar metabolic profiles. Col-0 and *old3-2* were clustered together at each time point and temperature. *old3-1*^{rec} clades at 20 ^{o}C and 28 ^{o}C were close to Col-0 and *old3-2* clades. L*er*-0 and the *old3-1* mutant were separated from other three genotypes because of differences in accumulation of metabolite and changes in levels of secondary metabolites. *old3-1* mutant at *t2* and *t3* at 20 ^{o}C forms a separate clade from others because of strong accumulation of metabolites.

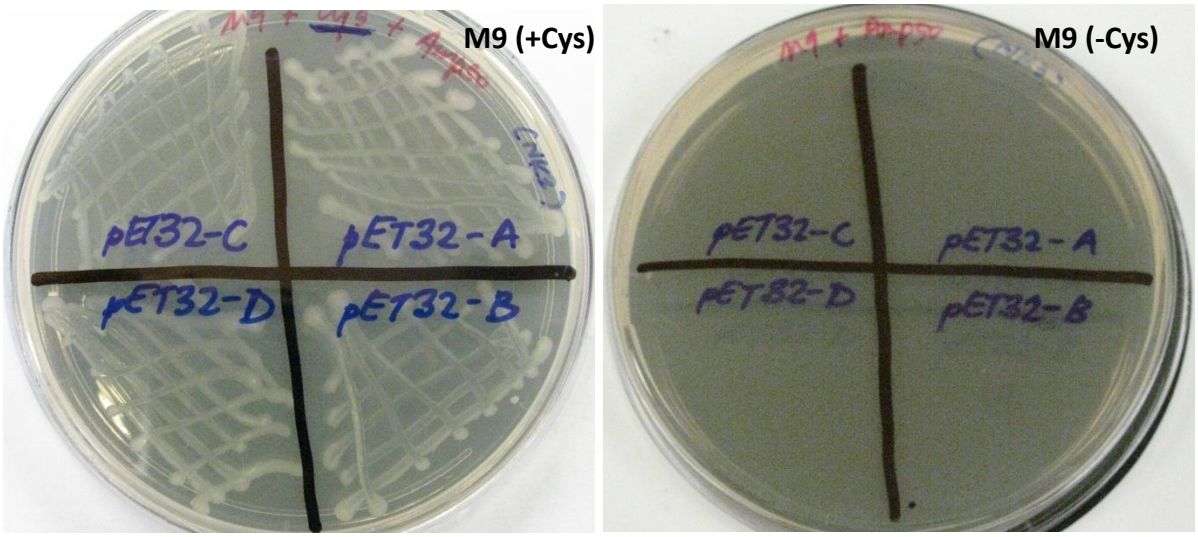

Appendix 17. Growth of the NK3 strain transformed with the vector pET32 on M9 minimal medium supplemented with or without cysteine.

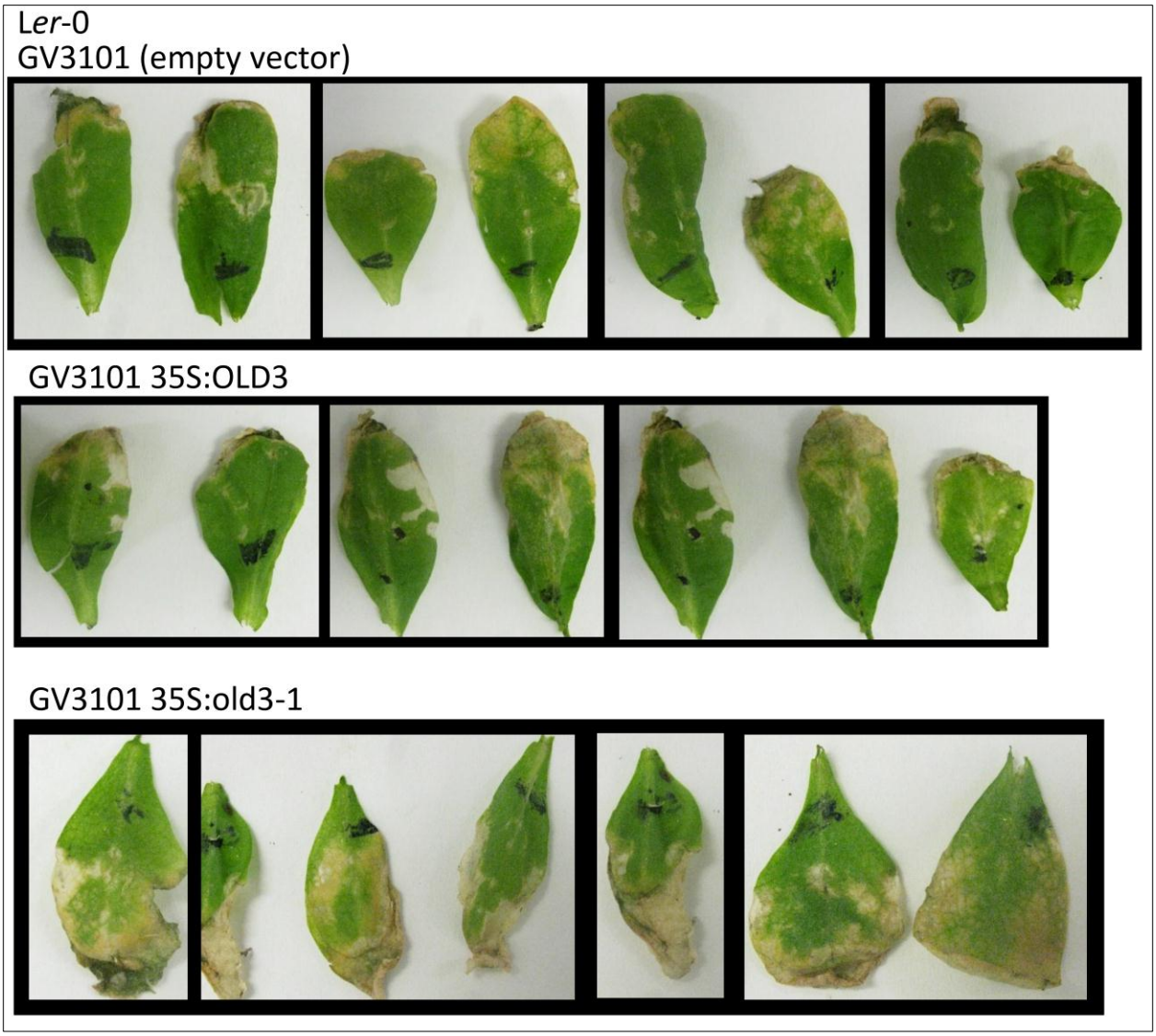

Appendix 18. Effects of *Agrobacterium* infection in leaves of L*er*-0, Col-0 and *old3-2 odd-ler* lines. Phenotypes in *Arabidopsis* plant lines, L*er*-0, Col-0 and *old3-2 odd-ler* lines -34 and -80, against infection with *Agrobactierum GV3101, Agrobactierum GV3101* carrying pGreen 0229 35s:OASTL-A1/OLD3 and *Agrobactierum GV3101* carrying pGreen 0229 35s:old3-1. Syringe inoculation of 1 x 10^4 cfu/mL was performed on plants grown for 4-6 weeks under long days (16 hr day/8 hr night; 21 °C/21 °C). Mock inoculated leaves (10 mM MgCl2) showed absence of any visible lesions and are not shown here. Leaf tissues were photographed 4 days post-infection.

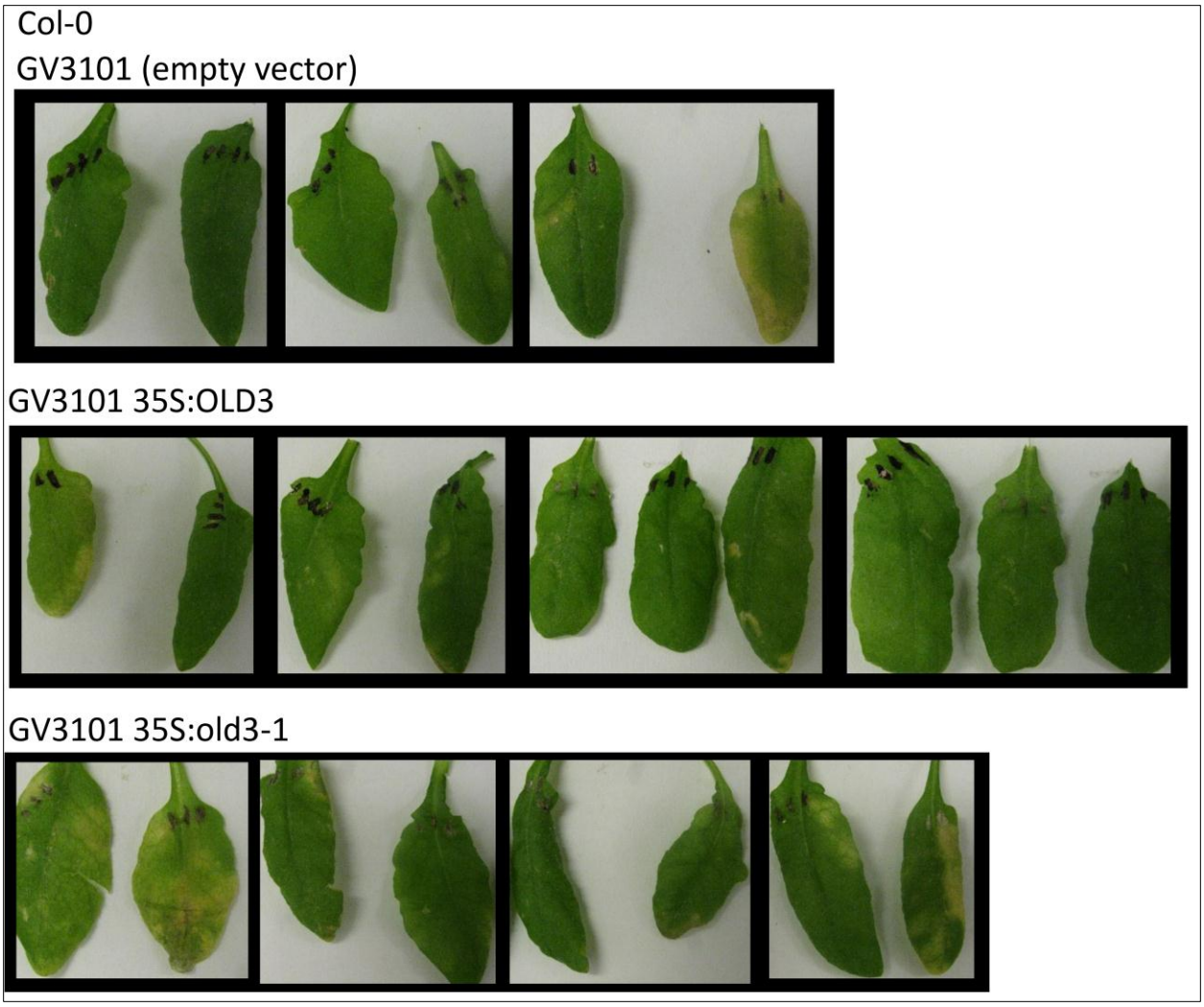

Appendix 18 *contd*. Effects of *Agrobacterium* infection in leaves of L*er*-0, Col-0 and *old3-2 odd-ler* lines.

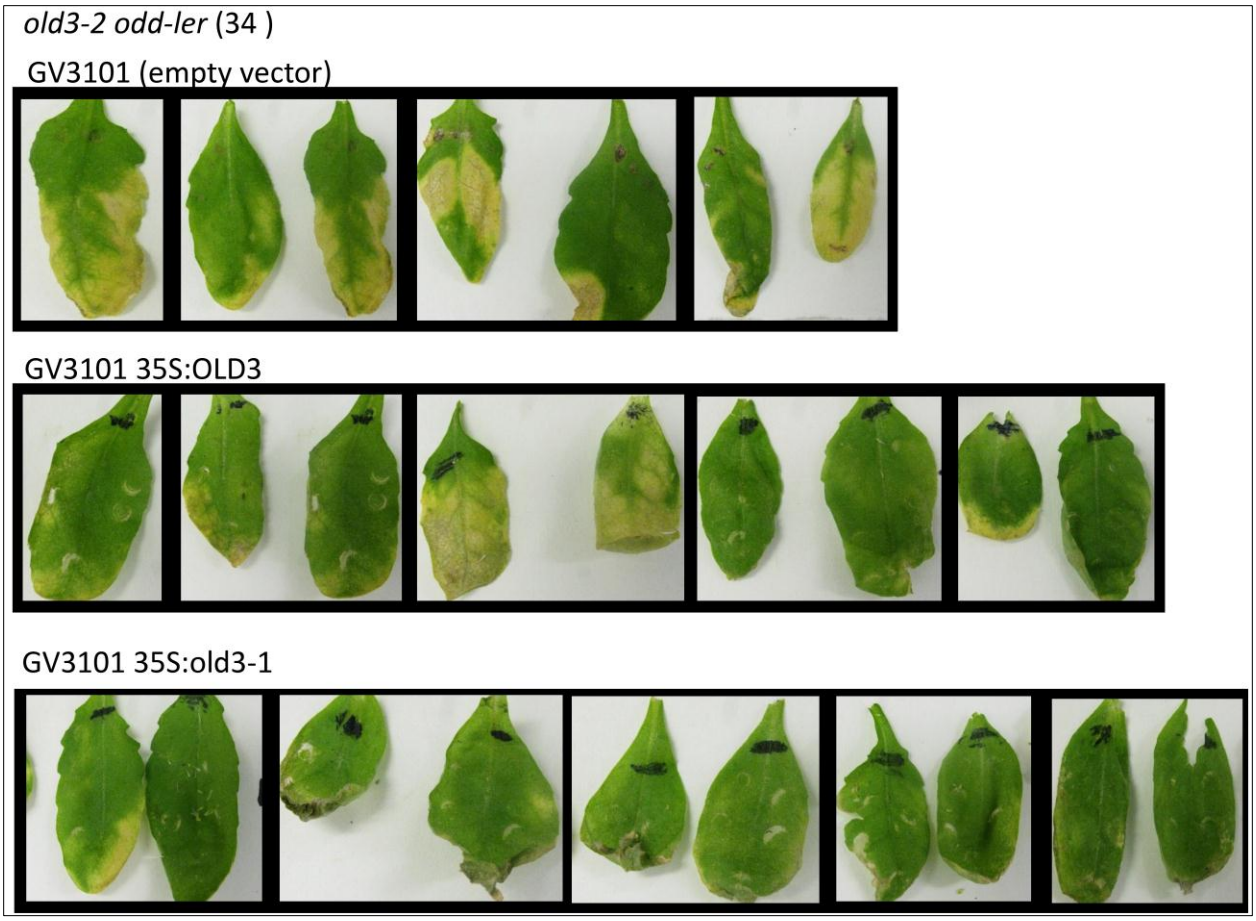

Appendix 18 *contd*. Effects of *Agrobacterium* infection in leaves of L*er*-0, Col-0 and *old3-2 odd-ler* lines.

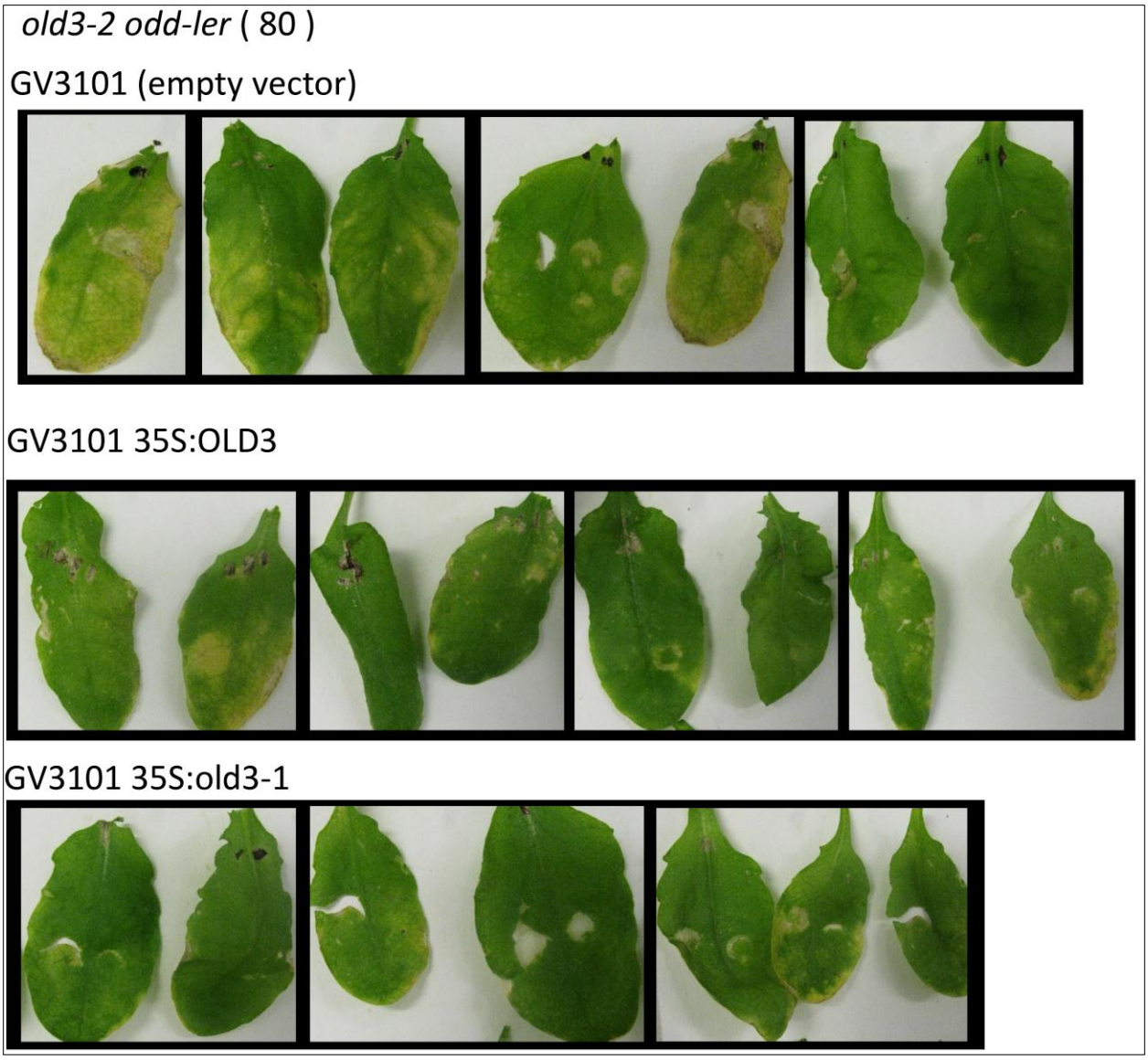

Appendix 18 *contd*. Effects of *Agrobacterium* infection in leaves of L*er*-0, Col-0 and *old3-2 odd-ler* lines.

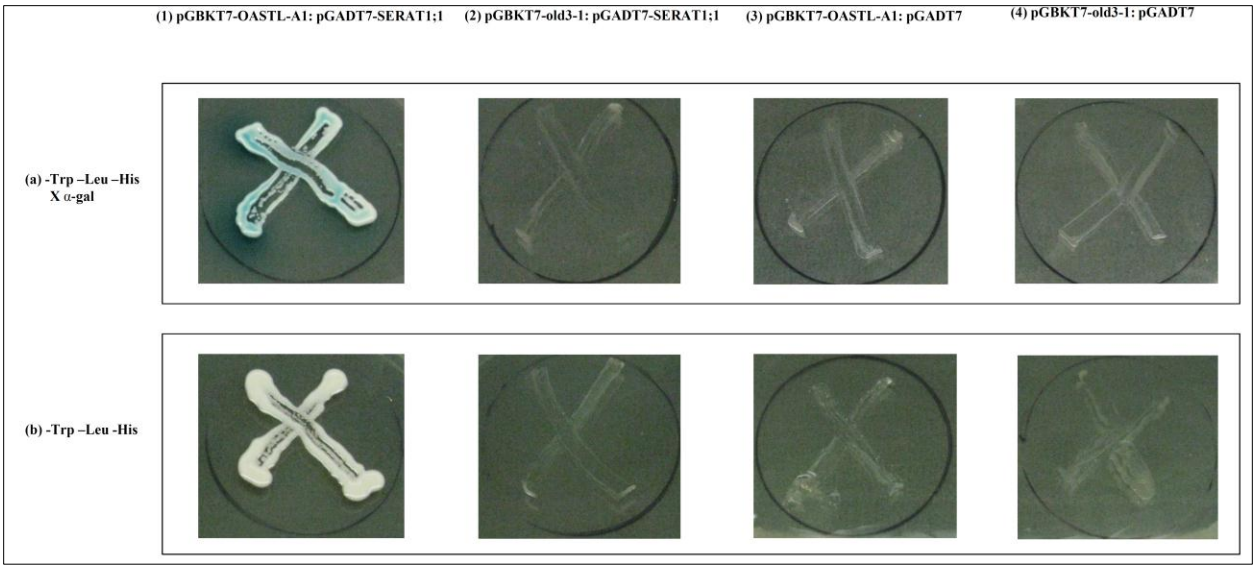

Appendix 19. Analysis of protein-protein interaction of cytosolic SERAT1;1 with OASTL-A1 and old3-1 in yeast. Figure show Yeast-2-hybrid test for protein-protein interaction between old3-1 and OASTL-A1/OLD3 and cytosolic SERAT1;1/SAT5. AH109 yeast strains carrying the old3-1 or OASTL cDNA fused with GAL4 binding domain in the bait vector pGBKT7 were transformed with the prey vector pGADT7 containing SERAT1;1/SAT5 cDNA fused with the GAL4 activation domain or empty pGADT7 vector, as a control. After transformation and selection at the basic SD mediums -Trp –Leu, colonies were streaked in a) -Leu -Trp -His X α-gal and b) -Leu -Trp -His, plates to see the activation of reporter gene. Development of blue colour and growth in plates in a) and growth in b) are indicator of positive for protein-protein interaction. To test the test reporter activity, cross streaked plates were kept at 30 °C for six days and afterwards at room temperatures for 5 days and then photographed.

Bibliography

Alcazar, R., Garcia, A.V., Kronholm, I., de Meaux, J., Koornneef, M., Parker, J.E., and Reymond, M. (2010a). Natural variation at Strubbelig Receptor Kinase 3 drives immune-triggered incompatibilities between Arabidopsis thaliana accessions. Nat. Genet. **42,** 1135-1139.

Alcazar, R., Altabella, T., Marco, F., Bortolotti, C., Reymond, M., Koncz, C., Carrasco, P., and Tiburcio, A. (2010b). Polyamines: molecules with regulatory functions in plant abiotic stress tolerance. Planta **231,** 1237-1249.

Alcázar, R., García, A.V., Parker, J.E., and Reymond, M. (2009). Incremental steps toward incompatibility revealed by Arabidopsis epistatic interactions modulating salicylic acid pathway activation. Proc. Natl. Acad. Sci. U. S. A. **106,** 334-339.

Alvarez, C., García, I., Romero, L.C., and Gotor, C. (2012a). Mitochondrial Sulfide Detoxification Requires a Functional Isoform O-Acetylserine(thiol)lyase C in Arabidopsis thaliana. Mol. Plant.

Alvarez, C., Calo, L., Romero, L.C., Garcia, I., and Gotor, C. (2010). An O-acetylserine(thiol)lyase homolog with L-cysteine desulfhydrase activity regulates cysteine homeostasis in Arabidopsis. Plant Physiol **152,** 656-669.

Alvarez, C., Bermudez, M.A., Romero, L.C., Gotor, C., and Garcia, I. (2012b). Cysteine homeostasis plays an essential role in plant immunity. New Phytol. **193,** 165-177.

Alvarez, C., Lozano-Juste, J., Romero, L.C., Garcia, I., Gotor, C., and Leon, J. (2011). Inhibition of Arabidopsis O-Acetylserine(thiol)lyase A1 by Tyrosine Nitration. J. Biol. Chem. **286,** 578-586.

Anderson, M.E. (1985). Determination of glutathione and glutathione disulfide in biological samples. Methods Enzymol. **113,** 548.

Aravind, L., and Koonin, E.V. (2000). The STAS domain - a link between anion transporters and antisigma-factor antagonists. Curr. Biol. **10,** R53-R55.

Arvidsson, S., Kwasniewski, M., Riaño-Pachón, D.M., and Mueller-Roeber, B. (2008). QuantPrime–a flexible tool for reliable high-throughput primer design for quantitative PCR. BMC Bioinformatics **9,** 465.

Ausubel, F.M. (2005). Are innate immune signaling pathways in plants and animals conserved? Nat. Immunol. **6,** 973-979.

Avonce, N., Leyman, B., Mascorro-Gallardo, J.O., Van Dijck, P., Thevelein, J.M., and Iturriaga, G. (2004). The Arabidopsis Trehalose-6-P Synthase AtTPS1 Gene Is a Regulator of Glucose, Abscisic Acid, and Stress Signaling. Plant Physiol. **136,** 3649-3659.

Balk, J., and Pilon, M. (2011). Ancient and essential: the assembly of iron–sulfur clusters in plants. Trends Plant Sci. **16,** 218-226.

Ball, L., Accotto, G.-P., Bechtold, U., Creissen, G., Funck, D., Jimenez, A., Kular, B., Leyland, N., Mejia-Carranza, J., Reynolds, H., Karpinski, S., and Mullineaux, P.M. (2004). Evidence for a Direct Link between Glutathione Biosynthesis and Stress Defense Gene Expression in Arabidopsis. Plant Cell **16,** 2448-2462.

Barberon, M., Berthomieu, P., Clairotte, M., Shibagaki, N., Davidian, J.C., and Gosti, F. (2008). Unequal functional redundancy between the two Arabidopsis thaliana high-affinity sulphate transporters SULTR1;1 and SULTR1;2. New Phytol. **180,** 608-619.

Barroso, C., Romero, L., Cejudo, F., Vega, J., and Gotor, C. (1999). Salt-specific regulation of the cytosolic O-acetylserine(thiol)lyase gene from Arabidopsis thaliana is dependent on abscisic acid. Plant Mol. Biol. **40,** 729-736.

Baxter, L., Tripathy, S., Ishaque, N., Boot, N., Cabral, A., Kemen, E., Thines, M., Ah-Fong, A., Anderson, R., Badejoko, W., Bittner-Eddy, P., Boore, J.L., Chibucos, M.C., Coates, M., Dehal, P., Delehaunty, K., Dong, S., Downton, P., Dumas, B., Fabro, G., Fronick, C., Fuerstenberg, S.I., Fulton, L., Gaulin, E., Govers, F., Hughes, L., Humphray, S., Jiang, R.H.Y., Judelson, H., Kamoun, S., Kyung, K., Meijer, H., Minx, P., Morris, P., Nelson, J., Phuntumart, V., Qutob, D., Rehmany, A., Rougon-Cardoso, A., Ryden, P., Torto-Alalibo, T., Studholme, D., Wang, Y., Win, J., Wood, J., Clifton, S.W., Rogers, J., Van den Ackerveken, G., Jones, J.D.G., McDowell, J.M., Beynon, J., and Tyler, B.M. (2010). Signatures of Adaptation to Obligate Biotrophy in the Hyaloperonospora arabidopsidis Genome. Science **330,** 1549-1551.

Becker, T., Loch, G., Beyer, M., Zinke, I., Aschenbrenner, A.C., Carrera, P., Inhester, T., Schultze, J.L., and Hoch, M. (2010). FOXO-dependent regulation of innate immune homeostasis. Nature **463,** 369-373.

Bednarek, P., Pislewska-Bednarek, M., Svatos, A., Schneider, B., Doubsky, J., Mansurova, M., Humphry, M., Consonni, C., Panstruga, R., Sanchez-Vallet, A., Molina, A., and Schulze-Lefert, P. (2009). A glucosinolate metabolism pathway in living plant cells mediates broad-spectrum antifungal defense. Science **323,** 101-106.

Beekwilder, J., van Leeuwen, W., van Dam, N.M., Bertossi, M., Grandi, V., Mizzi, L., Soloviev, M., Szabados, L., Molthoff, J.W., Schipper, B., Verbocht, H., de Vos, R.C.H., Morandini, P., Aarts, M.G.M., and Bovy, A. (2008). The Impact of the Absence of Aliphatic Glucosinolates on Insect Herbivory in Arabidopsis. PLoS One **3,** e2068.

Belkhadir, Y., Nimchuk, Z., Hubert, D.A., Mackey, D., and Dangl, J.L. (2004). Arabidopsis RIN4 Negatively Regulates Disease Resistance Mediated by RPS2 and RPM1 Downstream or Independent of the NDR1 Signal Modulator and Is Not Required for the Virulence Functions of Bacterial Type III Effectors AvrRpt2 or AvrRpm1. Plant Cell **16,** 2822-2835.

Berkowitz, O., Wirtz, M., Wolf, A., Kuhlmann, J., and Hell, R. (2002). Use of biomolecular interaction analysis to elucidate the regulatory mechanism of the cysteine synthase complex from Arabidopsis thaliana. J. Biol. Chem. **277,** 30629-30634.

Bermúdez, M.A., Páez-Ochoa, M.A., Gotor, C., and Romero, L.C. (2010a). *Arabidopsis* S-sulfocysteine synthase activity is essential for chloroplast function and long-day light-dependent redox control. The Plant Cell Online **22,** 403-416.

Bermúdez, M.A., Páez-Ochoa, M.A., Gotor, C., and Romero, L.C. (2010b). Arabidopsis S-Sulfocysteine Synthase Activity Is Essential for Chloroplast Function and Long-Day Light-Dependent Redox Control. Plant Cell **22,** 403-416.

Bernoux, M., Ellis, J.G., and Dodds, P.N. (2011). New insights in plant immunity signaling activation. Curr. Opin. Plant Biol. **14,** 512-518.

Bernoux, M., Timmers, T., Jauneau, A., Brière, C., de Wit, P.J.G.M., Marco, Y., and Deslandes, L. (2008). RD19, an Arabidopsis Cysteine Protease Required for RRS1-R–Mediated Resistance, Is Relocalized to the Nucleus by the Ralstonia solanacearum PopP2 Effector. Plant Cell **20,** 2252-2264.

Bikard, D., Patel, D., Le Mette, C., Giorgi, V., Camilleri, C., Bennett, M.J., and Loudet, O. (2009). Divergent Evolution of Duplicate Genes Leads to Genetic Incompatibilities Within A-thaliana. Science **323,** 623-626.

Birke, H., Haas, F.H., De Kok, L.J., Balk, J., Wirtz, M., and Hell, R. (2012). Cysteine biosynthesis, in concert with a novel mechanism, contributes to sulfide detoxification in mitochondria of Arabidopsis thaliana. Biochem. J. **445,** 275-283.

Blanco, F., Salinas, P., Cecchini, N., Jordana, X., Hummelen, P., Alvarez, M., and Holuigue, L. (2009). Early genomic responses to salicylic acid in Arabidopsis. Plant Mol. Biol. **70,** 79-102.

Bleecker, A.B., and Kende, H. (2000). Ethylene: a gaseous signal molecule in plants. Annu. Rev. Cell Dev. Biol. **16,** 1-18.

Bloem, E., Haneklaus, S., Salac, I., Wickenhäuser, P., and Schnug, E. (2007). Facts and Fiction about Sulfur Metabolism in Relation to Plant-Pathogen Interactions. Plant Biol. **9,** 596-607.

Bogdanova, N., and Hell, R. (1997). Cysteine synthesis in plants: protein-protein interactions of serine acetyltransferase from Arabidopsis thaliana. Plant J. **11,** 251-262.

Bolton, M.D. (2009). Primary Metabolism and Plant Defense—Fuel for the Fire. Mol. Plant-Microbe Interact. **22,** 487-497.

Bomblies, K., Lempe, J., Epple, P., Warthmann, N., Lanz, C., Dangl, J.L., and Weigel, D. (2007). Autoimmune response as a mechanism for a Dobzhansky-Muller-type incompatibility syndrome in plants. PLoS Biol. **5,** 1962-1972.

Bonner, E.R., Cahoon, R.E., Knapke, S.M., and Jez, J.M. (2005). Molecular basis of cysteine biosynthesis in plants: structural and functional analysis of O-acetylserine sulfhydrylase from Arabidopsis thaliana. J. Biol. Chem. **280,** 38803-38813.

Bordenstein, S.R., and Drapeau, M.D. (2001). Genotype-by-environment interaction and the Dobzhansky–Muller model of postzygotic isolation. J. Evol. Biol. **14,** 490-501.

Botella, M.A., Parker, J.E., Frost, L.N., Bittner-Eddy, P.D., Beynon, J.L., Daniels, M.J., Holub, E.B., and Jones, J.D.G. (1998). Three Genes of the Arabidopsis RPP1 Complex Resistance Locus Recognize Distinct Peronospora parasitica Avirulence Determinants. Plant Cell **10,** 1847-1860.

Bottcher, C., Westphal, L., Schmotz, C., Prade, E., Scheel, D., and Glawischnig, E. (2009). The multifunctional enzyme CYP71B15 (PHYTOALEXIN DEFICIENT3) converts cysteine-indole-3-acetonitrile to camalexin in the indole-3-acetonitrile metabolic network of Arabidopsis thaliana. Plant Cell **21,** 1830-1845.

Bruinsma, J. (1961). A comment on the spectrophotometric determination of chlorophyll. Biochim. Biophys. Acta **52,** 576.

Buchner, P., Takahashi, H., and Hawkesford, M.J. (2004). Plant sulphate transporters: co-ordination of uptake, intracellular and long-distance transport. J. Exp. Bot. **55,** 1765-1773.

Cairns, N.G., Pasternak, M., Wachter, A., Cobbett, C.S., and Meyer, A.J. (2006). Maturation of Arabidopsis seeds is dependent on glutathione biosynthesis within the embryo. Plant Physiol. **141,** 446-455.

Campanini, B., Speroni, F., Salsi, E., Cook, P.F., Roderick, S.L., Huang, B., Bettati, S., and Mozzarelli, A. (2005). Interaction of serine acetyltransferase with O-acetylserine sulfhydrylase active site: evidence from fluorescence spectroscopy. Protein Sci. **14,** 2115-2124.

Cañas, C.A., and Cañas, F. (2012). The Biological Significance of Evolution in Autoimmune Phenomena. Autoimmune Diseases **2012,** 12.

Candore, G., Lio, D., Colonna Romano, G., and Caruso, C. (2002). Pathogenesis of autoimmune diseases associated with 8.1 ancestral haplotype: effect of multiple gene interactions. Autoimmun. Rev. **1,** 29-35.

Cao, M.-J., Wang, Z., Wirtz, M., Hell, R., Oliver, D.J., and Xiang, C.-B. (2012). SULTR3;1 is a chloroplast-localized sulfate transporter in Arabidopsis thaliana. Plant J.**,** 10.1111/tpj.12059.

Cazale, A.C., and Clemens, S. (2001). Arabidopsis thaliana expresses a second functional phytochelatin synthase. FEBS Lett. **507,** 215-219.

Chaouch, S., Queval, G., Vanderauwera, S., Mhamdi, A., Vandorpe, M., Langlois-Meurinne, M., Van Breusegem, F., Saindrenan, P., and Noctor, G. (2010). Peroxisomal Hydrogen Peroxide Is Coupled to Biotic Defense Responses by ISOCHORISMATE SYNTHASE1 in a Daylength-Related Manner. Plant Physiol. **153,** 1692-1705.

Chattopadhyay, A., Meier, M., Ivaninskii, S., Burkhard, P., Speroni, F., Campanini, B., Bettati, S., Mozzarelli, A., Rabeh, W.M., Li, L., and Cook, P.F. (2007). Structure, mechanism, and conformational dynamics of O-acetylserine sulfhydrylase from Salmonella typhimurium: comparison of A and B isozymes. Biochemistry **46,** 8315-8330.

Chen, H.C., Yokthongwattana, K., Newton, A.J., and Melis, A. (2003). SulP, a nuclear gene encoding a putative chloroplast-targeted sulfate permease in Chlamydomonas reinhardtii. Planta **218,** 98-106.

Chen, J., Wu, F.H., Wang, W.H., Zheng, C.J., Lin, G.H., Dong, X.J., He, J.X., Pei, Z.M., and Zheng, H.L. (2011). Hydrogen sulphide enhances photosynthesis through promoting chloroplast biogenesis, photosynthetic enzyme expression, and thiol redox modification in Spinacia oleracea seedlings. J. Exp. Bot. **62,** 4481-4493.

Chiu, J., March, P.E., Lee, R., and Tillett, D. (2004). Site-directed, Ligase-Independent Mutagenesis (SLIM): a single-tube methodology approaching 100% efficiency in 4 h. Nucleic Acids Res. **32,** e174.

Chung, E.-H., da Cunha, L., Wu, A.-J., Gao, Z., Cherkis, K., Afzal, A.J., Mackey, D., and Dangl, J.L. (2011). Specific Threonine Phosphorylation of a Host Target by Two Unrelated Type III Effectors Activates a Host Innate Immune Receptor in Plants. Cell Host Microbe **9,** 125-136.

Clarkson, D.T., Saker, L.R., and Purves, J.V. (1989). Depression of Nitrate and Ammonium Transport in Barley Plants with Diminished Sulfate Status - Evidence of Co-Regulation of Nitrogen and Sulfate Intake. J. Exp. Bot. **40,** 953-963.

Clay, N.K., Adio, A.M., Denoux, C., Jander, G., and Ausubel, F.M. (2009). Glucosinolate Metabolites Required for an Arabidopsis Innate Immune Response. Science **323,** 95-101.

Coates, M.E., and Beynon, J.L. (2010). Hyaloperonospora arabidopsidis as a Pathogen Model. Annu. Rev. Phytopathol. **48,** 329-345.

Cobbett, C., and Goldsbrough, P. (2002). Phytochelatins and metallothioneins: Roles in heavy metal detoxification and homeostasis. Annu. Rev. Plant Biol. **53,** 159-182.

Cobbett, C.S., May, M.J., Howden, R., and Rolls, B. (1998). The glutathione-deficient, cadmium-sensitive mutant, cad2-1, of Arabidopsis thaliana is deficient in gamma-glutamylcysteine synthetase. Plant J. **16,** 73-78.

Collins, R.M., Afzal, M., Ward, D.A., Prescott, M.C., Sait, S.M., Rees, H.H., and Tomsett, A.B. (2010). Differential Proteomic Analysis of <italic>Arabidopsis thaliana</italic> Genotypes Exhibiting Resistance or Susceptibility to the Insect Herbivore, <italic>Plutella xylostella</italic>. PLoS One **5,** e10103.

Cooper, A.J. (1983). Biochemistry of sulfur-containing amino acids. Annu. Rev. Biochem. **52,** 187-222.

Cooper, C., and Brown, G. (2008). The inhibition of mitochondrial cytochrome oxidase by the gases carbon monoxide, nitric oxide, hydrogen cyanide and hydrogen sulfide: chemical mechanism and physiological significance. J. Bioenerg. Biomembr. **40,** 533-539.

Coyne, J.A., and Orr, H.A. (2004). Speciation. (Sinauer Associates).

Dan, H., Yang, G., and Zheng, Z.-L. (2007). A negative regulatory role for auxin in sulphate deficiency response in Arabidopsis thaliana. Plant Mol. Biol. **63,** 221-235.

Dangl, J.L., and Jones, J.D. (2001). Plant pathogens and integrated defence responses to infection. Nature **411,** 826-833.

Dardick, C., and Ronald, P. (2006). Plant and animal pathogen recognition receptors signal through non-RD kinases. PLoS Pathog. **2,** 14-28.

Darling, A.E., Mau, B., and Perna, N.T. (2010). *progressiveMauve*: multiple genome alignment with gene gain, loss and rearrangement. PloS One **5,** e11147.

Daum, S., Tai, C.-H., and Cook, P.F. (2002). Characterization of the S272A,D Site-Directed Mutations of O-Acetylserine Sulfhydrylase: Involvement of the Pyridine Ring in the α,β-Elimination Reaction†. Biochemistry **42,** 106-113.

Dellaporta, S., Wood, J., and Hicks, J. (1983). A plant DNA minipreparation: Version II. Plant Mol. Biol. Report. **1,** 19-21.

Diner, E.J., Beck, C.M., Webb, J.S., Low, D.A., and Hayes, C.S. (2012). Identification of a target cell permissive factor required for contact-dependent growth inhibition (CDI). Genes Dev. **26,** 515-525.

Dodds, P.N., and Rathjen, J.P. (2010). Plant immunity: towards an integrated view of plant-pathogen interactions. Nat. Rev. Genet. **11,** 539-548.

Dominguez-Solis, J.R., Lopez-Martin, M.C., Ager, F.J., Ynsa, M.D., Romero, L.C., and Gotor, C. (2004). Increased cysteine availability is essential for cadmium tolerance and accumulation in Arabidopsis thaliana. Plant Biotechnol. J. **2,** 469-476.

Domínguez-Solís, J.R., Gutiérrez-Alcalá, G., Romero, L.C., and Gotor, C. (2001). The Cytosolic O-Acetylserine(thiol)lyase Gene Is Regulated by Heavy Metals and Can Function in Cadmium Tolerance. J. Biol. Chem. **276,** 9297-9302.

Donahue, J.L., Alford, S.R., Torabinejad, J., Kerwin, R.E., Nourbakhsh, A., Ray, W.K., Hernick, M., Huang, X., Lyons, B.M., Hein, P.P., and Gillaspy, G.E. (2010). The Arabidopsis thaliana Myo-Inositol 1-Phosphate Synthase1 Gene Is Required for Myo-inositol Synthesis and Suppression of Cell Death. Plant Cell **22,** 888-903.

Droge, W. (2005). Oxidative stress and ageing: is ageing a cysteine deficiency syndrome? Philos. Trans. R. Soc. Lond. B Biol. Sci. **360,** 2355-2372.

Droux, M., Ruffet, M.-L., Douce, R., and Job, D. (1998). Interactions between serine acetyltransferase and O-acetylserine (thiol) lyase in higher plants. Eur. J. Biochem. **255,** 235-245.

Drummond, A.J., Ashton, B., Buxton, S., Cheung, M., Cooper, A., Duran, C., Field, M., Heled, J., Kearse, M., Markowitz, S., Moir, R., Stones-Havas, S., Sturrock, S., Thierer, T., and Wilson, A. (2011). Geneious v5.4, . Available from http://www.geneious.com/.

Dubery, I., Sanabria, N., and Huang, J.-C. (2012). Nonself Perception in Plant Innate Immunity. In Self and Nonself, C. López-Larrea, ed (Springer US), pp. 79-107.

El Kassis, E., Cathala, N., Rouached, H., Fourcroy, P., Berthomieu, P., Terry, N., and Davidian, J.-C. (2007). Characterization of a Selenate-Resistant Arabidopsis Mutant. Root Growth as a Potential Target for Selenate Toxicity. Plant Physiol. **143,** 1231-1241.

Eulgem, T., and Somssich, I.E. (2007). Networks of WRKY transcription factors in defense signaling. Curr. Opin. Plant Biol. **10,** 366-371.

Fahey, R.C., and Newton, G.L. (1987). Determination of low-molecular-weight thiols using monobromobimane fluorescent labeling and high-performance liquid chromatography. Methods Enzymol. **143,** 85-96.

Fediuc, E., Lips, S.H., and Erdei, L. (2005). O-acetylserine (thiol) lyase activity in Phragmites and Typha plants under cadmium and NaCl stress conditions and the involvement of ABA in the stress response. J. Plant Physiol. **162,** 865-872.

Feldman-Salit, A., Wirtz, M., Hell, R., and Wade, R.C. (2009). A mechanistic model of the cysteine synthase complex. J. Mol. Biol. **386,** 37-59.

Feldman-Salit, A., Wirtz, M., Lenherr, E.D., Throm, C., Hothorn, M., Scheffzek, K., Hell, R., and Wade, R.C. (2012). Allosterically gated enzyme dynamics in the cysteine synthase complex regulate cysteine biosynthesis in Arabidopsis thaliana. Structure **20,** 292-302.

Fernie, A.R., Aharoni, A., Willmitzer, L., Stitt, M., Tohge, T., Kopka, J., Carroll, A.J., Saito, K., Fraser, P.D., and DeLuca, V. (2011). Recommendations for reporting metabolite data. Plant Cell **23,** 2477-2482.

Feys, B.J., Moisan, L.J., Newman, M.-A., and Parker, J.E. (2001). Direct interaction between the Arabidopsis disease resistance signaling proteins, EDS1 and PAD4. EMBO J **20,** 5400-5411.

Fitzpatrick, K.L., Tyerman, S.D., and Kaiser, B.N. (2008). Molybdate transport through the plant sulfate transporter SHST1. FEBS Lett. **582,** 1508-1513.

Foyer, C.H., and Noctor, G. (2003). Redox sensing and signalling associated with reactive oxygen in chloroplasts, peroxisomes and mitochondria. Physiol. Plant **119,** 355-364.

Foyer, C.H., and Noctor, G. (2005). Redox Homeostasis and Antioxidant Signaling: A Metabolic Interface between Stress Perception and Physiological Responses. Plant Cell **17,** 1866-1875.

Francois, J.A., Kumaran, S., and Jez, J.M. (2006). Structural basis for interaction of O-acetylserine sulfhydrylase and serine acetyltransferase in the Arabidopsis cysteine synthase complex. Plant Cell **18,** 3647-3655.

Freeman, J.L., Garcia, D., Kim, D., Hopf, A., and Salt, D.E. (2005). Constitutively Elevated Salicylic Acid Signals Glutathione-Mediated Nickel Tolerance in Thlaspi Nickel Hyperaccumulators. Plant Physiol. **137,** 1082-1091.

Freeman, J.L., Persans, M.W., Nieman, K., Albrecht, C., Peer, W., Pickering, I.J., and Salt, D.E. (2004). Increased glutathione biosynthesis plays a role in nickel tolerance in thlaspi nickel hyperaccumulators. Plant Cell **16,** 2176-2191.

Gaitonde, M. (1967). A spectrophotometric method for the direct determination of cysteine in the presence of other naturally occurring amino acids. Biochem. J. **104,** 627.

García, I., Castellano, J.M., Vioque, B., Solano, R., Gotor, C., and Romero, L.C. (2010). Mitochondrial β-Cyanoalanine Synthase Is Essential for Root Hair Formation in Arabidopsis thaliana. Plant Cell **22,** 3268-3279.

Garrido-Franco, M., Ehlert, S., Messerschmidt, A., Marinković, S., Huber, R., Laber, B., Bourenkov, G.P., and Clausen, T. (2002). Structure and Function of Threonine Synthase from Yeast. J. Biol. Chem. **277,** 12396-12405.

Ghezzi, P. (2011). Role of glutathione in immunity and inflammation in the lung. Int J Gen Med **4,** 105-113.

Gill, S.S., and Tuteja, N. (2010). Reactive oxygen species and antioxidant machinery in abiotic stress tolerance in crop plants. Plant Physiol. Biochem. **48,** 909-930.

Gleave, A. (1992). A versatile binary vector system with a T-DNA organisational structure conducive to efficient integration of cloned DNA into the plant genome. Plant Mol. Biol. **20,** 1203-1207.

Glowacki, S., Macioszek, V.K., and Kononowicz, A.K. (2011). R Proteins as Fundamentals of Plant Innate Immunity. Cell. Mol. Biol. Lett. **16,** 1-24.

Grossman, A., and Takahashi, H. (2001). Macronutrient Utilization by Photosynthetic Eukaryotes and the Fabric of Interactions. Annu. Rev. Plant Physiol. Plant Mol. Biol. **52,** 163-210.

Gullner, G., Komives, T., and Rennenberg, H. (2001). Enhanced tolerance of transgenic poplar plants overexpressing gamma-glutamylcysteine synthetase towards chloroacetanilide herbicides. J. Exp. Bot. **52,** 971-979.

Ha, S.B., Smith, A.P., Howden, R., Dietrich, W.M., Bugg, S., O'Connell, M.J., Goldsbrough, P.B., and Cobbett, C.S. (1999). Phytochelatin synthase genes from Arabidopsis and the yeast Schizosaccharomyces pombe. Plant Cell **11,** 1153-1164.

Haas, F.H., Heeg, C., Queiroz, R., Bauer, A., Wirtz, M., and Hell, R. (2008). Mitochondrial Serine Acetyltransferase Functions as a Pacemaker of Cysteine Synthesis in Plant Cells. Plant Physiol. **148,** 1055-1067.

Halkier, B.A., and Gershenzon, J. (2006). BIOLOGY AND BIOCHEMISTRY OF GLUCOSINOLATES. Annu. Rev. Plant Biol. **57,** 303-333.

Harada, E., Kusano, T., and Sano, H. (2000). Differential expression of genes encoding enzymes involved in sulfur assimilation pathways in response to wounding and jasmonate in Arabidopsis thaliana. J. Plant Physiol. **156,** 272-276.

Hatzfeld, Y., Lee, S., Lee, M., Leustek, T., and Saito, K. (2000a). Functional characterization of a gene encoding a fourth ATP sulfurylase isoform from Arabidopsis thaliana. Gene **248,** 51-58.

Hatzfeld, Y., Maruyama, A., Schmidt, A., Noji, M., Ishizawa, K., and Saito, K. (2000b). beta-Cyanoalanine synthase is a mitochondrial cysteine synthase-like protein in spinach and Arabidopsis. Plant Physiol **123,** 1163-1171.

Hawkesford, M.J. (2003). Transporter gene families in plants: the sulphate transporter gene family — redundancy or specialization? Physiol. Plant **117,** 155-163.

Hay, I.D., Rehman, Z.U., and Rehm, B.H.A. (2010). Membrane Topology of Outer Membrane Protein AlgE, Which Is Required for Alginate Production in Pseudomonas aeruginosa. Appl. Environ. Microbiol. **76,** 1806-1812.

Heeg, C., Kruse, C., Jost, R., Gutensohn, M., Ruppert, T., Wirtz, M., and Hell, R. (2008). Analysis of the Arabidopsis O-acetylserine(thiol)lyase gene family demonstrates compartment-specific differences in the regulation of cysteine synthesis. Plant Cell **20,** 168-185.

Heidrich, K., Wirthmueller, L., Tasset, C., Pouzet, C., Deslandes, L., and Parker, J.E. (2011). Arabidopsis EDS1 connects pathogen effector recognition to cell compartment-specific immune responses. Science **334,** 1401-1404.

Hell, R., and Bergmann, L. (1990). Gamma-Glutamylcysteine Synthetase in Higher-Plants - Catalytic Properties and Subcellular-Localization. Planta **180,** 603-612.

Hell, R., and Wirtz, M. (2008). Metabolism of Cysteine in Plants and Phototrophic Bacteria. In Sulfur Metabolism in Phototrophic Organisms, R. Hell, C. Dahl, D. Knaff, and T. Leustek, eds (Springer Netherlands), pp. 59-91.

Hell, R., and Wirtz, M. (2011). Molecular Biology, Biochemistry and Cellular Physiology of Cysteine Metabolism in Arabidopsis thaliana. Arabidopsis Book **9,** e0154.

Hell, R., Jost, R., Berkowitz, O., and Wirtz, M. (2002). Molecular and biochemical analysis of the enzymes of cysteine biosynthesis in the plant Arabidopsis thaliana. Amino Acids **22,** 245-257.

Hellens, R.P., Edwards, E.A., Leyland, N.R., Bean, S., and Mullineaux, P.M. (2000). pGreen: a versatile and flexible binary Ti vector for Agrobacterium-mediated plant transformation. Plant Mol. Biol. **42,** 819-832.

Hendriks, J.H.M., Kolbe, A., Gibon, Y., Stitt, M., and Geigenberger, P. (2003). ADP-glucose pyrophosphorylase is activated by posttranslational redox-modification in response to light and to sugars in leaves of *Arabidopsis* and other plant species. Plant Physiol. **133,** 838-849.

Hernàndez-Sebastiá, C., Varin, L., and Marsolais, F. (2008). Sulfotransferases from Plants, Algae and Phototrophic Bacteria. In Sulfur Metabolism in Phototrophic Organisms, R. Hell, C. Dahl, D. Knaff, and T. Leustek, eds (Springer Netherlands), pp. 111-130.

Howarth, J.R., Fourcroy, P., Davidian, J.C., Smith, F.W., and Hawkesford, M.J. (2003). Cloning of two contrasting high-affinity sulfate transporters from tomato induced by low sulfate and infection by the vascular pathogen Verticillium dahliae. Planta **218,** 58-64.

Hruz, T., Laule, O., Szabo, G., Wessendorp, F., Bleuler, S., Oertle, L., Widmayer, P., Gruissem, W., and Zimmermann, P. (2008). Genevestigator v3: a reference expression database for the meta-analysis of transcriptomes. Adv Bioinformatics **2008,** 420747.

Hunter, D.A., Pinkney, T.T., Watson, L.M., Trivellini, A., Janssen, B.J., Brummell, D.A., and Heyes, J.A. (2011). Effect of postharvest water deficit stress on gene expression in heads of broccoli (*Brassica oleracea* var. *italica*). Postharvest Biol. Technol. **59,** 113-123.

Hwang, C.S., Shemorry, A., and Varshavsky, A. (2010). N-terminal acetylation of cellular proteins creates specific degradation signals. Science **327,** 973-977.

Hyde, C.C., Ahmed, S.A., Padlan, E.A., Miles, E.W., and Davies, D.R. (1988). Three-dimensional structure of the tryptophan synthase alpha 2 beta 2 multienzyme complex from Salmonella typhimurium. J. Biol. Chem. **263,** 17857-17871.

Inoue, H., Nojima, H., and Okayama, H. (1990). High efficiency transformation of Escherichia coli with plasmids. Gene **96,** 23-28.

Jang, E.-K., Min, K.-H., Kim, S.-H., Nam, S.-H., Zhang, S., Kim, Y.C., Cho, B.H., and Yang, K.-Y. (2009). Mitogen-Activated Protein Kinase Cascade in the Signaling for Polyamine Biosynthesis in Tobacco. Plant Cell Physiol. **50,** 658-664.

Jeuken, M.J.W., Zhang, N.W., McHale, L.K., Pelgrom, K., den Boer, E., Lindhout, P., Michelmore, R.W., Visser, R.G.F., and Niks, R.E. (2009). Rin4 Causes Hybrid Necrosis and Race-Specific Resistance in an Interspecific Lettuce Hybrid. Plant Cell **21,** 3368-3378.

Jing, H.C. (2005). Regulation of leaf senescence in Arabidopsis : isolation and characterisation of onset of leaf death mutants. Doctoral Thesis **University of Groningen. - With summary in Dutch.**

, http://irs.ub.rug.nl/ppn/274535092.

Jing, H.C., Sturre, M.J., Hille, J., and Dijkwel, P.P. (2002). Arabidopsis onset of leaf death mutants identify a regulatory pathway controlling leaf senescence. Plant J. **32,** 51-63.

Jones, J.D., and Dangl, J.L. (2006). The plant immune system. Nature **444,** 323-329.

Jones, P.R., Manabe, T., Awazuhara, M., and Saito, K. (2003). A new member of plant CS-lyases. A cystine lyase from Arabidopsis thaliana. J. Biol. Chem. **278,** 10291-10296.

Jost, R., Berkowitz, O., Wirtz, M., Hopkins, L., Hawkesford, M.J., and Hell, R. (2000). Genomic and functional characterization of the oas gene family encoding O-acetylserine (thiol) lyases, enzymes catalyzing the final step in cysteine biosynthesis in Arabidopsis thaliana. Gene **253,** 237-247.

Jost, R., Altschmied, L., Bloem, E., Bogs, J., Gershenzon, J., Hahnel, U., Hansch, R., Hartmann, T., Kopriva, S., Kruse, C., Mendel, R.R., Papenbrock, J., Reichelt, M., Rennenberg, H., Schnug, E., Schmidt, A., Textor, S., Tokuhisa, J., Wachter, A., Wirtz, M., Rausch, T., and Hell, R. (2005). Expression profiling of metabolic genes in response to methyl jasmonate reveals regulation of genes of primary and secondary sulfur-related pathways in Arabidopsis thaliana. Photosynth. Res. **86,** 491-508.

Katagiri, F., Thilmony, R., and He, S.Y. (2002). The *Arabidopsis thaliana-Pseudomonas syringae* interaction. In The Arabidopsis Book/American Society of Plant Biologists (Somerville, C.R., and Meyerowitz, E.M., eds) Rockville, MD: American Society of Plant Biologists. doi/10.1199/tab.0039. **1**.

Kataoka, T., Watanabe-Takahashi, A., Hayashi, N., Ohnishi, M., Mimura, T., Buchner, P., Hawkesford, M.J., Yamaya, T., and Takahashi, H. (2004). Vacuolar sulfate transporters are essential determinants controlling internal distribution of sulfate in Arabidopsis. Plant Cell **16,** 2693-2704.

Kaul et al. (2000). Analysis of the genome sequence of the flowering plant Arabidopsis thaliana. Nature **408,** 796-815.

Kawashima, C.G., Berkowitz, O., Hell, R., Noji, M., and Saito, K. (2005). Characterization and expression analysis of a serine acetyltransferase gene family involved in a key step of the sulfur assimilation pathway in Arabidopsis. Plant Physiol **137,** 220-230.

Kawashima, C.G., Matthewman, C.A., Huang, S.Q., Lee, B.R., Yoshimoto, N., Koprivova, A., Rubio-Somoza, I., Todesco, M., Rathjen, T., Saito, K., Takahashi, H., Dalmay, T., and Kopriva, S. (2011). Interplay of SLIM1 and miR395 in the regulation of sulfate assimilation in Arabidopsis. Plant J. **66,** 863-876.

Khan, M.S., Haas, F.H., Samami, A.A., Gholami, A.M., Bauer, A., Fellenberg, K., Reichelt, M., Hansch, R., Mendel, R.R., Meyer, A.J., Wirtz, M., and Hell, R. (2010). Sulfite Reductase Defines a Newly Discovered Bottleneck for Assimilatory Sulfate Reduction and Is Essential for Growth and Development in Arabidopsis thaliana. Plant Cell **22,** 1216-1231.

Kim, H., Awazuhara, M., Hayashi, H., Chino, M., and Fujiwara, T. (1997). Analysis of O-acetyl-L-serine in in vitro cultured soybean cotyledons. (In Sulphur metabolism in higher plants: molecular, ecophysiological and nutritional aspects. (Cram, W.J., De Kok, L.J., Stulen, I., Brunold, C., and Rennenberg, H. eds) Leiden, the Netherlands: Backhuys Publishers, pp. 307-309

Kim, J.H., Lee, B.W., Schroeder, F.C., and Jander, G. (2008). Identification of indole glucosinolate breakdown products with antifeedant effects on Myzus persicae (green peach aphid). Plant J. **54,** 1015-1026.

Klein, M., and Papenbrock, J. (2004). The multi-protein family of Arabidopsis sulphotransferases and their relatives in other plant species. J. Exp. Bot. **55,** 1809-1820.

Klonus, D., Hofgen, R., Willmitzer, L., and Riesmeier, J.W. (1994). Isolation and characterization of two cDNA clones encoding ATP-sulfurylases from potato by complementation of a yeast mutant. Plant J. **6,** 105-112.

Komori, R., Amano, Y., Ogawa-Ohnishi, M., and Matsubayashi, Y. (2009). Identification of tyrosylprotein sulfotransferase in Arabidopsis. Proc. Natl. Acad. Sci. U. S. A. **106,** 15067-15072.

Kopriva, S. (2006). Regulation of sulfate assimilation in Arabidopsis and beyond. Ann Bot **97,** 479-495.

Kopriva, S., Wiedemann, G., and Reski, R. (2007). Sulfate Assimilation in Basal Land Plants - What Does Genomic Sequencing Tell Us? Plant Biol. **9,** 556-564.

Kopriva, S., Mugford, S., Matthewman, C., and Koprivova, A. (2009). Plant sulfate assimilation genes: redundancy versus specialization. Plant Cell Rep. **28,** 1769-1780.

Kopriva, S., Büchert, T., Fritz, G., Suter, M., Weber, M., Benda, R., Schaller, J., Feller, U., Schürmann, P., Schünemann, V., Trautwein, A.X., Kroneck, P.M.H., and Brunold, C. (2001). Plant Adenosine 5′-Phosphosulfate Reductase Is a Novel Iron-Sulfur Protein. J. Biol. Chem. **276,** 42881-42886.

Koprivova, A., and Kopriva, S. (2008). Lessons from investigation of regulation of APS reductase by salt stress. Plant Signal Behav **3,** 567-569.

Koprivova, A., Melzer, M., von Ballmoos, P., Mandel, T., Brunold, C., and Kopriva, S. (2001). Assimilatory Sulfate Reduction in C3, C3-C4, and C4 Species ofFlaveria. Plant Physiol. **127,** 543-550.

Koprivova, A., Meyer, A.J., Schween, G., Herschbach, C., Reski, R., and Kopriva, S. (2002). Functional knockout of the adenosine 5'-phosphosulfate reductase gene in Physcomitrella patens revives an old route of sulfate assimilation. J. Biol. Chem. **277,** 32195-32201.

Krasileva, K.V., Dahlbeck, D., and Staskawicz, B.J. (2010). Activation of an Arabidopsis Resistance Protein Is Specified by the in Planta Association of Its Leucine-Rich Repeat Domain with the Cognate Oomycete Effector. Plant Cell **22,** 2444-2458.

Kredich, N.M. (1971). Regulation of L-cysteine biosynthesis in Salmonella typhimurium. I. Effects of growth of varying sulfur sources and O-acetyl-L-serine on gene expression. J. Biol. Chem. **246,** 3474-3484.

Kredich, N.M., Becker, M.A., and Tomkins, G.M. (1969). Purification and characterization of cysteine synthetase, a bifunctional protein complex, from Salmonella typhimurium. J. Biol. Chem. **244,** 2428-2439.

Krueger, S., Niehl, A., Lopez Martin, M.C., Steinhauser, D., Donath, A., Hildebrandt, T., Romero, L.C., Hoefgen, R., Gotor, C., and Hesse, H. (2009). Analysis of cytosolic and plastidic serine acetyltransferase mutants and subcellular metabolite distributions suggests interplay of the cellular compartments for cysteine biosynthesis in Arabidopsis. Plant Cell Environ. **32,** 349-367.

Kruger, J., Thomas, C.M., Golstein, C., Dixon, M.S., Smoker, M., Tang, S., Mulder, L., and Jones, J.D. (2002). A tomato cysteine protease required for Cf-2-dependent disease resistance and suppression of autonecrosis. Science **296,** 744-747.

Krüger, J., Thomas, C.M., Golstein, C., Dixon, M.S., Smoker, M., Tang, S., Mulder, L., and Jones, J.D.G. (2002). A Tomato Cysteine Protease Required for Cf-2-Dependent Disease Resistance and Suppression of Autonecrosis. Science **296,** 744-747.

Kruse, C., Jost, R., Lipschis, M., Kopp, B., Hartmann, M., and Hell, R. (2007). Sulfur-Enhanced Defence: Effects of Sulfur Metabolism, Nitrogen Supply, and Pathogen Lifestyle. Plant Biol. **9,** 608-619.

Krusell, L., Krause, K., Ott, T., Desbrosses, G., Kramer, U., Sato, S., Nakamura, Y., Tabata, S., James, E.K., Sandal, N., Stougaard, J., Kawaguchi, M., Miyamoto, A., Suganuma, N., and Udvardi, M.K. (2005). The sulfate transporter SST1 is crucial for symbiotic nitrogen fixation in Lotus japonicus root nodules. Plant Cell **17,** 1625-1636.

Kuang, H., Caldwell, K.S., Meyers, B.C., and Michelmore, R.W. (2008). Frequent sequence exchanges between homologs of RPP8 in Arabidopsis are not necessarily associated with genomic proximity. Plant J. **54,** 69-80.

Kuang, H., Woo, S.S., Meyers, B.C., Nevo, E., and Michelmore, R.W. (2004). Multiple genetic processes result in heterogeneous rates of evolution within the major cluster disease resistance genes in lettuce. Plant Cell **16,** 2870-2894.

Kumaran, S., and Jez, J.M. (2007). Thermodynamics of the interaction between O-Acetylserine sulfhydrylase and the C-terminus of serine acetyltransferase. Biochemistry **46,** 5586-5594.

Kumaran, S., Yi, H., Krishnan, H.B., and Jez, J.M. (2009). Assembly of the cysteine synthase complex and the regulatory role of protein-protein interactions. J. Biol. Chem. **284,** 10268-10275.

Lappartient, A.G., and Touraine, B. (1996). Demand-Driven Control of Root ATP Sulfurylase Activity and SO42- Uptake in Intact Canola (The Role of Phloem-Translocated Glutathione). Plant Physiol **111,** 147-157.

Lappartient, A.G., Vidmar, J.J., Leustek, T., Glass, A.D., and Touraine, B. (1999). Inter-organ signaling in plants: regulation of ATP sulfurylase and sulfate transporter genes expression in roots mediated by phloem-translocated compound. Plant J. **18,** 89-95.

Leustek, T., and Saito, K. (1999). Sulfate transport and assimilation in plants. Plant Physiol **120,** 637-644.

Leustek, T., Murillo, M., and Cervantes, M. (1994). Cloning of a cDNA encoding ATP sulfurylase from Arabidopsis thaliana by functional expression in Saccharomyces cerevisiae. Plant Physiol **105,** 897-902.

Leustek, T., Martin, M.N., Bick, J.A., and Davies, J.P. (2000). Pathways and regulation of sulfur metabolism revealed through molecular and genetic studies. Annu. Rev. Plant Physiol. Plant Mol. Biol. **51,** 141-165.

Liang, G., Yang, F.X., and Yu, D.Q. (2010). MicroRNA395 mediates regulation of sulfate accumulation and allocation in Arabidopsis thaliana. Plant J. **62,** 1046-1057.

Lindermayr, C., and Durner, J. (2009). S-Nitrosylation in plants: pattern and function. J. Proteomics **73,** 1-9.

Lindermayr, C., Saalbach, G., and Durner, J. (2005). Proteomic identification of S-nitrosylated proteins in Arabidopsis. Plant Physiol. **137,** 921-930.

Lindermayr, C., Saalbach, G., Bahnweg, G., and Durner, J. (2006). Differential inhibition of Arabidopsis methionine adenosyltransferases by protein S-nitrosylation. J. Biol. Chem. **281,** 4285-4291.

Lindroth, P., and Mopper, K. (1979). High performance liquid chromatographic determination of subpicomole amounts of amino acids by precolumn fluorescence derivatization with O-phthaldialdehyde. Anal. Chem. **51,** 1667-1674.

Lisec, J., Schauer, N., Kopka, J., Willmitzer, L., and Fernie, A.R. (2006). Gas chromatography mass spectrometry–based metabolite profiling in plants. Nat. Protoc. **1,** 387-396.

Liszewska, F., Gaganidze, D., and Sirko, A. (2005). Isolation of Nicotiana plumbaginifolia cDNAs encoding isoforms of serine acetyltransferase and O-acetylserine (thiol) lyase in a yeast two-hybrid system with Escherichia coli cysE and cysK genes as baits. Acta Biochim. Pol. **52,** 117-128.

Liu, J., Elmore, J.M., Lin, Z.-J.D., and Coaker, G. (2011). A Receptor-like Cytoplasmic Kinase Phosphorylates the Host Target RIN4, Leading to the Activation of a Plant Innate Immune Receptor. Cell Host Microbe **9,** 137-146.

Lopez-Martin, M.C., Becana, M., Romero, L.C., and Gotor, C. (2008). Knocking out cytosolic cysteine synthesis compromises the antioxidant capacity of the cytosol to maintain discrete concentrations of hydrogen peroxide in Arabidopsis. Plant Physiol. **147,** 562-572.

Loudet, O., Saliba-Colombani, V., Camilleri, C., Calenge, F., Gaudon, V., Koprivova, A., North, K.A., Kopriva, S., and Daniel-Vedele, F. (2007). Natural variation for sulfate content in Arabidopsis thaliana is highly controlled by APR2. Nat. Genet. **39,** 896-900.

Lowicka, E., and Beltowski, J. (2007). Hydrogen sulfide (H2S) - the third gas of interest for pharmacologists. Pharmacol Rep **59,** 4-24.

Luedemann, A., Strassburg, K., Erban, A., and Kopka, J. (2008). TagFinder for the quantitative analysis of gas chromatography—mass spectrometry (GC-MS)-based metabolite profiling experiments. Bioinformatics **24,** 732-737.

Lunn, J.E., Droux, M., Martin, J., and Douce, R. (1990). Localization of ATP Sulfurylase and O-Acetylserine(thiol)lyase in Spinach Leaves. Plant Physiol. **94,** 1345-1352.

Mackey, D., Belkhadir, Y., Alonso, J.M., Ecker, J.R., and Dangl, J.L. (2003). Arabidopsis RIN4 Is a Target of the Type III Virulence Effector AvrRpt2 and Modulates RPS2-Mediated Resistance. Cell **112,** 379-389.

Marshall, O.J. (2004). PerlPrimer: cross-platform, graphical primer design for standard, bisulphite and real-time PCR. Bioinformatics **20,** 2471-2472.

Martin, M.N., Tarczynski, M.C., Shen, B., and Leustek, T. (2005). The role of 5'-adenylylsulfate reductase in controlling sulfate reduction in plants. Photosynth. Res. **86,** 309-323.

Maruyama-Nakashita, A., Nakamura, Y., Yamaya, T., and Takahashi, H. (2004a). Regulation of high-affinity sulphate transporters in plants: towards systematic analysis of sulphur signalling and regulation. J. Exp. Bot. **55,** 1843-1849.

Maruyama-Nakashita, A., Nakamura, Y., Yamaya, T., and Takahashi, H. (2004b). A novel regulatory pathway of sulfate uptake in Arabidopsis roots: implication of CRE1/WOL/AHK4-mediated cytokinin-dependent regulation. Plant J. **38,** 779-789.

Maruyama-Nakashita, A., Inoue, E., Watanabe-Takahashi, A., Yamaya, T., and Takahashi, H. (2003). Transcriptome profiling of sulfur-responsive genes in Arabidopsis reveals global effects of sulfur nutrition on multiple metabolic pathways. Plant Physiol. **132,** 597-605.

Maruyama-Nakashita, A., Nakamura, Y., Tohge, T., Saito, K., and Takahashi, H. (2006). Arabidopsis SLIM1 is a central transcriptional regulator of plant sulfur response and metabolism. Plant Cell **18,** 3235-3251.

Maruyama-Nakashita, A., Nakamura, Y., Watanabe-Takahashi, A., Inoue, E., Yamaya, T., and Takahashi, H. (2005). Identification of a novel cis-acting element conferring sulfur deficiency response in Arabidopsis roots. Plant J. **42,** 305-314.

Mathai, J.C., Missner, A., Kügler, P., Saparov, S.M., Zeidel, M.L., Lee, J.K., and Pohl, P. (2009). No facilitator required for membrane transport of hydrogen sulfide. Proc. Natl. Acad. Sci. U. S. A. **106,** 16633-16638.

Maughan, S.C., Pasternak, M., Cairns, N., Kiddle, G., Brach, T., Jarvis, R., Haas, F., Nieuwland, J., Lim, B., Muller, C., Salcedo-Sora, E., Kruse, C., Orsel, M., Hell, R., Miller, A.J., Bray, P., Foyer, C.H., Murray, J.A., Meyer, A.J., and Cobbett, C.S. (2010). Plant homologs of the Plasmodium falciparum chloroquine-resistance transporter, PfCRT, are required for glutathione homeostasis and stress responses. Proc. Natl. Acad. Sci. U. S. A. **107,** 2331-2336.

Maxwell, D.P., Wang, Y., and McIntosh, L. (1999). The alternative oxidase lowers mitochondrial reactive oxygen production in plant cells. Proc. Natl. Acad. Sci. U. S. A. **96,** 8271-8276.

May, M.J., and Leaver, C.J. (1994). Arabidopsis thaliana gamma-glutamylcysteine synthetase is structurally unrelated to mammalian, yeast, and Escherichia coli homologs. Proc. Natl. Acad. Sci. U. S. A. **91,** 10059-10063.

McDowell, J.M., and Woffenden, B.J. (2003). Plant disease resistance genes: recent insights and potential applications. Trends Biotechnol. **21,** 178-183.

Meng, P.H., Raynaud, C., Tcherkez, G., Blanchet, S., Massoud, K., Domenichini, S., Henry, Y., Soubigou-Taconnat, L., Lelarge-Trouverie, C., Saindrenan, P., Renou, J.P., and Bergounioux, C. (2009). Crosstalks between Myo-Inositol Metabolism, Programmed Cell Death and Basal Immunity in Arabidopsis. PLoS One **4,** e7364.

Meyers, B.C., Kaushik, S., and Nandety, R.S. (2005). Evolving disease resistance genes. Curr. Opin. Plant Biol. **8,** 129-134.

Meyers, B.C., Kozik, A., Griego, A., Kuang, H., and Michelmore, R.W. (2003). Genome-Wide Analysis of NBS-LRR–Encoding Genes in Arabidopsis. Plant Cell **15,** 809-834.

Mhamdi, A., Hager, J., Chaouch, S., Queval, G., Han, Y., Taconnat, L., Saindrenan, P., Gouia, H., Issakidis-Bourguet, E., Renou, J.-P., and Noctor, G. (2010). Arabidopsis GLUTATHIONE REDUCTASE 1 plays a crucial role in leaf responses to intracellular H2O2 and in ensuring appropriate gene expression through both salicylic acid and jasmonic acid signaling pathways. Plant Physiol. **153,** 1144-1160.

Mizuno, N., Hosogi, N., Park, P., and Takumi, S. (2010). Hypersensitive Response-Like Reaction Is Associated with Hybrid Necrosis in Interspecific Crosses between Tetraploid Wheat and Aegilops tauschii Coss. PLoS One **5,** e11326.

Mizuno, N., Shitsukawa, N., Hosogi, N., Park, P., and Takumi, S. (2011). Autoimmune response and repression of mitotic cell division occur in inter-specific crosses between tetraploid wheat and Aegilops tauschii Coss. that show low temperature-induced hybrid necrosis. Plant J. **68,** 114-128.

Moldrup, M.E., Geu-Flores, F., Olsen, C.E., and Halkier, B.A. (2011). Modulation of sulfur metabolism enables efficient glucosinolate engineering. BMC Biotechnol. **11**.

Moore, J.W., Loake, G.J., and Spoel, S.H. (2011). Transcription Dynamics in Plant Immunity. Plant Cell **23,** 2809-2820.

Mugford, S.G., Yoshimoto, N., Reichelt, M., Wirtz, M., Hill, L., Mugford, S.T., Nakazato, Y., Noji, M., Takahashi, H., Kramell, R., Gigolashvili, T., Flugge, U.I., Wasternack, C., Gershenzon, J., Hell, R., Saito, K., and Kopriva, S. (2009). Disruption of adenosine-5'-phosphosulfate kinase in Arabidopsis reduces levels of sulfated secondary metabolites. Plant Cell **21,** 910-927.

Murillo, M., and Leustek, T. (1995). Adenosine-5'-triphosphate-sulfurylase from Arabidopsis thaliana and Escherichia coli are functionally equivalent but structurally and kinetically divergent: nucleotide sequence of two adenosine-5'-triphosphate-sulfurylase cDNAs from Arabidopsis thaliana and analysis of a recombinant enzyme. Arch. Biochem. Biophys. **323,** 195-204.

Nocito, F.F., Lancilli, C., Crema, B., Fourcroy, P., Davidian, J.C., and Sacchi, G.A. (2006). Heavy metal stress and sulfate uptake in maize roots. Plant Physiol **141,** 1138-1148.

Noctor, G., Mhamdi, A., Chaouch, S., Han, Y.I., Neukermans, J., Marquez-Garcia, B., Queval, G., and Foyer, C.H. (2012). Glutathione in plants: an integrated overview. Plant Cell Environ. **35,** 454-484.

Noji, M., and Saito, K. (2002). Molecular and biochemical analysis of serine acetyltransferase and cysteine synthase towards sulfur metabolic engineering in plants. Amino acids **22,** 231-243.

Noji, M., Inoue, K., Kimura, N., Gouda, A., and Saito, K. (1998). Isoform-dependent differences in feedback regulation and subcellular localization of serine acetyltransferase involved in cysteine biosynthesis from Arabidopsis thaliana. J. Biol. Chem. **273,** 32739-32745.

Noji, M., Saito, M., Nakamura, M., Aono, M., Saji, H., and Saito, K. (2001). Cysteine synthase overexpression in tobacco confers tolerance to sulfur-containing environmental pollutants. Plant Physiol. **126,** 973-980.

Oldroyd, G.E.D., and Staskawicz, B.J. (1998). Genetically engineered broad-spectrum disease resistance in tomato. Proc. Natl. Acad. Sci. U. S. A. **95,** 10300-10305.

Palma, K., Thorgrimsen, S., Malinovsky, F.G., Fiil, B.K., Nielsen, H.B., Brodersen, P., Hofius, D., Petersen, M., and Mundy, J. (2010). Autoimmunity in Arabidopsis acd11 Is Mediated by Epigenetic Regulation of an Immune Receptor. PLoS Pathog. **6,** e1001137.

Parisy, V., Poinssot, B., Owsianowski, L., Buchala, A., Glazebrook, J., and Mauch, F. (2007). Identification of PAD2 as a gamma-glutamylcysteine synthetase highlights the importance of glutathione in disease resistance of Arabidopsis. Plant J. **49,** 159-172.

Park, S., and Imlay, J.A. (2003). High levels of intracellular cysteine promote oxidative DNA damage by driving the fenton reaction. J. Bacteriol. **185,** 1942-1950.

Parker, J.E., Szabó, V., Staskawicz, B.J., Lister, C., Dean, C., Daniels, M.J., and Jones, J.D.G. (1993). Phenotypic characterization and molecular mapping of the Arabidopsis thaliana locus RPP5, determining disease resistance to Peronospora parasitica. Plant J. **4,** 821-831.

Parmar, S., Buchner, P., and Hawkesford, M.J. (2007). Leaf developmental stage affects sulfate depletion and specific sulfate transporter expression during sulfur deprivation in Brassica napus L. Plant Biol. **9,** 647-653.

Pasternak, M., Lim, B., Wirtz, M., Hell, R., Cobbett, C.S., and Meyer, A.J. (2008). Restricting glutathione biosynthesis to the cytosol is sufficient for normal plant development. Plant J. **53,** 999-1012.

Peiser, G.D., Wang, T.T., Hoffman, N.E., Yang, S.F., Liu, H.W., and Walsh, C.T. (1984). Formation of cyanide from carbon 1 of 1-aminocyclopropane-1-carboxylic acid during its conversion to ethylene. Proc. Natl. Acad. Sci. U. S. A. **81,** 3059-3063.

Pellny, T.K., Locato, V., Vivancos, P.D., Markovic, J., De Gara, L., Pallardo, F.V., and Foyer, C.H. (2009). Pyridine nucleotide cycling and control of intracellular redox state in relation to poly (ADP-ribose) polymerase activity and nuclear localization of glutathione during exponential growth of Arabidopsis cells in culture. Mol Plant **2,** 442-456.

Penn, D.J., and Potts, W.K. (1999). The evolution of mating preferences and major histocompatibility complex genes. Am. Nat. **153,** 145-164.

Pesaresi, P., Gardner, N.A., Masiero, S., Dietzmann, A., Eichacker, L., Wickner, R., Salamini, F., and Leister, D. (2003). Cytoplasmic N-terminal protein acetylation is required for efficient photosynthesis in Arabidopsis. Plant Cell **15,** 1817-1832.

Pfaffl, M.W. (2001). A new mathematical model for relative quantification in real-time RT–PCR. Nucleic Acids Res. **29,** e45-e45.

Piotrowski, M. (2008). Primary or secondary? Versatile nitrilases in plant metabolism. Phytochemistry **69,** 2655-2667.

Presgraves, D.C., Balagopalan, L., Abmayr, S.M., and Orr, H.A. (2003). Adaptive evolution drives divergence of a hybrid inviability gene between two species of Drosophila. Nature **423,** 715-719.

Rabeh, W.M., and Cook, P.F. (2004). Structure and mechanism of O-acetylserine sulfhydrylase. J. Biol. Chem. **279,** 26803-26806.

Rausch, T., and Wachter, A. (2005). Sulfur metabolism: a versatile platform for launching defence operations. Trends Plant Sci. **10,** 503-509.

Ravanel, S., Gakiere, B., Job, D., and Douce, R. (1998). The specific features of methionine biosynthesis and metabolism in plants. Proc. Natl. Acad. Sci. U. S. A. **95,** 7805-7812.

Ravanel, S., Block, M.A., Rippert, P., Jabrin, S., Curien, G., Rebeille, F., and Douce, R. (2004). Methionine metabolism in plants - Chloroplasts are autonomous for de novo methionine synthesis and can import S-adenosylmethionine from the cytosol. J. Biol. Chem. **279,** 22548-22557.

Rawlins, M.R., Leaver, C.J., and May, M.J. (1995). Characterization of an Arabidopsis-Thaliana Cdna-Encoding Glutathione Synthetase. FEBS Lett. **376,** 81-86.

Rehmany, A.P., Gordon, A., Rose, L.E., Allen, R.L., Armstrong, M.R., Whisson, S.C., Kamoun, S., Tyler, B.M., Birch, P.R.J., and Beynon, J.L. (2005). Differential Recognition of Highly Divergent Downy Mildew Avirulence Gene Alleles by RPP1 Resistance Genes from Two Arabidopsis Lines. Plant Cell **17,** 1839-1850.

Renosto, F., Patel, H.C., Martin, R.L., Thomassian, C., Zimmerman, G., and Segel, I.H. (1993). ATP sulfurylase from higher plants: kinetic and structural characterization of the chloroplast and cytosol enzymes from spinach leaf. Arch. Biochem. Biophys. **307,** 272-285.

Richman, P.G., and Meister, A. (1975). Regulation of gamma-glutamyl-cysteine synthetase by nonallosteric feedback inhibition by glutathione. J. Biol. Chem. **250,** 1422-1426.

Riemenschneider, A., Riedel, K., Hoefgen, R., Papenbrock, J., and Hesse, H. (2005). Impact of Reduced O-Acetylserine(thiol)lyase Isoform Contents on Potato Plant Metabolism. Plant Physiol. **137,** 892-900.

Roden, L.C., and Ingle, R.A. (2009). Lights, Rhythms, Infection: The Role of Light and the Circadian Clock in Determining the Outcome of Plant-Pathogen Interactions. Plant Cell **21,** 2546-2552.

Roine, E., Wei, W., Yuan, J., Nurmiaho-Lassila, E.-L., Kalkkinen, N., Romantschuk, M., and He, S.Y. (1997). Hrp pilus: An hrp-dependent bacterial surface appendage produced by Pseudomonas syringae pv. tomato DC3000. Proc. Natl. Acad. Sci. U. S. A. **94,** 3459-3464.

Romero-Puertas, M.C., Campostrini, N., Matte, A., Righetti, P.G., Perazzolli, M., Zolla, L., Roepstorff, P., and Delledonne, M. (2008). Proteomic analysis of S-nitrosylated proteins in Arabidopsis thaliana undergoing hypersensitive response. Proteomics **8,** 1459-1469.

Rotte, C., and Leustek, T. (2000). Differential Subcellular Localization and Expression of ATP Sulfurylase and 5′-Adenylylsulfate Reductase during Ontogenesis of Arabidopsis Leaves Indicates That Cytosolic and Plastid Forms of ATP Sulfurylase May Have Specialized Functions. Plant Physiol. **124,** 715-724.

Rouached, H., Secco, D., and Arpat, A.B. (2009). Getting the most sulfate from soil: Regulation of sulfate uptake transporters in Arabidopsis. J. Plant Physiol. **166,** 893-902.

Rouached, H., Secco, D., Arpat, B., and Poirier, Y. (2011). The transcription factor PHR1 plays a key role in the regulation of sulfate shoot-to-root flux upon phosphate starvation in Arabidopsis. BMC Plant Biol. **11**.

Rouached, H., Berthomieu, P., El Kassis, E., Cathala, N., Catherinot, V., Labesse, G., Davidian, J.C., and Fourcroy, P. (2005). Structural and functional analysis of the C-terminal STAS (sulfate transporter and anti-sigma antagonist) domain of the Arabidopsis thaliana sulfate transporter SULTR1.2. J. Biol. Chem. **280,** 15976-15983.

Rouached, H., Wirtz, M., Alary, R., Hell, R., Arpat, A.B., Davidian, J.C., Fourcroy, P., and Berthomieu, P. (2008). Differential regulation of the expression of two high-affinity sulfate transporters, SULTR1.1 and SULTR1.2, in Arabidopsis. Plant Physiol. **147,** 897-911.

Ruegger, M., and Chapple, C. (2001). Mutations that reduce sinapoylmalate accumulation in Arabidopsis thaliana define loci with diverse roles in phenylpropanoid metabolism. Genetics **159,** 1741-1749.

Saito, K. (2000). Regulation of sulfate transport and synthesis of sulfur-containing amino acids. Curr. Opin. Plant Biol. **3,** 188-195.

Saito, K., Yokoyama, H., Noji, M., and Murakoshi, I. (1995). Molecular cloning and characterization of a plant serine acetyltransferase playing a regulatory role in cysteine biosynthesis from watermelon. J. Biol. Chem. **270,** 16321-16326.

Saito, K., Kurosawa, M., Tatsuguchi, K., Takagi, Y., and Murakoshi, I. (1994). Modulation of Cysteine Biosynthesis in Chloroplasts of Transgenic Tobacco Overexpressing Cysteine Synthase [O-Acetylserine(thiol)-Iyase]. Plant Physiol. **106,** 887-895.

Sakakibara, H. (2006). Cytokinins: activity, biosynthesis, and translocation. Annu. Rev. Plant Biol. **57,** 431-449.

Sambrook, J. (2001). Molecular cloning : a laboratory manual. (Cold Spring Harbor, N.Y. :: Cold Spring Harbor Laboratory Press).

Scharte, J., SchÖN, H., and Weis, E. (2005). Photosynthesis and carbohydrate metabolism in tobacco leaves during an incompatible interaction with Phytophthora nicotianae. Plant Cell Environ. **28,** 1421-1435.

Schlaeppi, K., Bodenhausen, N., Buchala, A., Mauch, F., and Reymond, P. (2008). The glutathione-deficient mutant pad2-1 accumulates lower amounts of glucosinolates and is more susceptible to the insect herbivore Spodoptera littoralis. Plant J. **55,** 774-786.

Schulze-Lefert, P., and Panstruga, R. (2011). A molecular evolutionary concept connecting nonhost resistance, pathogen host range, and pathogen speciation. Trends Plant Sci. **16,** 117-125.

Sharma, S.S., and Dietz, K.-J. (2006). The significance of amino acids and amino acid-derived molecules in plant responses and adaptation to heavy metal stress. J. Exp. Bot. **57,** 711-726.

Shelp, B.J., Bown, A.W., and McLean, M.D. (1999). Metabolism and functions of gamma-aminobutyric acid. Trends Plant Sci. **4,** 446-452.

Shibagaki, N., and Grossman, A.R. (2004). Probing the function of STAS domains of the Arabidopsis sulfate transporters. J. Biol. Chem. **279,** 30791-30799.

Shibagaki, N., and Grossman, A.R. (2010). Binding of cysteine synthase to the STAS domain of sulfate transporter and its regulatory consequences. J. Biol. Chem. **285,** 25094-25102.

Shibagaki, N., Rose, A., McDermott, J.P., Fujiwara, T., Hayashi, H., Yoneyama, T., and Davies, J.P. (2002). Selenate-resistant mutants of Arabidopsis thaliana identify Sultr1;2, a sulfate transporter required for efficient transport of sulfate into roots. Plant J. **29,** 475-486.

Shin, R., Jez, J.M., Basra, A., Zhang, B., and Schachtman, D.P. (2011). 14-3-3 Proteins fine-tune plant nutrient metabolism. FEBS Lett. **585,** 143-147.

Shirzadian-Khorramabad, R., Jing, H.C., Everts, G.E., Schippers, J.H., Hille, J., and Dijkwel, P.P. (2010). A mutation in the cytosolic O-acetylserine (thiol) lyase induces a genome-dependent early leaf death phenotype in Arabidopsis. BMC Plant Biol. **10,** 80.

Siegień, I., and Bogatek, R. (2006). Cyanide action in plants — from toxic to regulatory. Acta Physiol. Plant. **28,** 483-497.

Smith, F.W., Ealing, P.M., Hawkesford, M.J., and Clarkson, D.T. (1995). Plant members of a family of sulfate transporters reveal functional subtypes. Proc. Natl. Acad. Sci. U. S. A. **92,** 9373-9377.

Smith, F.W., Hawkesford, M.J., Ealing, P.M., Clarkson, D.T., Vanden Berg, P.J., Belcher, A.R., and Warrilow, A.G. (1997a). Regulation of expression of a cDNA from barley roots encoding a high affinity sulphate transporter. Plant J. **12,** 875-884.

Smith, F.W., Hawkesford, M.J., Ealing, P.M., Clarkson, D.T., VandenBerg, P.J., Belcher, A.R., and Warrilow, G.S. (1997b). Regulation of expression of a cDNA from barley roots encoding a high affinity sulphate transporter. Plant J. **12,** 875-884.

Soutourina, O., Dubrac, S., Poupel, O., Msadek, T., and Martin-Verstraete, I. (2010). The pleiotropic CymR regulator of Staphylococcus aureus plays an important role in virulence and stress response. PLoS Pathog. **6,** e1000894.

Spadaro, D., Yun, B.-W., Spoel, S.H., Chu, C., Wang, Y.-Q., and Loake, G.J. (2010). The redox switch: dynamic regulation of protein function by cysteine modifications. Physiol. Plant **138,** 360-371.

Spoel, S.H., and Loake, G.J. (2011). Redox-based protein modifications: the missing link in plant immune signalling. Curr. Opin. Plant Biol. **14,** 358-364.

Spoel, S.H., Tada, Y., and Loake, G.J. (2010). Post-translational protein modification as a tool for transcription reprogramming. New Phytol. **186,** 333-339.

Spoel, S.H., Koornneef, A., Claessens, S.M.C., Korzelius, J.P., Van Pelt, J.A., Mueller, M.J., Buchala, A.J., Métraux, J.-P., Brown, R., Kazan, K., Van Loon, L.C., Dong, X., and Pieterse, C.M.J. (2003). NPR1 Modulates Cross-Talk between Salicylate- and Jasmonate-Dependent Defense Pathways through a Novel Function in the Cytosol. Plant Cell **15,** 760-770.

Staal, J., Kaliff, M., Dewaele, E., Persson, M., and Dixelius, C. (2008). RLM3, a TIR domain encoding gene involved in broad-range immunity of Arabidopsis to necrotrophic fungal pathogens. Plant J. **55,** 188-200.

Stitt, M., Lilley, R.M., Gerhardt, R., and Heldt, H.W. (1989). Metabolite Levels in Specific Cells and Subcellular Compartments of Plant-Leaves. Methods Enzymol. **174,** 518-552.

Stuttmann, J., Hubberten, H.-M., Rietz, S., Kaur, J., Muskett, P., Guerois, R., Bednarek, P., Hoefgen, R., and Parker, J.E. (2011). Perturbation of Arabidopsis Amino Acid Metabolism Causes Incompatibility with the Adapted Biotrophic Pathogen Hyaloperonospora arabidopsidis. Plant Cell.

Su, T., Xu, J., Li, Y., Lei, L., Zhao, L., Yang, H., Feng, J., Liu, G., and Ren, D. (2011). Glutathione-Indole-3-Acetonitrile Is Required for Camalexin Biosynthesis in Arabidopsis thaliana. The Plant Cell Online.

Swarbrick, P.J., Schulze-Lefert, P., and Scholes, J.D. (2006). Metabolic consequences of susceptibility and resistance (race-specific and broad-spectrum) in barley leaves challenged with powdery mildew. Plant Cell Environ. **29,** 1061-1076.

Tada, Y., Spoel, S.H., Pajerowska-Mukhtar, K., Mou, Z.L., Song, J.Q., Wang, C., Zuo, J.R., and Dong, X.N. (2008). Plant immunity requires conformational charges of NPR1 via S-nitrosylation and thioredoxins. Science **321,** 952-956.

Takahashi, H. (2010). Chapter 4 - Regulation of Sulfate Transport and Assimilation in Plants. In International Review of Cell and Molecular Biology, W.J. Kwang, ed (Academic Press), pp. 129-159.

Takahashi, H., Buchner, P., Yoshimoto, N., Hawkesford, M.J., and Shiu, S.H. (2011a). Evolutionary relationships and functional diversity of plant sulfate transporters. Front Plant Sci **2,** 119.

Takahashi, H., Kopriva, S., Giordano, M., Saito, K., and Hell, R. (2011b). Sulfur assimilation in photosynthetic organisms: molecular functions and regulations of transporters and assimilatory enzymes. Annu. Rev. Plant Biol. **62,** 157-184.

Takahashi, H., Watanabe-Takahashi, A., Smith, F.W., Blake-Kalff, M., Hawkesford, M.J., and Saito, K. (2000). The roles of three functional sulphate transporters involved in uptake and translocation of sulphate in Arabidopsis thaliana. Plant J. **23,** 171-182.

Takahashi, H., Yamazaki, M., Sasakura, N., Watanabe, A., Leustek, T., Engler, J.A., Engler, G., Van Montagu, M., and Saito, K. (1997). Regulation of sulfur assimilation in higher plants: a sulfate transporter induced in sulfate-starved roots plays a central role in Arabidopsis thaliana. Proc. Natl. Acad. Sci. U. S. A. **94,** 11102-11107.

Takken, F.L.W., and Goverse, A. (2012). How to build a pathogen detector: structural basis of NB-LRR function. Curr. Opin. Plant Biol. **15,** 375-384.

Takken, F.L.W., Albrecht, M., and Tameling, W.I.L. (2006). Resistance proteins: molecular switches of plant defence. Curr. Opin. Plant Biol. **9,** 383-390.

Takumi, S., and Mizuno, N. (2011). Low temperature-induced necrosis shows phenotypic plasticity in wheat triploid hybrids. Plant Signal. Behav. **6,** 1431-1433.

Tang, S.W., and Presgraves, D.C. (2009). Evolution of the Drosophila Nuclear Pore Complex Results in Multiple Hybrid Incompatibilities. Science **323,** 779-782.

Thomazeau, K., Curien, G., Dumas, R., and Biou, V. (2001). Crystal structure of threonine synthase from Arabidopsis thaliana. Protein Sci. **10,** 638-648.

Thordal-Christensen, H., Zhang, Z., Wei, Y., and Collinge, D.B. (1997). Subcellular localization of H2O2 in plants. H2O2 accumulation in papillae and hypersensitive response during the barley—powdery mildew interaction. Plant J. **11,** 1187-1194.

Todesco, M., Balasubramanian, S., Hu, T.T., Traw, M.B., Horton, M., Epple, P., Kuhns, C., Sureshkumar, S., Schwartz, C., Lanz, C., Laitinen, R.A.E., Huang, Y., Chory, J., Lipka, V., Borevitz, J.O., Dangl, J.L., Bergelson, J., Nordborg, M., and Weigel, D. (2010). Natural allelic variation underlying a major fitness trade-off in Arabidopsis thaliana. Nature **465,** 632-636.

Tohge, T., and Fernie, A.R. (2010). Combining genetic diversity, informatics and metabolomics to facilitate annotation of plant gene function. Nat. Protoc. **5,** 1210-1227.

Tomatsu, H., Takano, J., Takahashi, H., Watanabe-Takahashi, A., Shibagaki, N., and Fujiwara, T. (2007). An Arabidopsis thaliana high-affinity molybdate transporter required for efficient uptake of molybdate from soil. Proc. Natl. Acad. Sci. U. S. A. **104,** 18807-18812.

Tornero, P., and Dangl, J.L. (2001). A high-throughput method for quantifying growth of phytopathogenic bacteria in *Arabidopsis thaliana*. Plant J. **28,** 475-481.

Treutter, D. (2006). Significance of flavonoids in plant resistance: a review. Environmental Chemistry Letters **4,** 147-157.

Valpuesta, V., and Botella, M.A. (2004). Biosynthesis of L-ascorbic acid in plants: new pathways for an old antioxidant. Trends Plant Sci. **9,** 573-577.

Van Breusegem, F., and Dat, J.F. (2006). Reactive Oxygen Species in Plant Cell Death. Plant Physiol. **141,** 384-390.

Vauclare, P., Kopriva, S., Fell, D., Suter, M., Sticher, L., von Ballmoos, P., Krahenbuhl, U., den Camp, R.O., and Brunold, C. (2002). Flux control of sulphate assimilation in Arabidopsis thaliana: adenosine 5 '-phosphosulphate reductase is more susceptible than ATP sulphurylase to negative control by thiols. Plant J. **31,** 729-740.

Vernoux, T., Wilson, R.C., Seeley, K.A., Reichheld, J.P., Muroy, S., Brown, S., Maughan, S.C., Cobbett, C.S., Van Montagu, M., Inze, D., May, M.J., and Sung, Z.R. (2000). The ROOT MERISTEMLESS1/CADMIUM SENSITIVE2 gene defines a glutathione-dependent pathway involved in initiation and maintenance of cell division during postembryonic root development. Plant Cell **12,** 97-109.

Vidmar, J.J., Tagmount, A., Cathala, N., Touraine, B., and Davidian, J.E. (2000). Cloning and characterization of a root specific high-affinity sulfate transporter from Arabidopsis thaliana. FEBS Lett. **475,** 65-69.

Vivancos, P.D., Wolff, T., Markovic, J., Pallardo, F.V., and Foyer, C.H. (2010). A nuclear glutathione cycle within the cell cycle. Biochem. J. **431,** 169-178.

Vlot, A.C., Dempsey, D.M.A., and Klessig, D.F. (2009). Salicylic Acid, a Multifaceted Hormone to Combat Disease. Annu. Rev. Phytopathol. **47,** 177-206.

Voll, L.M., Jamai, A., Renne, P., Voll, H., McClung, C.R., and Weber, A.P.M. (2006). The photorespiratory Arabidopsis shm1 mutant is deficient in SHM1. Plant Physiol. **140,** 59-66.

Wachter, A., Wolf, S., Steininger, H., Bogs, J., and Rausch, T. (2005). Differential targeting of GSH1 and GSH2 is achieved by multiple transcription initiation: implications for the compartmentation of glutathione biosynthesis in the Brassicaceae. Plant J. **41,** 15-30.

Warrilow, A.G.S., and Hawkesford, M.J. (2000). Cysteine synthase (O-acetylserine (thiol) lyase) substrate specificities classify the mitochondrial isoform as a cyanoalanine synthase. J. Exp. Bot. **51,** 985-993.

Watanabe, M., Kusano, M., Oikawa, A., Fukushima, A., Noji, M., and Saito, K. (2008a). Physiological roles of the *β-substituted alanine synthase* gene family in *Arabidopsis*. Plant physiology **146,** 310-320.

Watanabe, M., Mochida, K., Kato, T., Tabata, S., Yoshimoto, N., Noji, M., and Saito, K. (2008b). Comparative genomics and reverse genetics analysis reveal indispensable functions of the serine acetyltransferase gene family in Arabidopsis. Plant Cell **20,** 2484-2496.

Wei, J., Tang, Q.X., Varlamova, O., Roche, C., Lee, R., and Leyh, T.S. (2002). Cysteine biosynthetic enzymes are the pieces of a metabolic energy pump. Biochemistry **41,** 8493-8498.

Wei, W., Plovanich-Jones, A., Deng, W.L., Jin, Q.L., Collmer, A., Huang, H.C., and He, S.Y. (2000). The gene coding for the Hrp pilus structural protein is required for type III secretion of Hrp and Avr proteins in *Pseudomonas syringae* pv. tomato. Proc. Natl. Acad. Sci. U. S. A. **97,** 2247.

Weigel, D., and Glazebrook, J. (2006). In planta transformation of Arabidopsis. CSH Protoc **2006**.

Weigel, D., and Mott, R. (2009). The 1001 genomes project for Arabidopsis thaliana. Genome Biol **10,** 107.

Wiermer, M. (2005). Molecular and spatial characterisation of Arabidopsis EDS1 defence regulatory complexes (Universität).

Wirtz, M., and Hell, R. (2006). Functional analysis of the cysteine synthase protein complex from plants: structural, biochemical and regulatory properties. J. Plant Physiol. **163,** 273-286.

Wirtz, M., Droux, M., and Hell, R. (2004). O-acetylserine (thiol) lyase: an enigmatic enzyme of plant cysteine biosynthesis revisited in Arabidopsis thaliana. J. Exp. Bot. **55,** 1785-1798.

Wirtz, M., Berkowitz, O., Droux, M., and Hell, R. (2001). The cysteine synthase complex from plants. Mitochondrial serine acetyltransferase from Arabidopsis thaliana carries a bifunctional domain for catalysis and protein-protein interaction. Eur. J. Biochem. **268,** 686-693.

Wirtz, M., Heeg, C., Samami, A., Ruppert, T., and Hell, R. (2010). Enzymes of cysteine synthesis show extensive and conserved modifications patterns that include Nα-terminal acetylation. Amino Acids **39,** 1077-1086.

Wirtz, M., Beard, K.F.M., Lee, C.P., Boltz, A., Schwarzländer, M., Fuchs, C., Meyer, A.J., Heeg, C., Sweetlove, L.J., Ratcliffe, R.G., and Hell, R. (2012). Mitochondrial Cysteine Synthase Complex Regulates O-Acetylserine Biosynthesis in Plants. J. Biol. Chem. **287,** 27941-27947.

Wise, A., Liu, Z., and Binns, A. (2006). Nucleic Acid Extraction from Agrobacterium Strains. In Agrobacterium Protocols, K. Wang, ed (Humana Press), pp. 67-76.

Xiang, C., and Oliver, D.J. (1998). Glutathione Metabolic Genes Coordinately Respond to Heavy Metals and Jasmonic Acid in Arabidopsis. Plant Cell **10,** 1539-1550.

Yamaguchi, Y., Nakamura, T., Kusano, T., and Sano, H. (2000). Three Arabidopsis Genes Encoding Proteins with Differential Activities for Cysteine Synthase and β-Cyanoalanine Synthase. Plant Cell Physiol. **41,** 465-476.

Yamamoto, E., Takashi, T., Morinaka, Y., Lin, S.Y., Wu, J.Z., Matsumoto, T., Kitano, H., Matsuoka, M., and Ashikari, M. (2010). Gain of deleterious function causes an autoimmune response and Bateson-Dobzhansky-Muller incompatibility in rice. Mol. Genet. Genomics **283,** 305-315.

Yang, S., and Hua, J. (2004). A haplotype-specific Resistance gene regulated by BONZAI1 mediates temperature-dependent growth control in Arabidopsis. Plant Cell **16,** 1060-1071.

Yao, M., Ose, T., Sugimoto, H., Horiuchi, A., Nakagawa, A., Wakatsuki, S., Yokoi, D., Murakami, T., Honma, M., and Tanaka, I. (2000). Crystal Structure of 1-Aminocyclopropane-1-carboxylate Deaminase from Hansenula saturnus. J. Biol. Chem. **275,** 34557-34565.

Yatusevich, R., Mugford, S.G., Matthewman, C., Gigolashvili, T., Frerigmann, H., Delaney, S., Koprivova, A., Flügge, U.-I., and Kopriva, S. (2010). Genes of primary sulfate assimilation are part of the glucosinolate biosynthetic network in Arabidopsis thaliana. Plant J. **62,** 1-11.

Ye, B., Muller, H.H., Zhang, J., and Gressel, J. (1997). Constitutively elevated levels of putrescine and putrescine-generating enzymes correlated with oxidant stress resistance in Conyza bonariensis and wheat. Plant Physiol. **115,** 1443-1451.

Yi, H., and Richards, E.J. (2007). A cluster of disease resistance genes in Arabidopsis is coordinately regulated by transcriptional activation and RNA silencing. Plant Cell **19,** 2929-2939.

Yoshimoto, N., Takahashi, H., Smith, F.W., Yamaya, T., and Saito, K. (2002). Two distinct high-affinity sulfate transporters with different inducibilities mediate uptake of sulfate in Arabidopsis roots. Plant J. **29,** 465-473.

Yoshimoto, N., Inoue, E., Saito, K., Yamaya, T., and Takahashi, H. (2003). Phloem-localizing sulfate transporter, Sultr1;3, mediates re-distribution of sulfur from source to sink organs in Arabidopsis. Plant Physiol **131,** 1511-1517.

Youssefian, S., Nakamura, M., Orudgev, E., and Kondo, N. (2001). Increased cysteine biosynthesis capacity of transgenic tobacco overexpressing an O-acetylserine(thiol) lyase modifies plant responses to oxidative stress. Plant Physiol **126,** 1001-1011.

Yun, B.-W., Spoel, S.H., and Loake, G.J. (2012). Synthesis of and signalling by small, redox active molecules in the plant immune response. Biochimica et Biophysica Acta (BBA) - General Subjects **1820,** 770-776.

Zhang, X., Henriques, R., Lin, S.S., Niu, Q.W., and Chua, N.H. (2006). *Agrobacterium*-mediated transformation of *Arabidopsis thaliana* using the floral dip method. Nat. Protoc. **1,** 641-646.

Zhang, Y., Shi, J., Liu, J.Y., Zhang, J.D., and Guo, X.Q. (2010). Identification of a novel NPR1-like gene from Nicotiana glutinosa and its role in resistance to fungal, bacterial and viral pathogens. Plant Biol. **12,** 23-34.

Zhao, C., Kumada, Y., Imanaka, H., Imamura, K., and Nakanishi, K. (2006). Cloning, overexpression, purification, and characterization of O-acetylserine sulfhydrylase-B from Escherichia coli. Protein Expr. Purif. **47,** 607-613.

Zhou, H., Lin, J., Johnson, A., Morgan, Robyn L., Zhong, W., and Ma, W. (2011). Pseudomonas syringae Type III Effector HopZ1 Targets a Host Enzyme to Suppress Isoflavone Biosynthesis and Promote Infection in Soybean. Cell Host Microbe **9,** 177-186.

Zhu, Y., Qian, W., and Hua, J. (2010). Temperature Modulates Plant Defense Responses through NB-LRR Proteins. PLoS Pathog. **6,** e1000844.

Zhu, Y.L., Pilon-Smits, E.A.H., Jouanin, L., and Terry, N. (1999a). Overexpression of glutathione synthetase in Indian mustard enhances cadmium accumulation and tolerance. Plant Physiol. **119,** 73-79.

Zhu, Y.L., Pilon-Smits, E.A.H., Tarun, A.S., Weber, S.U., Jouanin, L., and Terry, N. (1999b). Cadmium tolerance and accumulation in Indian mustard is enhanced by overexpressing gamma-glutamylcysteine synthetase. Plant Physiol. **121,** 1169-1177.

Zook, M. (1998). Biosynthesis of camalexin from tryptophan pathway intermediates in cell-suspension cultures of arabidopsis. Plant Physiol. **118,** 1389-1393.

Zuber, H., Davidian, J.C., Aubert, G., Aime, D., Belghazi, M., Lugan, R., Heintz, D., Wirtz, M., Hell, R., Thompson, R., and Gallardo, K. (2010). The Seed Composition of Arabidopsis Mutants for the Group 3 Sulfate Transporters Indicates a Role in Sulfate Translocation within Developing Seeds. Plant Physiol. **154,** 913-926.

Zybailov, B., Rutschow, H., Friso, G., Rudella, A., Emanuelsson, O., Sun, Q., and van Wijk, K.J. (2008). Sorting signals, N-terminal modifications and abundance of the chloroplast proteome. PLoS One **3,** e1994.

Publication

Most of the work presented in Chapter 4 and Chapter 5 was accepted for publication in the Plant Journal. Following is the accepted proof of the manuscript in the press.

The Plant Journal (2012) doi: 10.1111/tpj.12021

Activation of *R*-mediated innate immunity and disease susceptibility is affected by mutations in a cytosolic *O*-acetylserine (thiol) lyase in Arabidopsis

Jibran Tahir[1,†], Mutsumi Watanabe[2,†], Hai-Chun Jing[3], Donald A. Hunter[4], Takayuki Tohge[2], Adriano Nunes-Nesi[2], Yariv Brotman[2], Alisdair R. Fernie[2], Rainer Hoefgen[2] and Paul P. Dijkwel[1,*]

[1]*Institute of Molecular BioSciences, Massey University, Private Bag 11222, Palmerston North, New Zealand,*
[2]*Max-Planck-Institut fuer Molekulare Pflanzenphysiologie, Wissenschaftspark Golm, Am Muehlenberg 1, Potsdam-Golm, 14476, Germany,*
[3]*Centre for Bioenergy Plants Research and Development, Institute of Botany, Chinese Academy of Sciences, Beijing, 100093, China, and*
[4]*The New Zealand Institute for Plant & Food Research Limited, Private Bag 11600, Palmerston North, 4442, New Zealand*

Received 8 June 2012; revised 05 September 2012; accepted 10 September 2012.
*For correspondence (e-mail p.dijkwel@massey.ac.nz).
†These authors contributed equally to this work.

SUMMARY

***O*-acetylserine (thiol) lyases (OASTLs) are evolutionarily conserved proteins among many prokaryotes and eukaryotes that perform sulfur acquisition and synthesis of cysteine. A mutation in the cytosolic OASTL-A1 protein ONSET OF LEAF DEATH3 (OLD3) was previously shown to reduce the OASTL activity of the old3-1 protein *in vitro* and cause auto-necrosis in specific Arabidopsis accessions. Here we investigated why a mutation in this protein causes auto-necrosis in some but not other accessions. The auto-necrosis was found to depend on *Recognition of Peronospora Parasitica 1* (*RPP1*)-like disease resistance *R* gene(s) from an evolutionarily divergent *R* gene cluster that is present in L*er*-0 but not the reference accession Col-0. *RPP1*-like gene(s) show a negative epistatic interaction with the *old3-1* mutation that is not linked to reduced cysteine biosynthesis. Metabolic profiling and transcriptional analysis further indicate that an effector triggered-like immune response and metabolic disorder are associated with auto-necrosis in *old3-1* mutants, probably activated by an *RPP1*-like gene. However, the old3-1 protein in itself results in largely neutral changes in primary plant metabolism, stress defence and immune responses. Finally, we showed that lack of a functional OASTL-A1 results in enhanced disease susceptibility against infection with virulent and non-virulent *Pseudomonas syringae* pv. *tomato DC3000* strains. These results reveal an interaction between the cytosolic OASTL and components of plant immunity.**

Keywords: RPP1, OASTL-A1, disease resistance, auto-necrosis, cysteine biosynthesis, innate immunity.

To access the full article please follow the link below;

http://onlinelibrary.wiley.com/doi/10.1111/tpj.12021/full